Dissertation

submitted to the
combined faculties for the Natural Sciences and for Mathematics of the
Ruperto-Carola University of Heidelberg, Germany

for the degree of
Doctor of Natural Sciences

presented by

M. Sc. **Irina Meln**
born in Leningrad, USSR

oral examination: 15th of December 2016, Heidelberg

Conditioning fat for the future: adipose tissue expansion during childhood

Referees:

Prof. Dr. Ingrid Lohmann

Prof. Dr. Stephan Herzig

Statement of authorship

I hereby declare that this thesis has been written only by the undersigned, without any unauthorized use of services of a third party. No sources or aids have been used in the preparation of this thesis other than those indicated in the thesis itself. Where the work of others has been quoted or reproduced, the source is always given. This thesis, in same or similar form, has not been available to any audit authority yet.

Ich erkläre hiermit, dass Ich die vorliegende Arbeit selbstständig und ohne unzulässige Hilfe Dritter verfasst habe. Ich habe keine anderen als die angegebenen Hilfsmittel und Quellen verwendet. Insbesondere habe ich wörtlich oder sinngemäß aus anderen Werken übernommene Inhalte als solche kenntlich gemacht. Die Arbeit ist in dieser oder ähnlicher Form noch nicht als Prüfungsarbeit eingereicht worden.

Irina Meln
Heidelberg, October 2016

SUMMARY

Obesity has become a global health problem for both children and adults. White adipose tissue (WAT) displays unique plasticity upon excessive feeding by expanding its mass through proliferation and differentiation of resident adipocyte progenitor cells (AP). Studies have shown that excessive accumulation of WAT is pre-determined during early childhood. However, mechanisms of the body weight programming and effect of WAT expansion during childhood on metabolic disease risk later in life are still elusive. In order to investigate regulation of AP expansion by obesogenic diet, we established a diet-induced obesity model. We observed a rapid gain in body weight and increased accumulation of WAT already one week after high-fat diet (HFD) feeding in young, sexually immature female mice, but not adult mice. Moreover, HFD induced WAT growth via proliferation of APs and partially through mature adipocyte hypertrophy. Employing an isocaloric, pair feeding approach, we found that dietary fat content is able to induce proliferation of APs, while the amount of consumed calories seems to promote inflammation. Moreover we demonstrated that AP proliferation could occur without initial hypertrophy of mature adipocytes. Although we demonstrated that the concentration of insulin-like growth factor 1 (IGF-1) was regulated by calorie load as little as 2 days of HFD, it was not changed upon isocaloric HFD thus could not fully explain the proliferation we observed in APs. Additionally, we found lipids transiently increased after feeding and could be potentially involved in AP activation. In order to identify genes involved in regulating AP responses in the niche upon excessive feeding during childhood, we performed gene expression profiling from whole tissue and specific cellular subpopulations of WAT. A large portion of the differentially expressed genes from WAT profiles were associated with key events in tissue remodeling and cell-to-cell communication, such as inflammation, cytokine production, and extracellular matrix proteins/remodeling enzymes. In order to functionally validate candidate genes, a novel co-culture system with APs and feeder niche-like cells was established to mimic WAT physiological conditions. This system was used for siRNA screening by high-content microscopy to identify alterations in cell proliferation and differentiation. Several gene targets related to increased proliferation of APs in response to HFD feeding have been validated including epithelial membrane protein 1 (EMP1), which known to play a role in cell junctions. EMP1 modulation in feeder cells (siRNA mediated knockdown or overexpression) altered AP-derived colony growth. Our results suggested that high fat feeding induces activation of the network of cell-cycle related genes triggering AP proliferation in early development.

ZUSAMMENFASSUNG

Fettleibigkeit ist ein globales Gesundheitsproblem für Kinder und Erwachsene geworden. Weißes Fettgewebe (WF) zeigt eine einzigartige Plastizität bei übermäßiger Kalorienaufnahme durch Expansion seiner Masse durch Proliferation und Differenzierung von residenten Adipozyten-Vorläuferzellen (AV). Studien haben gezeigt, dass eine übermäßige Akkumulation von WF in der frühen Kindheit vorausbestimmt wird. Allerdings sind die Mechanismen der Körpergewichts-Programmierung und Wirkung der WF-Expansion während der Kindheit auf das metabolische Krankheitsrisiko später im Leben noch schwer fassbar. Um die Regulation der AV-Expansion durch obesogene Ernährung zu untersuchen, haben wir ein Diät-induziertes Fettleibigkeitsmodell etabliert. Wir beobachteten einen raschen Anstieg des Körpergewichts und eine erhöhte Akkumulation von WF bereits eine Woche nach Beginn der Hochfettdiät (HFD) bei jungen, aber nicht bei erwachsenen Mäusen. Darüber hinaus induzierte Hochfettdiät das WF-Wachstum durch die frühe Zellproliferation und auch teilweise durch Adipozytenhypertrophie. Mittels eines isokalorischen Fütterungsansatz es haben wir festgestellt, dass hoher Fettgehalt in der Nahrung die Proliferation von AVs induzieren kann, während die Menge der verbrauchten Kalorien die Entzündung zu fördern scheint. Darüber hinaus haben wir gezeigt, dass AV-Proliferation ohne anfängliche Hypertrophie von reifen Adipozyten auftreten konnte. Obwohl wir gezeigt haben, dass die Konzentration von IGF-1 durch Kalorienbelastung bereits nach 2 Tagen HFD reguliert wurde, wurde sie bei isokalorischer HFD nicht verändert, was die in AVs beobachtete Proliferation nicht vollständig erklären konnte. Darüber hinaus fanden wir vorübergehend erhöhte Lipide nach der Fütterung, welche möglicherweise an der AV-Aktivierung beteiligt sein könnten. Um Gene, die an der Regulation der AV-Antwort bei übermäßiger Fütterung während der Kindheit beteiligt sind, zu identifizieren, führten wir eine Transkriptomanalyse aus dem gesamten WF und aus spezifischen zellulären Subpopulationen durch. Ein großer Teil der differentiell exprimierten Gene aus WF-Profilen wurde mit wichtigen Ereignissen in der Geweberegenerierung und der Zell-Zell-Kommunikation, wie Entzündung, Zytokinproduktion und extrazelluläre Matrixproteine/ Remodelingenzyme, in Verbindung gebracht. Um die funktionelle Validierung von Kandidatengenen durchzuführen, wurde ein Kokultursystem von AV und Feeder-Zellten entwickelt, um die physiologischen Bedingungen der WF-Nische nachzuahmen. Dieses System wurde für das siRNA-Screening verwendet, mittels High-Content Mikroskopie, um Veränderungen in der Zellproliferation/ -differenzierung zu identifizieren. Mehrere Gen-Targets, die im Zusammenhang mit AVs Reaktion auf fettreiche Fütterung stehen wurden im Co-Kultur-System validiert, einschließlich epithelial membrane protein 1 (EMP1), von dem bekannt ist, dass es eine Rolle im Zellkontakt spielt. EMP1-Manipulation in Feeder-Zellen (siRNA-vermittelter Knockdown oder Überexpression) veränderte AV-abgeleitetes Kolonienwachstum. Unsere Ergebnisse deuten darauf hin, dass eine fettreiche Fütterung die Aktivierung des Netzwerks von zellzyklusbezogenen Genen induziert, die die AV-Proliferation in der frühen Entwicklung auslösen.

CONTRIBUTIONS

All experiments were performed in DKFZ Junior Group Metabolism and Stem Cell Plasticity (A171) at the German Cancer Research Center (DKFZ), Heidelberg, Germany. Initial design of the project done by Dr. Alexandros Vegiopoulos, design of all experiments done by Irina Meln and Dr. Alexandros Vegiopoulos. Additionally, experiment with controlled circadian rhythm (Fig. 2.17) was designed together with Dr. Gretchen Wolff. Many animal experiments were done with the assistance of Dr. Gretchen Wolff, Sarah Lerch, Oksana Seibert and Annika Zota. Concentration of EdU administration for mice was optimised with assistance of Dr. Gretchen Wolff. Embedding of tissues, section cutting and H&E staining were done by Sarah Lerch, I have performed microscopy and further analysis. Serum factor mesurments were performed with assistance of Sarah Lerch. Pipeline for automatic image analysis of adipose tissue histology and EdU-labeled nuclei count were developed together with Dr. Damir Krunic. FASC antibody staining and gaiting scheme was designed and set on the FACS machine by Irem Bayindir-Buchhalter. FACS machine for sorting of subpopulations was operated by Klaus Hexel. Pipeline for cell/colony recognition and count for co-culture experiments was developed with Dr. Jürgen Reymann and automated algorithm was written by Dr. Jürgen Reymann. Affymetrix gene expression arrays were hybridized in Genomics & Proteomics Core Facility, DKFZ. I was provided with raw CEL files and all further analysis was performed by me. Some graphical representation of expression data was done with assistance of Dr. Daria Bunina. Validation of targets from gene expression profiling via qPCR was done by Liza Harbrecht under my supervision. The last described experiment for functional validation of EMP1 (Fig. 2. 39) was performed by Wujun Hong, master student supervised by me. I performed all other experiments and analyses, unless indicated above.

ACKNOWLEDGMENTS

First of all I would like to acknowledge my current supervisor Dr. Alexandros Vegiopoulos for providing to me the opportunity to do PhD project in his lab and for teaching me a multitude of different techniques. I am very grateful that Dr. Vegiopoulos has been a great mentor to me, helped me in many difficult moments and contributed to developing my strategical scientific thinking for experimental design and project management.

I would like to thank all former and current members of Vegiopoulos lab for their expertise and support, especially Dr. Gretchen Wolff for significant contribution to continuation of this project, for scientific discussions and experiment design and for proofreading of this thesis. Also I would like to thank Sarah Lerch for daily assistance and support, and all trainee who genotyped UBC-GFP mice. I would like to acknowledge Irem Bayindir-Buchhalter for establishing FACS antibody and gating scheme which we have used in this project, for great lab protocols and all help. I would like to mention all former members of Prof. Herzig department; they provided useful feedback on my project during lab meetings and established many protocols in the lab. Especially I am very grateful to Oksana Seibert and Annika Zota for helping with animal experiments. I would like to mention and thank my extremely talented students Liza Harbrecht and Wujun Hong for their contribution to this project, for being independent and motivated.

I am very grateful for excellent support of DKFZ core facilities, especially to with Dr. Damir Krunic from Light Microscopy facility for constant help with image acquisition and postprocessing, for teaching me Fiji (ImageJ) and many other advice. Also I am thankful to Klaus Hexel from Flow Cytometry core facility for sorting my samples and useful advice during FACS data acquisition. I would also like to mention our collaborators from ViroQuant-CellNetworks RNAi Screening Facility, Bioquant, University of Heidelberg, Dr. Holger Erfle, Dr. Jürgen Reymann, Jürgen Beneke and Nina Beil. I would like to thank Dr. Jürgen Reymann for developed automated algorithm for this project and Jürgen Beneke and Nina Beil for assistance in image acquisition.

I would like to thank all members of TAC committee, Prof. Dr. Bruce Edgar, Prof. Dr. Ingrid Lohmann, Dr. Holger Erfle, and Dr. Jürgen Reymann for useful feedback on my project. I would like to thank the DKFZ training team for an opportunity to attend interesting courses and workshops. I am very grateful to The Helmholtz International Graduate School for Cancer Research in Heidelberg for financial and personal support, for excellent scientific communication workshops and networking events.

TABLE OF CONTENT

1. INTRODUCTION

1.1 Adipose tissue

Adipose or fat tissue (AT) is a complex organ with metabolic and endocrine functions in the body. AT can be classified into two main types: white adipose tissue (WAT) and brown adipose tissue (BAT) (Peirce et al. 2014). WAT consists of unilocular adipocytes (fat cells) with one big lipid droplet, specialized for storage of calories. BAT is composed of multilocular cells with many small lipid droplets enriched with mitochondria for dissipating energy by heat production. Another distinct type of adipocyte is the “beige” or “bright”, a brown-like adipocyte found within WAT upon special stimuli, e.g. cold exposure (Cinti 2012). Recently, the “pink” adipocyte was observed during lactation deriving from mammary gland alveolar epithelial cells (Giordano et al. 2014). The main focus of this work is the WAT, as it is the main source for storage of calories.

1.1.1 Location of different types of white adipose tissue in human and mouse

Although WAT is found throughout the body, there are some specialization, with distinct characteristics and functions, depending on the location. WAT is subdivided as subcutaneous (sc), which is the fat located under the skin, and visceral (v), which is the fat positioned inside of peritoneum; scWAT in humans can be further divided into abdominal, gluteal and femoral (Fig. 1.1 - A). In mice, scWAT is classified by anterior and posterior position in the body. The anterior scWAT is subdivided into deep cervical, superficial cervical, interscapular, subscapular, and axillo-thoracic depots, whereas the posterior, into dorso-lumbar, inguinal and gluteal (Fig. 1.1 - B). Visceral fat in humans is divided into periental, retroperitoneal, omental and mesenteric (Fig. 1.1 - A). In mice there are several vWAT depots as peritoneal, retroperitoneal, mesenteric, and perigonadal (epididymal) (Fig. 1.1 - B). Taking into consideration the differences between mouse and human physiology, the mouse perigonadal WAT (gWAT) is used as a model for the human vWAT. The mouse counterpart of human scWAT is the inguinal WAT (ingWAT).

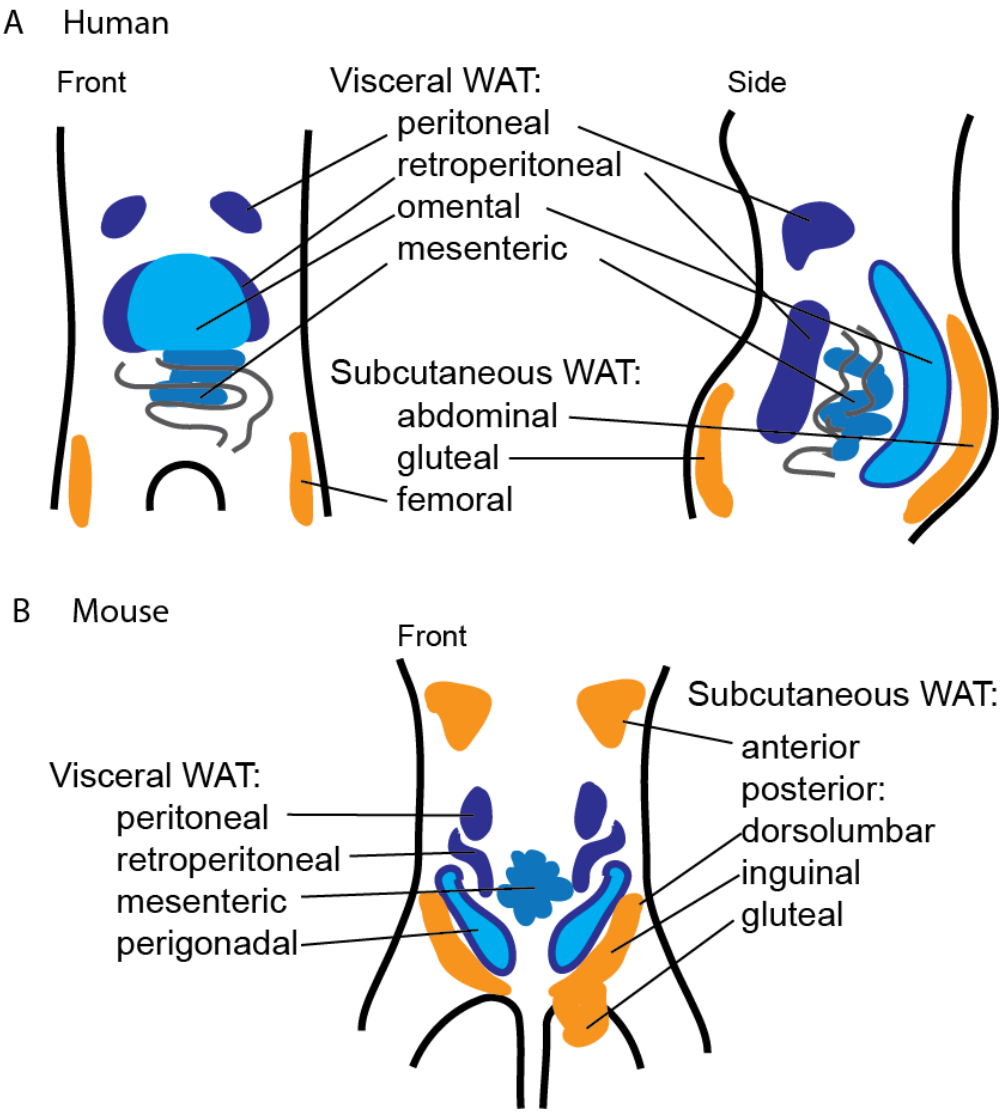

Figure 1.1 Location of different types of WAT in human and mouse.

1.1.2 Main functions of white adipose tissue

Among other vital functions, the key function of WAT is to be the main source of energy for the organism, storing calories during food availability and releasing them in time of need. By buffering energy, adipose tissue plays a pivotal role in organism homeostasis (Rosen & Spiegelman 2014), (Rutkowski et al. 2015). Mature adipocytes are the main cell type within the adipose tissue and responsible for sustaining this function. These specialized cells can store triglycerides in the form of lipid droplets. After feeding, energy is transported in the form of fatty acids into the adipocytes directly from food or through *de novo* lipogenesis in hepatocytes/adipocytes. Non-esterified fatty acids (NEFAs or free fatty acids – FFAs) are taken up from the circulation by fatty acids binding and transporting proteins like CD36 and FATPs, which are highly expressed on adipocytes (Rutkowski et al. 2015). Then FFA are esterified into triglycerides and stored in the lipid droplets leading to an increase of adipocyte size. Another source of energy from food are carbohydrates. Glucose is transported into mature adipocyte in the presence of insulin by the Glut4 transporter (Stry & Renold 1965).

During glycolysis, dihydroxyacetone phosphate is produced from glucose and converted to glycerol-3-phosphate going for triglyceride synthesis. Around 25% of glucose taken by mature adipocyte is used for triglyceride synthesis (Frayn & Humphreys 2012). Alternatively, glucose can enter the tricarboxylic acid (TCA) cycle leading to the production of citrate, which is used for fatty acids synthesis. During fasting, adipose tissue has a central role in body homeostasis by providing fatty acids via lipolysis, which are released to the circulation. Fatty acids can be used as source of energy in different tissues, sparing glucose for the brain and red blood cells (Rosen & Spiegelman 2014).

1.1.2.1 Lipodystrophy

To understand the importance of adipose tissue functions, transgenic mice A-ZIP/F-1 lacking fat were generated in 1998 by the group of Dr. Charles Vinson. Lipodystrophic mice have no WAT and reduced BAT, which leads to a severe metabolic phenotype with enlarged liver filled with lipids, elevated serum glucose (3-fold), insulin (50-400 fold), FFA (2-fold), triglycerides (3-5 fold) (Moitra et al. 1998). Recently the first model of an inducible lipoatrophic mouse was created, FAT-ATTAC (fat apoptosis through targeted activation of caspase 8). Within 2 weeks of induction of adipocytes apoptosis FAT-ATTAC mice had reduced adipose tissue and became glucose intolerant with reduced glucose-stimulated insulin secretion (Pajvani et al. 2005). Lipodystrophy is known in humans as partial or complete loss of adipose tissue, which is often associated with other symptoms as ectopic fat accumulation, metabolic disorders as insulin resistance, diabetes mellitus, hypertriglyceridemia and hepatic steatosis (Endocrinology et al. 2012). Another example of atrophy of adipose tissue is a part of complex disorder called cancer-associated cachexia (CAC) (Petruzzelli & Wagner 2016). Provided examples of lipodystrophic phenotype underlined that AT plays a key role in “save” storing of toxic lipids which can cause ectopic fat accumulation in other organs, e.g. liver.

1.1.2.2 Obesity

Obesity is a result of a positive energy balance, when energy intake is higher than energy expenditure involving the combination of resting metabolic rate, energy spend for absorption and metabolism of dietary macronutrients, and during physical activity (Hill et al. 2012), (Spiegelman & Flier 2001), (Gesta et al. 2007). Although adipose tissue serves as a reservoir for excess calories, increased abdominal fat mass, the so–called central obesity, is strongly associated with increased risk of developing cardiometabolic diseases and increased mortality (Coutinho et al. 2011), (J. J. Lee et al. 2014). Dysfunction of AT expansion is one of the key factors in development of insulin resistance due to impaired lipid storage. Accumulating of vWAT during obesity is associated with chronic inflammation and

insulin resistance induced by tissue macrophages producing proinflammatory cytokines (tumor necrosis factor-alpha (TNF-alpha) and interleukin-6 (IL-6)) (Girard & Lafontan 2008). According to the World Health Organization, the number of people suffering from obesity has doubled since 1980 and totaling over 1.9 billion adults (18 years and older). Obesity leads to life threatening conditions as cardiovascular diseases (CVD) (mainly heart disease and stroke), diabetes, musculoskeletal disorders like osteoarthritis, and some cancers (including endometrial, breast, ovarian, prostate, liver, gallbladder, kidney, and colon) (WHO, 2016).

Nevertheless, not all obese individuals are metabolically unhealthy. It has been shown that some overweight/obese individuals have no association with CVD. These "metabolically healthy obese" (MHO) individuals, despite excess body fat, have no hypertension and display normal metabolic parameters as high insulin sensitivity, normal level of lipids, liver enzymes, hormones and immune profile (Denis & Obin 2013), (Primeau et al. 2011), (Sims 2001). Intriguingly, population studies have shown that moderate obesity can be beneficial effect for health (Andres 1980). More recently some molecular details of healthy expansion of adipose tissue were shown. Type II transmembrane protein tenomodulin (TNMD) is upregulated in AT of individuals with insulin resistance compared with insulin sensitive ones from body mass index (BMI) - matched group. Mice overexpressing Tnmd under an adipose tissue-specific promoter, despite having increased gWAT upon high-fat diet, exhibit improved systemic insulin sensitivity, decreased fibrogenic collagen production and inflammation of AT (Senol-Cosar et al. 2016). Another example is using thiazolidinediones (TZD) for treating patients with diabetes mellitus type 2 (T2DM). TZD are known as agonists of PPARs (peroxisome proliferator-activated receptors), increasing storage of fatty acids in adipocytes, thus decreasing amount of fatty acids in the circulation. TZD increases amount of triglyceride (TG) in WAT and decreasing in liver, which leads to improved insulin sensitivity (Yamauchi et al. 2001). Additionally, TZD induces adipogenesis *in vivo* as rosiglitazone (Tang et al. 2011). Although patients under TZD treatment have improved hepatic and peripheral insulin sensitivity, it leads to weight gain as a side effect (Fonseca 2003). Weight gain was observed to be directly proportional to the level of metabolic improvement (Wilding 2006). It is becoming clear that the functional quality of adipose tissue contributes to metabolic complications during obesity. Comparison studies on the quality and components of extracellular matrix (ECM) in health obese and metabolically compromised women demonstrated that some types of collagen (COL6A3) and enzymes involved in tissue remodeling could discriminate these two groups of obese people (Lackey et al. 2014). Interestingly, MHO individuals have smaller adipocyte size and less macrophage infiltration (Klöting et al. 2010).

1.1.3 Early adipose tissue growth

1.1.3.1 Epidemiology of childhood obesity

Childhood obesity has become a serious public health problem of modern society (Nishtar et al. 2016). Accordingly to the WHO, in 2013 42 million children were overweight or obese (31 million are leaving in developing countries) and this trend predicted continues to grow (Fig. 1.2).

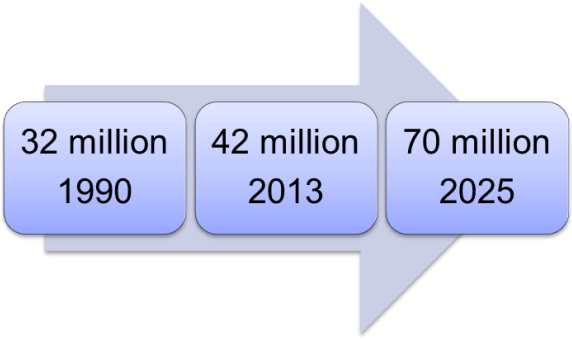

Figure 1.2 Global increase in number of overweight and obese children (WHO, 2016).

1.1.3.2 Chronic problems related to childhood obesity

Obesity is harmful to many organ systems as cardiovascular, endocrine, renal, and can cause physiological and psychological damage for a child as illustrated on Figure 1.3 (Garver et al. 2013). Obese children have a higher risk to remain obese during adult life. It was reported that although obese children before age of 3 years without obese parents have low risk, 80% of children being obese in age 10-15 became obese adults in age of 25 years regardless parental status (Whitaker et al. 1997). In 2014 longitude study was conducted with 7738 participants demonstrating that overweight children in age of 5 have 4 times higher risk to become obese at age fourteen (31.8% vs. 7.9%) (Cunningham et al. 2014).

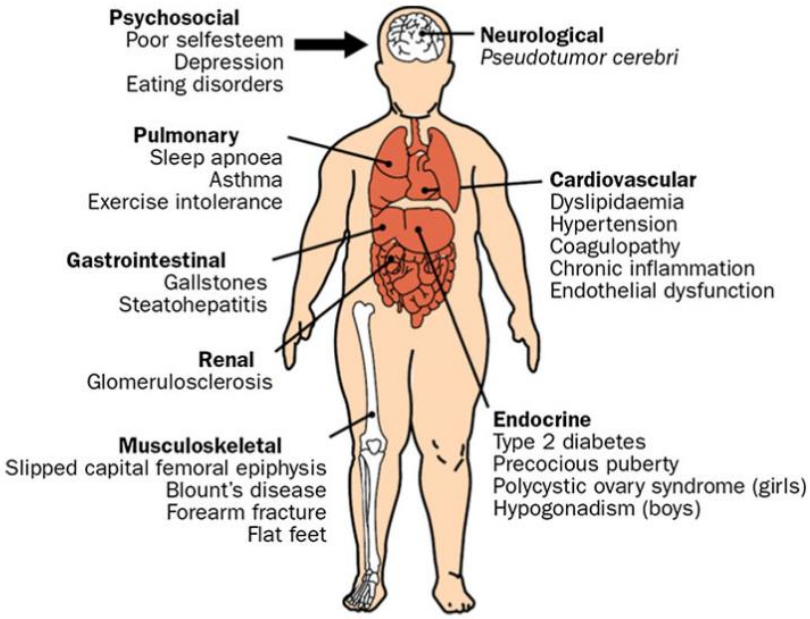

Figure 1.3 Health consequences of childhood obesity. Adapted from (Garver et al. 2013)**.**

1.1.3.3 Risk factors and etiology

While the most common form of childhood obesity is polygenic, studies support that rare monogenic forms are not contributing to the current epidemic of obesity in children (Garver et al. 2013). Having obese parents increases more than 2 times the risk of obesity in adulthood among obese and non-obese children below age of 10 years (Whitaker et al. 1997). The National Health and Nutrition Examination Survey (2005–2006, USA) investigated pre-diabetic status among adolescents (12–19 years) from different ethnic and gender groups; they measured fasting blood glucose and performed glucose tolerance tests (GTT). They showed that Caucasian (white) and Latino- children have the highest prevalence when African-American children have the lowest (Alderete et al. 2014). Accordingly, the same study showed a higher prevalence in boys than girls (Alderete et al. 2014). Although regulation of body weight is considered highly heritable (Kannel et al. 1977), genetic factors interact with environmental ones as adaptation to nutritional/behavior changes (Garver et al. 2013). One obesogenic environmental factor is consuming a diet high in fat and sweet beverages. Studies and surveys in the USA from 1989 till 2008 measuring the intake of sugar from sweetened beverages e.g. fruit drinks, soda, high fat, high sugar milk, and sports drinks have reported increased consumption among children 6-11 years old (Lasater et al. 2011). High- fat diet enriched with saturated fatty acids has a strong association with increased adiposity in obese children (Aeberli et al. 2008). Recently, associations between different food composition as saturated fat on body weight increase in adults were found (Lin et al. 2012). Correlations have been found between sleeping quality/duration and obesity in adolescents. From 1586 individuals aged 11–14 years 24% were overweight/obese. Self-

reported short sleep duration and poor sleep, according to the questionnaires, were associated with increased BMI, fat mass and consuming more unhealthy food (Ferranti et al. 2016). Many studies have investigated the effects of maternal feeding effects on metabolic health of offspring. Increased maternal fructose consumption was associated with obesity of children in humans (Goran et al. 2013). In mice, sucrose feeding during pregnancy leads to obesity in female offspring (Samuelsson et al. 2013). One of the mechanisms proposed is that maternal obesity leads to mitochondrial dysfunction within the oocyte. After transplantation to recipient mothers fertilized oocytes from obese mice gave rise to heavier fetuses (Wu et al. 2015).

1.1.3.4 Models to study early adipose tissue growth

To study early adipose tissue growth, a model of early postnatal overfeeding (PNOF) was developed. In this rodent model, investigators achieved increased body and fat accumulation by reducing litter size (reduced number of offspring). Sprague-Dawley rats, raised in a smaller litter size (4 vs. 22 siblings) from birth till weaning (21 day later) and later had free access to food, had increased body weigh already during weaning and heavier gWAT 10 weeks after weening (Knittle & Hirsch 1968). A more recent study demonstrated that PNOF leads to increased vWAT, lipogenic activity and inflammatory status, while pancreatic and hepatic responsiveness, BAT thermogenic activity were reduced (Consequences et al. 2013). Moreover, PNOF mice are more susceptible to ischemia-reperfusion injury of the heart potentially due to changes in extracellular matrix genes (Habbout et al. 2013). A porcine model of restricted feeding during suckling was also utilized to study early adipose tissue growth and feeding behavioral (Houpt et al. 1979). There are many different methods and model organisms that have been used to study early adipose tissue growth. Each presents its own challenge to study this dynamic tissue, which is becoming a global target for therapy.

1.1.3.5 Global perspective and treatments

Several initiatives have been taken around the world to combat the growing childhood obesity epidemic. An association was found between childhood obesity and low levels of growth hormone (GH). Through inhibition of FFA, a pilot study was conducted with administration of Niacin and results are coming (Galescu et al. 2016). Sleep- lengthening programs for infants with combination of teaching techniques for mothers gave significant results toward preventing obesity during the first year after birth (Paul et al. 2011), (Yanovski 2011). In 2016 WHO published „Report of the commission on ending childhood obesity", in which prevention of childhood obesity was highlighted as crucial for health of future generations (WHO 2016).

1.2 Adipose tissue expansion

WAT has a unique capacity of adapting to changes in nutrient environment. Tissue expansion is one of the features of WAT presented upon excess feeding. As it was mentioned before, mature adipocytes are the main units of adipose tissue. However, adipose tissue consists of many cell types as adipose tissue progenitor cells, endothelial cells in vessels, fibroblasts, many types of immune cells, nerves and extracellular matrix, building together a adipose tissue niche (Fig. 1.4). Moreover physiological turnover of adipose tissue is possible due to proliferation and differentiation immature stromal cells called adipose tissue progenitor cells resisting in the low number in adipose tissue.

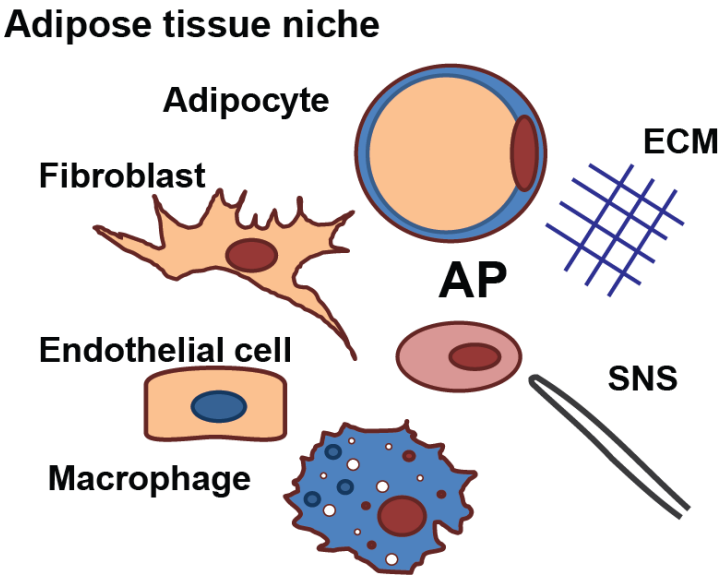

Figure 1.4 Adipose tissue niche components. Adipose tissue consists of many cell types and extracellular structures as extracellular matrix (ECM).

1.2.1 Adipose tissue progenitor cells

For long time it was common to use adherent cells of stroma vascular fraction (SVF) from adipose tissue after digestion to culture so-called mesenchymal stem cells. The surface markers of the heterogeneous population were defined after several passages (Baer 2014). However, very little was known about specific progenitor subpopulations inside of adipose tissue. Recently several groups have contributed substantially to our understanding what adipose tissue progenitors (APs) are. In 2008 Rodeheffer et al. described subpopulations of APs with high adipogenic capacity as Lin-CD29+CD34+Sca-1+CD24+ cells. These cells could differentiate towards mature adipocytes *in vitro* and *in vivo* after transplantation to lipodystrophic mice reversing the diabetic complications of this model by giving rise new adipocytes (Rodeheffer et al. 2008). In a follow up study the same group demonstrated a hierarchy of APs, that Lin-CD29+CD34+Sca-1+CD24+ cells lose the CD24 marker during differentiation and leave the early progenitor pool (Berry & Rodeheffer 2013). The

Granneman group has identified platelet- derived growth factor receptor alpha positive cells (PDGFRα+ cells) as a population of cells with high *in vivo* adipogenic potential. PDGFRα+ cells have unique morphology characterized by cytoplasm with long lamellipodias. They were located in between of mature adipocytes and very often close to blood capillaries. PDGFRα+ cells are CD34+ and Sca-1+, but negative for endothelial marker (IB4), or B-cell marker (CD24), or other family member PDGFRβ, for SMA and PPARγ. PDGFRα+ cells can give rise to white adipocytes after high-fat diet (HFD) feeding or after transplantation into Matrigel in mice (Lee et al. 2012). Resent reporter-linage studies demonstrated that adipose progenitor cells ($PDGFR\beta^{+}$) expressing the zinc-finger transcription factor Zfp423 are contributing to *de novo* adipogenesis *in vivo* (Vishvanath et al. 2016).

1.2.2 Hypertrophy and hyperplasia

AT expansion can be mainly achieved by two mechanisms: increasing size of preexisting adipocytes (hypertrophy) by filling lipid droplets or through proliferation and differentiation of resident APs (hyperplasia). A combination of both hyperplasia and hypertrophy can also occur. The currently accepted model of AT expansion upon calorie excess can be divided on 3 steps: mature adipocyte hypertrophy, death of mature adipocytes and then recruitment of new ones from APs pool (Choe et al. 2016) is shown on Fig. 1.5.

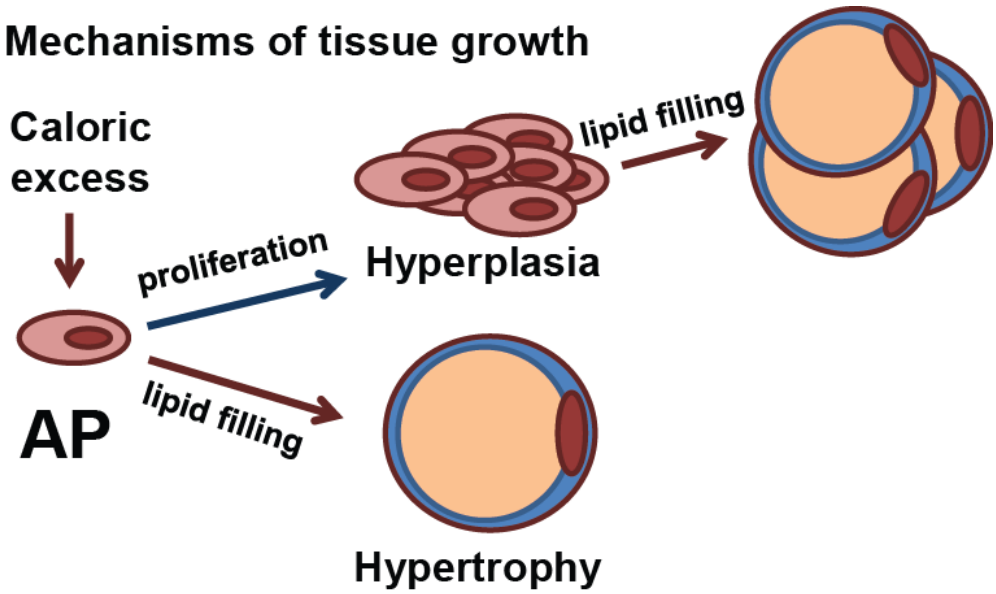

Figure 1.5 Cellular mechanism of adipose tissue growth. Upon calorie excess adipose tissue grows via hypertrophy (increased cell size) of exciting adipocytes and by recruitment of adipose progenitors - hyperplasia (increased cell number).

1.2.2.1 Adipocyte hypertrophy

Upon excess of calories, adipocytes increase their size up to a pre-determined limit, which is estimated as maximum fat cell weight equivalent to 0.7- 0.8 μg/cell (Krotkiewski et al. 1983). Many studies suggested that hypertrophic fat cell has different functions showing a

necrotic phenotype attracting macrophages and secreting pro-inflammatory cytokines (Cinti et al. 2005), (Strissel et al. 2007). Frequency of such necrotic-like adipocytes is higher in diet-induced obesity rodent models and during development of obesity in humans (Cinti et al. 2005). Apparently mice vWAT has greater rate of adipocyte death upon HFD, reaching up to 80% after 4 months of HFD compared with first indication of adipocyte death in scWAT after 3 months of HFD (Strissel et al. 2007). There are many studies showing how hypertrophy and death of adipocytes leads to insulin resistance, but also it is one of the mechanisms to recruit adipose progenitors to proliferate and differentiate.

1.2.2.2 Adipogenesis

The process of AP differentiation towards mature adipocytes (adipogenesis) is very complex and regulated by multiple transcription factors, co-activators and miRNAs (Peirce et al. 2014). The key regulators of adipogenesis are peroxisome proliferator-activated receptor γ (PPARγ) (Spiegelman et al. 1997) and CCAAT/enhancer binding protein family (C/EBP-α, C/EBP-β and C/ EBP-δ) (Rosen et al. 2000), (Hansen & Kristiansen 2006) responsible for triggering and maintenance of the process. Another transcriptional factor that drives expression of genes involved in lipogenesis is sterol regulatory element binding transcription factor 1c (SREBP1c). Additionally, activation of SREBP1c leads to through secretion of lipid ligands directly activating PPARγ (Kim et al. 1998). Some other pathways are playing role in fate determination of APs as bone morphogenetic proteins (BMPs) (Schulz & Tseng 2016), insulin and insulin-like growth factors (IGFs) (Smith et al. 1988), Wnt/β-catenin signaling (Jeon et al. 2016). However most of molecular studies of adipogenesis were performed in cell lines or primary APs and not much known about *in vivo* adipogenesis. The latest study shown contribution of APs in *in vivo* adipogenesis will be discussed in 1.2.3 section.

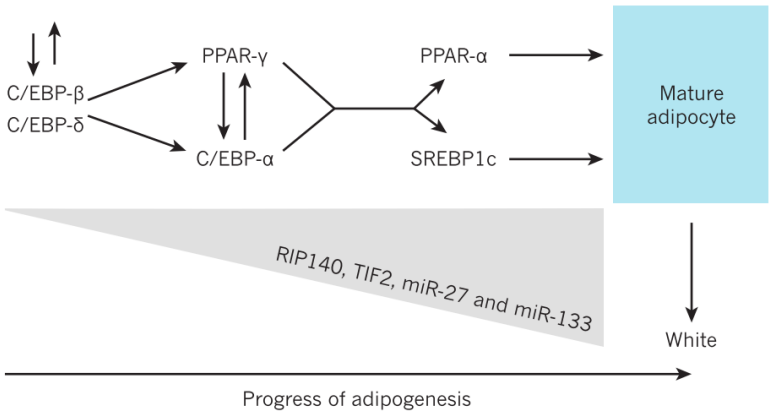

Figure 1.6 Transcriptional regulation of adipocyte differentiation. Adapted from (Peirce et al. 2014)**.**

1.2.2.3 Adipose tissue plasticity decline in adulthood

According to the currently accepted paradigm (Rosen & Spiegelman 2014), (Choe et al. 2016), the number of adipocytes is set during childhood and remains stable through the life. scWAT arise in humans from 12-24 weeks till 28 weeks of embryonic development via increasing number of cells (Poissonnet et al. 1984). In rats, it was shown that primary after birth scWAT fat pad was grown via increased number of cell and then by combination of both hyperplasia and hypertrophy (Knittle & Hirsch 1968). Another independent study showed that adipocyte number is determined (288 individuals from 4th month till 19 years). This study revealed the dynamic process of increasing cell number from birth till 8 years then a 3 times elevation in cell number until 19 years of age on Fig. 1.7 (Knittle et al. 1979). Interestingly, obese children had an increased number of cells already one year after birth.

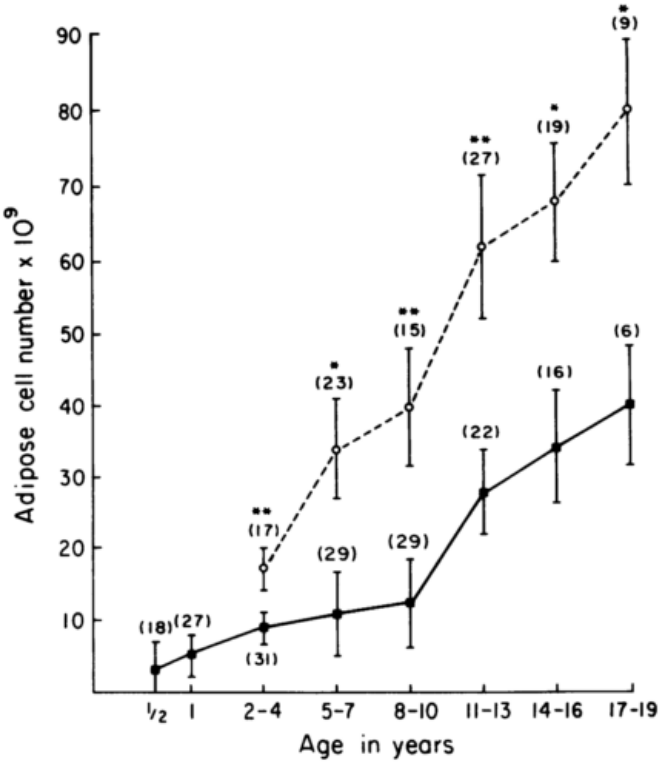

Figure 1.7 Dynamic of scWAT adipocyte number after birth in lean and obese children. Adapted from (Knittle et al. 1979). Obese individuals shown as open circles, lean as black squares. n= number of individuals. Data represented as mean ± SEM, ***,** pV < 0.05; ****,** pV < 0.01; *****,** pV < 0.001; obese vs. lean Student's t test.

Due to difficulties to access vWAT, little is known about cellular dynamic of this fat depot in humans in early age. Several studies were performed on 6 to 18 - year-old children using magnetic resonance (MR) imaging or ultrasound revealed strong correlation between total fat volume/vWAT thickness and obesity (Fox et al. 1993), (Siegel et al. 2007), (Jung et al. 2016). Contribution of hypertrophy vs. hyperplasia during early development of vWAT is still elusive.

Number of adipocytes was not increased upon experimental over/restricted feeding in adult humans (Salans et al. 1971). In this study, metabolically healthy male volunteers were overfed for 3-4 months to gain weight, later they had restricted feeding to lose weight (Salans et al. 1971). Three subcutaneous depots (gluteal, anterior abdominal wall and from triceps) were analyzed to determine adipose tissue cellularity dynamic upon excess/restricted feeding. During the experiment volunteers gained around 10 kg of fat mass, but the number of adipocytes did not change rather only the size of adipocytes was increased. This process was reversible and adipocyte size decreased upon dietary restriction (Salans et al. 1971). A more recent study showed that scWAT from upper-body (abdominal part) increased mass upon overfeeding through hypertrophy, but scWAT from lower-body (femoral part) grow via hyperplasia (Tchoukalova et al. 2010). Both these studies were limited to scWAT depots. The same effect was observed in pigs, in which growth of adipose tissue was achieved by increased size of existing adipocytes, but no changes in cell number per gram of tissue was observed (Mersminn et al. 1975). Stable isotope labeling studies confirmed that the number of adipocytes is set early in life and remain stable during life in mice (Kim et al. 2014) and humans (Spalding et al. 2008). Kim et al. showed adipocyte and SVF cell turnover in adult mice. vWAT had greater rate of adipogenesis comparing to scWAT (1.05% vs. 21.57%). The key point of this study is the age-dependent comparison of adipogenic potential in which the authors came to the conclusion that diet-induced hyperplasia acures only in young mice (4-week old), but not in the adult mice. In this study, 4 or 10-week old male C57Bl/6 mice were fed with high-fat diet for 5 weeks in combination of ^{15}N-thymidine- labeling. An increased % of labeled adipocytes in both vWAT and scWAT was observed only in young mice (Kim et al. 2014). Similar conclusions were achieved in another independent study using isotopes that number of adipocites is set during childhood and early adolescence and remain the same in lean and obese individuals. Even after bariatric surgery and substantial weight loss number of adipocytes remain the same, but size was decreased (Spalding et al. 2008). Interestingly, another group showed that proliferation of APs has time and depot specific dynamics (Jeffery et al. 2015). Employing bromodeoxyuridine (BrdU) to label proliferating cells, it was demonstrated that APs proliferate in response to high-fat diet only during first week and only in vWAT. The human study has shown as well that vWAT growth more dependent on increased cell number, than cell size in mails (Arner et al. 2013). The potential of APs to give rise to mature adipocytes declines with age due to multiple reasons, including the expression of the tumor suppressor as p16Ink4a (Nishino et al. 2008). Since adipose tissue plasticity declines with age, it is important to study molecular mechanism of early adipose tissue growth.

1.2.3 Molecular mechanisms of adipose tissue expansion (systemic and local factors)

1.2.3.1 Overnutrition and rapid fat expansion

Molecular mechanisms of adipose tissue expansion have been long a challenge to be uncovered. In 2015, Rodeheffer at al. (Jeffery et al. 2015) proposed that phosphoinositide 3-kinase (PI3K) - AKT2 pathway is a required element for diet-induced explanation of WAT. In this study, it was shown that APs proliferate upon HFD, with the highest proliferation rate on the 3rd day. They demonstrated that proliferating APs differentiate to mature adipocytes contributing to *in vivo* adipogenesis. To reveal molecular mechanism of APs proliferation they analyzed well known nutrient sensing pathway PI3K-AKT and found that AKT2, but not AKT1, is phosphorylated in response to 3 days of HFD in vWAT APs. Using conditional knockout of *Akt2* crossed with the PdgfRα promoter lacking *Akt2* only in specific population of APs and pharmacological inhibitor of PI3K, they showed that AKT2- pathway is required for vWAT AP activation during HFD feeding. Specifically, mice lacking *Akt2* in specific population of APs - PdgfRα+ cells (PdgfRα-cre; Akt2fl/fl) has no increase in percentage of BrdU labeled (proliferating) cells after one week of high fat diet (HFD) vs. SD (standard diet) when Akt2fl/fl line is showing a similar to wild type phenotype with increased labeling of APs after HFD feeding (Jeffery et al. 2015). This study demonstrates that one particular pathway can influence AP activation upon nutritional challenges and it would be expected that our knowledge about other contributors will grow next years.

1.2.3.2 Role of local inflammation

vWAT contributes to systemic inflammation during obesity via production of pro-inflammatory cytokines affecting liver and inducing insulin resistance (Girard & Lafontan 2008). However, until recently, little was known about local molecular events leading to AP recruitment and differentiation *in vivo*. In 2013, Granneman et al. (Lee et al. 2013) demonstrated the importance of immune cells creating a special signaling environment for APs to proliferate and differentiate. The chain of cellular and molecular events was elegantly untangled: b3-adrenergic receptor stimulation or HFD feeding or physical injury involves the death of mature adipocytes that are cleared by immune cells as M2-polarized macrophages. Proliferating EdU-labeled APs are located in places with are clusters of immune cells (F4/80+ macrophages) so-called crown-like structures (CLS). Macrophages expressing osteopontin, receptors to which are present on PDGFRa+ progenitors, which in turn are recruited to side of clearance of dying mature adipocyte (Lee et al. 2013). Other research groups also demonstrated contribution of local inflammation to adipose tissue remodeling. Adipogenesis *in vivo* can be induced by local injection of lipopolysaccharides (LPS) into fat pad (Wernstedt Asterholm et al. 2014). In the same study, it was shown that knocking out of

some pro-inflammatory cytokines, specifically in adipose tissue, leads to adipose tissue dysfunction and metabolic disorders (Wernstedt Asterholm et al. 2014). It was also reported that activation of type 2 innate lymphoid cells (ILC2s) is sufficient to induce proliferation and differentiation of bipotential APs, which can give rise to beige fat *in vivo* (M.-W. Lee et al. 2014). This data indicates that immune signals can affect expansion and functional property of adipose tissue.

1.2.3.3 Role of sympathetic nervous system innervation

Sympathetic nervous system (SNS) is involved into regulation of blood flow and fatty acids metabolism in WAT (Y.-H. Lee et al. 2014). It was shown that sympathetic denervation leads to increased number of fat cells (Bowers et al. 2004), (Foster & Bartness 2006). It was proposed that increased sympathetic innervation leading to increased norepinephrine (NE) release and that could inhibit proliferation of cell in fat pat in depot specific manure (Foster & Bartness 2006). This data in line with *in vitro* work when it was shown that NE can inhibit proliferation of progenitors (Lin & Scott 2012).

1.2.3.4 Gut microbiota

Luck has shown that altered due to high-fat diet feeding immunity in the intestine causes increased gut permeability. Followed by leaking bacterial and dietary components increased systemic inflammation leads to insulin resistance (Luck et al. 2015). Recently another mechanism was proposed by Perry and colleagues. They found that altered gut microbiota produce increased amount of acetate which activates parasympathetic nerve system promoting glucose-stimulated insulin secretion, hyperphagia and obesity (Perry et al. 2016). Resent progress in sequencing allowed to identify specific bacterial spices which were driven by HFD feeding and associated with obesity (Heo et al. 2016).

1.2.3.5 Role of insulin-like growth factor 1

Recently it was postulated in several reviews that insulin-like growth factor 1 (IGF-1) is a crucial factor in pre-adipocyte proliferation, differentiation and survival (Garten et al. 2012) and it contributes to development of obesity (Berryman et al. 2013), (Kreitschmann-Andermahr et al. 2010). Also it was reported that IGF-1 stimulates proliferation of cancer cell lines (Davison et al. 2011), proliferation and adipogenic differentiation of human MSCs (Scavo et al. 2004). IGF-1 seems to play important role in adipocyte differentiation of 3T3-L1 (Smith et al. 1988). Recently importance of AKT2-signaling pathway in induction of AP proliferation were shown (Jeffery et al. 2015) which can be mediated through IGF-1. However direct prove of contribution of IGF-1 in *in vivo* adipogenesis was not available.

1.3 Aims of the project

This project aimed to understand how systemic and local factors can affect the fate of adipose tissue progenitors and contribute to adipose tissue growth. Since it has been shown that the number of adipocytes is set during childhood and plasticity of adipose tissue progenitors decline with age, we focused our efforts on investigating dietary models of early childhood obesity. The specific objectives were:

1 To develop and characterize a diet-induced model of childhood obesity;

2 To demonstrate mechanisms by with adipose tissue growth achieved in the developed model;

3 To study contributions of adipose tissue progenitors to adipose tissue growth;

4 To evaluate systemic factors potentially involved in adipose tissue growth;

5 To identify novel genes that could play a role in adipose tissue remodeling;

6 To describe gene networks regulating adipose tissue remodeling upon dietary challenges;

7 To develop an *in vitro* system for functional investigation of candidate factors that control the fate and activation of the APs using high content automated microscopy screening;

8 To validate several candidate factors involved to adipose tissue remodeling using the *in vitro* system;

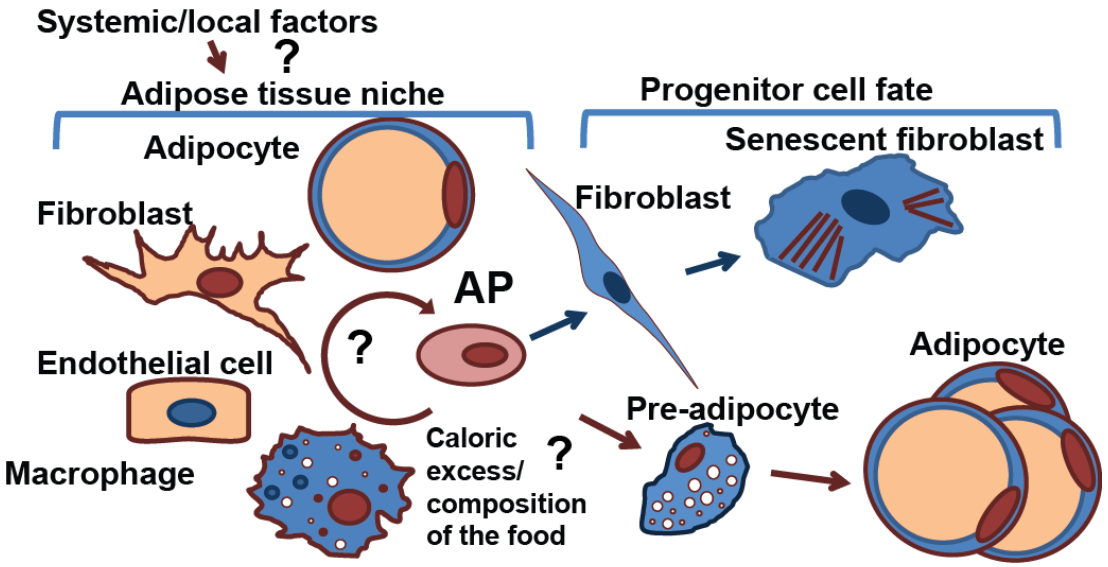

Figure 1.8 Aim of the study. Adipose progenitors (APs) are known to contribute to *in vivo* adipogenesis. However little is known about systemic and local factors regulating behavior and fate of APs inside of adipose tissue niche.

2. RESULTS

2.1 Diets high in fat lead to rapid growth of adipose tissue

2.1.1 The long-term effects of high-fat diet feeding in a model of early onset obesity

In order to investigate cellular and molecular mechanisms that lead to white adipose tissue (WAT) remodeling, a diet-induced obesity model in mice before sexual maturation had to be established. Although high-fat diet (HFD) feeding is a well-established model of diet-induced obesity in rodents (Buettner et al. 2006), there was lack of information on the effect of HFD feeding in early age on WAT growth and developing of childhood obesity. Most of the studies conducted to date have used male mice shortly after sexual maturation (5-6 week-old) (Jeffery et al. 2015), (Rabot et al. 2016). Additionally, the intake of sugar-sweetened beverages has increased dramatically among school-aged children over the past years and became the top calorie source (Lasater et al. 2011), which could be one of the main factors contributing to the increased incidence of obesity amongst teenagers. It was demonstrated that diet-induced proliferation occurs in both fat depots, inguinal and perigonadal WAT (ingWAT and gWAT, respectively) in young male mice (Kim et al. 2014), but it was not investigated in sexually immature female mice. In order to find a combination of diet and sugary drink, which would efficiently stimulate obesity in early age, 40 female 3-week-old pups were weaned and randomized between 4 groups with different diets: control diet (CD) with water vs. high-fat diet with water (HFD, 60% of fat), CD with sucrose/fructose solution (S/F) vs. HFD with S/F. Diets were applied for 15 weeks. For the first 5 weeks, low concentration of S/F was applied to acclimatize mice to sweet drinks and, for the remaining 10 weeks, concentration was increased (see methods section 4.1.2). Body weight dynamic, body composition and food/drink intake were measured weekly as shown in Figure 2.1 – A. Food intake was measured during the first 8 weeks and, as expected, HFD groups consumed significantly more calories than CD groups (Appendix Fig. 1 – A, B). Mice drinking S/F in combination with HFD consumed more calories as compared with HFD group drinking water. Interestingly, there was no significant difference between the groups drinking water and S/F under CD (Appendix Fig. 1 – A, B). As expected, mice under HFD had higher body weight and accumulated fat mass more rapidly compared with CD (Fig. 2.1 – B, C, and D). However, S/F had no additional effect on body and fat mass growth in any time point measured in this experiment (Fig. 2.1 – B, C, and D). Nevertheless, S/F seemed to trigger an increase of lean mass after week 11, when compared in CD group (Appendix Fig. 1 – C). Blood glucose level is well-regulated by hormone systems. Insulin decreases level of glucose whereas another hormones as glucagon, cortisol and

catecholamines increase blood glucose. There are several methods to challenge endocrine system which allow to reveal altered metabolic condition as hyperglycemia/ hypoglycemia. The most commonly used is analysis of glucose level after long fasting (16h). To analyze diet-dependent effects on blood glucose regulation, fasting blood glucose level was measured after 12 weeks of diet. HFD leads to increased fasting glucose levels, whereas S/F solution intake had no effect (Fig. 2.1 – E). Another method is to observe time-course clearance of glucose after injection of glucose solution - glucose tolerance tests (GTT). Insulin tolerance test (ITT) is time course analysis of blood glucose level after injection of insulin. Glucose tolerance test (GTT) and insulin tolerance test (ITT) also revealed increased levels of glucose in both HFD groups independently of S/F solution (Appendix Fig. 1– D, E). All mice were euthanized after 15 weeks of diet, organs were weighed, and collected for gene expression and histological analysis. Significant increase was observed in tissue weight from 3 different adipose depots after HFD compared with CD (Fig. 2.1 – E and Appendix Fig. 2). The gWAT was 6-fold heavier after HFD as compared with CD (2.97 +/- 0.1g vs. 0.53 +/- 0.04 g) (Fig. 2.1 – E). Similarly, a 4-fold increase in the weight of ingWAT was observed (1.82 +/- 0.21g vs. 0.4 +/- 0.01g; Appendix Fig. 2 – A). Interscapular brown adipose tissue (isBAT) was 2 times heavier after HFD compared to CD (0.163 +/- 0.013 g vs. 0.08 +/- 0.0008 g) (Appendix Fig. 2 – B). S/F showed no additive effect for all three adipose tissue depots. In contrast, liver weight was affected by S/F treatment in CD group (1.236 +/- 0.16 g vs. 1.594 +/- 0.4 g), which can contribute to changed lean mass (Appendix Fig. 2 – C). Gastrocnemius (Gc) muscles were not affected by neither diet nor S/F treatment (Appendix Fig. 2 – D).

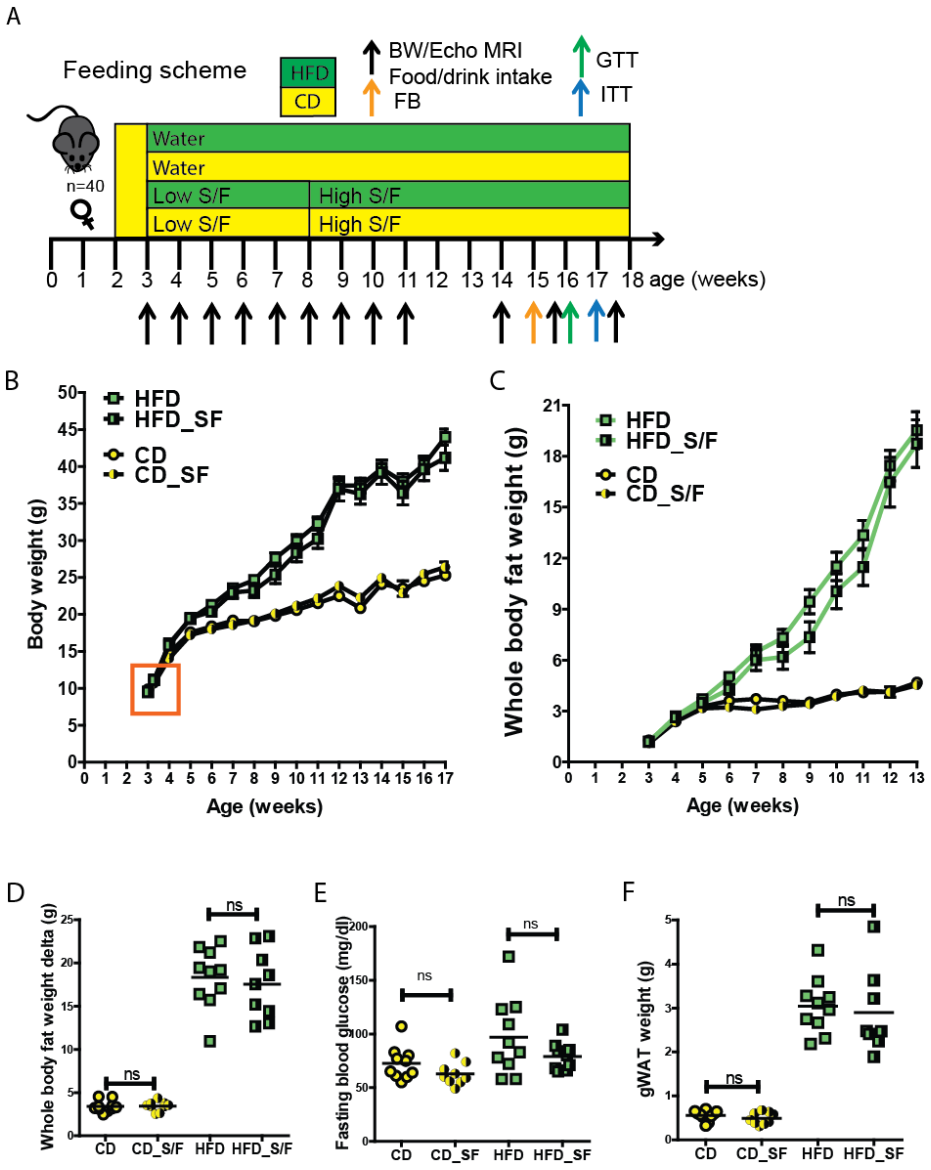

Figure 2.1: Long-term effects of high-fat diet and sucrose/fructose in early onset obesity. A) Scheme of animal experiment; 40 two-week old female C57BL/6NCrl mice were acclimatized on control diet (CD) for one week and then fed with 4 different diets: CD with water, high-fat diet with water (HFD, 60% of fat), CD with sucrose/fructose solution (S/F) and HFD with S/F. Diets were applied for 15 weeks. For the first 5 weeks, low concentration of S/F (18.9/23.1 g/l) was applied to acclimatize mice to sweet drinks and for the remaining 10 weeks concentration was increased (94.5/115.5 g/l). During the course of experiment food/drink intake, body weight and body composition were measured weekly. Fasting blood glucose (FB), glucose tolerance test (GTT), insulin tolerance test (ITT) were measured in different time points indicated by arrows. **B)** Weekly body weight dynamic, data represented as mean ± SEM. Area in orange, one week (7 days) is the first time point for significant weight gain in HFD in comparison to CD. **C)** Weekly whole body fat mass (by EchoMRI), data represented as mean ± SEM. **D)** Delta of whole body fat mass in the end of experiment. **E)** Fasting blood glucose (after 16 hours of fasting) on 12 week after start of diets. **F)** Perigonadal WAT (gWAT) weight at the end of experiment. For D, E and F each dot represented individual mouse, line is mean of the group, two-way Anova with Bonferroni post-hoc test was used to assess significance, ns, no statistically significant difference.

In conclusion, long-term HFD caused severe obesity with elevated fasting glucose level and impaired glucose clearances occurring during development of type 2 diabetes mellitus (T2DM). S/F treatment did not affect fat mass accumulation during the course of experiment and thus it will not be part of this model for WAT accumulation. The main observation contributing to the next step of the project was the significant increase in body weight upon HFD, which was achieved already after one week of treatment (Figure 2. 2). This indicated rapid early growth upon HFD in young age and determined the one week as the shortest period of treatment leading to a significant body weight increased. Successfully established model of HFD-induced obesity directly after weaning provided us a model for studying WAT remodeling during development of childhood obesity.

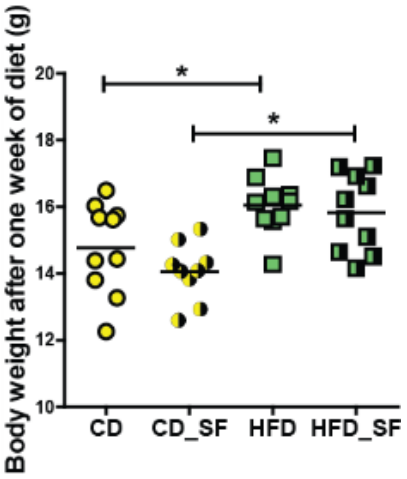

Figure 2.2: Body weight comparison after one-week diet. Each dot represents individual mouse, line is mean of the group, two-way Anova with Bonferroni post-hoc test was used to assess significance, *, pV< 0.05.

2.1.2 Acute high-fat diet leads to adipose tissue growth via increased number of adipose tissue progenitor cells in sexually immature mice

The data in section 2.1.1 showed that HFD feeding leads to a significant increase in body weight of sexually immature female mice after one week. The next question was to discriminate which cell types are contributing to this increase in fat mass. In order to study early adipose tissue accumulation and remodeling, 42 three-week old female C57BL/6NCrl mice were fed with HFD or CD for one week as shown on Fig. 2.3 – A. Mice from the HFD-fed group were consuming significantly more calories every day (Fig. 2.3 – B). After 2 and 7 days upon diet, mice were euthanized, organs weighted and tissues collected for RNA and histological analysis. We found significant increases in body weight (Fig. 2.3 – C, D), gWAT (Fig. 2.3 – E) and ingWAT (Fig. 2.3 – F) after 7 days of HFD, but not after 2 days (Appendix Fig. 3 – A, B, C). This confirmed that one week of HFD feeding leads to significant increased body weight in sexually

immature female mice. Furthermore, this increase was due to acute fat mass accumulation in both gWAT and ingWAT (Fig. 2.3 – E, F). This rapid accumulation of WAT served as an experimental model to investigate mechanisms of WAT remodeling.

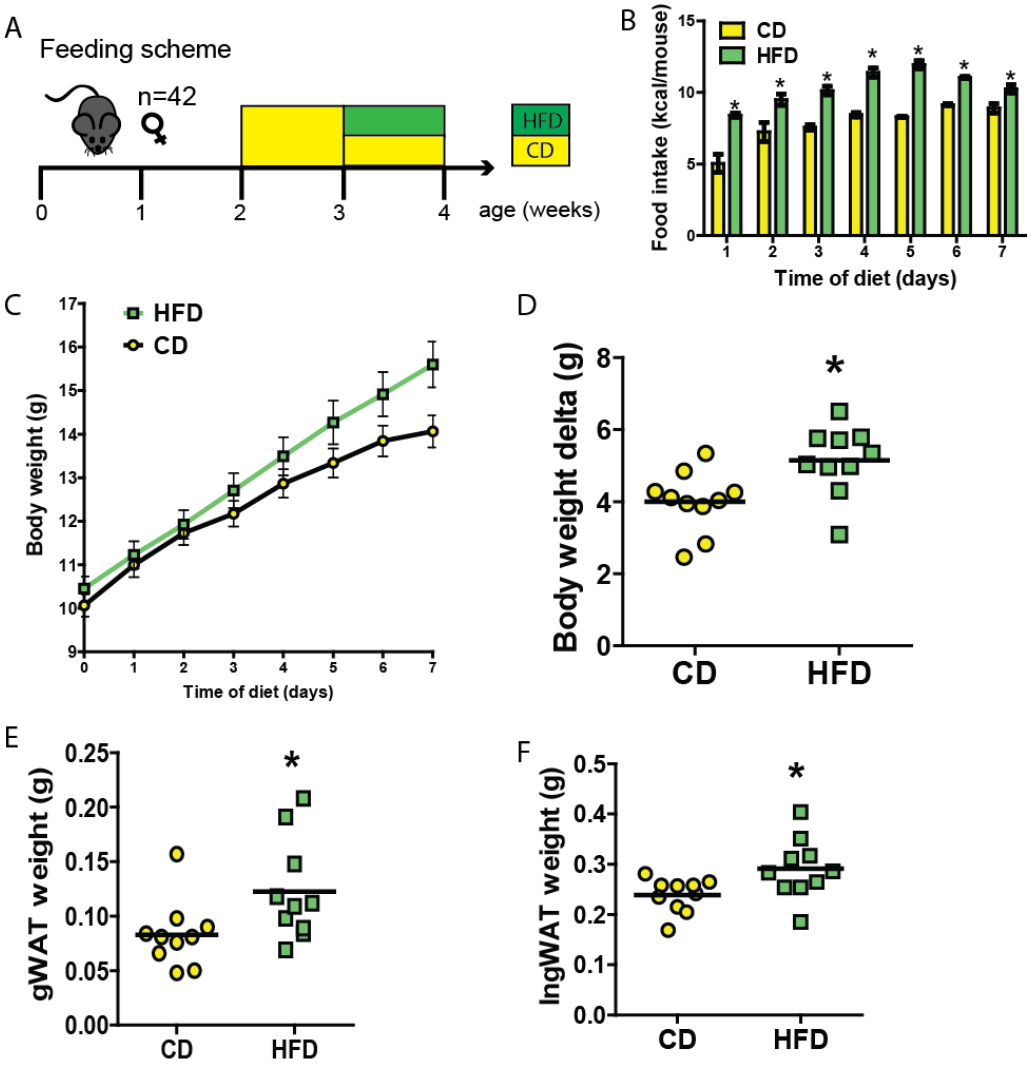

Figure 2.3: Fat accumulation and adipose tissue growth on one week of high-fat diet. A) Scheme of animal experiment; 42 two-week old female C57BL/6NCrl mice were acclimatized on control diet (CD) for one week and then fed with high-fat (HFD) or CD for one week. **B)** Daily food intake (kcal/mouse) was measured from 4 cages per group (n= 5-6 mice per cage), data represented as mean ± SEM, two-way Anova for repeated measurements was used to assess significance, *, pV< 0.05. **C)** Daily body weight dynamic, data represented as mean ± SEM. **D)** Body mass gain between day 0 and day 7 (delta). **E)** Perigonadal WAT (gWAT) weight in day 7. **F)** inguinal WAT (IngWAT) weight in day 7. For D, E and F each dot represents individual mouse, line is mean of the group, Mann-Whitney t- test was used to assess significance, *, pV< 0.05.

To investigate cellular mechanisms contributing to rapid WAT growth, the main constituents of WAT were analyzed: mature adipocytes by microscopic sections (gWAT) and the stroma vascular fraction (SVF) by cell counting (Fig. 2.4 – A-H). A shift in the frequency distribution of lipid droplets area was observed in gWAT after 7 days of HFD (Fig. 2.4 – B). Bigger lipid droplets were more frequent in HFD samples compared to CD, indicating adipocyte

hypertrophy. Adipocyte diameter (Fig. 2.4 – D) and volume (Fig. 2.4 – E) were increased following HFD; however the total number of adipocytes in the whole depot remained the same between diets (Fig. 2.4 – F). These data showed that, upon one week of HFD feeding, mature adipocytes increased their size by lipid filling, rather than by cell proliferation. To investigate the effect of HFD on the stromal component of adipose tissue, the number of cells from the gWAT SVF was counted. After one week of HFD, an increased number of SVF cells per gram of gWAT (Fig. 2.4 – G) and per mouse (Fig. 2.4 – H) was observed, indicating tissue hyperplasia. These data suggested that one week of HFD feeding leads to rapid WAT growth via 2 independent mechanisms: increased number of SVF cells and hypertrophy of existing mature adipocytes.

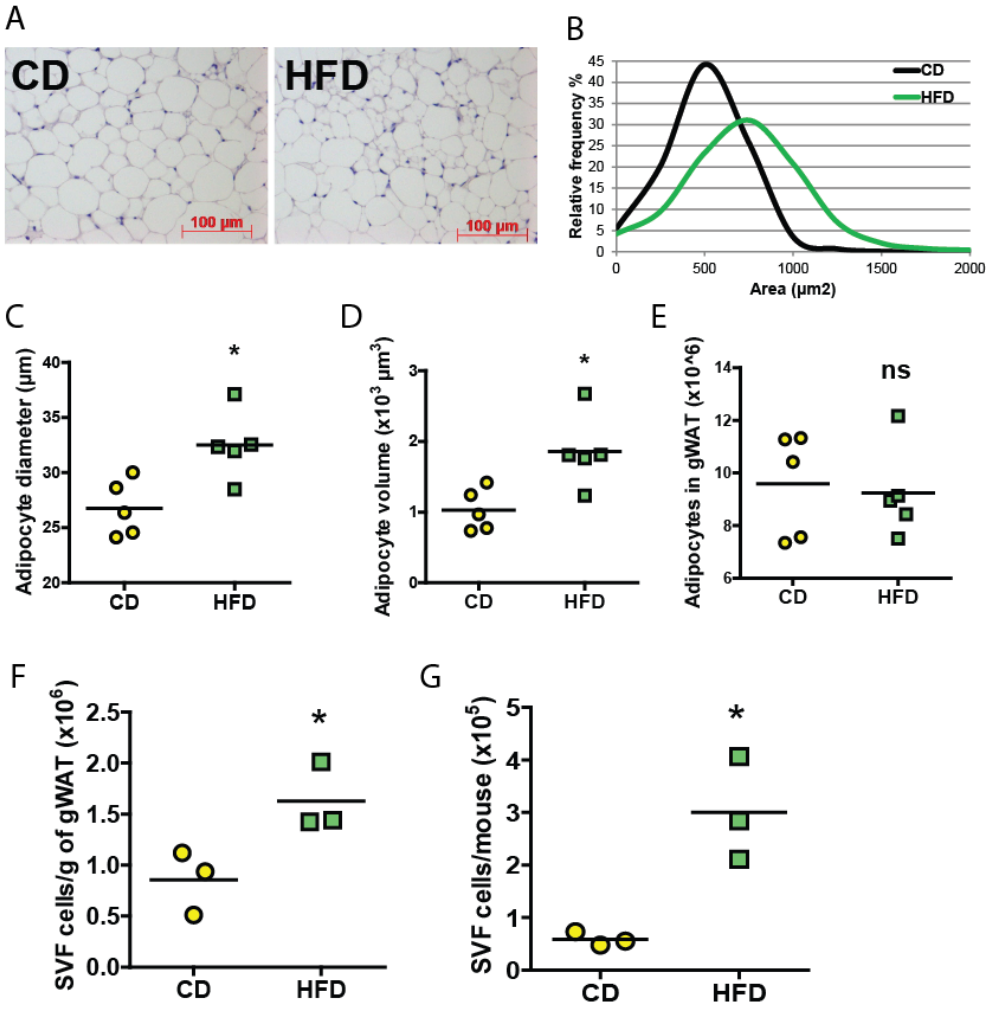

Figure 2.4: Mechanisms of early adipose tissue growth: contribution of hyperplasia and hypertrophy. A) Histological analysis of perigonadal WAT (gWAT) of sexually immature female mice after one week of CD and HFD, scale bar, 100 µm. **B)** Relative frequency distribution of lipid droplets area (μm^2) based on histological slides from A. **C)** Adipocyte diameter (µm). **D)** Adipocyte volume (x10 μm^3). **E)** Absolute number of mature adipocytes in gWAT. For B, C, D and E 5 mice per group were used, 3 pictures per mouse were acquired, each dot represents individual mouse. **F)** Stroma vascular fraction (SVF) cell count obtained after one week of CD vs. HFD normalized per gram of gWAT. **G)** SVF cell count obtained after one week of CD vs. HFD calculated per one mouse. For F and G each dot represents pooled sample from 3-6 mice. For C-G line is mean of the group, Mann Whitney t-test was used to assess significance, *, pV< 0.05; ns, no statistically significant difference.

The SVF is non-homogeneous, consisting of many different cell types such as endothelial cells (CD31+), immune cells (CD45+) and adipose tissue progenitor cells (Sca-1+). To investigate the contribution of different cell subpopulations to the proliferation of SVF cells upon HFD, after 1-week of HFD gWAT was digested and cells were sorted. To estimate number of cells per gram of tissue and absolute number per mouse, gWAT was weighted and number of SVF cells was counted after digestion. An increased number of Sca-1+ cells per gram of gWAT (Fig. 2.5 – A) and per mouse (Fig. 2.5 – B) was observed. The number of CD31+ cells per gram of gWAT was not different between diets (Fig. 2.5 – C). However, when calculated per mouse, the number of CD31+ cells was higher upon HFD (Fig. 2.5 – D). The number of CD45+ cells was increased per gram of gWAT (Fig. 2.5 – E) and per mouse upon HFD (Fig. 2.5 – F). Additionally, no changes in the number of CD34^{low} cells (potentially an important cell type for adipose tissue fibrosis) per gram of gWAT were observed (Fig. 2.5 – G). Nevertheless, there is an increase in the total number per mouse upon HFD (Fig. 2.5 – H). These data indicated that number of Sca-1+ APs and CD45+ cells per gram of gWAT/ per mouse has increased, which contributes to increase WAT mass during growth. Additionally, we observed increased total number of potentially profibrotic CD34 ^{low} and endothelial cells, which are also contributing to the WAT remodeling.

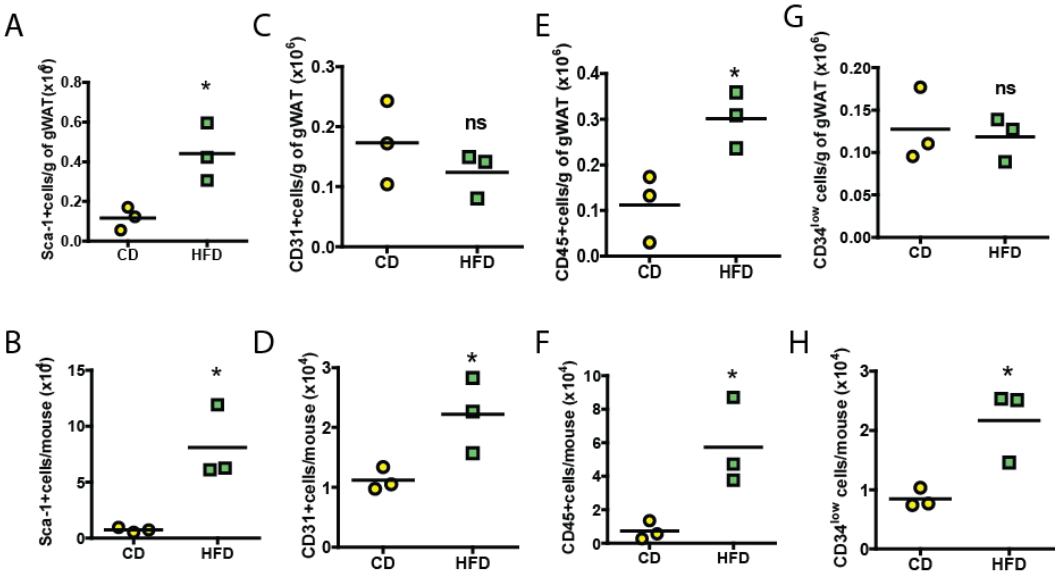

Figure 2.5: Contribution of different cell subpopulations to perigonadal WAT (gWAT) increased cell number upon one week of HFD. First replicate with 25 and second with 60 two-week old female C57BL/6NCrl mice were acclimatized on control diet (CD) for one week and then fed with high-fat (HFD) or CD for one week. FACS was performed on SVF cells from gWAT. **A)** Number of Sca-1+ cell per gram of gWAT. **B)** Absolut number of Sca-1+ cell per mouse. **C)** Number of CD31+ endothelial cell per gram of gWAT. **D)** Absolut number of CD31+ endothelial cell per mouse. **E)** Number of CD45+ hematopoietic cell per gram of gWAT. **F)** Absolut number of CD45+ hematopoietic cell per mouse. **G)** Number of CD34^{low} cell per gram of gWAT. **H)** Absolut number of CD34^{low} cell per mouse. For A-H each dot represents pooled sample from 3-6 mice, line is mean of the group, Mann Whitney t-test was used to assess significance, *, pV< 0.05, ns, no statistically significant difference.

To compare adipose tissue plasticity in early age and adulthood, 27-week old mice were fed with CD and HFD as previously described for young mice (Fig. 2.6 – A). The HFD group consumed daily more calories and gained significantly more weight compared with CD (Fig. 2.6 – B, C, and D). However the weight of two WAT depots did not change between feeding groups (Fig. 2.6 – E, F).

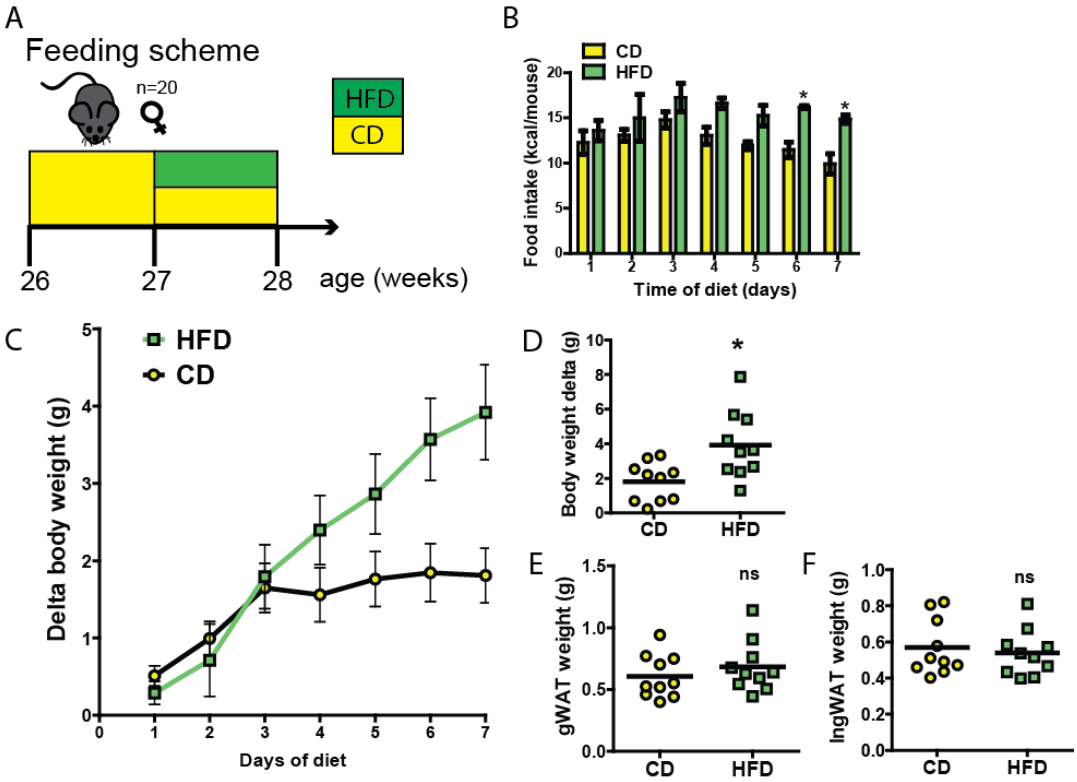

Figure 2.6: Absence of rapid adipose tissue gain in adult mice. A) Scheme of animal experiment: 20 female 26-week-old female C57BL/6NCrl mice were acclimatized on control diet (CD) for one week and then fed with high-fat (HFD) or CD for one week. **B)** Daily food intake (kcal/mouse) from 2 cages per group (5 mice per cage); t-test inside of each time point was used. **C)** Daily delta of body weight, data represented as mean ± SEM. **D)** Delta body weight in the end of experiment. **E)** Weight of perigonadal WAT (gWAT). **F)** Weight of inguinal WAT (ingWAT). For D, E and F every dot represents individual mouse, line is mean of the group, Mann Whitney t-test was used to assess significance, *, pV< 0.05, ns, no statistically significant difference.

To investigate cellular mechanisms contributing to adipose tissue growth in adult mice in our dietary setup, we used histological analysis of gWAT sections (Fig. 2.7 – A). We did not observe changes in lipid droplet area frequency distribution after one week of HFD (Fig. 2.7 – B). Additionally, the number of SVF was not increased upon one week of HFD in adult mice (Fig. 2.7 – C). There is a trend for decrease number of SVF cells per gram of gWAT (Fig. 2.7 – C), but not per mouse (Fig. 2.7 – D). Decreased numbers of SVF cells suggested to us that APs may be leaving the progenitor pool and differentiating into mature adipocytes.

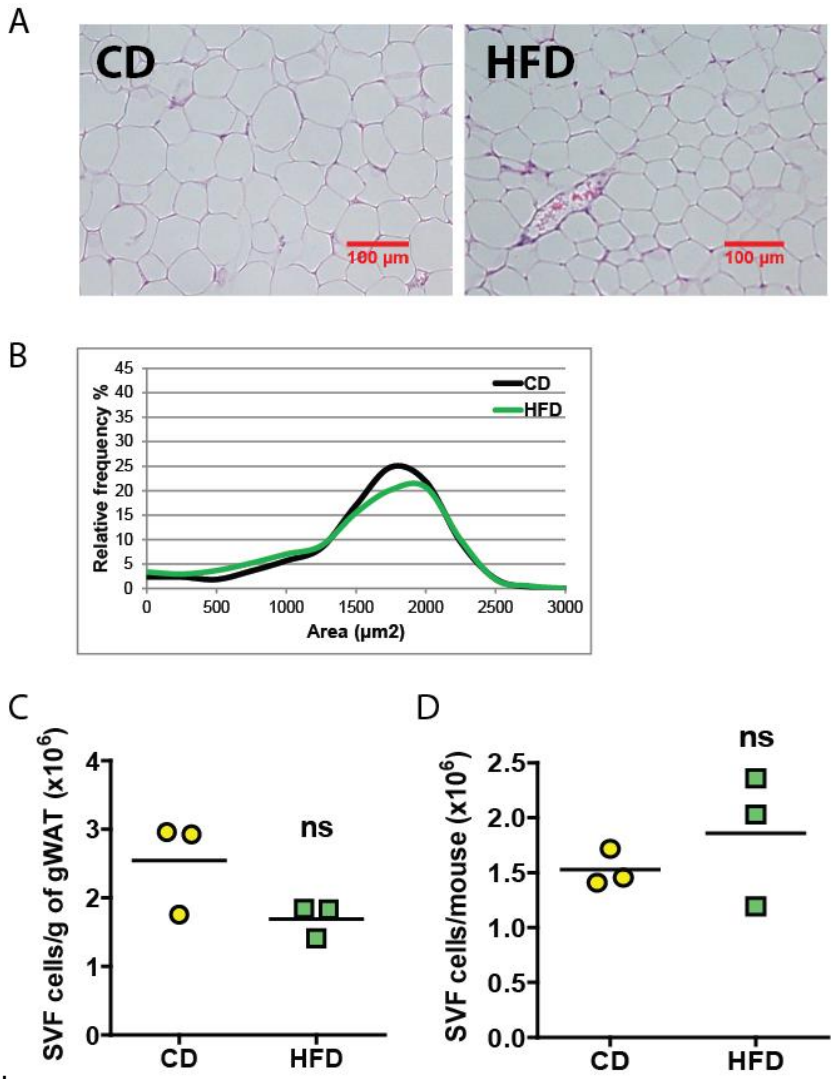

Figure 2.7: Absence of adipocyte hypertrophy or hyperplasia upon one week of HFD in adult mice. Female 26-week-old C57BL/6NCrl mice were acclimatized on control diet (CD) for one week and then fed with high-fat (HFD) or CD for one week. **A)** Histological analysis of perigonadal WAT (gWAT) after one week of CD and HFD in adult mice, scale bar, 100 µm. **B)** Relative frequency distribution of lipid droplets area (μm^2) based on histological slides from A, 6 mice were used per group (3 images per mouse). **C)** Stroma vascular fraction (SVF) cell count obtained from gWAT of adult mice after one week of CD vs. HFD normalized per gram of gWAT. **D)** Absolute number of SVF cells per mouse. For C and D each dot represents pooled sample from 3-5 mice, line is mean of the group, Mann Whitney t-test was used to assess significance, ns, no statistically significant difference.

To further analyze the effect of HFD in cell populations we performed FACS for adult mice fed with HFD for one week. There were no significant difference between feeding groups for the number of Sca-1+ cell per gram of gWAT (Fig. 2.8 – A) or per mouse (Fig. 2.8 – B). The number of CD31+ endothelial cells per gram of gWAT was significantly decreased (Fig. 2.8 – C), but not per mouse (Fig. 2.8 – D). Number of CD45+ cells per gram of gWAT was not affected by diets (Fig. 2.8 – E, F). There was significantly less $CD34^{low}$ cells per gram of gWAT (Fig. 2.8 – G), but not per mouse (Fig. 2.8 – H).

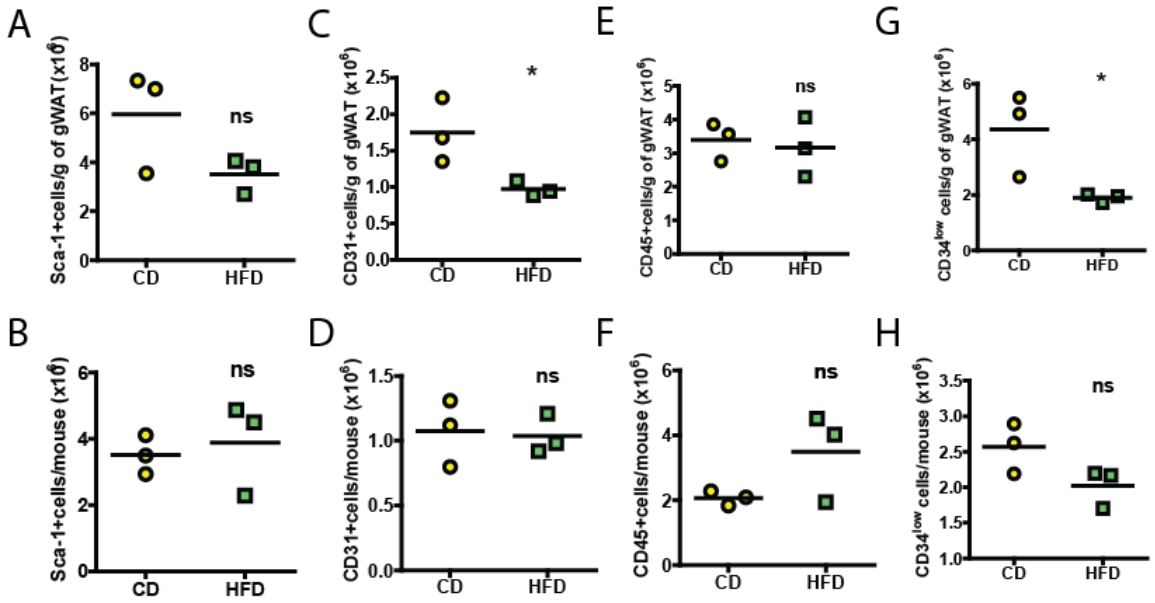

Figure 2.8: Contribution of different cell subpopulations to perigonadal WAT (gWAT) cell number upon one week of HFD in adult mice. Female 28-week-old C57BL/6NCrl mice were acclimatized on control diet (CD) for one week and then fed with high-fat (HFD) or CD for one week. FACS was performed on SVF cells from gWAT. **A)** Number of Sca-1+ cell per gram of gWAT. **B)** Absolut number of Sca-1+ cell per mouse. **C)** Number of CD31+ endothelial cell per gram of gWAT. **D)** Absolut number of CD31+ endothelial cell per mouse. E) Number of CD45+ hematopoietic cell per gram of gWAT. **F)** Absolut number of CD45+ hematopoietic cell per mouse. **G)** Number of $CD34^{low}$ cell per gram of gWAT. **H)** Absolut number of $CD34^{low}$ cell per mouse. For A-H each dot represents pooled sample from 3-5 mice, line is mean of the group, one-way Anova with Tukey's post-hoc test was used to assess significance, *, pV< 0.05, ns, no statistically significant difference.

Our data demonstrated that HFD increases body weight and fat mass via an increase in the number of Sca-1+ APs after one week of feeding in sexually immature female mice, but not adult female mice. These data open questions for a following study about the exact mechanism driving AP proliferation and the early remodeling of WAT.

2.1.3 Fat content in the food induces adipose tissue progenitor cell proliferation

In this work, we have shown that one week of HFD feeding of sexually immature female mice leads to gWAT accumulation and increased number of Sca-1+ APs. However, since CD and HFD have a different composition of macronutrients and animals were fed *ad libitum*, there were two factors that could play a role in our observations: the delta in calorie consumption among the groups and/or different food composition. To investigate the independent effect of these two factors, 40 three-week old female mice were fed either with CD, high protein diet (HPD), HFD *ad libitum* and one group was fed with restricted HFD (HFD-R) for 7 days. HFD-R and HPD groups received the same number of calories as CD, but the macronutrient composition was different (see methods section 4.1.2). Using this approach, we had 3 groups enriched with different macronutrients (CD with carbohydrates, HPD with proteins and HFD-R with fat) and the same energy intake from them. The comparison between HFD with HFD-R would allow us to observe the role of higher calorie consumption on adipose tissue growth but

under the same diet. Previous works have reported that the CD used is actually enriched in simple carbohydrates (sucrose) and can have an effect on experiments/gene expression at least in intestine and liver (Wang et al. 2009). Therefore, HPD served as an additional control, since it has the same amount of fat as CD but enriched proteins instead of carbohydrates. Scheme of animal experiment is shown in Fig. 2.9 – A. Energy intake was elevated in HFD compared to CD, HPD and HFD-R (Fig. 2.9 – B). During 1 week upon HFD, mice gained significantly more body weight (Fig. 2.9 – C, D), gWAT (Fig. 2.9 – E) and ingWAT (Fig. 2.9 – F) weight than all other groups. These data suggested that new dietary scheme worked accordingly our experimental design and allowed using well-controlled feeding groups for investigation WAT remodeling process.

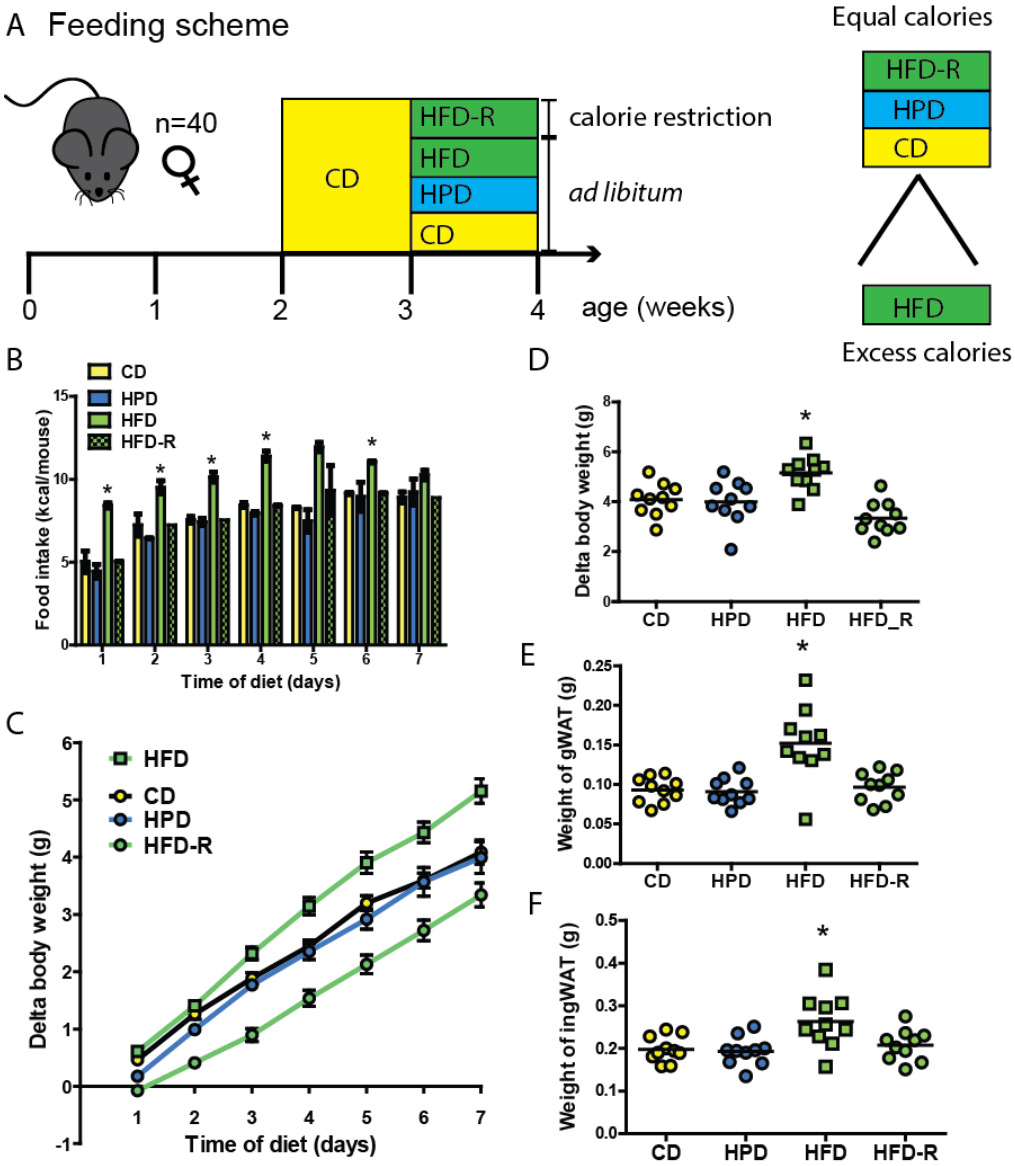

Figure 2.9: Contribution of diet composition to weight gain. Excess calories but not food composition, induces body and adipose tissue weight gain in sexually immature mice. **A)** Scheme of animal experiment: 40 two-week old female C57BL/6NCrl mice were acclimatized on control diet (CD) for one week and then fed with CD or high-protein diet (HPD), high-fat diet (HFD) or restricted HFD (HFD-R)

for one week. CD, HPD and HFD-R received equal calorie amounts, while HFD consumed significantly more calories. **B)** Daily food intake from 2 cages per group (5 mice per cage), data represented as mean ± SD, two-way Anova for repeated measurements was used to assess significance, *, pV< 0.05. **C)** Daily body weight increase during one week of different diets, data represented as mean ± SEM. **D)** Delta of body mass after 7 days of diets. **E)** Weight of perigonadal WAT (gWAT). **F)** Weight of inguinal WAT (ingWAT). For D, E and F every dot represents individual mouse, line is mean of the group, one-way Anova with Tukey's post-hoc test was used to assess significance, *, pV< 0.05.

First we investigated histology of gWAT (Fig. 2.10 – A) to estimate mature adipocyte size by measuring area of lipid droplets. In accordance with the previous experiment (see section 2.1.2), bigger lipid droplets were observed upon HFD, when compared to all other groups (Fig. 2.10 – B). These data indicated that, on the tissue level, only HFD *ad libitum* leads to hypertrophy of mature adipocytes.

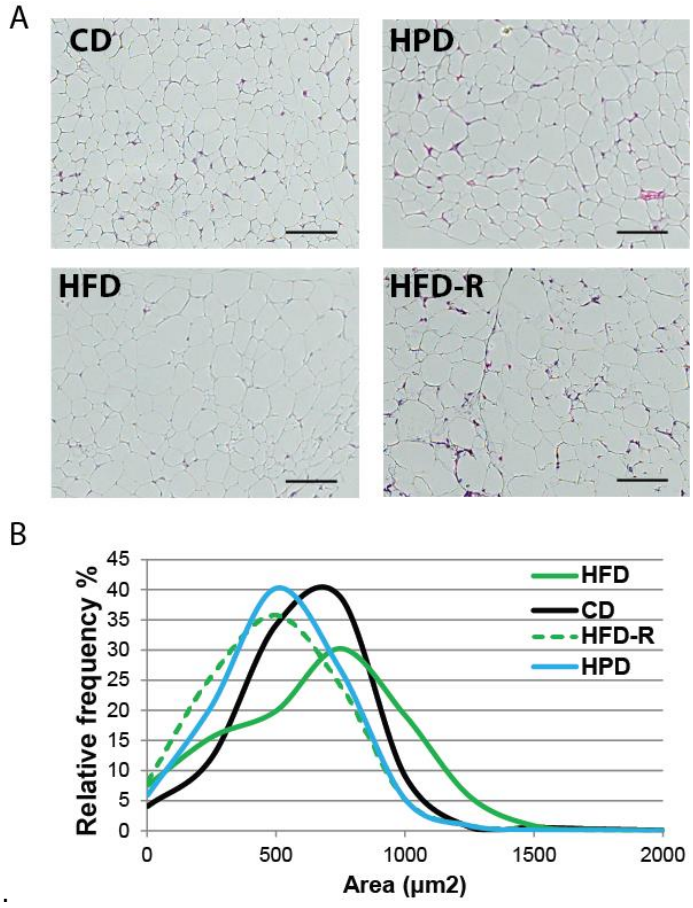

Figure 2.10: One week of high-fat diet (HFD) leads to mature adipocyte hypertrophy but not in isocaloric to control diet amount (HFD-R). Two-week old female C57BL/6NCrl mice were acclimatized on control diet (CD) for one week and then fed with CD or high-protein diet (HPD), high-fat diet (HFD) or restricted HFD (HFD-R) for one week. Then histological analysis of perigonadal WAT (gWAT) was performed. **A)** Histological analysis of gWAT after one week of CD, HPD, HFD and HFD-R, 6 mice were used per group (3 images per mouse), scale bar, 100 µm. **B)** Relative frequency distribution of lipid droplets area (μm^2) based on histological cuts.

The next question was how different macronutrients directly affect proliferation of SVF cells. To investigate this, 3-week old female mice were fed with CD and HFD *ad libitum* and

HFD-R. To identify the proliferating subpopulations, 5-ethynyl-2'-deoxyuridine (EdU) was applied in drinking water for one week during the diet challenges as on Fig. 2.11 – A. After one week, mice were euthanized; gWAT and ingWAT were dissected, weighted and digested. Erythrocytes were depleted and SVF cells were counted, stained and FACS was performed. HFD *ad libitum* increased percentage and amount of Sca-1+ EdU+ APs per gram of tissue in both fat pats, when compared to CD (Fig. 2.11 – B, C, D, and E). Although mice from HFD-R group received the same number of calories as CD group, there was significantly higher percentage of Sca-1+ EdU+ APs for both fat depots (Fig. 2.11 – B, D). In gWAT, the number of Sca-1+ EdU+ APs per gram of tissue was increased upon HFD-R in comparison to CD (Fig. 2.11 – C). In ingWAT, no significant changes were observed (Fig. 2.11 – E). Additionally, when HFD compared with HFD-R we observed an increased percentage of Sca-1+ EdU+ APs in gWAT, but not in ingWAT (Fig. 2.11 – B, D). The number of Sca-1+ EdU+ APs per gram of tissue was not changed upon HFD when compared with HFD-R in both fat depots (Fig. 2.11 – C, E). This data indicated that dietary fat content can stimulate proliferation of APs independent of calorie load.

Although there was no significant effect of diets on the percentage of parent of CD31+ EdU+ cells in gWAT and ingWAT (Fig. 2.12 – A, C), we noticed a trend toward decreases numbers of CD31+ cells per gram of tissue upon HFD. In gWAT only in comparison of HFD-R with CD was significant (Fig. 2.12 – B), but in ingWAT both HFD and HFD-R lead to a significant decrease in the number of CD31+ EdU+ cells compared to CD group (Fig. 2.12 – D). These data indicated that fat content in the food is capable to negatively regulate endothelial cell proliferation. There were no significant differences between dietary groups on the amount of CD45+ EdU+ cells in both fat pats (Fig. 2.12 – E, G). We noticed significant increases in the number of CD45+ EdU+ cells per gram of tissue upon HFD compared to CD in gWAT (Fig. 2.12– F), but not in ingWAT (Fig. 2.12– H). Although previously we observed an increased number of CD45+ cells in gWAT upon HFD, it is not due to proliferation of these cells (section 2.1.2, Fig. 2.5 – E and F). We also investigated $CD34^{low}$ cells with fibroblastic surface marker phenotype. No dietary effects were observed in this subpopulation in gWAT (Fig. 2.12 – I, J). However, in ingWAT there were significantly increased percentages of parent and total number of CD34 $CD34^{low}$ EdU+ cells per gram of tissue upon HFD when compared to CD (Fig. 2.12 – K, L). This observation may indicate that different fat depots have distinct cellular response to HFD suggesting that ingWAT is more proud to fibrosis upon HFD.

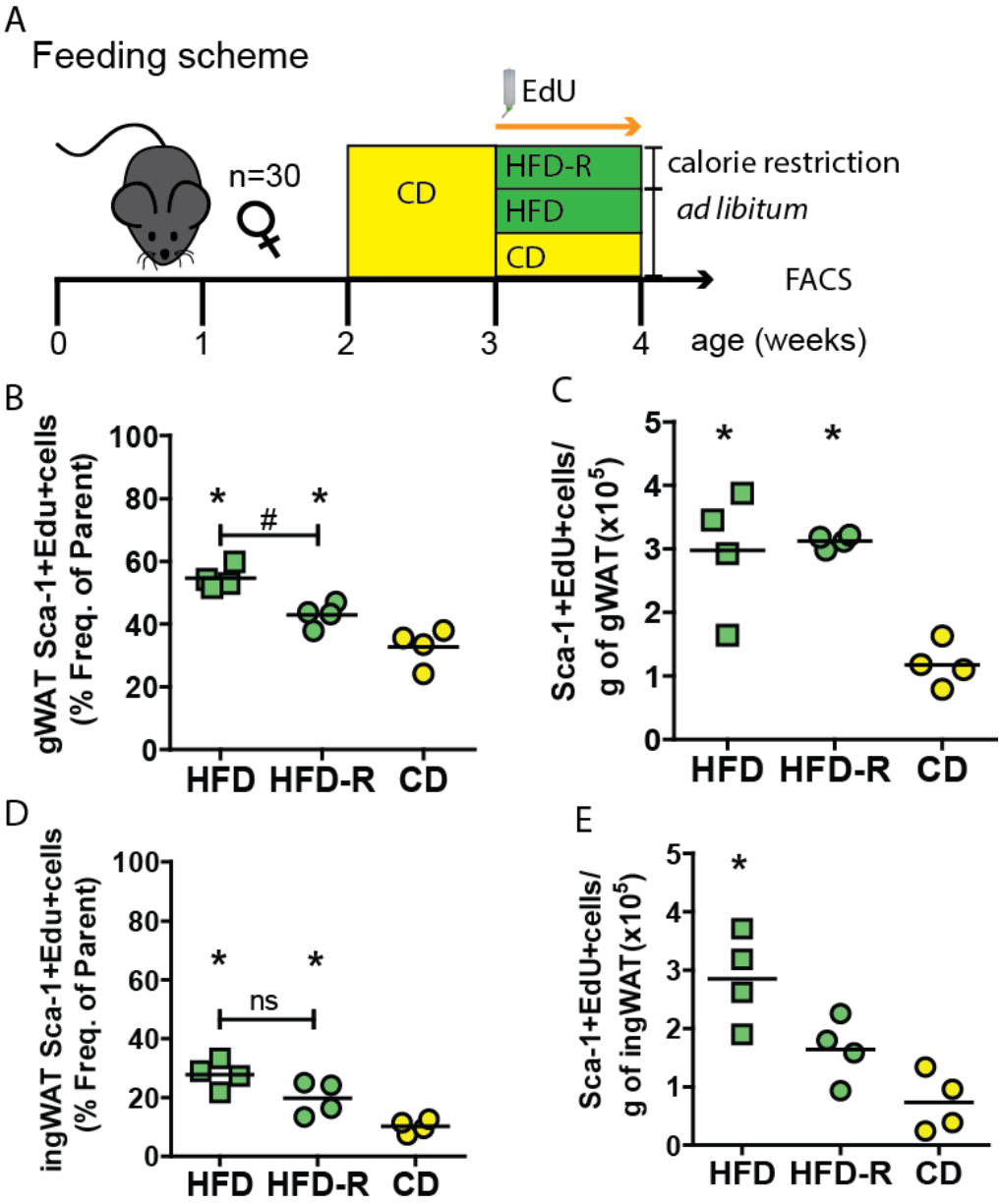

Figure 2.11: High-fat diet induces Sca-1+ AP proliferation in both fat depots in female sexually immature mice. A) Scheme of animal experiment: 30 two-week old female C57BL/6NCrl mice were acclimatized on control diet (CD) for one week and then fed with CD, high-fat diet (HFD) or restricted HFD (HFD-R) for one week in combination with 5-ethynyl-2'-deoxyuridine (EdU) administered in drinking water. Then FACS was performed on SVF cells from perigonadal WAT (gWAT) and inguinal WAT (IngWAT). **B)** Frequency of parent (%) of Sca-1+ EdU+ APs from gWAT. **C)** Number of Sca-1+ EdU+ APs per gram of gWAT. **D)** Frequency of parent (%) of Sca-1+ EdU+ APs from ingWAT. **E)** Number of Sca-1+ EdU+ APs per gram of ingWAT. For B-E each dot represents pooled sample from 2.5 mice, line is mean of the group, one-way Anova with Tukey's post-hoc test was used to assess significance, *, comparison with CD, #, comparison between indicated groups, pV< 0.05, ns, no statistically significant difference.

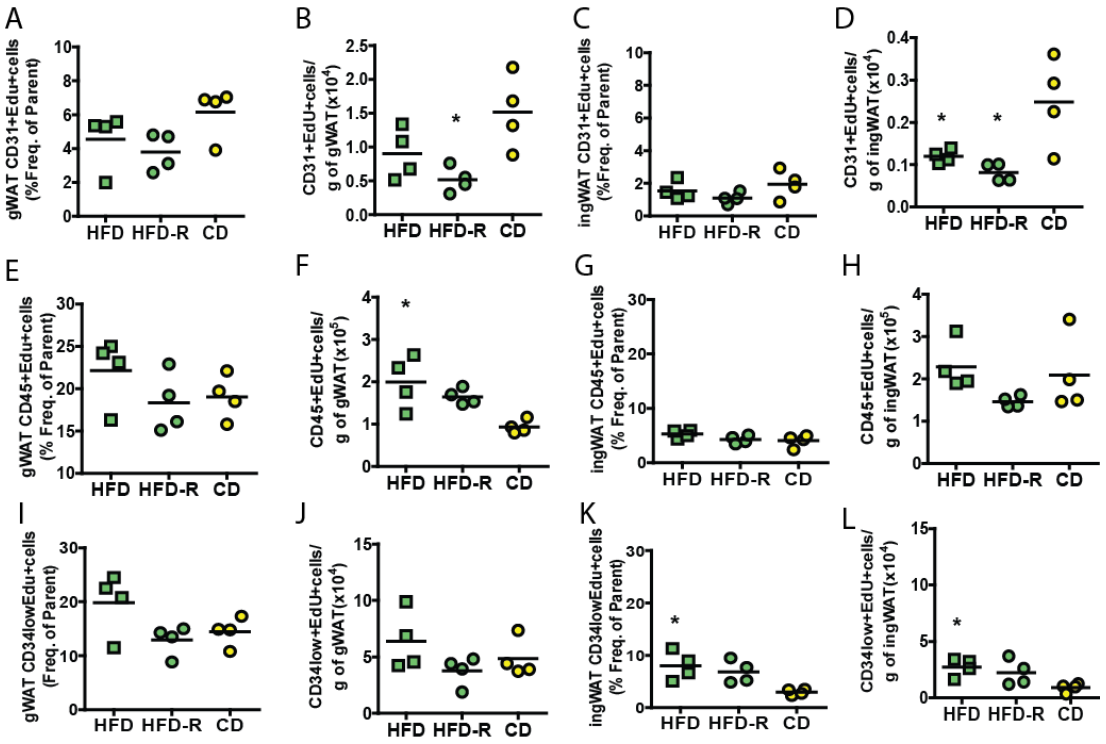

Figure 2.12: High-fat diet does not induce proliferation of other cell subpopulations.
A) Frequency of parent (%) of CD31+ EdU+ endothelial cells (ECs) from gWAT. **B)** Number of CD31+ EdU+ ECs per gram of gWAT. **C)** Frequency of parent (%) of CD31+ EdU+ ECs from ingWAT. **D)** Number of CD31+ EdU+ ECs per gram of ingWAT. **E)** Frequency of parent (%) of CD45+ EdU+ hematopoietic cells (HCs) from gWAT. **F)** Number of CD45+ EdU+ HCs per gram of gWAT. **G)** Frequency of parent (%) of CD45+ EdU+ HCs from ingWAT. **H)** Number of CD45+ EdU+ HCs per gram of ingWAT. **I)** Frequency of parent (%) of $CD34^{low}$ EdU+ cells from gWAT. **J)** Number of $CD34^{low}$ EdU+ cells per gram of gWAT. **K)** Frequency of parent (%) of $CD34^{low}$ EdU+ cells from ingWAT. **L)** Number of $CD34^{low}$ EdU+ cells per gram of ingWAT. For A-L each dot represents pooled sample from 2.5 mice, line is mean of the group, one-way Anova with Tukey's post-hoc test was used to assess significance, *, comparison with CD, pV< 0.05, ns, no statistically significant difference.

In summary, HFD induces Sca-1+ AP proliferation in both fat depots in sexually immature, female mice independently from the amount of consumed calories. This raises the question as which systemic factors can regulate proliferation of APs in response to dietary stimulus, furthermore what regulatory networks are contributing to the WAT remodeling. Established one-week HFD model allow us to investigate dietary regulation of AP proliferation, since we have the short time between stimulus (nutrient) and response of adipose tissue via AP proliferation.

2.2 Systemic factors in the regulation of adipose tissue growth

2.2.1 Dynamic of systemic factors in blood serum upon high-fat diet feeding

Systemic factors, nutrients, metabolites circulate in the blood and communicate direct/indirect metabolic signals to WAT. To investigate systemic factors regulated tissue growth upon HFD in young mice, we measured metabolic factors in blood serum as glucose, insulin

and insulin-like growth factor 1 (IGF-1). Insulin system directly affects adipocyte hypertrophy by regulating glucose uptake. We measured blood glucose and insulin after 2 and 7 days of HFD feeding. Random fed blood glucose was not changed between groups after 2 days (Fig. 2.13 – A). However, it was increased at day 7 in both groups being significantly higher upon HFD (Fig. 2.13 – A). Insulin level was higher in CD-fed group after 2 days and stayed on the same level at day 7 (Fig. 2.13 – B). In HFD-fed group, insulin was lower as compared with CD-fed group at 2 days, but increased after 7 days of diet (Fig. 2.13 – B). Playing an important role in cell growth, IGF-1 was also interesting for us. IGF-1 levels were higher upon HFD at both time points, when compared with CD-fed group (Fig. 2.13 – C). To investigate lipid species involved in energy homeostasis and contributing to WAT growth, we measured triglycerides (TG), non-esterified fatty acids (NEFA) and cholesterol in blood serum. TG was on the same level between HFD and CD on day two (Fig. 2.13 – D). However, level of TG elevated upon HFD after 7 days and decreased upon CD as compared with two days (Fig. 2.13 – D). As for true TG, NEFA levels were the same after 2 days of diet (Fig. 2.13 – E). Interestingly, NEFA levels slightly decreased upon HFD and slightly increased upon CD after 7 days when compared to levels at day 2 (Fig. 2.13 – E). This data indicates that upon HFD mice accumulate excess amount of TG in the blood. The level of cholesterol was significantly higher upon HFD after 2 days of diet when compared to CD-fed group and remained unchanged after 7 days of diet (Fig. 2.13 – F). Cholesterol in CD-fed group increased from day 2 to day 7, reaching the level of HFD-fed group at day 7 (Fig. 2.13 – E).

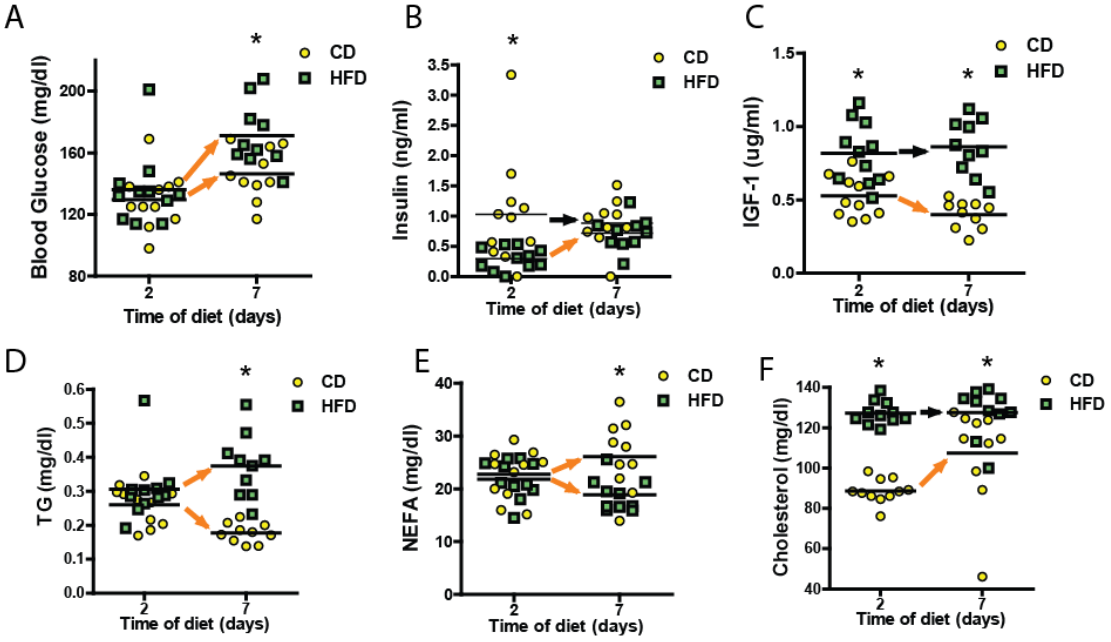

Figure 2.13: Dynamic of systemic factors in blood serum upon high-fat diet feeding.
Forty two 2-week old female C57BL/6NCrl mice were acclimatized on control diet (CD) for one week and then fed with high-fat (HFD) or CD for one week. After euthanizing blood was collected after 2 and 7 days of diets and blood serum factors were measured. Mice were in random fed state. **A)** Blood glucose. **B)** Insulin. **C)** Insulin-like growth factor 1 (IGF-1). **D)** Triglycerides (TG). **E)** Non-esterified fatty

acids (NEFA). **F)** Cholesterol. For A-F each dot represents individual mouse, line is mean of the group, two-way Anova with Bonferroni post-hoc test was used to assess significance, *, comparison with CD of each time point, pV< 0.05, orange arrows indicate dynamic inside of one group from day 2 to day 7, black arrows indicate consistent level on both time points.

We found several systemic factors altered upon HFD feeding, which potentially can contribute to adipose tissue growth by directly affecting APs such as IGF-1 or indirectly through lipid metabolism as TG and NEFA. The next question was the calorie and nutritional regulation of systemic factor which we answered in following section.

2.2.2 Nutritional regulation of systemic factors in blood serum

To understand the influence of diet composition on systemic factors, we used a similar approach as described in section 2.1.3, with CD, HPD, HFD and HFD-R. There was no difference in random fed glucose and insulin level between all groups after 7 days of diets (Fig. 2.14 – A, B). IGF-1 was elevated upon HFD after 7 days as compare with CD, HPD, and HFD-R (Fig. 2.14 – C), indicating that amount of consumed calories affecting level of IFG-1 rather than food composition. TG was elevated upon HFD as compared with CD and upon HPD as compared with CD and HFD-R group (Fig. 2.14 – D). We found significant decrease in NEFA level upon HFD, HFD-R and HPD as compared with CD after 7 days (Fig. 2.14 – E), which correlates with abundance of carbohydrates in CD. There was no difference in the level of cholesterol upon HFD as compared with CD and HFD-R (Fig. 2.14 – F), which is in line with our previous observation for 7 day time point. Decrease of cholesterol level was detected upon HPD as compared with HFD (Fig. 2.14 – F). Also increased amount of ketone bodies was observed, which can indicate active gluconeogenesis upon carbohydrate restriction. The level of ketone bodies was higher in HFD-R as compared with all diets (Fig. 2.14 – G), which possibly indicates that mice were fasted before blood collection in HFD-R group due to limited amount of food. Summary of nutritional regulation of systemic factors in blood 7 days after different diets is represented in Table 1.

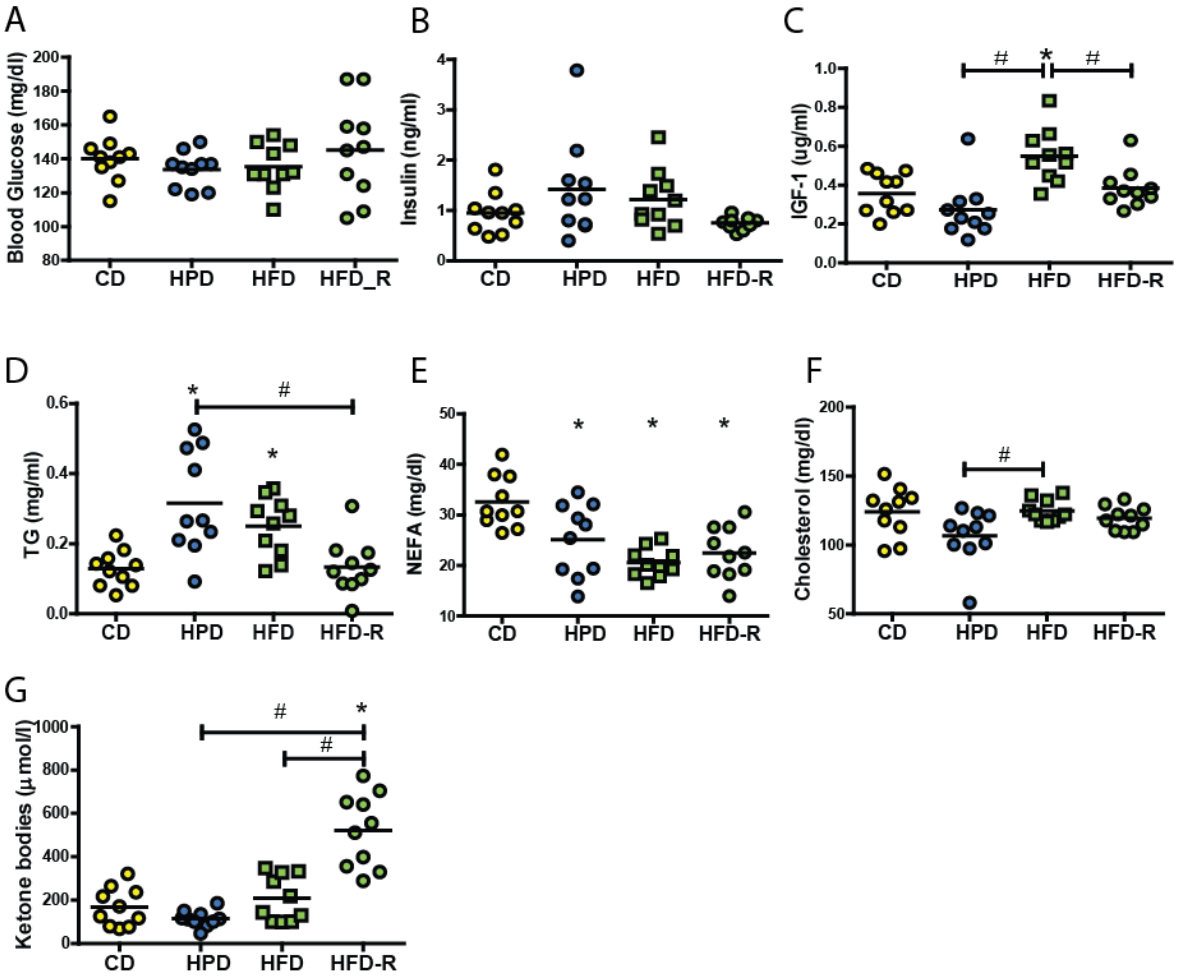

Figure 2.14: Nutritional regulation of systemic factors in blood serum in sexually immature mice after one week of diet. Forty two-week old female C57BL/6NCrl mice were acclimatized on control diet (CD) for one week and then fed with CD or high-protein diet (HPD), high-fat diet (HFD) or restricted HFD (HFD-R) for one week. After euthanizing blood was collected and blood serum factors were measured. Mice were in random fed state. **A)** Blood glucose. **B)** Insulin. **C)** Insulin-like growth factor 1 (IGF-1). **D)** Triglycerides (TG). **E)** Non-esterified fatty acids (NEFA). **F)** Cholesterol. **G)** Ketone bodies. For A-G each dot represents individual mouse, line is mean of the group, one-way Anova with Tukey's post-hoc test was used to assess significance, *, comparison with CD, #, comparison between indicated groups, pV< 0.05.

Table 1: Nutritional regulation of systemic factors in blood serum one week after of diet,

noΔ – was not significantly changed, Δ↑ significantly increased, Δ↓ significantly decreased.

Serum factor	**HFD *ad libitum* vs. CD**	**HFD-R vs. CD**	**HPD vs. CD**
Random fed glucose	noΔ	noΔ	noΔ
Insulin	noΔ	noΔ	noΔ
IGF-1	Δ↑	noΔ	Δ↓
TG	Δ↑	noΔ	Δ↑
NEFA	Δ↓	Δ↓	Δ↓
Cholesterol	noΔ	noΔ	noΔ
Ketone bodies	noΔ	Δ↑	noΔ

To evaluate the same parameters in adult mice, we have performed similar experiment with 26-week old female mice. No difference was observed on the levels of random glucose (Fig. 2.15 – A), insulin (Fig. 2.15 – B), IGF-1 (Fig. 2.15 – C), TG (Fig. 2.15 – D), NEFA (Fig. 2.15 – E) and cholesterol (Fig. 2.15 – F). The level of ketone bodies was elevated in HFD-R as compared with all diets (Fig. 2.15 – G).

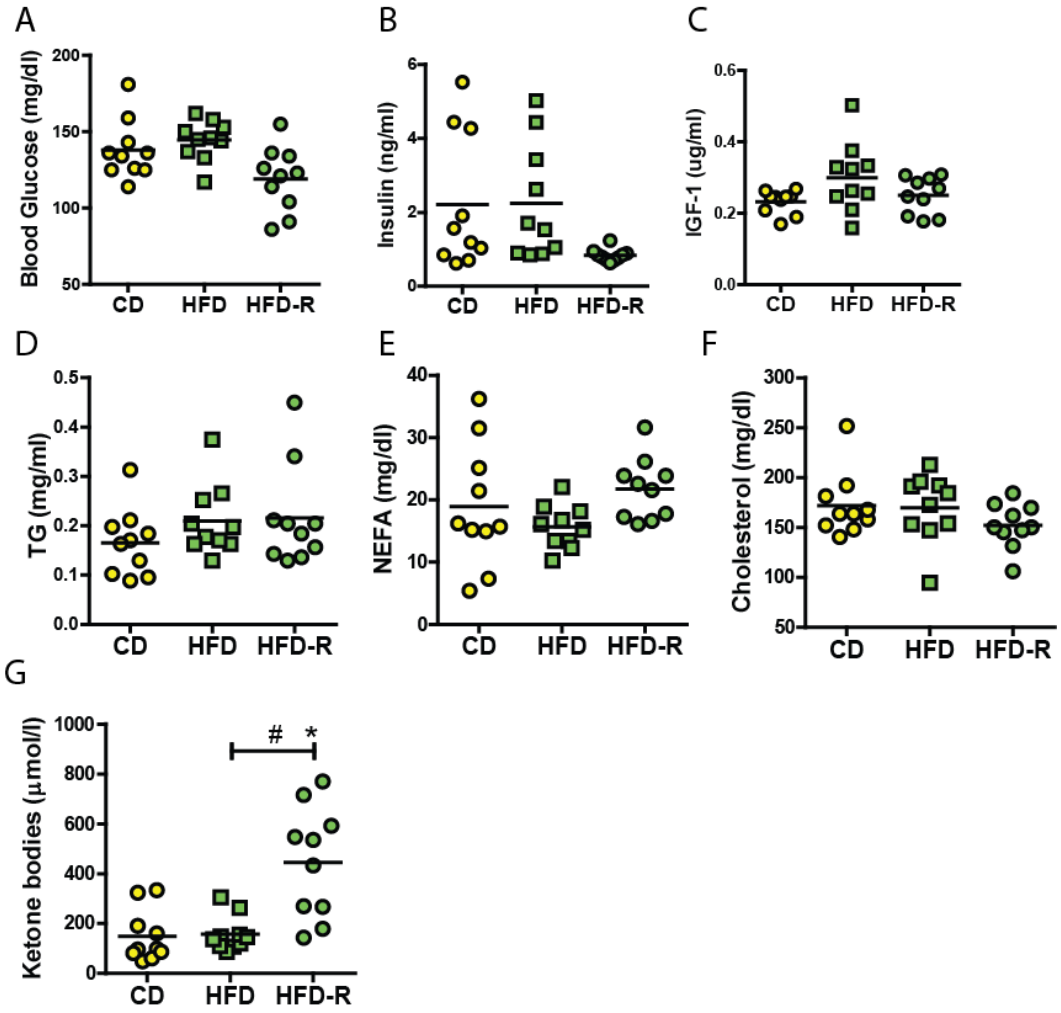

Figure 2.15: Nutritional regulation of systemic factors in blood serum in adult mice after one week of diet. Thirty female 26-week-old female C57BL/6NCrl mice were acclimatized on control diet (CD) for one week and then fed with CD, high-fat (HFD) or restricted HFD (HFD-R) for one week. After euthanizing blood was collected and blood serum factors were measured. Mice were in random fed state. **A)** Blood glucose. **B)** Insulin. **C)** Insulin-like growth factor 1 (IGF-1). **D)** Triglycerides (TG). **E)** Non-esterified fatty acids (NEFA). **F)** Cholesterol. **G)** Ketone bodies. For A-G each dot represents individual mouse, line is mean of the group, one-way Anova with Tukey's post-hoc test was used to assess significance, *, comparison with CD, #, comparison between indicated groups, pV< 0.05.

We demonstrated that regulation of IGF-1 depends on calorie load, but not on food composition in young mice. Some lipids, e.g. NEFA, were regulated by food composition and were decreased upon HFD and HFD-R in young, but not adult mice. TG had combined regulation since they were elevated upon HPD as compared with groups with same calorie load and also by HFD with excess calories.

Many circulated serum factors have dynamic regulation due to fasting/refeeding or day/night phases. To understand which factors can be transiently increased upon feeding, 30 female, sexually immature mice were fed with CD, HFD and HFD-R diets for 3 days. To achieve maximal nutrient load and anabolic response mice were euthanized in their active phase (dark phase), 3 hours after receiving diet. Blood glucose was increased in both HFD and HFD-R groups (Fig. 2.16 – A), but levels of insulin did not change (Fig. 2.16 – B). IGF-1 was higher upon HFD, but no differences were observed between HFD-R and CD (Fig. 2.16 – C). These data indicated that increased on IGF-1 levels depend on overall calorie load and this was not observed in the HFD-R group at least 3 hours after meal. No difference in TG could be observed (Fig. 2.16 – D). NEFA was higher in both HFD-R and HFD groups as compared with CD (Fig. 2.16 – E and F). Additionally cholesterol was significantly higher in HFD group compared to HFD-R (Fig. 2.16 – F). Ketone bodies were higher in both HFD and HFD-R groups (Fig. 2.16 – G). Summary of nutritional regulation of systemic factors 3 hours after feeding is represented in Table 2.

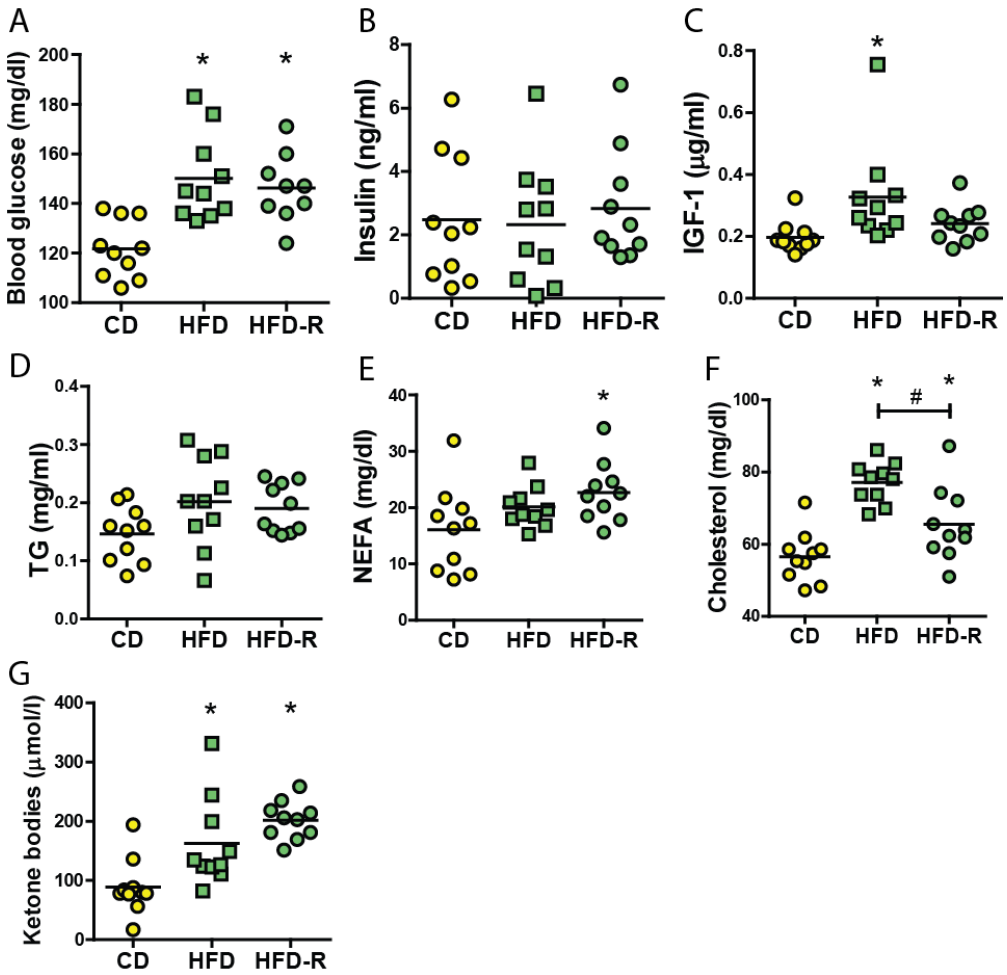

Figure 2.16: Level of systemic factors 3 hours after feeding in sexually immature mice. Thirty two-week old female C57BL/6NCrl mice were acclimatized on control diet (CD) for one week and then fed with CD, high-fat diet (HFD) or restricted HFD (HFD-R) for one week. Food was applied only during dark/active phase and removed during light/resting phase. Blood was collected 3 hours after beginning of

feeding and blood serum factors were measured. **A)** Blood glucose. **B)** Insulin. **C)** Insulin-like growth factor 1 (IGF-1). **D)** Triglycerides (TG). **E)** Non-esterified fatty acids (NEFA). **F)** Cholesterol. **G)** Ketone bodies. For A-G each dot represents individual mouse, line is mean of the group, one-way Anova with Tukey's post-hoc test was used to assess significance, *, comparison with CD, #, comparison between indicated groups, pV< 0.05.

Table 2: Nutritional regulation of systemic factors in blood 3 hours after feeding, noΔ – was not significantly changed, Δ↑ significantly increased, Δ↓ significantly decreased.

Serum factor	**HFD *ad libitum* vs. CD**	**HFD restricted vs. CD**
Glucose	Δ↑	Δ↑
Insulin	noΔ	noΔ
IGF-1	Δ↑	noΔ
TG	noΔ	noΔ
NEFA	noΔ	Δ↑
Cholesterol	Δ↑	Δ↑
Ketone bodies	Δ↑	Δ↑

These data showed that regulation of blood glucose was affected by HFD 3 hours after beginning of food consumption. Increase on IGF-1 levels 3 hours *post cibum* was dependent only on the amount of calories consumed, but not on the food composition. Interestingly, cholesterol is affected by both food composition and amount of calories. These observations provide important information for future investigation of systemic factors contributing to the WAT remodeling.

2.2.4 Mouse serum does not affect adipose progenitor proliferation *in vitro*

To investigate direct effects of blood serum factors on proliferation of APs, we stimulated APs from gWAT *in vitro* with mouse serum collected after 2 and 7 days of CD and HFD feeding. After 21 hours of stimulation and EdU labeling, automated images were acquired and analyzed (Fig. 2.17 – A). We found that there was no significant difference in percentage of labeled cells between dietary conditions in both time points (Fig. 2.17 – B). This experiment indicated that direct short-term treatment of APs with serum form mice fed with HFD and CD cannot stimulate proliferation of APs.

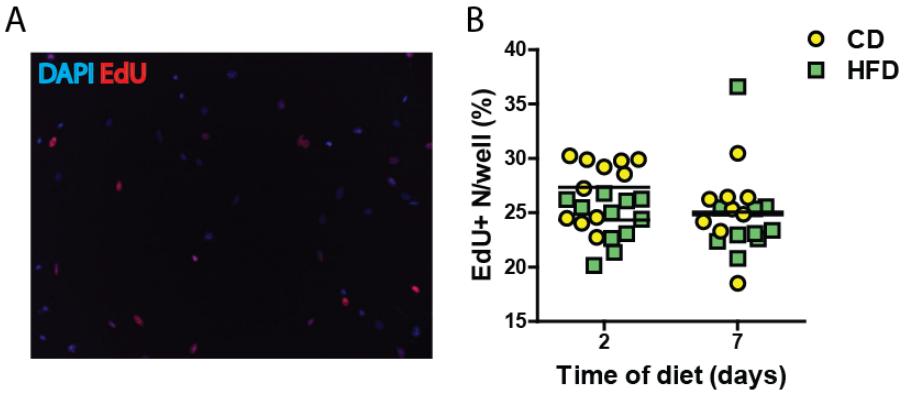

Figure 2.17: Proliferation rate of adipose progenitors after treatment with serum collected from CD and HFD-fed mice. Forty two 3-week old female C57BL/6NCrl mice were fed with control diet (CD) or high-fat (HFD) for one week. After 2 and 7 days of diets blood serum was collected. gWAT Sca-1+ APs were isolated from 3-week old female C57BL/6NCrl mice and seeded in monoculture. Serums from CD-fed and HFD-fed mice were applied on gWAT Sca-1+ APs for 21 hour following with EdU pulse. **A)** Representative image of nuclei stained with DAPI (blue) /EdU (red). **B)** Percentage of EdU+ nuclei based on automated analysis, each dot represents individual mouse serum (25 images per mouse), line is mean of the group, two-way Anova with Bonferroni post-hoc test was used to assess significance.

2.3 Local molecular networks of adipose tissue remodeling and growth in response to high-fat diet

2.3.1 High-fat diet feeding induces acute adipose tissue remodeling

To identify the regulatory networks leading to adipose tissue remodeling upon HFD, we performed microarray hybridizations using RNA isolated from gWAT after 2 and 7 days of diet. Analysis via gene set enrichment analysis (GSEA) showed 69 and 126 gene sets enriched after 2 and 7 days of HFD as compared with CD, respectively, with false discovery rate (FDR) of less than 0.1. We selected 116 gene sets, out of the total 195, from representative pathways related to tissue remodeling process. A complete list of pathways with an enrichment scores and false discovery values is displayed in the Appendix table 1. There are 31 unique pathways characterizing early process in tissue remodeling identified 2 days upon HFD (Fig. 2.18 - A). Among these, there were genes involved in key processes such as angiogenesis, inflammation, leukocyte migration, T-cell activation and differentiation, and cell-cell communication, including receptor signaling protein activity and transmembrane receptor protein kinase activity (Fig. 2.18 – B and Appendix table 1). There are 38 gene sets overlapping between the 2 time points (Fig. 2.18 – A). Among the common pathways, the most relevant to tissue remodeling are: 1) inflammation as immune responses; 2) cytokine and chemokine regulation; 3) neurogenesis (Fig. 2.18 – B and Appendix table 1). After 7 days of HFD, there are 88 pathways enriched (Fig. 2.18 – A). These pathways are involved in extracellular matrix (ECM) remodeling as collagen and cell signaling and in the Jak/STAT and cAMP cascades. Additionally, regulation and

progression of cell cycle pathways were enriched further supporting our data indicating cell proliferation upon HFD (Fig. 2.18 – B and Appendix table 1).

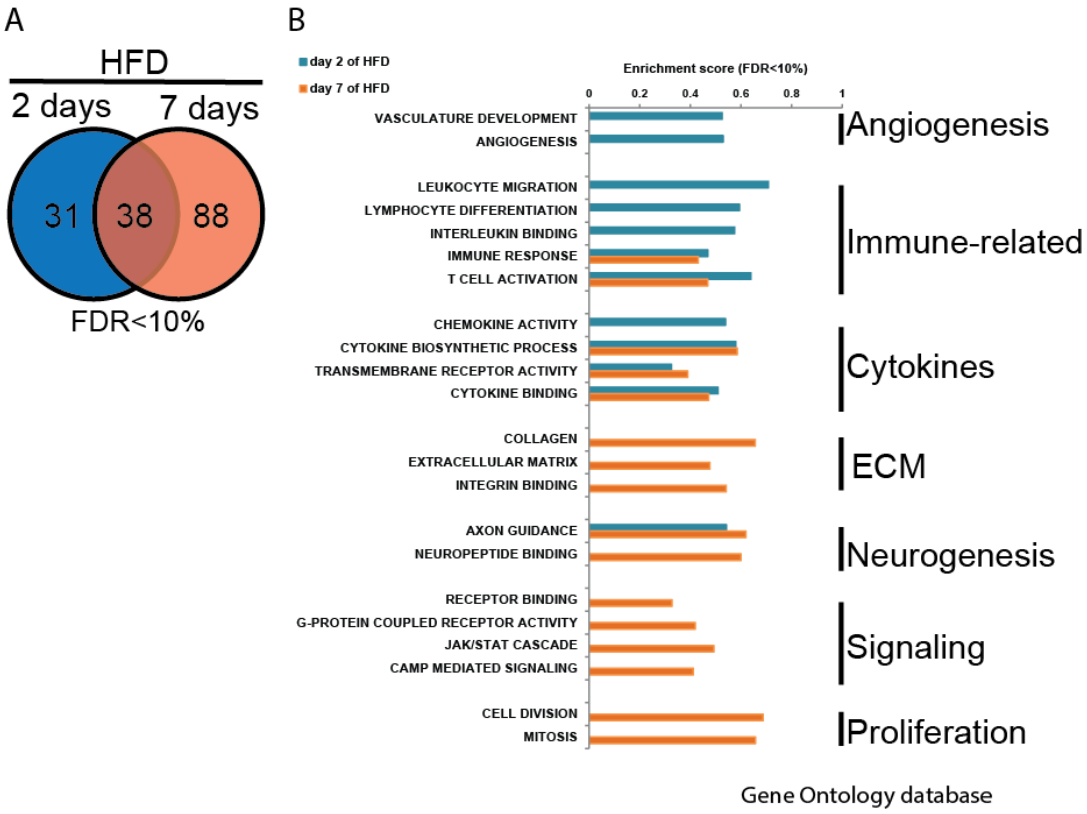

Figure 2.18: Enriched gene sets upon HFD. Three-week old mice were fed with high-fat diet (HFD) vs. control diet (CD) for 2 and 7 days followed by perigonadal WAT (gWAT) dissection, RNA isolation and microarray hybridizations for gene expression profiling. Gene set enrichment analysis was performed for each time point using Gene Ontology database **A)** Enriched upon HFD gene sets represents as Venn diagram with false discovery rate (FDR) <10%. **B)** Enriched upon HFD gene sets related to adipose tissue remodeling represented as bar plot for day 2 (blue) and day 7 (orange) with indicated enrichment score.

We found 68 and 69 gene sets enriched after 2 and 7 days of CD respectively with a false discovery rate of less than 0.1 (Fig. 2.19 – A). Interestingly, 80 from 137 pathways were related to metabolic process. A complete list of pathways with enrichment scores and false discovery values is displayed in Appendix table 2. After 2 days of CD we found 28 pathways related to carbohydrates catabolism and cellular respiration (Fig. 2.19 – B) which continued after 7 days of CD as well. Another prevalent metabolic process was lipid biosynthesis which is largely represented in the 40 common pathways (Fig. 2.19 – B). After 7 days of CD we observed 29 unique gene sets related to secondary metabolic processes and intracellular transport (Appendix table 2). We noticed that proteasome related gene sets were enriched upon CD after 2 and 7 days (Fig. 2.19 – B), which is in line with fact that upon HFD gene set responsible for positive regulation of cellular protein metabolism was enriched (Appendix table 2).

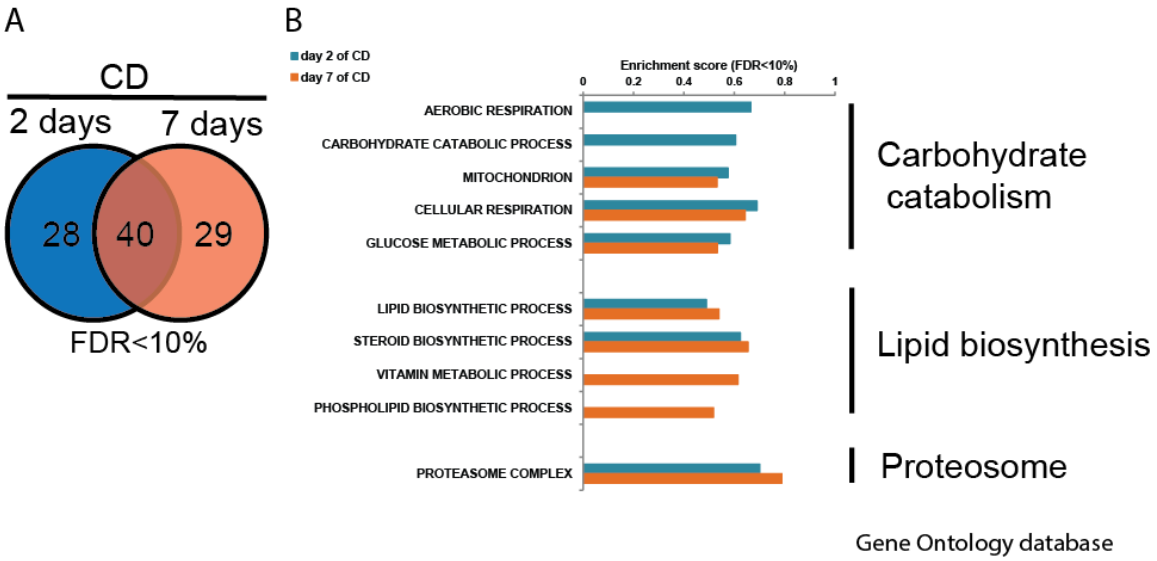

Figure 2.19: Enriched gene sets upon CD. Three-week old mice were fed with high-fat diet (HFD) vs. control diet (CD) for 2 and 7 days followed by perigonadal WAT (gWAT) dissection, RNA isolation and microarray hybridizations for gene expression profiling. Gene set enrichment analysis was performed for each time point using Gene Ontology database **A)** Number of enriched gene sets upon 2 and 7 days of CD in comparison with HFD represents as Venn diagram with false discovery rate (FDR) <10%. **B)** Enriched upon CD gene sets related increased carbohydrate catabolism and lipid biosynthesis represented as bar plot for day 2 (blue) and day 7 (orange) with indicated enrichment score.

These data indicated that activation of gene network related to adipose tissue remodeling was already observed 2 days upon high-fat diet and many processes continue to be driven by HFD until 7 days. We identified dynamic in pathway enrichment as inflammation, cytokine-receptor interaction, cell-cell communication and angiogenesis start early following by extracellular matrix remodeling and activation of proliferation. Additionally, many metabolic related gene sets were upregulated upon CD meaning downregulated upon high-fat diet as carbohydrates catabolism and lipid biosynthesis.

2.3.2 Fat content, but not calorie, induces cell proliferation in adipose tissue

As the diets used have different content of macronutrients (see section 2.1.3), it would be possible that the results of the first expression profile could have been influenced by these differences. To identify which gene sets are induced by excess calorie versus the macronutrient content, we performed a new profile with HFD, HFD-R, CD and HPD and compared the enriched gene sets. We included the HPD in order to compare with our previous observations by manipulating dietary content. The HFD group had excess calories compared with CD and HPD (Fig. 2.20 – A). We found 32 pathways exclusively enriched in HFD vs. CD with a false discovery rate of less than 0.1 (Fig. 2.20 – B). Interestingly, some of the gene sets are related to regulation of immune process (Appendix table 3). Most of the 38 common pathways were related to cell cycle and to immune- related processes, confirmed our previous observations (see section 2.3.1). HFD vs. HPD gave rise to 17 pathways exclusively enriched, mostly related

to ECM as collagen. The complete comparison of pathways with enrichment scores and false discovery values are displayed in the Appendix table 3. Also we looked into downregulated gene sets upon HFD with a false discovery rate of less than 0.1. We found 63 gene sets downregulate upon HFD mostly related to metabolism as carbohydrate catabolism and lipid biosynthesis, corroborating our previous result (see section 2.3.1). Surprisingly, no gene set was downregulated comparing HFD with HPD (Fig. 2.20 – C).

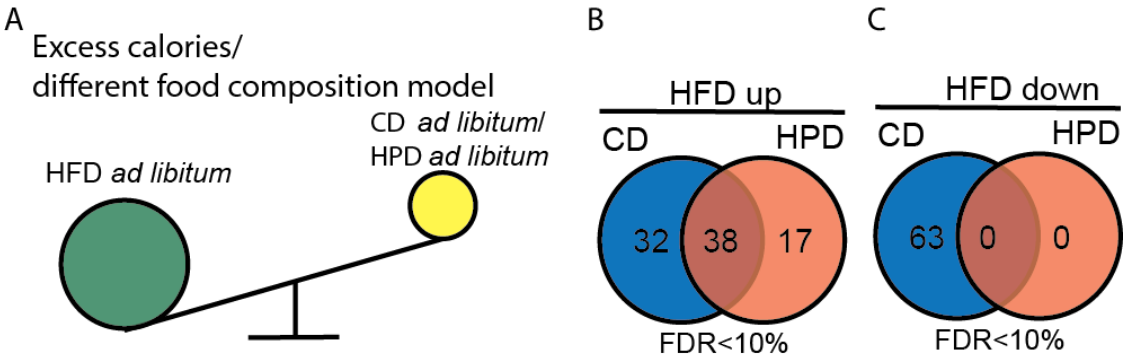

Figure 2.20: Scheme of analysis of enriched genes using excess calorie model.
A) In this type of experiment 2 factors are present: excess calories from high-fat diet (HFD) *ad libitum* feeding and different composition of food of comparison as control diet (CD) or high-protein diet (HPD). **B)** Number of enriched gene sets upon HFD in comparison with CD (blue) or HPD (orange) represents as Venn diagram with false discovery rate (FDR) <10%. **C)** Number of enriched gene sets upon CD (blue) or HPD (orange) in comparison with HFD represents as Venn diagram with FDR <10%.

To identify pathways enriched depending on different food components, but not calorie excess, the following pairs were compared: HFD-R vs. CD and HFD-R vs. HPD (Fig. 2.21 – A). There were 18 pathways enriched exclusively between HFD-R and CD and 19 between HFD-R and HPD and 44 common gene sets (Fig. 2.21 – B and Appendix table 4). Proliferation-related pathways were enriched in both comparisons as well as cell cycle phase (Appendix table 4). These data suggested HFD leads to adipose tissue cell proliferation independently of the calorie load. These data was confirmed by the increased number of EdU-labeled APs seen in section 2.1.3. To understand the effects of high-fat content in the diet we performed additional comparisons of HFD and HFD-R to CD (Fig. 2.21 – D). There were 30 pathways exclusively enriched in HFD mostly with immune-related functions (Fig. 2.21 – E), indicating that activation of immune-related processes depends on excess calorie load. Most of common enriched gene sets belong to cell-cycle progress (Fig. 2.20 – E), confirming again that fat content was able to activate cell proliferation in adipose tissue independent on calorie load. We found 22 gene sets enriched in response to food restriction mostly muscle-related (Fig. 2.21 – E).

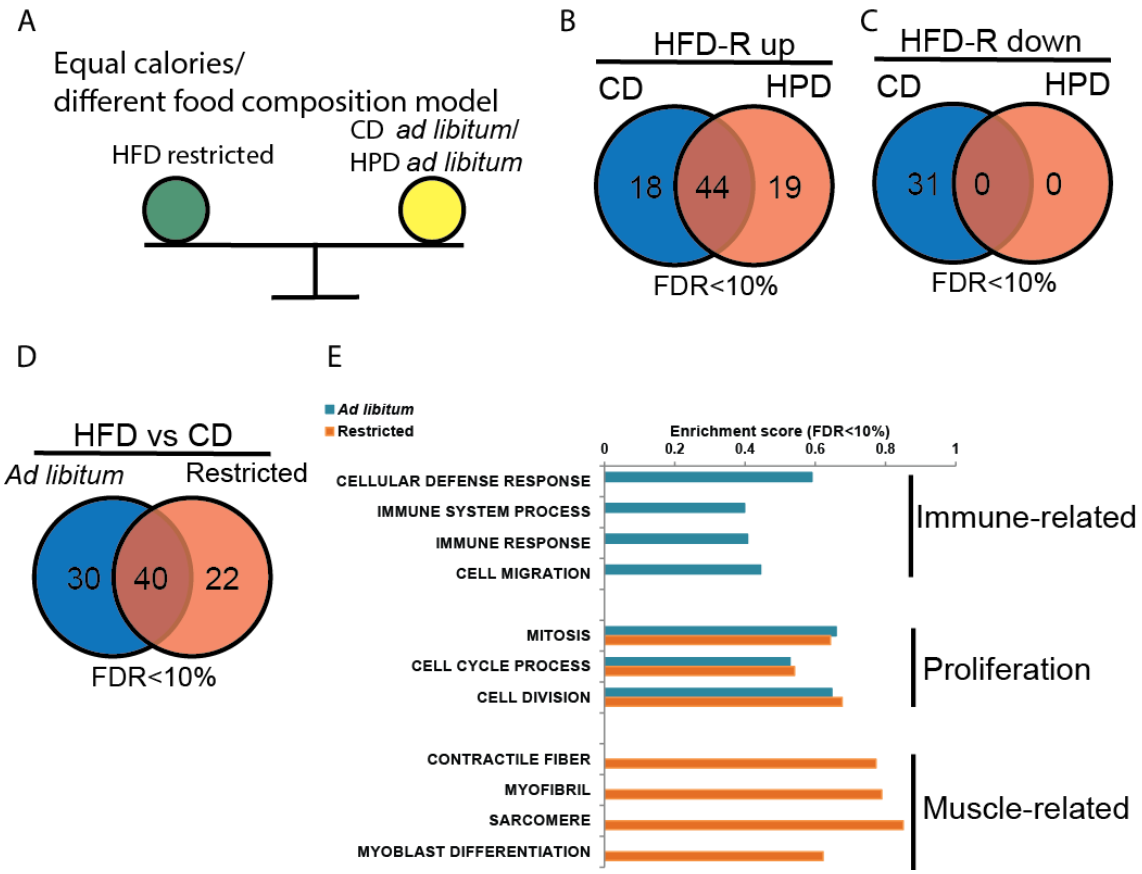

Figure 2.21: Scheme of analysis of enriched genes using isocaloric model. A) In this type of experiment using pair feeding approach mice received the same amount of calories from high-fat diet (HFD-R) as control groups: control diet (CD) and high-protein diet (HPD). **B)** Number of enriched gene sets upon HFD-R in comparison with CD (blue) or HPD (orange) represents as Venn diagram with false discovery rate (FDR) <10%. **C)** Number of enriched gene sets upon CD (blue) or HPD (orange) in comparison with HFD-R represents as Venn diagram with false discovery rate (FDR) <10%. **D)** Number of enriched gene sets upon HFD in comparison with CD (blue) and HFD-R in comparison with CD (orange) represents as Venn diagram with false discovery rate (FDR) <10%. **E)** Enriched upon HFD gene sets related to adipose tissue remodeling represented as bar plot for *ad libitum* (blue) and restricted (orange) with indicated enrichment score.

To investigate the effect of the amount of consumed calories on gene regulation, a comparison between HFD and HFD-R was performed, as these groups received the same type of diet but in different amounts, reflecting different calorie load (Fig. 2.22 – A). Surprisingly, only one gene set was found to be enriched upon HFD in this comparison – Carboxylesterase activity. This pathway is important for hydrolyze of esters and also long-chain fatty acid esters and thioesters. We also found 14 pathways downregulated upon HFD related to muscle as regulation of muscle cell differentiation and muscle constriction.

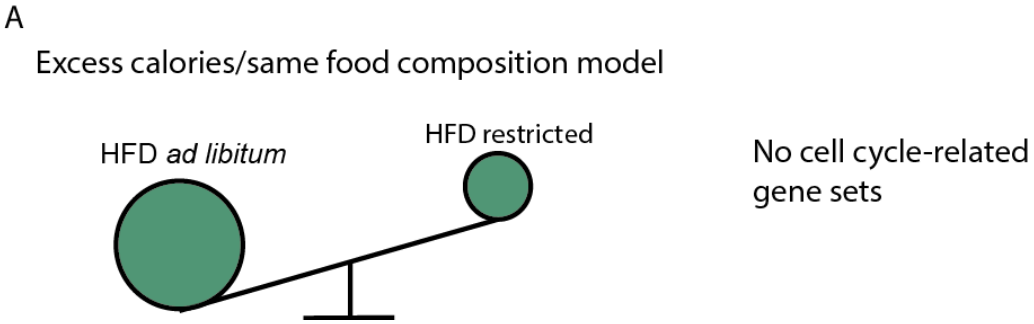

Figure 2.22: Scheme of analysis of enriched genes using same composition of the food.
In this type of experiment mice were fed with HFD only either *ad libitum* or in restricted form. No cell cycle related gene sets were enriched.

We demonstrated that cell cycle gene sets enriched in HFD *ad libitum and* HFD-R when compared with CD, but not in comparison HFD *ad libitum* vs. HFD-R. These data indicated that fat content can alone trigger AP proliferation which can contribute to WAT remodeling during development of childhood obesity. Additionally we demonstrated that inflammation-related gene sets were not significantly different in HFD-R vs. CD that indirectly indicated independence of inflammation from induction of AP proliferation in response to high-fat diet.

2.3.3 Cell population response to high-fat diet

To investigate response of different cell subpopulations in AT remodeling upon HFD feeding, we performed 2 independent mouse experiments followed by cell sorting. Female sexually immature mice were fed with HFD and CD for 7 days, then gWAT was dissected, digested and SVF cells were stained (as described in methods section 4.2.5), 5 different cell subpopulations were collected: mature adipocytes, CD45+ cells, CD31+ endothelial cells, Sca-1+ APs and $CD34^{low}$ cells. We performed microarray hybridizations using RNA isolated from Sca-1+ APs, CD31+ and $CD34^{low}$ cells (Fig. 2.23 – A). Specificity of cell populations was confirmed by identifying the expression of markers that characterize these cells CD45 antigen (Ptprc) for hematopoietic lineage, CD31 (Pecam1) for endothelial cells, Pdgfrα for Sca-1+ APs and Acta2 for $CD34^{low}$ cells (Fig. 2.23 – B). CD45 antigen was not expressed on any of cell subpopulations. CD31 was expressed only in sorted CD31+ cells samples, Pdgfrα was expressed on Sca-1+APs, and Acta2 was present only on $CD34^{low}$ cells (Fig. 2.23 – B). These data indicated that cell subpopulation was correctly sorted.

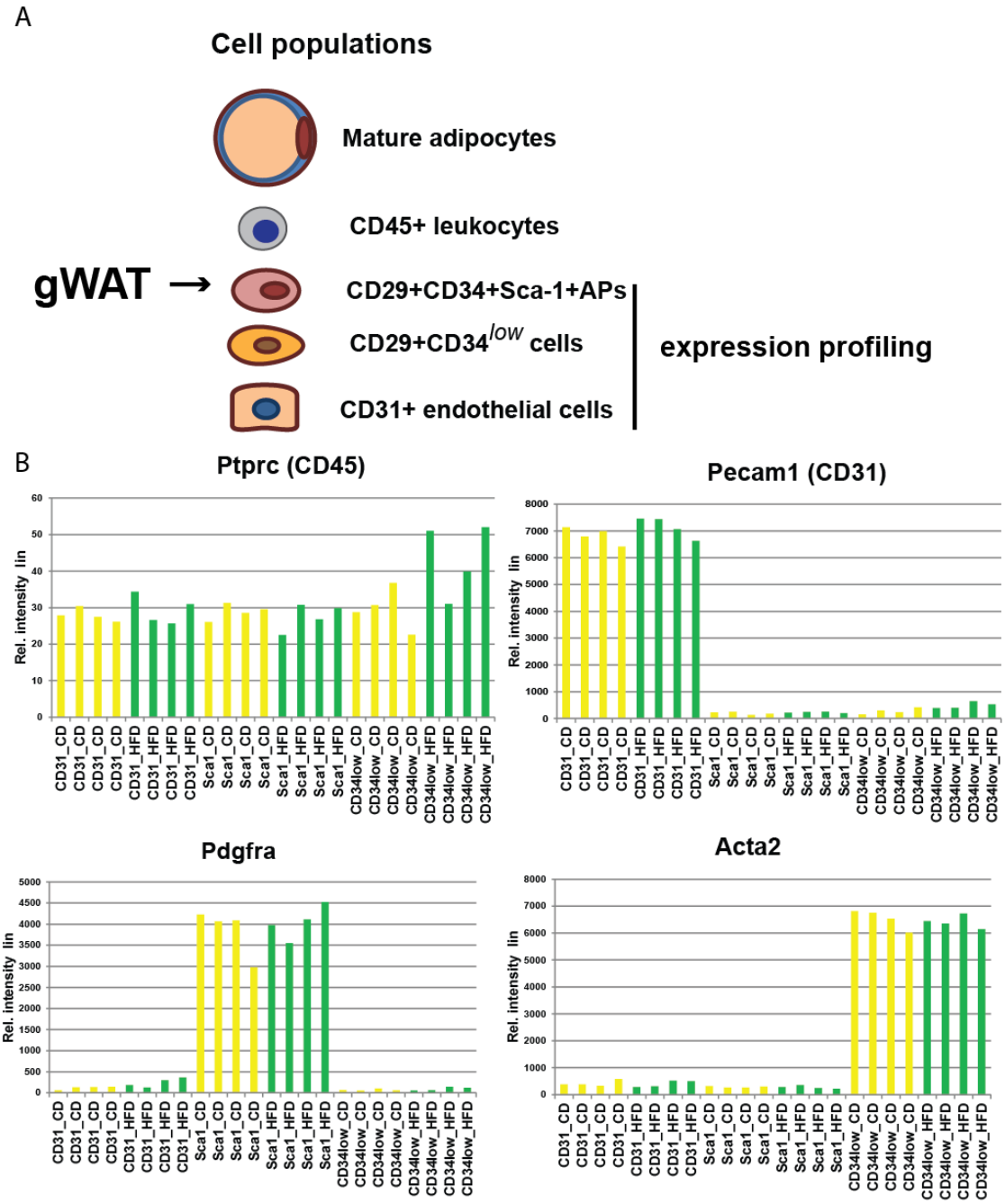

Figure 2.23: Validation of cell population-specific expression of sorted cells. A) Scheme of experiment: 3-week old female C57BL/6NCrl mice were fed with HFD or CD for one week, perigonadal WAT (gWAT) was dissected, digested and stroma vascular fraction cell were stained followed by FACS. Two independent animal experiments were conducted (n=25 and n=60), each sample was pooled from 3-12 mice. RNA was isolated from 3 subpopulations: Lin-CD29+CD34+Sca-1+ adipose progenitors (APs), Lin-CD29+CD34^{low} cells and from CD45-CD31+ endothelial cells (ECs) and microarray hybridizations for gene expression profiling was performed. **B)** Surface markers from gene expression profiling conforming purity of sorted subpopulations as all samples are negative for Ptprc (CD45), only ECs samples are positive for Pecam1 (CD31), only APs expressed Pdgfrα, only CD34^{low} cells expressed Acta2.

We investigated the effects of HFD feeding on specific cell subpopulations from gWAT using GSEA with a false discovery rate of less than 0.1. We found only 8 gene sets enriched upon HFD in Sca-1+ APs (Fig. 2.24 – A, B). Coagulation, wound healing, cytokine biosynthetic

processes, and peptide receptor activity indicate active cell-cell communicating upon HFD. There were no gene sets enriched upon CD in Sca-1+ APs. We found 34 enriched sets upon HFD in CD31+ cells. Most gene sets were related to ECM remodeling such as glycosaminoglycan binding and collagen (Fig. 2.24 – A, B). Also 14 gene sets were enriched upon CD in CD31+ cells related to cell adhesion as intercellular junction assembly (Fig. 2.24 – A, B). There were 35 gene sets enriched upon HFD in CD34^{low} cells. The majority of them were related to ECM regulation, T cell activation, negative regulation of angiogenesis and M-phase of cell cycle (Fig. 2.24 – A, B). There were no gene sets enriched upon CD diet. There was no overlap between the enriched gene sets among all different subpopulations, except for Sca-1+ cells, sharing 6 enriched gene sets with CD34^{low} cells including coagulation and wound healing (Fig. 2.24 – A, B). CD34^{low} cells shared 4 enriched gene sets with CD31+ endothelial cells related to extracellular region (Fig. 2.24 – A, B).

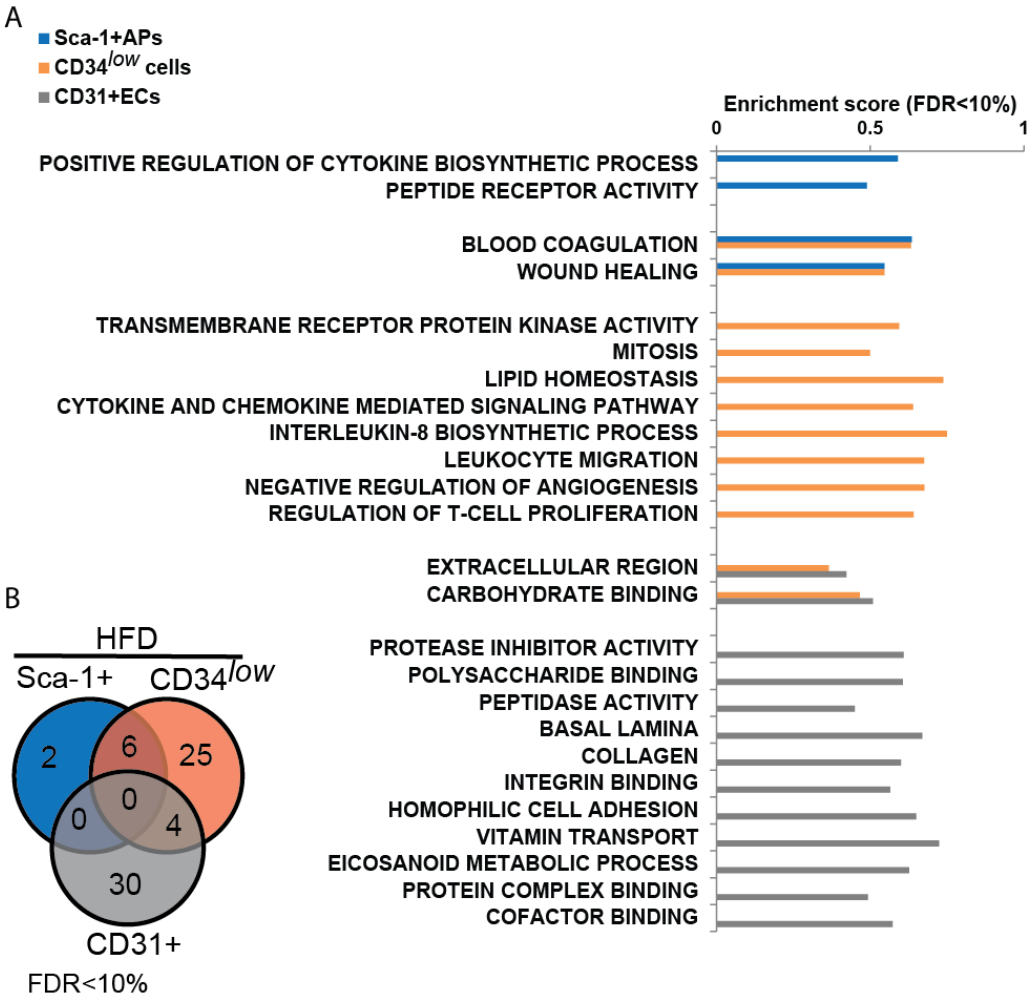

Figure 2.24: Cell specific enrichment of gene sets upon high-fat diet. A) Enriched upon high-fat diet (HFD) gene sets represented as bar plot for Sca-1+ adipose progenitors (APs) (blue), CD34l^{ow} cells (orange) and CD31+ endothelial cells (ECs) (grey) with indicated enrichment score with false discovery rate (FDR) <10%, each group was enriched in compared with CD. B) Number of enriched upon HFD gene sets represents as Venn diagram with FDR <10%.

These data indicate that different cell subpopulation in WAT had distinct cell response on HFD feeding and the understanding of cell-cell interactions could inform us about role of specific cell population in WAT remodeling.

2.3.4 Novel gene search – differentially expressed genes during early adipose tissue remodeling

In order to identify candidate targets for further functional screening, we investigated differentially expressed genes potentially involved in WAT remodeling and AP activation upon short term high-fat feeding. For that we performed microarray hybridizations using RNA isolated from gWAT after 2 and 7 days of HFD as described in section 2.3.1. We were interested in cell-cell crosstalk mediators such as secreted proteins, receptors, enzymes, extracellular matrix proteins/remodeling enzymes which could be manipulated by overexpression/siRNA silencing, or application of soluble factors. First, using linear modeling, we discriminated genes with interaction between two factors: time of diet and effect of diet. Although, we did not find genes with interaction satisfying filtering criteria (pV <0.05 and at least 1.5 -fold change in linear or 0.58 in log scale), there were 2 genes close with pV=0.06 (Appendix table 5, marked orange). We identified 230 genes with pV <0.05 for effect of diet (main effect- diet), but only 129 had at least 1.5-fold change in their expression level (Appendix table 5, marked blue). Two groups tests were used for HFD vs. CD comparison inside each time point (for 2 days and for 7 days separately). There were 72 genes which were significant for day 2 of diet with more than 1.5-fold change. However, 71 of them were already in the main effect list and only one was additional (Appendix table 5, marked green). When tested for day 7 of diet, 181 genes were significant with at least 1.5-fold change. Again 109 genes were already selected by main effect and 72 were added to the list (Appendix table 5, marked yellow). Insulin is a potent hormone for adipose tissue function. Genes upregulated upon CD were involved in glucose homeostasis and regulated by insulin were found as *Slc2a5* and *Slc2a4* (solute carrier family 2 (facilitated glucose transporter), member 5 and member 4 respectively, also known as GLUT5 and GLUT4), Insig1 (insulin induced gene 1) (Fig. 2.25 – A). We found genes involved in cell-cell communication such as ECM and adhesion proteins e.g. epithelial membrane protein 1 (*Emp1*), leucine-rich alpha-2-glycoprotein 1 (*Lrg1*), versican (*Vcan*), thrombospondin 2 (*Thbs2*) (Fig. 2.25 – B). Also genes involved in cytokine- receptor interaction were found such as BMP-binding endothelial regulator (*Bmper*), interleukin 4 receptor, alpha (*Il4ra*), bone morphogenetic protein 3 (*Bmp3*), TNF receptor associated factor 4 (*Traf4*) (Fig. 2.25 – C). Additionally we found genes with unknown function in adipose tissue and not related to the categories above as neuronatin (*Nnat*), fragile X mental retardation syndrome 1 (*Fmr1*), prostate transmembrane protein, androgen induced 1 (*Pmepa1*), procollagen-lysine, 2-oxoglutarate 5-dioxygenase 2 (*Plod2*), lipase, endothelial (*Lipg*) (Fig. 2.25 – D).

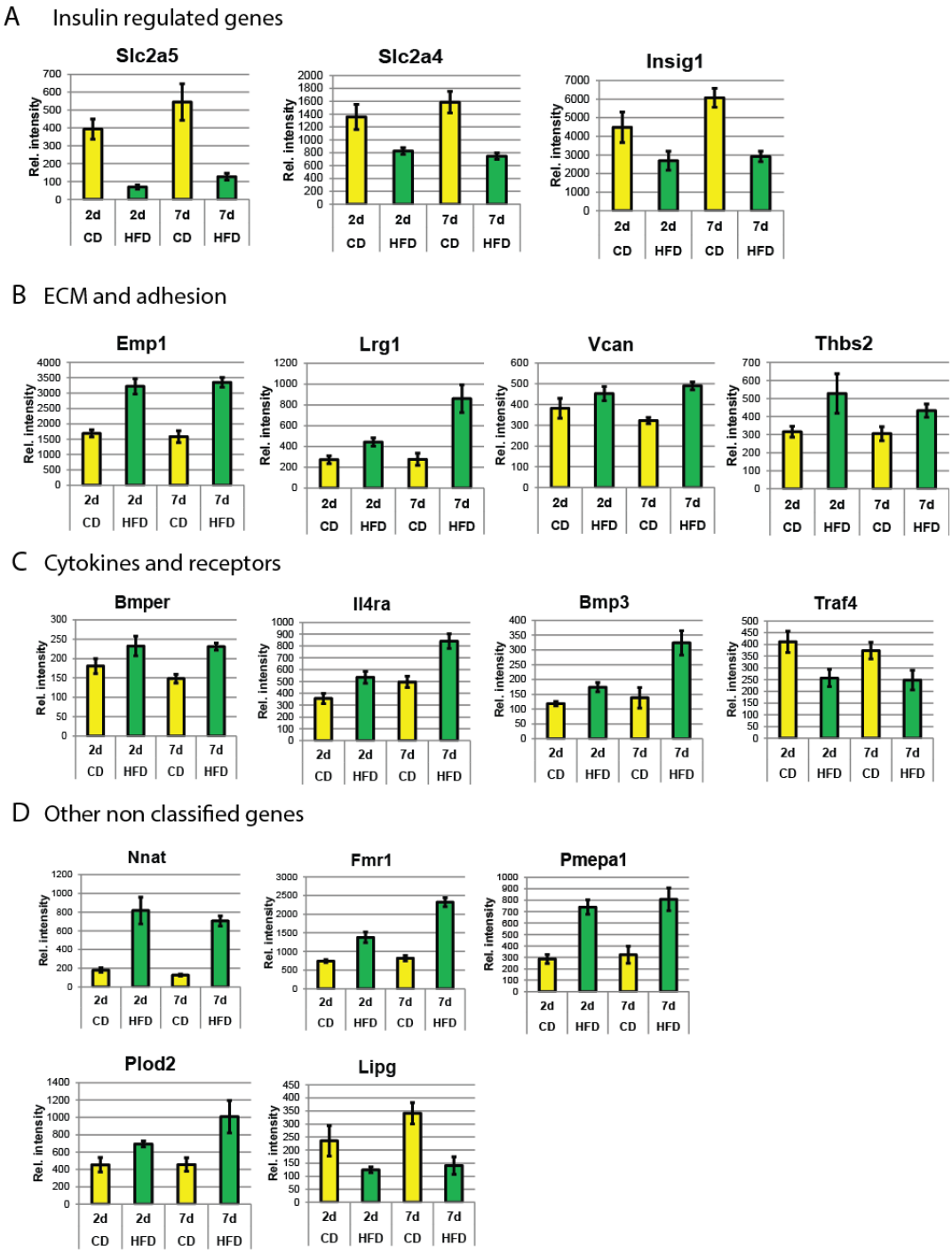

Figure 2.25: Change in expression pattern of representative candidate genes upon 2 and 7 days of HFD. RNA expression levels from microarray data. A-D – different gene category and the main representatives in each category. Data represented as mean ± SEM from 5 measurements.

2.3.5 Novel gene search – impact of fat content on gene expression

In order to investigate molecular signals leading to AP activation upon different dietary components we performed microarray hybridizations using RNA isolated from gWAT as described in section 2.3.2. Applying 2 filtering parameters with p value < 0.05 and at least 1.5-fold change, 65 genes were differentially expressed between HFD vs. CD (Appendix

table 6). There were 43 genes overlapping between this experiment and the one in described above (section 2.3.4). (Appendix table 6, marked orange). Genes of interest involved in cell-cell communication have the same pattern as in first profiling (Fig. 2.26). As in the first profiling insulin-regulated genes, *Slc2a5*, *Slc2a4* and *Insig1* were upregulated upon CD compared with HFD and HFD-R, but not when compared with HPD (Fig. 2.26 – A). Genes involved to ECM and cell adhesion exhibited a similar pattern as in first profiling: *Emp1*, *Lrg1*, and *Vcan* were upregulated in HFD compared with CD and HPD. However *Thbs2* did not show significant differences (Fig. 2.26 – B). Cytokines and receptors were upregulated upon HFD and HFD-R such as *Bmper*, *Il4ra*, *Bmp3*, while *Traf4* was downregulated with HFD and HFD-R (Fig. 2.26 – C). *Nnat* and *Pmepa1* were upregulated upon HFD and HFD-R diet compared with CD and HPD (Fig. 2.26 – D). *Fmr1* was upregulated only upon HFD compared with all other diets (Fig. 2.26 – D). However, *Plod2* did not show significant difference. *Lipg* was downregulated upon HFD and HFD-R (Fig. 2.26 – D). There were 22 genes that appeared elusively in the second profiling with a p value < 0.05 and at least 1.5-fold change (Appendix table 6, no color). One of these genes was particulary interesting so we followed it for further analysis. Lumican (*Lum*) as an ECM protein, was upregulated upon HFD and HFD-R (Fig. 2.26 – B). In order to find genes which were differentially expressed only in response to excess calories we compered HFD vs. HFD-R and found 83 genes with p value < 0.05 and at least 1.5-fold change (Appendix table 7). Interestingly when we compared HFD vs. CD and HFD vs. HFD-R we identified 4 overlapping genes: *Fmr1*, *Emp1*, oxytocin receptor (*Oxtr*) and solute carrier family 27 (fatty acid transporter), member 1 (*Slc27a1*). These genes were potentially acting independently of food composition but were sensitive to calorie load.

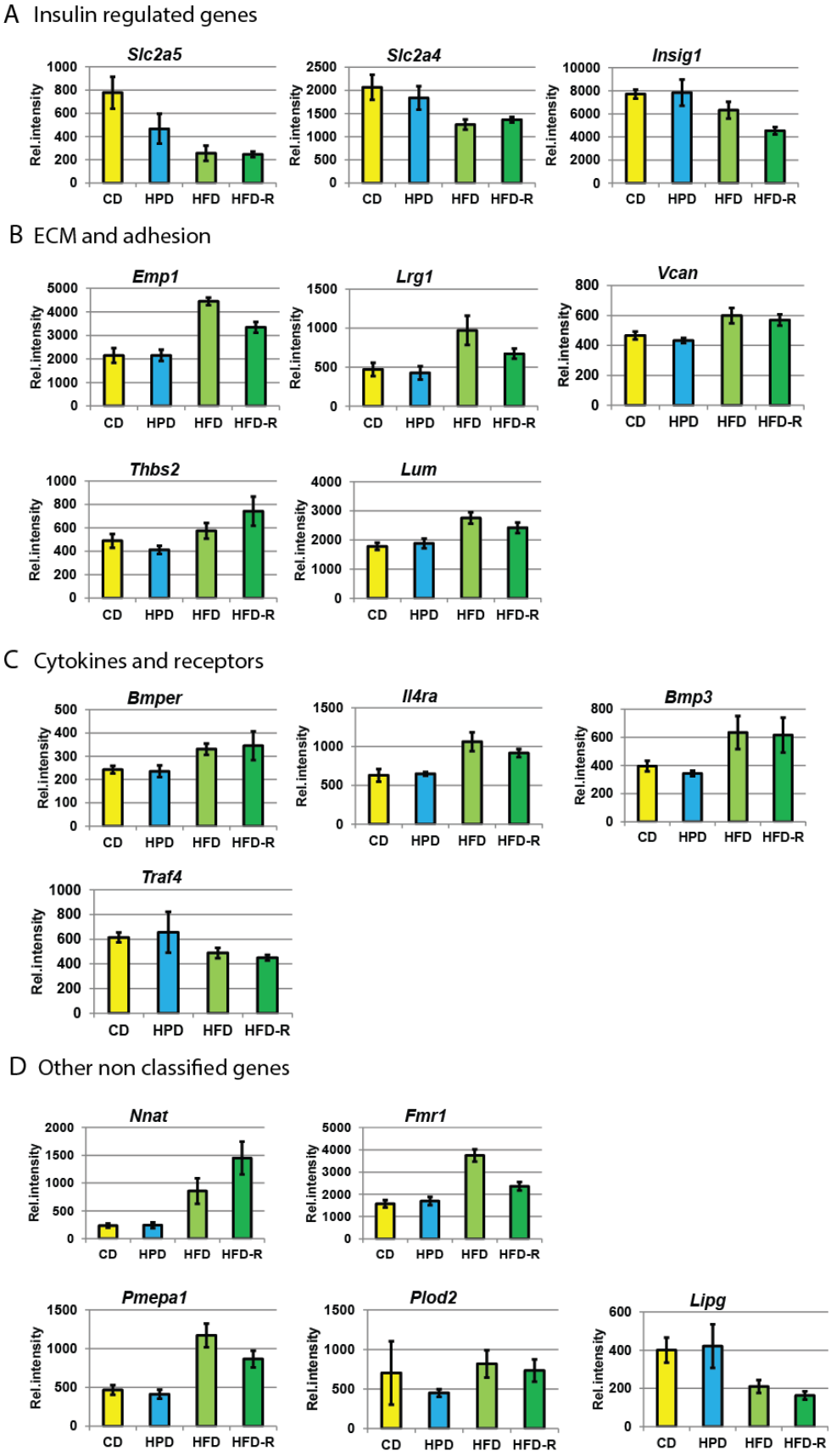

Figure 2.26: Change in expression pattern of representative candidate genes upon different diets. RNA expression levels from microarray data. A-D – different gene category and the main representatives in each category. Data represented as mean ± SEM from 5 measurements.

2.3.6 Novel gene search – different cell subpopulations response

In order to identify cell population specific genes altered in response to HFD, we performed microarray hybridizations using RNA isolated from 3 different cell subpopulations as described in section 2.3.3 and two groups analysis as it was described above. Appling 2 filtering parameters with p value < 0.05 and at least 1.5-fold change, 19 genes were differentially expressed in comparison HFD vs. CD in Sca-1+ APs (Fig. 2.27 – A). We found new targets which were not differentially expressed on whole tissue level, e.g. transforming growth factor, beta-induced (*Tgfbi*) specifically downregulated in Sca-1+ APs upon HFD (Fig. 2.27 – B). There were 109 genes differentially expressed in CD31+ ECs upon HFD (Fig. 2.27 – A, C). Interestingly as we have observed extracellular matrix related genes altered upon HFD in this subpopulation, e.g. *Vcan* was upregulated and collagen, type VIII, alpha 1 (*Col8a1*) was downregulated (Fig. 2.27 – C). In CD34^{low} cells 108 were differentially expressed upon HFD, e.g. reelin (*Reln*) and calsequestrin 2 (*Casq2*) (Fig. 2.27 – D).

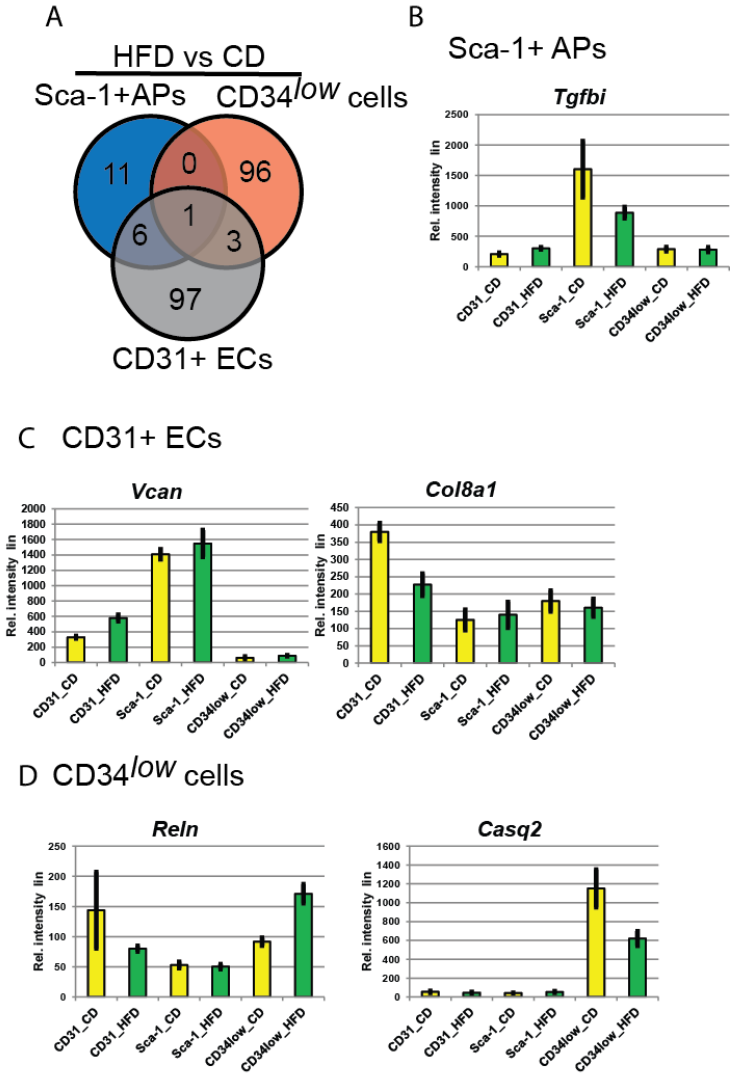

Figure 2.27: Change in expression pattern of representative candidate genes upon different diets in different cell subpopulation from gWAT. RNA expression levels from microarray data. **A)** Number of differentially expressed genes represented as Venn diagram for Sca-1+ adipose progenitors (APs) (blue),

CD34l^{ow} cells (orange) and CD31+ endothelial cells (ECs) (grey) **B-D**) Different gene category and the main representatives in each category. Data represented as mean ± SEM from 5 measurements.

We identified genes differentially expressed upon dietary challenges and selected several targets for futher validation.

2.3.7 Validation and function of candidate genes

We selected several genes described in sections 2.3.4 – 2.3.6 by following criteria: potentially involved in cell-cell communication, could be modified by siRNA/ overexpressin, function were not described in context of *in vivo* adipogenesis or/and AP proliferation/differentiation. First in order to validate target genes, we analyzed gene expression after 7 days of CD, HFD, HPD and HFD-R in young and adult female mice via qPCR. Summary of validation represented in table 3 and Appendix Fig. 4.

Table 3: Validation of selected from expression profiles genes by qPCR. Significance between groups were tested by one-way Anova with Tukey's post-hoc test, *, comparison between indicated conditions, pV< 0.05, ns, no statistically significant difference.

	Young mice			Adult mice		
Gene name	**CD vs HFD**	**CD vs HFD-R**	**HFD vs HFD-R**	**CD vs HFD**	**CD vs HFD-R**	**HFD vs HFD-R**
Emp1	*	*	*	*	*	*
Fmr1	*	*	*	ns	ns	*
Bmper	*	*	ns	ns	ns	ns
Fap	*	ns	*	ns	*	*
Plod2	ns	ns	ns	ns	ns	ns
Ngfr	*	ns	*	ns	ns	ns
Traf4	ns	*	ns	ns	ns	*
Vcan	*	ns	ns	ns	ns	*
Emb	ns	ns	ns	ns	ns	*
Pkp2	*	ns	*	ns	ns	ns
Lum	*	ns	*	ns	*	*

2.4 Functional characterization of genes related to adipose tissue remodeling and responding to high-fat diet using co-culture system in a niche-like setting

2.4.1 Establishment of co-culture system for modeling AP regulation

To investigate the functional role of identified genes, we established a co-culture system, in which Sca-1+ APs were seeded on top of feeders. One of the main advantages of this system is the single cell density of APs, which was not possible in classical monoculture because of high seeding density. This system allowed us to follow individual cells and the colonies

developing from them, which is important taking in consideration heterogeneity of AP population. Second, feeder cell layer provided a niche-like environment partially mimicking cell-cell interaction in the tissue *in vivo*, influencing gene expression and cell behaver by slowing proliferation of APs (Fig. 2.28).

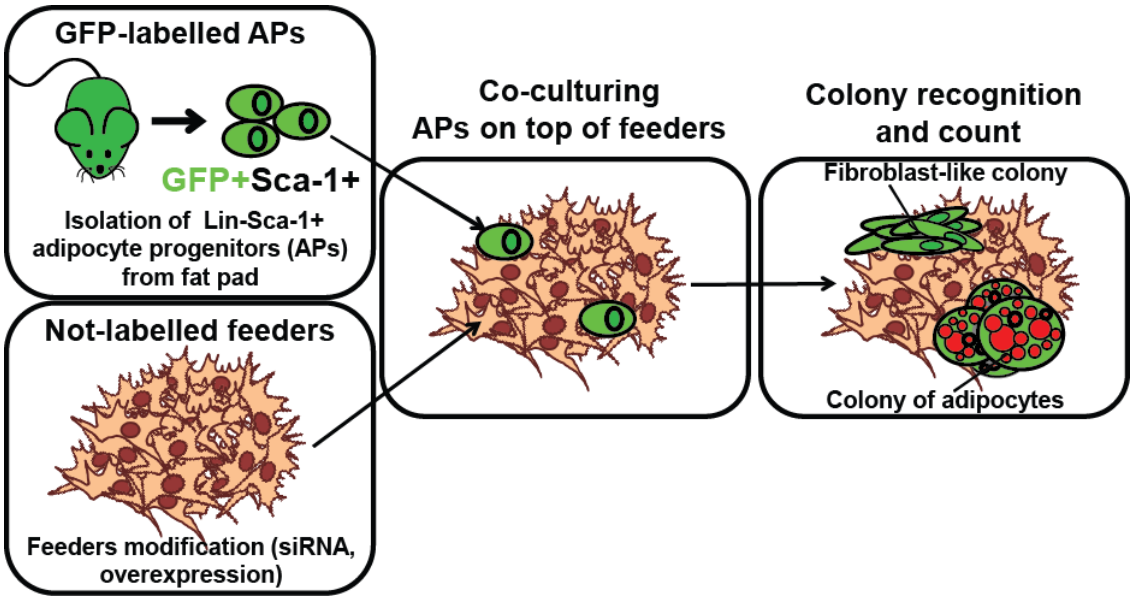

Figure 2.28: Scheme of co-culture system. Not-labeled feeders can be modified in order to mediate knockdown or overexpression for gene of interest. After isolation from adipose tissue GFP-labeled adipose progenitors (GFP+ Sca-1+ APs) are seeded on top of modified/unmodified feeders in the single cell density. In this moment different soluble factors can be added to the system. After co-culturing GFP+ APs form colonies with adipogenic and fibroblastic fate. To distinguish different colonies LipidTox staining can be utilized for natural lipids staining. Finally, colonies can be recognized and counted to asses function of the gene of interested in niche-like setting.

2.4.1.1 Testing GFP+ mice strains

In order to track and distinguish adipose progenitors from other cell types in a co-culture system, cells expressing detectable levels of GFP were introduced to the system. Two mice strains expressing enhanced GFP ubiquitously were tested: C57BL/6-Tg(UBC-GFP)30Scha/J and STOCK Tg(CAG-EGFP)D4Nagy/J. Lin-Sca-1+ progenitor cells (APs) were isolated from gWAT, ingWAT, isBAT and tested for their ability to sustain GFP signal during proliferation and differentiation in monoculture *in vitro*. Progenitor cells from mice without GFP served as negative control. Only cells derived from C57BL/6-Tg(UBC-GFP)30Scha/J mice strain expressed GFP on a detectable level with standard microscopy (Fig. 2.29 – A). To promote differentiation *in vitro*, we used common inducers of adipogenesis such as insulin, dexamethasone, 3,3'5'-triiodothyronine (T3), isobutylmethylxanthine (IBMX), prostacyclin (PGI2) and rosiglitazone (Rosi) (see materials and methods 4.2.1). Adipose progenitor cells from UBC-GFP mice differentiated with the same efficiency as cells derived

from control mice in depot- specific manner while sustaining high GFP signal (Fig. 2.29 – B). Therefore, these cells were further used in experiments.

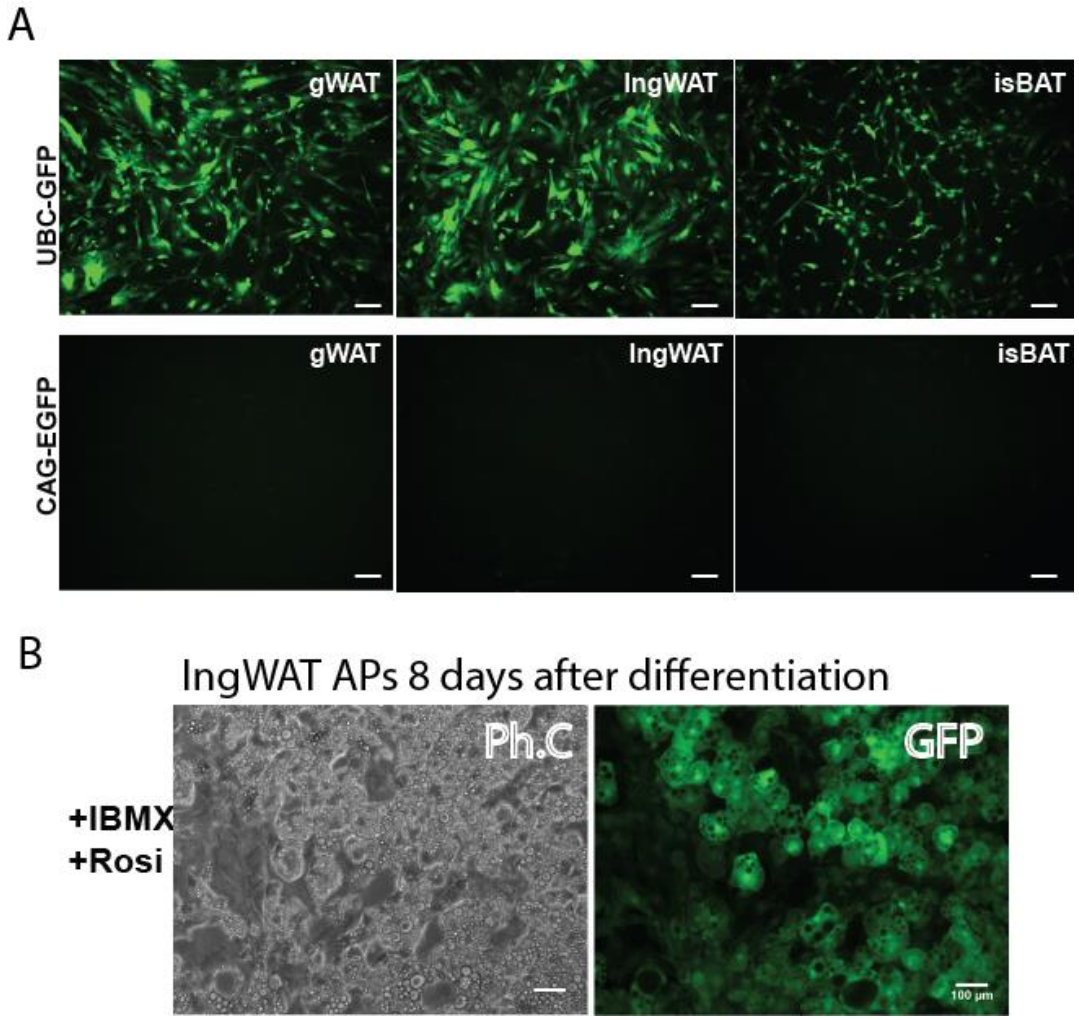

Figure 2.29: Comparison of GFP-signal intensity of cells isolated from two different mice strains. Sca-1+ adipose progenitors (APs) were isolated from three different fat depots: perigonadal WAT (gWAT), inguinal WAT (lngWAT) and interscapular brown adipose tissue (isBAT) of two mice strains expressing enhanced GFP ubiquitously: C57BL/6-Tg(UBC-GFP)30Scha/J (UBC-GFP) and STOCK Tg(CAG-EGFP)D4Nagy/J (CAG-GFP). **A)** Florescent microscopy of APs monoculture, scale bar, 100 µm. **B)** lngWAT APs from UBC-GFP were differentiated in a presence of isobutylmethylxanthine (IBMX) and rosiglitazone (Rosi) for 8 days. Phase contrast (Ph.C) and florescent (in GFP channel) images with differentiated adipocytes are represented, scale bar, 100 µm.

2.4.1.2 Feeder types and growing conditions for co-culture system

Several feeder systems were tested to address different questions. To mimic the physiological niche, differentiated to mature adipocytes pre-adipocyte cell lines (derived from mouse embryo fibroblasts) C3H10T1/2 were used. The C3H10T1/2 line can be terminally differentiated to adipocytes by presence of rosiglitazone (Rosi). Using this feature of the cell line, it is possible to obtain completely differentiated feeders with Rosi or just arrest the cells before accumulating lipid (Appendix Fig. 5). In the first experiment, C3H10T1/2 cells, which were induced to differentiate with or without Rosi (dif-C3H/ undif-C3H, respectively), were used

as feeders. ingWAT GFP+ APs were seeded on top of feeders with or without the potent growth factor - basic fibroblast growth factor (bFGF), promoting proliferation and survival of APs. Growth factors in the serum play an important role in AP proliferation/differentiation and were used to determine potential sensitivity of the system to growth factors. After 4 days of co-culturing, we observed first forming colonies (Fig. 2.30 – A). Colonies were counted manually and a significant interaction between stage of feeder differentiation and presence of bFGF was witnessed by two-way ANOVA. There were two times more colonies in the presence of bFGF on undif-C3H, but no effect of bFGF was observed when used differentiated feeders (Fig. 2.30 – B). After 10 days, GFP+ cells had spontaneously differentiated into adipocytes without any differentiating stimulus, which has not been yet achieved in standard monoculture (Fig. 2.30 – C). This result showed that a co-culture system is suitable to mimic the *in vivo* microenvironment and promotes natural cell fate. Additionally, functional heterogeneity inside of Lin-Sca-1+ progenitor population was observed. Some colonies differentiated into adipocytes, whereas others exhibited fibroblastic morphology (Fig. 2.30 – D). We concluded that co-culture system with feeder layer provided differentiation signals for progenitor cells and can be used for functional validation of target genes.

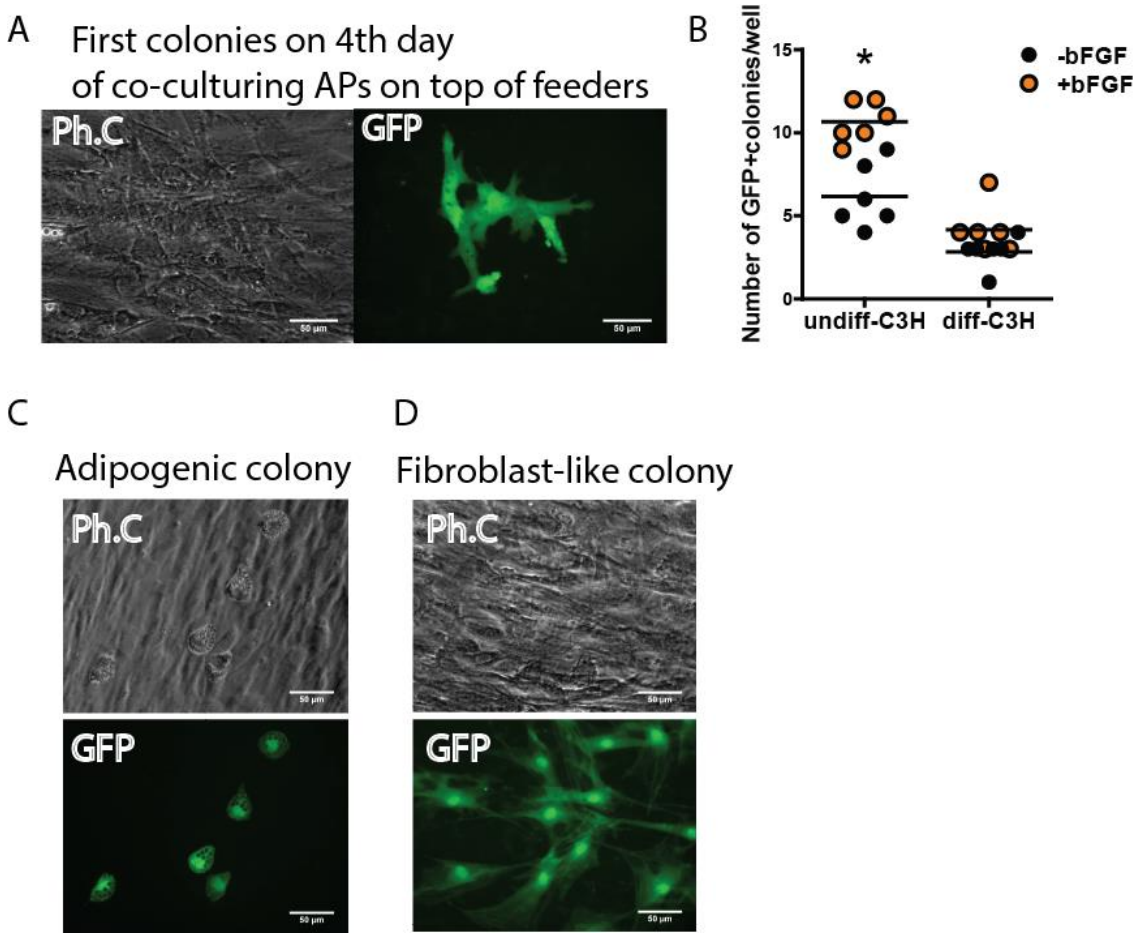

Figure 2.30: Colony formation in co-culture system. A) IngWAT APs gave rise to GFP+ colonies several days after seeding. Phase contrast (Ph.C) and florescent (in GFP channel) images of representative colony 4 days after seeding on top of undifferentiated C3H10T1/2 cells (undiff-C3H), scale

bar, 50 µm. **B)** Number of GFP+ colonies per well formed on undiff-C3H or differentiated C3H10T1/2 (diff-C3H) in presence bFGF (+bFGF) or absence (-bFGF) 4 days after seeding, each dot represents count per well, line is mean of the group, two-way Anova with Bonferroni post-hoc test was used to assess significance, *, pV< 0.05. **C)** Phase contrast (Ph.C) and florescent (in GFP channel) images of IngWAT GFP+ adipogenic and **D)** fibroblast-like colony formed on top of undiff-C3H 8 days after seeding, scale bar, 50 µm. bFGF - basic fibroblast growth factor.

2.4.1.3 Assessment of differentiation of APs in co-culture system

To test the ability of the co-culture system to provide a better environment to detect AP proliferation and differentiation upon gene expression manipulation, C3H10T1/2 cells were used as feeders, this time treated with Mitomycin C to prevent overgrowth (Appendix Fig. 5). We seeded GFP+ Sca-1+ progenitor cells from ingWAT on top of feeders in different growth conditions (Fig. 2.31 – A). In first 3 conditions, initial 2 days cells were cultured with bFGF or IGF-1 or control cells had no additional growth factors, after that growth factors were replaced with insulin until the end of experiment (Fig. 2.31 – A). In condition 4, 5 and 6, cells were grown ether without any additional factors or with insulin or with insulin + IGF1 for whole time of experiment (Fig. 2.31 – A). After 10 days, cells were fixed and stained with LipidTox to visualize lipid droplets (Fig. 2.31 – B). LipidTox positive colonies were manually counted and significantly more colonies with differentiated APs upon initial bFGF treatment were observed (Fig. 2.31 – C). Interestingly, the initial two-day treatment with IGF-1 did not lead to a higher number of colonies. The number of adipocytes inside of the colony was also manually counted (Fig. 2.31 – D). There was a shift in the frequency distribution upon bFGF treatment towards higher number of differentiated APs (Fig. 2.31 – D, E). Insulin or insulin combined with IGF-1 had no effect on number of colonies or number of cells inside of colony compared with control condition for whole course of experiment (Fig. 2.31 – F, G). These data indicated that using co-culture system allows us to identify factors influencing AP differentiation, e.g. IGF-1 and insulin had no effect on AP proliferation/differentiation. However bFGF seems to be important growth factor promoting AP proliferation and was included in following screening experiments.

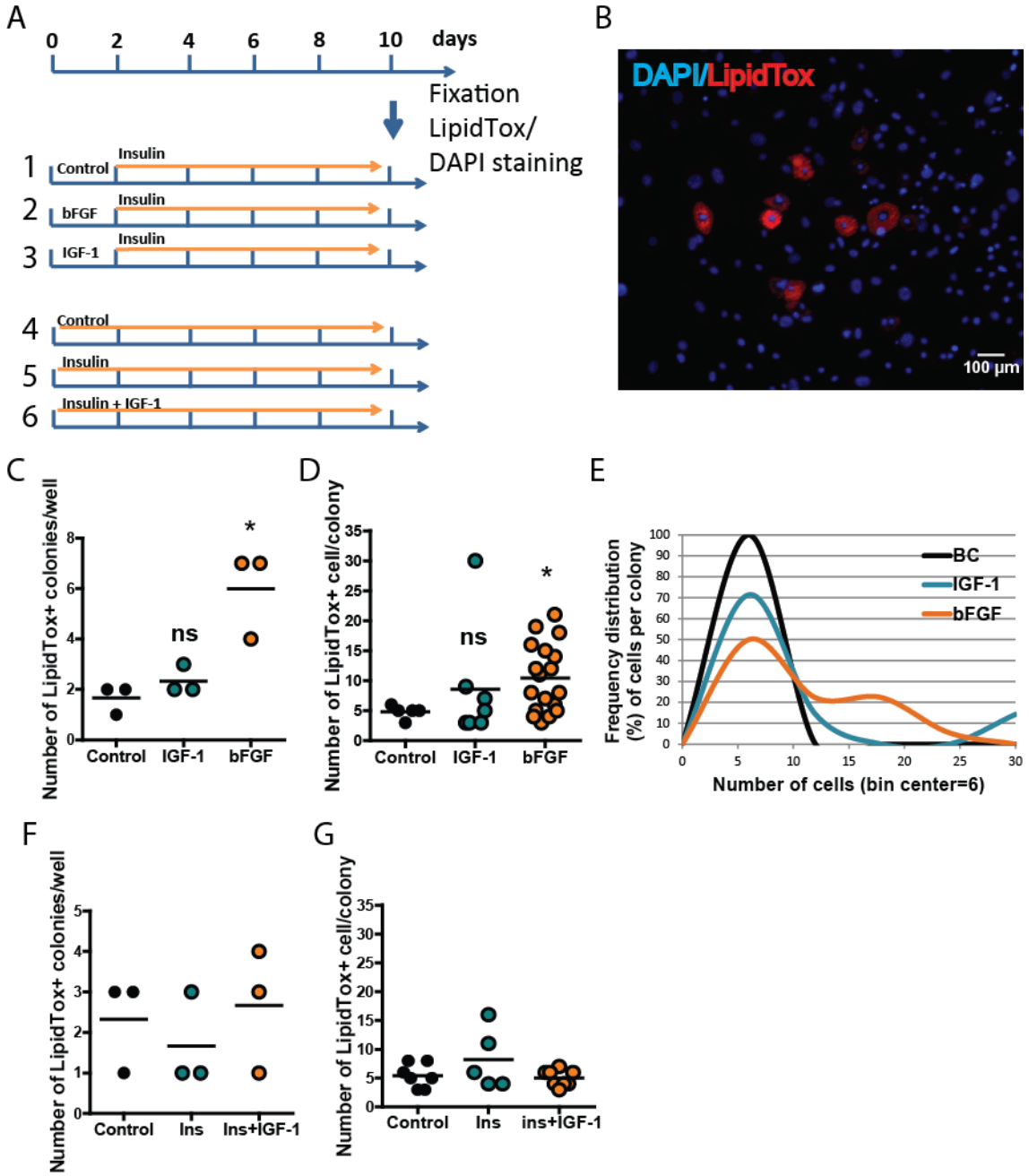

Figure 2.31: Assessment of adipogenesis in co-culture system. A) Experimental design: ingWAT GFP+ Sca-1+ APs were seeded on top of mitomycin C-treated C3H10T1/2 feeders in 6 different growing conditions: for initial days media was supplemented with bFGF (2) or IGF-1 (3) vs. control without any additives (1). After 2 days all cell were cultured in presence of insulin. Alternatively cells were cultured with insulin (5) or insulin and IGF-1 (6) vs. control without any additives (4) for whole course of experiment. Co-cultures were fixed after 10 days, stained with DAPI/LipidTox. **B)** Representative image of adipogenic LipidTox positive colony, scale bar, 100 µm. **C)** Number of LipidTox+ colonies per well upon control, IGF-1 and bFGF treatment for 2 initial days. **D)** Number of LipidTox+ cells per colony upon control, IGF-1 and bFGF treatment for 2 initial days. **E)** Relative frequency distribution (%) of cells per colony from D, bin center = 6 cells. **F)** Number of LipidTox+ colonies per well upon control, insulin (Ins) and insulin combined with IGF-1 treatment (Ins+IGF-1) for whole course of co-culture. **G)** Number of LipidTox+ cells per colony upon control, Ins and Ins+IGF-1 treatment for whole course of co-culture. For C, F each dot represents count per well, for D, G each dot represents count per colony, line is mean of the group, one-way Anova with Tukey's post-hoc test was used to assess significance, *, comparison with Control, pV< 0.05, ns, no statistically significant difference. bFGF- basic fibroblast growth factor, IGF-1 - insulin-like growth factor 1.

2.4.1.4 Developing an automated system for colony recognition and count

To increase and automate the data acquisition, an automated high content microscopy assay protocol was developed. Images were automatically acquired in 3 channels (100 pictures per channel - 30% of one 24- well) and analyzed. It is possible to observe difference between conditions in colony size, numbers, ratio GFP+ colonies/LipidTox+ colonies. For instance, GFP+ progenitors proliferated faster and had bigger area of colonies after prostacyclin treatment (cPGI2) that known as a specific effector of adipogenesis (Fig. 2.32).

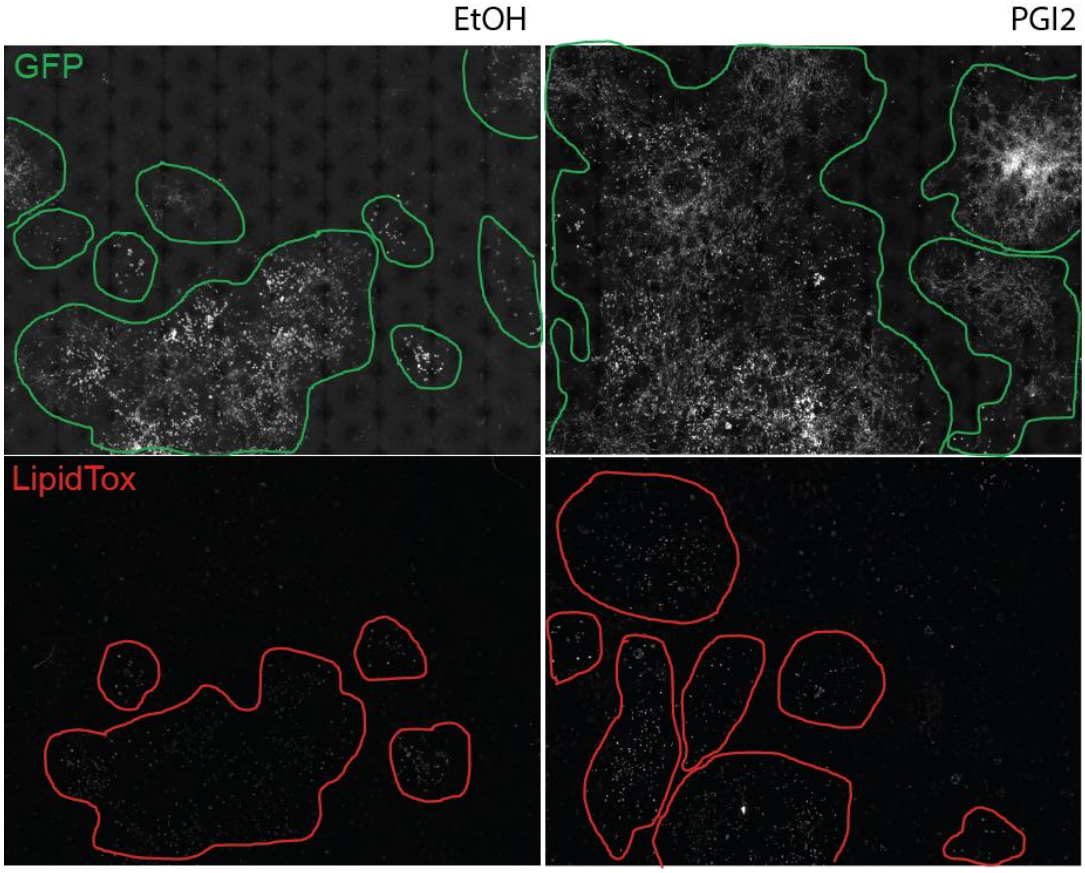

Figure 2.32: Developing of automated system for colony recognition and count. Upper panel represents GFP+ colonies, lower panel – LipidTox+ colonies on top of feeders with presence/ absence of prostacyclin (PGI2) treatment (etanol, EtOH serves as control). Stitched images from one well for GFP/LipidTox channels. Manual colony recognition was performed.

Further algorithms for image data analysis (GFP+/LipidTox colony recognition and count) were established. Automatic algorithms using KNIME Analytics Platform were created for colony recognition and count. A virtual stitching algorithm was created to analyze multiple images from one well. Analysis included assessment of proliferation by number (N) of GFP+ cells and differentiation capacity by N of double positive GFP+ LipidTox+ cells. First all nuclei were segmented based on DAPI staining and had individual labels, then each nucleus was crosschecked in the GFP channel based on the maximum intensity measurement around the nucleus. If the nucleus was assigned as GFP+, then it was checked in the LipidTox channel. Analysis was classified in two levels: cellular level (N of GFP+ cells per well/ per colony, N of

GFP+ LipidTox+ cells per well/ per colony) and colony level (N of GFP+ colonies per well, area of GFP+ colonies, N of GFP+ LipidTox+ colonies). This algorithm was further used for automated screening.

2.4.1.5 Development of an automated screening for characterization of candidate genes

To test established protocols for automated screening for distinct growth conditions, ingWAT GFP+ APs were seeded on top of two types of feeders, Mit-C treated C3H10T1/2 and 3T3-L1 (Appendix Fig. 5), in 4 different growing conditions (Fig. 2.33 – A). Co-culturing cells were fixed and stained with LipidTox/DAPI. Microscopy and image data analysis were performed according to the protocol developed in this project. When C3H10T1/2 was used as feeder, there were more colonies and we could discriminate differences between growing conditions (Fig. 2.33 – B, C.). It was same trend of increased number of colonies upon bFGF treatment as during manual count in section 2.4.1.2. Also we could confirm previous observation from section 2.4.1.3 that upon bFGF treatment during 2 initial days of co-culture number of LipidTox+ colonies was higher compared with control (Fig. 2.33 – E.). Only on C3H10T1/2 feeders this phenotype was exhibited, but not on 3T3-L1 (Fig. 2.33 – D). For further investigations we used only C3H10T1/2 feeders.

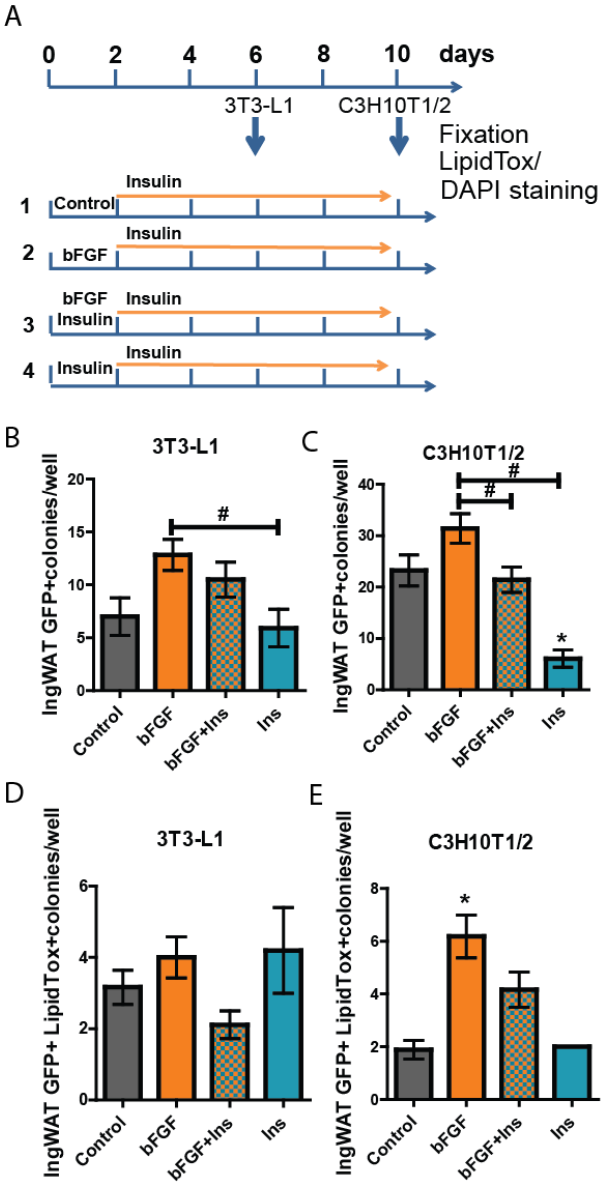

Figure 2.33: Automated screening for validation on example of different growing conditions. A) Experimental design: GFP+ APs were seeded on top of MitC-treated C3H10T1/2 and 3T3-L1, in 4 different growing conditions: for initial days media was supplemented with bFGF or insulin or combination of bFGF and insulin vs. control without any additives. After 2 days all cell were cultured in presence of insulin. On 6th day and 10th day of co-culturing on top of 3T3-L1 and C3H10T1/2, respectively, co-cultures were fixed. After staining an automated imaging was performed and algorithm for colony recognition was tested. **B)** Number of ingWAT GFP+ colonies per well after co-culturing on top of 3T3-L1 feeders. **C)** Number of ingWAT GFP+ colonies per well after co-culturing on top C3H10T1/2 feeders. **D)** Number of ingWAT GFP+ LipidTox+ colonies per well after co-culturing on top of 3T3-L1 feeders. **E)** Number of ingWAT GFP+ LipidTox+ colonies per well after co-culturing on top of C3H10T1/2 feeders. For B-D data represented as mean ± SEM, 8-16 wells per condition were used for analysis, one-way Anova with Tukey's post-hoc test was used to assess significance, *, comparison with Control, pV< 0.05, #, comparison between indicated conditions, pV< 0.05. bFGF - basic fibroblast growth factor.

2.4.1.6 Optimizing siRNA treatment in feeder cells

Ultimately, the co-culture system should be used for functional characterization of candidate genes. To test the efficiency of siRNA transfection in feeder cells, 3T3-L1 and C3H10T1/2 were

transfected with siRNA against *Cited2* gene, which is highly expressed in both cell lines (Fig. 2.34 – A). Two different concentrations of siRNA were tested (5 and 20nM). Cells were harvested 3 and 10 days after transfection for testing silencing efficiency via qPCR. One of the concentrations (5nM) showed 85-90% and 72-78% 3 and 10 days after transfection, respectively in both cell lines (Fig. 2.34 – B, C). These data indicated that using optimized siRNA treatment protocol allows us to sustain knockdown during prolonged co-culture.

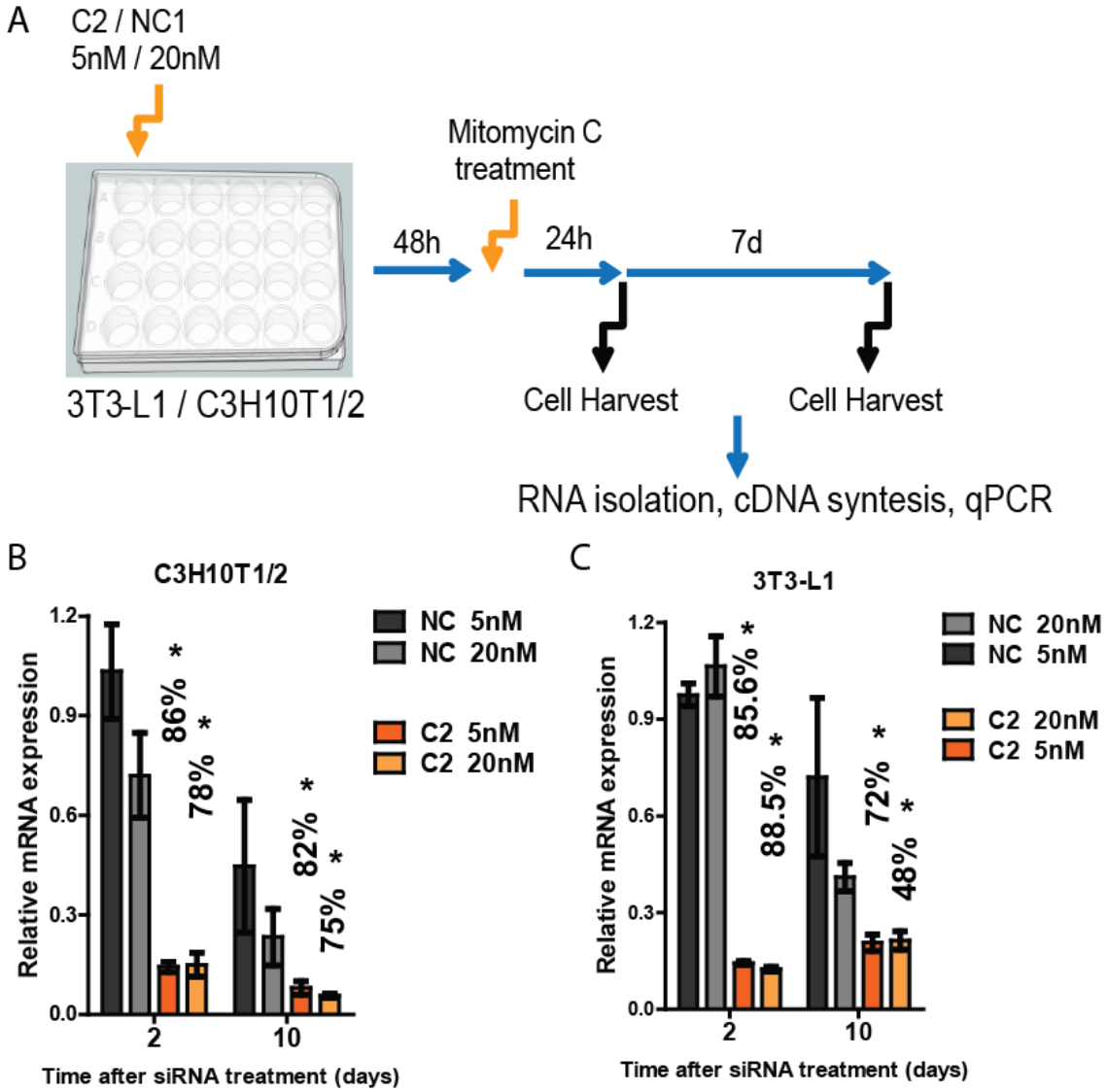

Figure 2.34: Measurement of siRNA knockdown efficiency in feeder cells. A) Experimental design: 3T3-L1 and C3H10T1/2 were transfected with siRNA against *Cited2* (C2) and negative control (NC) using 2 different concentrations 5 and 20nM, 2 days after cells were treated with Mitomycin C, RNA was isolated 2 and 10 days after transfection followed by cDNA synthesis and qPCR. **B)** Relative expression of C2 gene in C3H10T1/2. C) Relative expression of C2 gene in 3T3-L1. Data represented as mean ± SEM, efficiency of transfection was calculated in comparison with NC for each time point for each concentration, two-way Anova with Bonferroni post-hoc test was used to assess significance, *, pV< 0.05.

To conclude, a co-culture system was established with image analysis algorithms for automated assessment of proliferation and differentiation of adipose tissue progenitor cells. Automated algorithms were able to discriminate differences between growing conditions and

confirmed manual count observations indicating that the protocol developed for automated screening is sensitive to study candidate genes.

2.4.2 Functional validation of target genes in co-culture system

In order to characterize candidate genes found in our screening (section 2.3.4 – 2.37) we approached two different systems for each target: 1) in the co-culture system, gene knockdown in feeder cells for investigating niche-mediated effect on AP proliferation/ differentiation 2) in monoculture, AP knockdown for investigating direct effect on AP proliferation via EdU-labeling. We performed functional screening with several targets and two examples presented to illustrate abilities of functional screening via co-culture system.

2.4.2.1 Lumican as an example of gene with no co-culture phenotype

Lumican (*Lum*) is an extracellular matrix protein that involved in collagen fibrogenesis and suspected to be involved in cell proliferation (Nikitovic et al. 2008). Lumican upregulated in response to HFD (section 2.3.5) and highly expressed in Sca1+ APs. We hypothesize that this gene can be potentially involved in mediating APs proliferative response. Accordingly to biogps data *Lum* in not expressed in feeder cells and our first line strategy was to knock it down in APs monoculture. gWAT APs were seeded in monoculture with bFGF to induce growth of the cell, then cells were transfected with siRNA against *Lum* (2 different siRNAs) in comparison with negative control siRNA. Using EdU pulse 24 h after transfection to label proliferating cells and the automated algorithm to count the number of EdU-labeled nuclei and total number of nuclei, we demonstrated that *Lum* knockdown negatively regulated proliferation of APs (Fig. 2.35 – A). Additionally we used this gene as a negative control in co-culture screening, in which only feeder cells were transfected with siRNA against *Lum*. For co-culture experiment, GFP+ APs isolated from gWAT and ingWAT were seeded on top of feeders previously transfected with siRNA against *Lum* (Lum_1 and Lum_2). Afterward co-cultured cells were fixed and stained with LipidTox/DAPI (Fig. 2.35 – B). Following that, 96-well plates were screened and analyzed using the automated protocol described in section 2.4.1.4. The algorithm accessed cell proliferation by counting the number of GFP+ cells per well and per colony, GFP+ colonies per well and differentiation by the number of LipidTox+ cell/colonies inside GFP+ population. We did not observe consistently significant changes in the number of GFP+ cells (Fig. 2.35 – C) or colonies (Fig. 2.35 – D) as well as in LipidTox+ GFP+ cells (Fig. 2.35 – E) or colonies (Fig. 2.35 – F) from both fat depots.

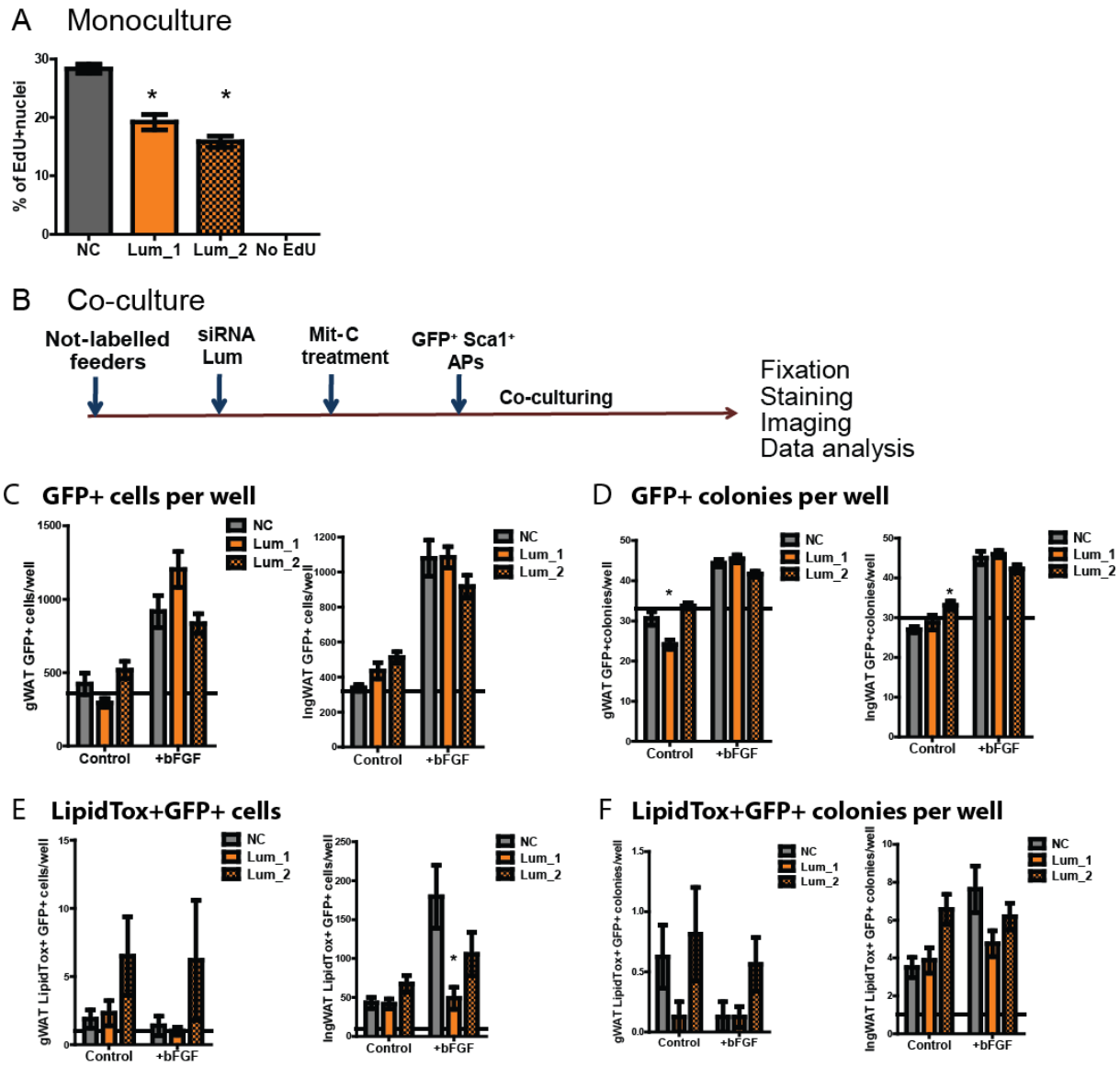

Figure 2.35: Effect of Lumican knockdown on AP proliferation and differentiation in monoculture and co-culture systems. A) Sca-1+APs isolated from perigonadal WAT (gWAT) were transfected with *Lum* siRNA (Lum_1 and Lum_2) vs. negative control siRNA (NC), after 2 days rate of proliferation was measured via Edu-labeling, data represented as mean ± SEM, one-way Anova with Tukey's post-hoc test was used to assess significance, *, comparison with NC. **B)** Experimental design: not-labeled C3H10T1/2 feeders were seeded, transfected with siRNA against *Lum* and with NC following by mitomycin C (MitC) treatment. GFP+ Sca-1+ APs isolated from gWAT and inguinal WAT (ingWAT) of 4-week old female mice were seeded on top of feeders with knockdown of *Lum*, co-cultured without (control) or with bFGF (+bFGF) for initial days, then after one week fixed, stained with DAPI/LipidTox and imaged. **C)** Number of gWAT and ingWAT GFP+ cells per well after co-culturing on top of feeders transfected with negative NC, Lum_1, Lum_2 without (control) or with bFGF (+bFGF). **D)** Number of gWAT and ingWAT GFP+ colonies per well after co-culturing on top of feeders transfected with negative NC, Lum_1, Lum_2 without (control) or with bFGF (+bFGF). **E)** Number of gWAT and ingWAT LipidTox+ GFP+ cells per well after co-culturing on top of feeders transfected with negative NC, Lum_1, Lum_2 without (control) or with bFGF (+bFGF). F) Number of gWAT and ingWAT LipidTox+ GFP+ colonies per well after co-culturing on top of feeders transfected with negative NC, Lum_1, Lum_2 without (control) or with bFGF (+bFGF). For C-F data represented as mean ± SEM, 8-16 wells were used for analysis, two-way Anova with Bonferroni post-hoc test was used to assess significance, *, comparison with NC of each condition, pV< 0.05, dashed line is level of background based on GFP-feeders. bFGF -basic fibroblast growth factor.

These data indicated that although knockdown of *Lum* had direct effect on AP proliferation in monoculture, we did not observe niche mediated effect, which served us a control of specificity in co-culture screening.

2.4.2.1 EMP gene family modulate AP response through the niche

Two genes from the EMP family (EMP1 and EMP3) were selected from our candidate gene list. EMP-1 is involved in tight-junctions formation (Durgan et al. 2015), thus cell remodeling. *Emp1* and *Emp3* was upregulated upon HFD, when compared with CD (Fig. 2.24 – B and Fig. 2.25 – B). Both genes were expressed in feeders and their role in adipose cell biology was still unknown. For co-culture experiment, GFP+ APs isolated from gWAT and ingWAT were seeded on top of feeders previously transfected with siRNA against *Emp1* and *Emp3*. After co-culture cells were fixed and stained with LipidTox/DAPI (Fig. 2.36 – A). Following, 10 96-well plates were screened and analyzed using the automated protocol described in section 2.4.1.4. First controls were analyzed. No effect of transfection was observed when compered negative control siRNA (NC) and non-treated cells (NT, only transfection reagents) for both fat depots gWAT and ingWAT (Fig. 2.36 – B, C). Also level of background was set accordingly GFP-feeder cells (Fig. 2.36 – B, C). Treatment with bFGF for 2 initial days of co-culture served us as positive control and as it was observed previously addition of bFGF increases cell count (Fig. 2.36 – B, C). When we mediated knockdown either *Emp1* or *Emp3* in feeder cells, a decrease in the number of GFP+ cells compared with NC was observed for both growing conditions (control and +bFGF) in ingWAT (Fig. 2.36 – E). However, in gWAT the decrease was significant only in combination with bFGF (Fig. 2.36 – D). The same results for colony count with all described above controls (Fig. 2.36 – F, G, H, I). These data suggested that mediated in feeders knockdown of *Emp1* and *Emp3* played a role in AP proliferation.

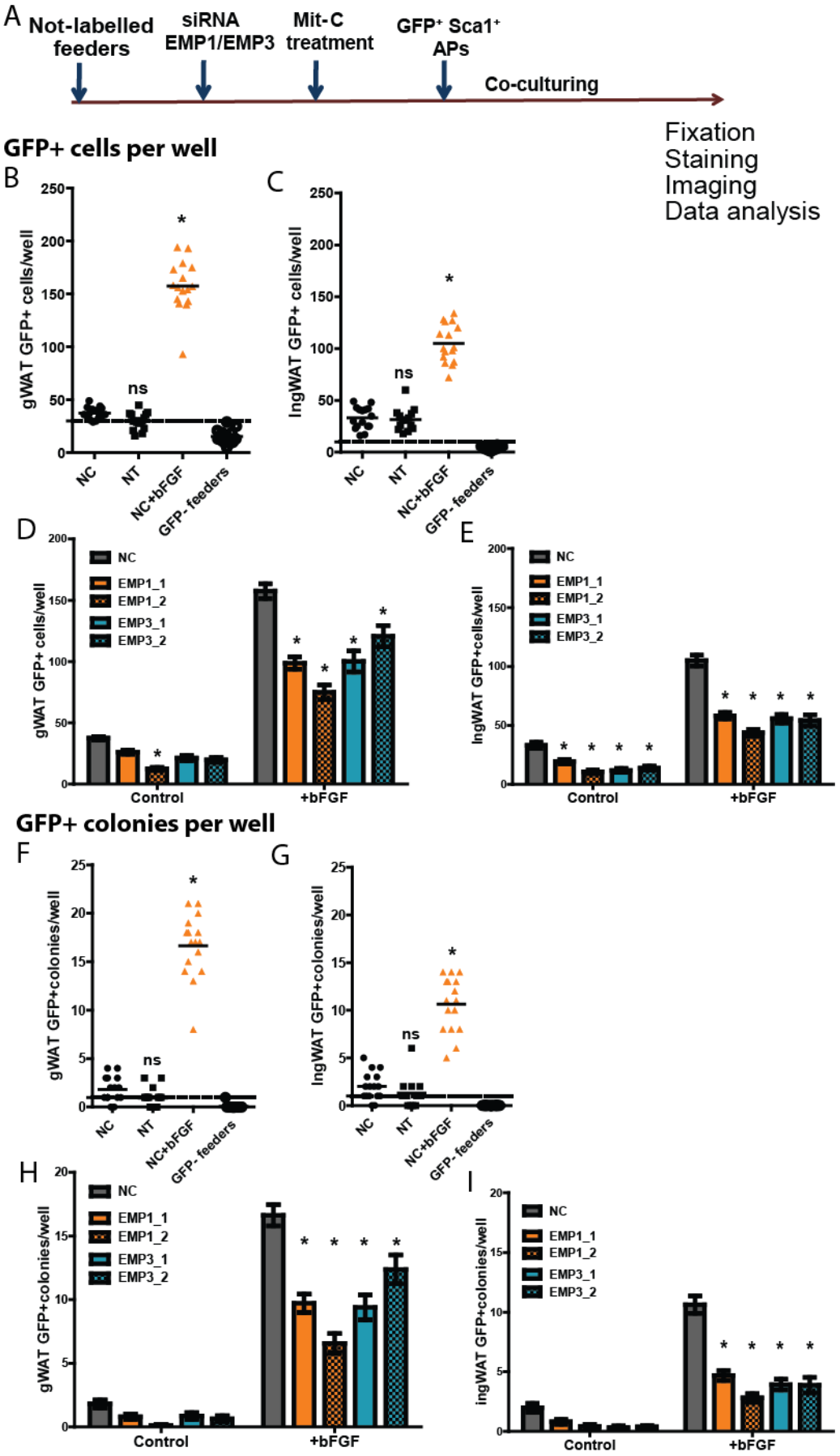

Figure 2.36: Effect of *Emp1* and *Emp3* knockdown in the feeder cells on proliferation of adipose progenitors. A) Experimental design: not-labeled C3H10T1/2 feeders were seeded, transfected

with siRNA against EMP1 (EMP1_1 and EMP1_2), EMP3 (EMP3_1 and EMP3_2) and with negative control siRNA following by mitomycin C (MitC) treatment. GFP+ Sca-1+ APs isolated from perigonadal WAT (gWAT) and inguinal WAT (ingWAT) of 4-week old female mice were seeded on top of feeders with knockdown of *Emp1* and *Emp3*, co-cultured without (control) or with bFGF (+bFGF) for initial days, then after one week fixed, stained with DAPI/LipidTox and imaged. **B)** Number of gWAT GFP+ cells per well after co-culturing on top of negative control (NC) and NC with bFGF (NC+bFGF), not treated feeders (NT). **C)** The same as B for ingWAT. **D)** Number of gWAT GFP+ cells per well after co-culturing on top of feeders transfected with negative control (NC), EMP1_1, EMP1_2, EMP3_1, EMP3_2 siRNAs without (control) or with bFGF (+bFGF). **E)** The same as D for ingWAT. **F)** Number of gWAT GFP+ colonies per well after co-culturing on top of NC and NC+bFGF, NT. **G)** The same as F for ingWAT. **H)** Number of gWAT GFP+ colonies per well after co-culturing on top of feeders transfected with NC, EMP1_1, EMP1_2, EMP3_1, EMP3_2 siRNAs in control or +bFGF. **I)** The same as H for ingWAT. For B, C, F, G each dot represents count per one well, line is mean of the group, one-way Anova with Tukey's post-hoc test was used to assess significance, *, comparison with NC, $pV < 0.05$, dashed line is level of background based on GFP-feeders. For D, E, H, I data represented as mean ± SEM, 8-16 wells were used for analysis, two-way Anova with Bonferroni post-hoc test was used to assess significance, *, comparison with NC of each condition, $pV < 0.05$. bFGF -basic fibroblast growth factor.

The second part of analysis was assessment of differentiation of co-cultured cells. Increased number of LipidTox+ colonies and cells were observed before (section 2.4.1.3) upon bFGF treatment using ingWAT APs, when counted manually. In this experiment we could confirm the same trend for ingWAT cells (Fig. 2.37 – B). Interestingly, APs from gWAT had the opposite phenotype and the number of LipidTox+ cells were reduced upon bFGF treatment (Fig. 2.37 – A). There was no significant difference between siRNA treatment in number of LipidTox+ cells in both gWAT and ingWAT (Fig. 2.37 – C, D). These data indicated that mediated in feeders knockdown of *Emp1* and *Emp3* had no effect on AP differentiation.

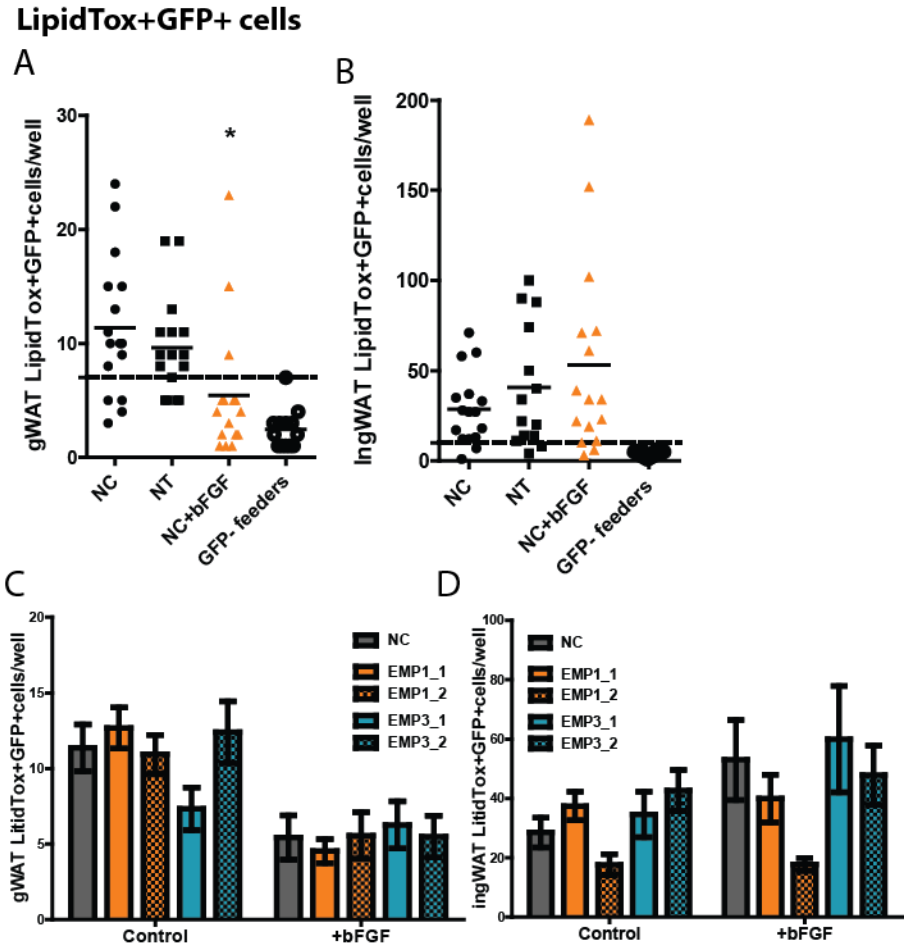

Figure 2.37: Effect of *Emp1* and *Emp3* knockdown in the feeder cells on differentiation of adipose progenitors. A) Number of gWAT GFP+ LipidTox+ cells per well after co-culturing on top of negative control (NC) and NC with bFGF (NC+bFGF), not treated feeders (NT). **B)** The same as A for ingWAT. **C)** Number of gWAT GFP+ LipidTox+ cells per well after co-culturing on top of feeders transfected with NC, EMP1_1, EMP1_2, EMP3_1, EMP3_2 siRNAs without (control) or with bFGF (+bFGF). **D)** The same as C for ingWAT. For A, B each dot represents count per one well, line is mean of the group, one-way Anova with Tukey's post-hoc test was used to assess significance, *, comparison with NC, pV< 0.05, dashed line is level of background based on level of spontaneous differentiation of feeder cells. For C, D data represented as mean ± SEM, 8-16 wells were used for analysis, two-way Anova with Bonferroni post-hoc test was used to assess significance. bFGF - basic fibroblast growth factor.

To investigate the direct effect of *Emp1* and *Emp3* knockdown on AP proliferation in monoculture we employed cell count and EdU-labeling. gWAT APs were seeded in monoculture with bFGF to induce growth of the cell, then cells were transfected with siRNA against *Emp1* and *Emp3* (3 different siRNAs per target) in comparison with negative control siRNA. Cells were manually counted daily up to 3 days after transfection. There was no effect of siRNA treatment on growth of gWAT APs (Fig. 2.38 – A). To confirm these data we used EdU pulse 24 h after transfection to label proliferating cells and used the automated algorithm (method section 4.5.2) to count the number of EdU-labeled nuclei and total number of nuclei. No direct effect of *Emp1* and *Emp3* transfection on ration of proliferating cells was observed, in agreement with our previous results (Fig. 2.38 – B).

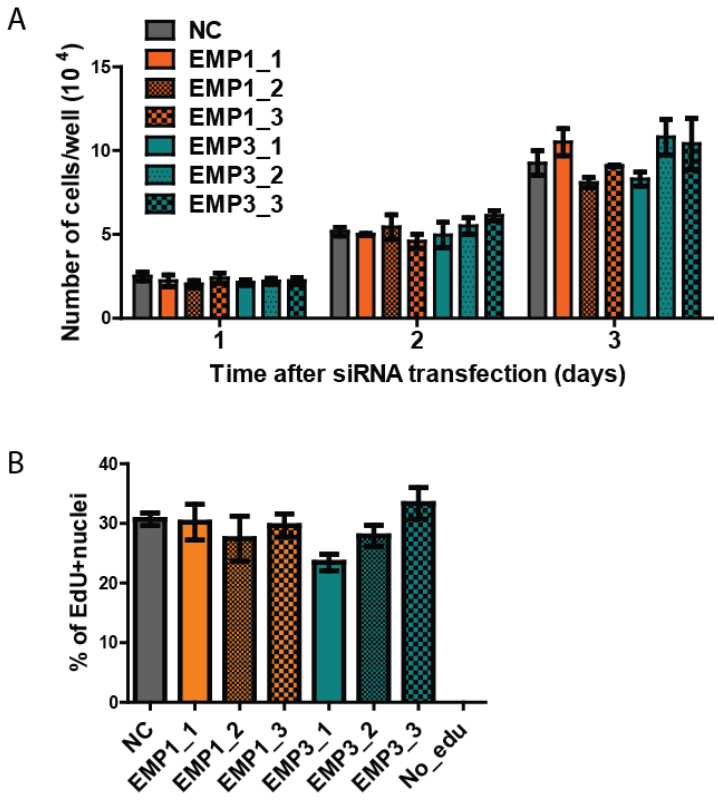

Figure 2.38: Effect of *Emp1* and *Emp3* knockdown on proliferation of adipose progenitors in monoculture. Isolated from perigonadal WAT (gWAT) Sca-1+ APs were seeded and transfected with siRNA agents *Emp1* (EMP1_1, EMP1_2 and EMP1_3), *Emp3* (EMP3_1, EMP3_2 and EMP3_3), and negative control (NC) **A)** Number of cell per well 1, 2 and 3 days after transfection with siRNAs. Data represented as mean ± SEM, 3 wells per condition were used, two-way Anova with Bonferroni post-hoc test was used to assess significance. **B)** Present (%) of EdU+ nuclei 2 days after transfection with siRNAs, data represented as mean ± SEM from 3 wells (5 images per well), one-way Anova with Tukey's post-hoc test was used to assess significance.

To confirm and further investigate effect of *Emp1* knockdown in feeders on proliferation of APs another co-culture experiment was performed by master student Wujun Hong supervised by me. In this experiment GFP+ APs were seeded on top of feeders transfected with empty vector pcDNA3.1 or overexpression construct pCMV-EMP1 and siRNA again *Emp1* vs. negative control siRNA. After 4 days of co-culture, EdU pulse were applied to label proliferating cells, then cells were fixed and analyzed by FACS. We demonstrated that upon overexpression in feeders % of GFP+ cells were increased and upon siRNA treatment decreased (Fig. 2.39 – A). However % GFP+ EdU+ cells were not changed among conditions, indicating that feeder-mediated changes in % of GFP+ cells were not due to proliferation. The next steps are measure feeder-mediated adhesion and apoptosis of APs.

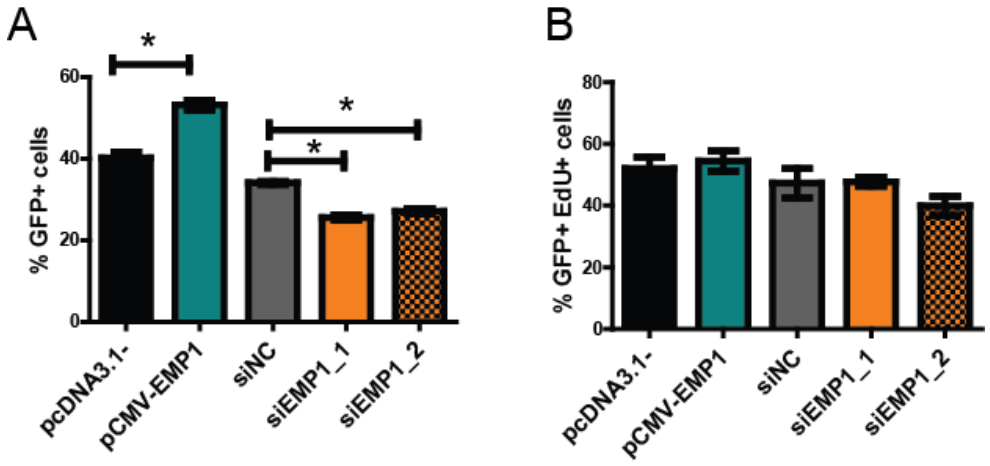

Figure 2.39: Effect of *Emp1* overexpression and knockdown on proliferation of adipose progenitors in co-culture. Experiment performed by Wujun Hong. GFP+ APs were seeded on top of feeders transfected with: empty vector pcDNA3.1 or with overexpression vector pCMV-EMP1, siRNA against *Emp1* (EMP1_1 and EMP1_2). After 4 days of co-culturing EdU pulse were performed and cells were fixed and analyzed by FACS. A) % of GFP+ cells B) % of GFP+ EdU+ cells. Data represented as mean ± SEM from 3 samples, each sample contained 2 pooled wells, one-way Anova with Tukey's post-hoc test was used to assess significance, *, comparison with NC of the group, pV< 0.05.

These data underlined that *Emp1* had no direct effect on AP proliferation but acted through another type of cells via cell-cell communication and affected number of APs.

3. DISCUSSION

3.1 Long-term impact of HFD feeding on young mice: WAT remodeling

We demonstrated that adipose tissue of young sexually immature mice grew rapidly in response to excess calories. In fact, HFD increased body weight, fat mass due to increased number of Sca-1+APs after one week of feeding of sexually immature female mice, but not adult female mice. These data were in line with other studies showing age-dependent decline of adipose tissue plasticity in mice (Kim et al. 2014) and human (Spalding et al. 2008). These data indicated that early remodeling of WAT is the set point for future metabolic outcome of adult tissue. Moreover, we have observed that the determination of AP cell fate occurs rapidly upon HFD, leading to visible phenotype upon 7 days of diet. It is interesting to notice that there seems to be a short window in time that can lead to significant consequences for the WAT constitution throughout the whole lifespan of a mouse. Although obesity is tightly associated with development of cardiovascular diseases and mortality, little is known about long-term impact of increased number of cells in adipose tissue during childhood. We can hypnotize that increased number of adipose progenitors in response to dietary challenges can be beneficial to future metabolic condition, since these cells can give rise to mature adipocytes and store more lipids preventing lipotoxicity of other tissues. Based on our experiments so far, we are still not able to have a clear picture of long-term impact, but we had a hint. During the experiment with the addition of sweetened beverage, we observed increased liver size upon sucrose/fructose treatment only in control diet, but not in high-fat diet. Potentially after hyperplastic response on high-fat diet, adipose tissue can store more energy preventing from ectopic accumulation in other organs, e.g. liver. Further experiments, considering initial HFD challenge, followed by CD (wash out effect) and re-challenge with HFD, are planned and could give more information on tissue memory upon diet stimuli. We still need to demonstrated direct prove that APs do not proliferate in adult mice upon one week of HFD employing EdU-labeling approach. Moreover, we have found target genes, e.g. *Fmr1*, *Bmper, Traf4, Vcan* which were exclusively differentially expressed in young mice upon HFD, but not in adults. As some of these genes could be involved in early adipose tissue remodeling, they could be used to potentially restore loss of plasticity in adults.

3.2 Sex-dependent proliferation of APs

There are some studies on adipose tissue proliferation in young male mice (Kim et al. 2014), but not female. To us, it was important not only to better define the window of time where HFD would lead to cell proliferation, but also to identify possible sex-specific differences. Two studies in male mice have shown slightly discrepant results. In the first, young male mice have proliferation in both fat depots (scWAT and vWAT) upon HFD (Kim et al. 2014). However, in the second, only APs from vWAT proliferated in response to HFD in

male adolescent mice (Jeffery et al. 2015). It is important to notice that there was a difference between the age of mice used in these studies (4 weeks and 6-8 weeks, respectively), which can explain that younger mice had diet-induced proliferation in both depots. Therefore, determining the earliest time point when phenotypical difference upon HFD could be observed had an importance. We demonstrated that APs from both fat depots proliferate in response to HFD in young female mice. Our data is consistent with recent study demonstrating sex- and depot-specific differences in response to HFD showing that adipogenesis occurs in both depots in female and only in vWAT in male (Jeffery et al. 2016). The limitation of this study was an adult age of used mice 6-8 weeks, so they still cannot conclude was sex-specific response determined by age. To address this question, we plan to conduct short-term HFD study with EdU- labeling using young sexually immature male mice.

3.3 Dietary fat content triggers expansion of adipose tissue in early development via hyperplasia

Most of obesity related conclusions were done based on diet-induced rodent models, in which animals consuming excess amount of calories upon HFD *ad libitum* compared with CD matched by protein content, but enriched with carbohydrates. However limitation of this model was that there were 2 factors interacting and contributing to results: mice upon HFD consuming more calories and two diets have different composition. To overcome this limitation and investigate the impact of food components to WAT growth we used isocaloric pair feeding approach, in which mice received restricted HFD equal to consumed calories from CD group. We demonstrated that dietary fat triggered proliferation of APs, but did not lead to WAT gain. We do not know about impact of this initial proliferation induced by dietary fat content and further experiments are required to address this point. Nevertheless, as lipids are the main component stored in adipocytes, we could hypothesize that an excess of fat content of the diet could trigger a signaling cascade, leading to a higher number of APs, which could give rise to adipocytes and allowing more efficient storage of the excess of calorie intake.

3.4 High sugar content does not induce additional adipose tissue weight gain

Another important observation regarding food composition was that the supplying of sweetened beverage, meaning additional calories, had no effect on WAT gain on both CD an HFD diet. Although we did not observe significant changes in glucose homeostasis, we still are not able to claim, that quality of adipocytes and functional property of WAT was not changed due to lack of functional studies. However we observed that upon CD many insulin responding genes were upregulated, level of insulin was higher after 2 days and level of EdU-labeling of AP was quit high (30-40%) compared with other studies in which it was less than 10% in both male in female adolescent mice (Jeffery et al. 2015), (Jeffery et al. 2016).

These observations gave us an idea that because of enriched sucrose content in CD no additive effect could be achieved with sucrose/fructose in drinking water. The effect of sweetened beverage on acute AP proliferation and long-term consciences plan to be tested, since now new matched CD with lower sucrose content is commercially available. We can conclude that nutrient content is very important for experiment design and type of diet can have a major impact in the outcome of experiments.

3.5 Contributions of adipocyte hypertrophy to AP proliferation

According to current paradigm, mature adipocytes grow via hypertrophy till their size limit upon calorie excess (Rosen & Spiegelman 2014). After that, hypertrophic mature adipocytes die and macrophages are recruited to sites of adipocyte death to remove the dead cells. This macrophages one of the factors recruiting APs (Lee et al. 2013). However we demonstrated that fat content in the food induces Sca-1+ AP proliferation without hypertrophy of mature adipocytes in gWAT of sexually immature female mice. These data suggested that nutritional stimulus can activate AP proliferation before mature adipocyte hypertrophy occurs and potentially prepare adipose tissue to following dietary challenges at least in young age.

3.6 Contributions of inflammation to AP proliferation

It was postulated that local inflammation in adipose tissue triggers *in vivo* angiogenesis (Wernstedt Asterholm et al. 2014), (Brestoff et al. 2014). Accordingly to our data immune-related gene sets were enriched in response to excess calorie load, but not in isocaloric groups. Taking in consideration our result that fat content in the food in isocaloric amount as in CD group leaded to AP proliferation, we could not conclude that inflammation was necessary to induce AP proliferation at least in sexually immature female mice.

3.7 Contributions of IGF-1 to AP proliferation

Although there is no consistency in observations of serum level of insulin-like growth factor 1 (IGF-1) in obese adults and children, IGF-1 is believed to play an important role in AP proliferation, differentiation and contributing to development of obesity (Garten et al. 2012), (Berryman et al. 2013), (Kreitschmann-Andermahr et al. 2010). In this project, we demonstrated that although IGF-1 was increased 2 days after HFD feeding, it was not increased upon isocaloric high fat diet (restricted HFD) and cannot fully explain AP proliferation. Additionally *in vitro* IGF-1 treatment of ingWAT APs showed no effect on number of differentiated colonies in co-culture system.

3.8 Contributions of insulin to AP proliferation

Insulin is one of the major players in sustaining glucose homeostasis by inducing glucose intake by mature adipocytes, liver and muscle cells (Rutkowski et al. 2015). We have observed increased insulin in serum 2 days upon CD, after 7 days there was no difference in

serum insulin level among diets. However we noticed upregulation of insulin-regulated genes in gene expression profiling upon CD in both time points. Taking into consideration data that peak of AP proliferation occurred on 3rd day of HFD (Jeffery et al. 2015) we could hypnotize that insulin could serve as an inhibitory factor for AP proliferation. This hypothesis has counter argument, since insulin level is increased during obesity. However it can play regulatory role just in short developmental window. We plan to address acute effect of insulin treatment on AP proliferation upon HFD. We observed decrease in ingWAT GFP+ colonies upon insulin treatment, but not in number of differentiated colonies. This data could indicate that insulin supported differentiation of committed APs from heterogenic progenitor pool, but not proliferation of immature progenitors. Additionally, since we have observed increased insulin already on days 2 of CD we planned to generate samples with time point 0 during switch from mother milk enriched in fat to high carbohydrate control diet. It would allow us to conclude about early dynamic of insulin.

3.9 Contributions of lipids to AP proliferation

It became clear form this project that dietary fat is able to promote proliferation of APs. However it is not clear through which systemic factor it can be communicated to adipose tissue niche. Since we know that initial burst of AP proliferation accrues 3 days after start of HFD feeding (Jeffery et al. 2015), we studied serum lipid dynamic in the random-fed state 2 and 7 days upon HFD. We observed no changes in triglycerides (TG) and non-esterified fatty acid (NEFA) 2 days after diet. However cholesterol was increased 2 days after HFD, which could indicate potential signaling role of cholesterol. Further NEFA was lower upon HFD and isocaloric HFD (HFD-R) 7 days after diets. Since signaling molecules should have a quick turnover, we hypothesized that we may not able to detect some differences in random-fed state. To overcome this problem, we collected blood 3 hours after feeding, which corresponded to highest peak of nutrients in the blood. We found that NEFA and cholesterol were increased upon HFD-R 3 hours after feeding which indicated their potential signaling role in induction of AP proliferation. TG was higher upon HFD *ad libitum and* was not significantly altered 3 hours after feeding between groups.

3.10 Gene expression patterns reveal a cascade of events leading to rapid tissue remodeling upon HFD

In order to identify which genes could play a role in AP expansion upon HFD, gene expression profile was performed using microarrays. From the 195 gene sets enriched upon HFD, there were 116 that function associated to tissue remodeling. When compared 2 and 7 days of HFD, it was possible to observe dynamic change in enriched genes. After 2 days of HFD we observed pathways, which characterized early process in tissue remodeling. Among the pathways, there were some related to inflammation as leukocyte migration, innate

immune response, B-cell activation and cell-cell communication as receptor signaling protein activity. We detected evidences indicating hypoxic condition and following angiogenesis. Common pathways between 2 time points were related 1) to inflammation as immune and defense responses, lymphocyte and leukocyte activation; 2) to cytokine and chemokine regulation as cytokine production and chemokine activity; 3) to extracellular matrix remodeling as collagen and 4) development of new vessels. We found that after 7 days of HFD pathways which were involved in a regulation and progression of cell cycle were enriched. This data indicates that inflammation, cytokine receptor interaction, cell-cell communication and angiogenesis start early following by extracellular matrix remodeling and activation of proliferation.

Despite being restrictive to the amount of information that is possible to gather, microarrays allowed identifying almost 200 differentially expressed genes that could be subject to further characterization of their role in AP proliferation and differentiation. Using other detection methods, like NGS, would be interesting in order to identify other elements that could also play a role here, as miRNAs, differential splicing, among others.

3.11 Co-culture system for studying AP functions

In parallel to target identification we established a co-culture system with feeders, on top of which we seeded GFP+ APs in a single cell density that allowed us to validate function of identified target genes in an adipose tissue niche in a way which close to physiological. The most common way of AP *in vitro* studies is following: isolation of whole SVF or APs by specific markers from fat, seeding in monoculture that activates their proliferation. When monolayer is completed differentiation can be induce by specific inductors. This approach is not physiological because progenitor cells are not sitting close to each other inside adipose tissue and proliferate only in response of certain stimulus, which we would like to study. To solve this methodological problem we developed new approach of co-culture system of feeder cells and progenitor cell in the low density on top of them. Co-culture approach was successfully used in other stem cell systems before, as human embryonic stem cells (Peerani et al. 2007) or hematopoietic stem cells (Butler et al. 2012), (Raynaud et al. 2013). However, to our knowledge it was not developed for APs from adipose tissue. This system allowed us to follow individual cells and colonies developing from them and we found that already after 4 days in co-culture Sca-1+ APs formed colonies which further had a different fate as they differentiated to adipogenic or fibrogenic colonies. It was not possible to observe AP heterogeneity before using classical monoculture and co-culture gave as a significant adventure over it. Feeder cell layer provided niche-like environment partially mimicking cell-cell interaction in the tissue *in vivo*. Thus, co-culture modulated cell behaver of APs and prevented AP senescence by slowing down proliferation rate of APs. Additionally this system allowed us easy to manipulate gene of interest in feeders by siRNA or overexpression

independently from APs and observe stroma-related phenotype. Our readouts were proliferation activity by measuring GFP+ cell number/colony size, differentiation capacity by ratio adipogenic vs. fibroblastic colonies. Using co-culture system we validated function of *Emp1*, which were deferentially expressed in profiling data. Co-culture system allows to measure functional property of APs beyond our target list, many biological questions can be addressed with this system, e.g. gender, depot or age- specific properties of APs. Additionally we planned to isolate APs from mice fed with different diets and asses proliferation/ differential property.

3.12 Role of EMP1 in adipose tissue remodeling

Epithelial Membrane Protein 1 (*Emp1*) is an integral multi-pass (tetra-span) membrane glycoprotein consisting of 160 amino acids, which is important in tight junction function, assembly and maintenance in lung epithelium (Durgan et al. 2015). EMP1 is expressed in micro vessels of the brain and involved in assembly of brain blood barrier tight junctions (Bangsow et al. 2008). However role of *Emp1* was not described in context of adipose tissue growth, function or *in vivo* adipogenesis. We demonstrated that *Emp1* was upregulated in gWAT within 2 and 7 days upon high-fat diet in young and adult female mice. Since it was reported that EMP1 has lower expression in tumor vs. normal surrounding tissues, e.g. on mRNA level in human lung cancer (Durgan et al. 2015), on protein level in human prostate, colorectal and breast cancer (G. G. Sun et al. 2014), (G.-G. Sun et al. 2014) and ovary tumor on mRNA and protein level (Demirag et al. 2016) we suspected role of EMP1 in cell proliferation. We found that in particular *Emp1* was highly expressed in Sca-1+ APs, endothelial cells and mature adipocytes. Our hypothesis was that *Emp1* modulates directly (in APs) or indirectly (through mature adipocytes) AP proliferation in WAT growth. To test it we modulated knockdown of *Emp1* in feeders and seeded APs on top and after co-culturing we demonstrated that number of GFP+ cells/colonies was lower than on top of feeders transfected with negative control siRNA. To test direct effect of loss of *Emp1* in APs, we generate knockdown in monoculture of APs and measured rate of cell divisions. No direct effect of *Emp1* knockdown was observed on AP proliferation. These data indicated that *Emp1* was playing role in cell-cell communication rather than directly affecting proliferation of APs. In order to explain observed decrease in number of GFP+ cells/colonies co-cultured on top of feeders with *Emp1* knockdown, we hypothesized that it could be decreased proliferation, increased apoptosis or impaired adhesion of APs to feeders. Preliminary data suggested that *Emp1* knockdown in feeders was not affecting proliferation and apoptosis of APs in co-culture (data were obtained by master student Wujun Hong supervised by me). In the next stet we would like to investigate the role of *Emp1* in landing of APs on feeders. Since we found that *Emp1* was upregulated upon HFD in mature adipocytes and Sca-1+ APs we intend to investigate effect of manipulation of *Emp1* expression in model of

mature adipocytes and its effect on cell-cell contacts between mature adipocytes and APs. Another open question is which factors /signals/ligands could modulate expression of *Emp1* in mature adipocytes and is currently being addressed.

3.13 Key findings at a glance

Key findings at a glance

Diets high in fat lead to rapid growth of adipose tissue:

1. One week of high-fat diet leads to body and adipose tissue gain in sexually immature female mice, but not in adult mice.
2. Adipose tissue gain after one week of high-fat diet occurs through hyperplasia of Sca1+ APs and partially via hypertrophy of mature adipocytes.
3. Enrichment of dietary fat with isocaloric content (HFD-R), when compared control diet, does not lead to body weight gain, far mass gain or hypertrophy of mature adipocytes, but induces proliferation of Sca1+ APs.
4. IGF-1 was regulated by calorie load, but not food content, and its levels were highly increased upon HFD *ad libitum* after 2 days of diet.
5. NEFA was regulated by food content: decreased upon HFD-R after 7 days in and transiently increased 3 hours after feeding upon HFD-R.
6. Cholesterol was transiently increased 3 hours after feeding upon HFD-R vs. CD.
7. Mouse serum from different feeding groups had no difference in effect on proliferation of AP in *ex vivo* system.

Molecular mechanisms of adipose tissue remodeling – novel gene search from tissue and cell subpopulations:

8. Activation of gene network related to adipose tissue remodeling was already observed 2 days upon HFD.
9. Fat content even in isocaloric diet (HFD-R) activates cell-cycle related pathways.
10. Inflammation-related genes were activated in response to excess calories and were enriched upon HFD *ad libitum* vs. CD, but were not the presence in isocaloric diets comparison.
11. 203 genes were differentially expressed upon high-fat feeding in adipose tissue in first gene expression profiling (selected by p value <0.05 and 1.5 fold-change.
12. Age- and subpopulation-specific genes were found, potentially involved in adipose tissue remodeling.

Functional characterization of genes responding to HFD using co-culture system in a niche-like setting:

13. Co-culture system was successfully established.
14. Adipocyte progenitor cells can form colonies and differentiate in co-culture into mature adipocytes without providing classical inductors of differentiation.

15. Microscopy screening settings/image data analysis algorithms were established and tested.
16. *Emp1* mediated knockdown in feeder cells decreased the number of GFP+ cells/colonies formed from APs in co-culture system.

3.14 Conclusions and future perspectives

In this project we established and characterized diet-induced model for investigating early adipose tissue growth during development of childhood obesity. We found molecular network connecting dietary stimulus and response of APs and investigated several genes using niche-like setting.

We opened new questions as:

1. What are the long-term consequences of AP proliferation on adipose tissue function and metabolic health?
2. Nutritional sensing mechanisms, which cells and how can sense nutrients and respond to them.
3. Which exact component of fat is able to promote AP proliferation?
4. Age and sex-specific AP response on dietary challenges.
5. *In vitro* and *in vivo* function of identified target genes.

4. MATERIALS and METHODS

4.1 Animal work

4.1.1 Mouse strains and housing

For dietary experiments/APs isolations female C57BL/6NCrl mice were obtained from Charles River Laboratories (Sulzfeld, Germany). For initial co-culture experiments female C57BL/6-Tg (UBC-GFP) 30Scha/J and STOCK Tg (CAG-EGFP) D4Nagy/J mice were obtained from The Jackson Laboratory (USA). For all following co-culture experiment female C57BL/6-Tg(UBC-GFP) 30Scha/J mice were bred in Unit 6 of University of Heidelberg (Germany). Mice were housed in IVC cages on RT in a 12-hour dark and 12-hour dark/light condition. All handling and tissue dissection was performed in the light phase of the day cycle, if not state differently.

4.1.2 Dietary regimes

Diet induced obesity mouse model

Two-week old pups were acclimatized with mothers on control diet (10% of fat) during the first week. After that, 3-week old pups were weaned and randomized equally based on their body weight between dietary groups as control diet (CD, 10% kcal from fat), high-fat diet (HFD, 60% kcal from fat), high-protein diet (HPD, 10% kcal from fat). Diets were applied for the time of experiment ad libitum if not mentioned other. To mimic consumption of sweet beverages sucrose/fructose syrup was provided for first 5 weeks in the low concentration = 18.9/23.1 g/l to acclimatize mice to sweet drinks. Then concentration was increased up to 94.5/115.5 g/l. Sucrose/fructose solution was filtered after preparation and bottles were changed 1-2 per week.

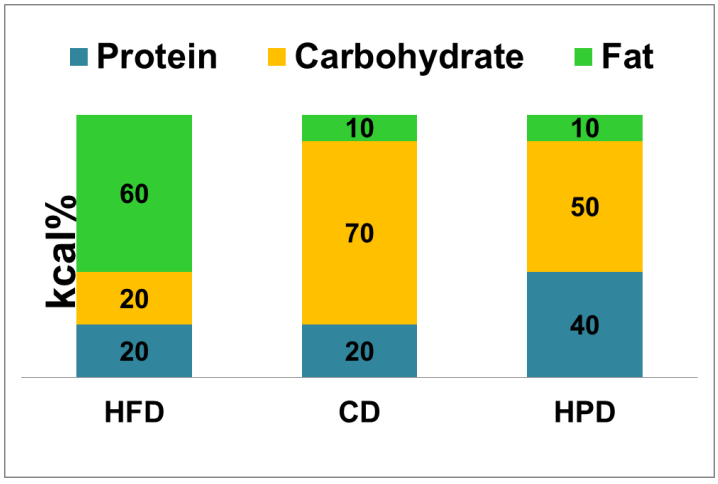

Figure 4.1: Dietary compositions, % of calories from different macronutrient sources as protein, carbohydrates and fat. High-fat diet (HFD), control diet (CD) and high-protein diet (HPD).

Table 4.1: Diets used in this study.

Diet	Cat. #	Distributor
Control Diet irradiated	D12450Bi	Research Diets Inc, OpenSource Diets
High Fat Diet irradiated	D12492i	Research Diets Inc, OpenSource Diets
High Protein Diet (Special customized composition order for Dr. Adam Rose)	D14032601	Research Diets Inc, OpenSource Diets

Pair feeding approach for equal calorie load

To equalize amount of consumed calories, control diet (CD) group served as a reference group. CD group mice were fed with CD and food was measured before and 24h after supplying. Then consumed calories were calculated every day and the same amount of calories was applied for high-fat diet restricted group (HFD-R). Since mice at 3 week age grow actively, food consumption was increasing every day in CD group. To take this in account measurement of food intake of reference CD group was done every 24 h till the end of experiment.

Pair feeding with controlled circadian rhythm

To measure peak of blood serum factors the scheme of pair feeding experiment was modified. CD reference group received food at the beginning of dark/active phase and food was taken away in 12 h at the beginning of light/rest phase. Consumed calories were calculated and provided for HFD-R group next day at the beginning of dark phase. For all groups food was applied at the beginning of dark phase and was removed and measured at the beginning of light phase. All mice were euthanized randomly between experimental groups 3-5 h after beginning of dark phase when food was just supplied.

4.1.3 Body composition measurements (EchoMRI)

Alterations in body composition were measured weekly by NMR quantitation (Echo MRI, Echo Medical Systems). The EchoMRI™-100H was calibrated by 32g oil sample. Body weight of mice was measured and fat mass, lean mass, free water, total water were determined accordingly to the body weight.

4.1.4 Fasting blood glucose, glucose and insulin tolerance tests

Fasted blood glucose was collected after overnight fasting (16 h). For that mice were transferred into new cages and only water was supplied, in 16 h tail vain blood glucose was measured by glucometer Accu-chek Aviva (Roche Diagnostic, Mannheim, Germany). Glucose and insulin tolerance tests were performed on overnight fasted mice (16 h and 5h,

respectively) with ip injection of glucose (Applichem, Germany) (2 mg/g of lean mass) or insulin (Humulin, 1 U/ kg lean mass, USA). Blood glucose from tail blood was measured prior to (0 min) and 10, 20, 30, 60 and 120 min after the injection using a glucometer Accu-chek Aviva (Roche Diagnostic, Mannheim Germany).

4.1.5 Tissues dissection

Mice were euthanized by cervical dislocation by FELASA B licensed investigators. Blood was collected from decapitated animal and stored on ice. The mouse peritoneal cavity (abdominal coelom) was opened. Abdominal WAT (gWAT) was dissected from area around uterus cutting along the uterine tubes. Liver was dissected without glad bladder. IngWAT was dissected from the dorsal side close to the lumbar sacrum, and isBAT from the intra scapular region. Triceps sureae bundle: gastrocnemius, soleus were dissected from the hind limb. Weights of tissues were determined, part was collected for histology and part was frozen in liquid nitrogen for RNA extraction. Blood serum was obtained by incubation of blood samples at RT for 30 min. and subsequent centrifugation for 30 min. at 5.000 rpm, 4°C. The serum (upper phase) was transferred to a new tube and stored at -80°C.

4.1.6 Edu administration

5-ethynyl-2-deoxyuridine (EdU, E10187, Thermo Fisher Scientific, Darmstadt, Germany) was administered in drinking water (for 1 week) in a final concentration 0.2 mg/ml. Water was supplied in the dark bottle and changed every 2 days. Control mice had their water supply without EdU (neg. control EdU).

4.1.7 Histology

Tissues were kept in histo-cassettes in 4% Histofix (Roth, Germany) at RT for 24 h in the fume hood. Histo-cassettes were rinsed with tap water for at least 2 h and transferred to 70% ethanol and store at 4°C until embedding in paraffin blocks. Embedding of paraffin blocks, cutting of the slides and hematoxylin and eosin (H&E) staining were as follows: for dehydration Tissue Processing Center (Medite, Germany) was used, to embed samples embedding street (Modite) and tissue embedding medium (paraffin) (VO-5-101, Vogel histo-comp) were used. After that paraffin blocks were cut using RM2245 microtome (Leica, Germany). For H&E staining: rehydration: xylene→100% EtOH →95% EtOH →70% EtOH→ water; hematoxylin (GHS332-1L, Sigma) for 5 min; water rinse; 0.4% HCl for 20 sec and then water rinse; eosin (HT110132-1L, Sigma, Germany) for 30-60 sec and water rinse for 1-2 min; dehydration: 70% EtOH→95% EtOH→100% EtOH→ xylene; mounting with Eukitt® (03989-100ML, Sigma).

4.2 Cell biology

4.2.1 Culture and differentiation of 3T3-L1 and C3H10T1/2

3T3-L1 and C3H10T1/2 were obtained from ATCC (USA) and from A170 cell bank, respectively (Heidelberg, Germany). 3T3-L1 was cultured in DMEM low glucose 1g/l (31885049, Thermo Fisher Scientific) supplied with 10% Fetal Bovine Serum (FCS) (10270106, Thermo Fisher Scientific) and 1% Penicillin-Streptomycin (P/S) (15140122, Thermo Fisher Scientific). Cells were re-fed every 2-3 days and passaged before they reach 80% confluency, normally 1:10 or 1:15 depending on experiment. To induce differentiation following protocol was used: 2 days of induction ->2 days of induction -> 4-6 days of maturation ->1 day of culturing media. Induction medium consisted of DMEM glucose 4.5g/l (41966052, Thermo Fisher Scientific), 10% FCS, 1% P/S and inductors of differentiation (1 µg/ml Insulin (I2643-50mg, Sigma), 0.25 µM Dexamethasone (D8893-1MG, Sigma) and 0.5 mM 3-Isobutyl-1-methylxanthin (IBMX) (I5879-1G, Sigma). Maturation medium consisted of DMEM glucose 4.5g/l, 10% FCS, 1% P/S supplied only with 1 µg/ml Insulin. C3H10T1/2 was cultured in DMEM glucose 4.5g/l, 10% FCS, and 1% P/S and differentiated similar to 3T3-L1, but to achieve differentiation 2µM of rosiglitazone was used during all course of differentiation.

4.2.2 Magnetic isolation of Lin-Sca1+ adipocyte progenitor cells from adipose tissue

gWAT and ingWAT were dissected, washed with 1x D-PBS stored on ice. Fat pads were minced until homogenous mass, transferred to15 ml tubes and digesting solution was applied following by warming up in water both on 37°C for 10 min. Than samples were gently shacked at 70rpm at 37°C for 20-40 min. Samples were meshed through 300µm nylon mesh and centrifuged at 145g at RT for 10 min. After separation into 3 phases: mature adipocyte layer were collected or/and removed as well as supernatant. The SVF cells pallet was washed with 12ml of BSA buffer (1xPBS, 0.5% BSA, 1mM EDTA). After spinning down at 300g at RT for 5 min pallet was resuspended in appropriate amount of BSA buffer (0.5 ml of buffer for up to 10 4week old mice) and incubated with blocking reagent CD16/32 (2µl/100µl BSA-Buffer) on ice for 5-10 min. To deplete erythrocytes (Ter119+), endothelial cells (CD31+) and leucocytes (CD45+) - Ter119-, CD31-, CD45-biotin-coupled antibodies were applied (1µl of each antibody/100µl BSA-Buffer) to the suspension and were incubated on ice for 30 min. After centrifugation at 300g at 4°C for 5 min cell pallet was resuspended in 10 ml of pre-cooled BSA buffer and centrifuged again using the same settings. The SVF pellet was resuspended in 180µl BSA buffer and 20µl of streptavidin-coupled microbeads were added per one magnetic column and incubated on ice for 15 min. Depending on amount of adipose tissue/mice 1 or 2 columns were used per sample and accordingly all reagents were adjusted. Cell suspension was washed with 4ml of BSA buffer and centrifuged at 300g at 4°C

for 5 min. Cell pellet was resuspended in 1m of BSA buffer and applied on pre-separation filter inserted into magnetic column. Flow-through and 3 subsequent washing solutions going through column were collected and centrifuged at 300g at 4°C for 5 min. For Sca1-enrichment cell pellet was resuspended in 80µl of BSA buffer and 20µl of Anti-Sca1-Microbeads were added and incubated for on ice for 15 min. Cell suspension was washed with 4 ml of BSA buffer and centrifuged at 300g at 4°C for 10 min. Cell were resuspended in 1 ml of BSA buffer, applied on pre-separation filter inserted into magnetic column and washed 3 times with 500µl BSA buffer. The columns were removed from the magnet field and cells were eluted by applying 1 ml of BSA buffer and pushing piston. After centrifugation cells were centrifuged at 300g at RT for 10 min and resuspended in culture medium. Cells were count and seeded accordingly to experimental need.

4.2.3 Co-culture system

Protocol is divided into 4 steps: 1) Feeder cell preparation; 2) APs seeding on top of feeder cells; 3) Co-culturing; 4) Fixing, staining, imaging, image data analysis.

Step 1: Feeder cell preparation

C3H10T1/2 or 3T3-L1 were used as a feeder layer in normal culturing. To prevent post confluence inhibition of cell division, cells were split at confluence not more than 80%.

Day 1 C3H10T1/2 cells were seeded on 24- or 96-well plates (7000 cells/well for 24-well plate or 1500 cells/well for 96-well plate).

Day 2: C3H10T1/2 reached 60-70% of confluency when were transfected with siRNA. See method section 4.2.4.

Day 3: 24 h after transfection culturing media was changed with fresh normal culturing media.

Day 4: Feeder cells formed complete monolayer. To privet father divisions, feeder cells we treated with 20µg/ml Mitomycin C in the normal culturing media for 2.5h at 37°C. Then, Mitomycin C solution was removed and cells were washed with normal culture medium 2 times. After 2nd wash cells were incubated for 30 min. at 37°C and the medium was changed again for fresh one. To test efficiency of transfection some plats were harvested next day after Mitomycin C treatment.

Step 2: Adipose progenitor cells seeding

Day 5: To isolate Lin-Sca1+ adipocyte progenitor cells from fat pads see section 4.2.2. C57BL/6-Tg(UBC-GFP)30Scha/J mice were used to isolate GFP-labelled APs. To achieve low density 300 APs per well of 24-well plate were seeded in normal culturing medium. For 96-well plate 50 APs per well were seeded. To induce APs growth bFGF were added in concentration 10ng/ml during first 2-4 days of co-culturing.

Step 3: Co-culturing

Day 7: Media was gently aspirated after 2 days and normal culturing media supplied with 100nM insulin was added.

Day 9, 11, 13: Normal culturing media supplied with 100nM insulin was changed every 2 days. GFP colonies can be detected in 4 days after seeding of APs. GFP colonies differentiated into adipocytes can be visualized in 7-10 days after seeding of APs.

Step 4: Fixing, staining, imaging, image data analysis

For fixation and LipidTox/DAPI staining see an additional protocol.

4.2.4 siRNA transfection

Lipofectamine RNAiMAX Transfection Reagent (Life Technologies, 13778075) and 5nM or 20nM Silencer® Select siRNA (Applied Biosystems) were used as recommended by manufacture (usually 1 µl of RNAiMAX was diluted with 50 µl OptiMEM). Transfection was done when cells reached 60-70% confluence. Then after 24 h cells were washed and used 24 or 48 h after transfection.

4.2.5 FACS for cell populations study

gWAT and ingWAT were dissected and processed with digestion as described above (section 4.2.2). Mature adipocyte fraction was collected. For erythrocyte depletion SVF cells were resuspended in 160 µl BSA buffer with 2% FCS plus 3.2ul FcBlock (CD16/32) (14-0161-85, e bioscience, Germany) on ice for 5-10 min. This amount for pellet from 3-5 four-week old mice was increased accordingly with final concentration 2ul/100ul. Then 40µl/column of Ter119-microbeads (130-049-901, Miltenyi Biotec, Cologne Germany) were added and incubated on ice for 15 min. Sample was washed with 4 ml of BSA buffer and centrifuged at 300g on 4 °C for 5 min. Cell pellet was resuspended in 1m of BSA buffer and applied on pre-separation filter inserted into magnetic column. Flow through was collected into 15 ml tubes. After flow through went completely magnetic column was washed 3 times with 500µl BSA buffer and washing solution was collected as well. Then cell number was determined for each sample. Cell suspension was centrifuged at 300g on 4 °C for 5 min and resuspended in antibody mix. Antibody staining: in order to make FACS gating single stained samples for all antibodies were prepared as unstained sample for initiating gating, CD45-AF700 (56-0451-82 Mouse CD45 Alexa Fluor®700 (30-F11), eBioscience) (1:40), CD31-APC (17-0311-82, Mouse CD31 APC (390), eBioscience) (1:40), CD34-eFluor450 (48-0341-82, Mouse CD34 eFluor®450 (RAM34), eBioscience) (1:10) CD29-PE (12-0291-81, Mouse/Rat CD29 PE (eBioHMb1-1) (50 ug), eBioscience) (1:40), Sca1-APC-Cy7 (56-0451-82, Mouse CD45 Alexa Fluor®700 (30-F11), eBioscience) (1:50). Additionally in case of EdU-labeling FMO for EdU staining was prepared. FACS gating system used is summarized in Figure 4.2. Further analysis was done using FlowJo software (FlowJo, LLC, USA).

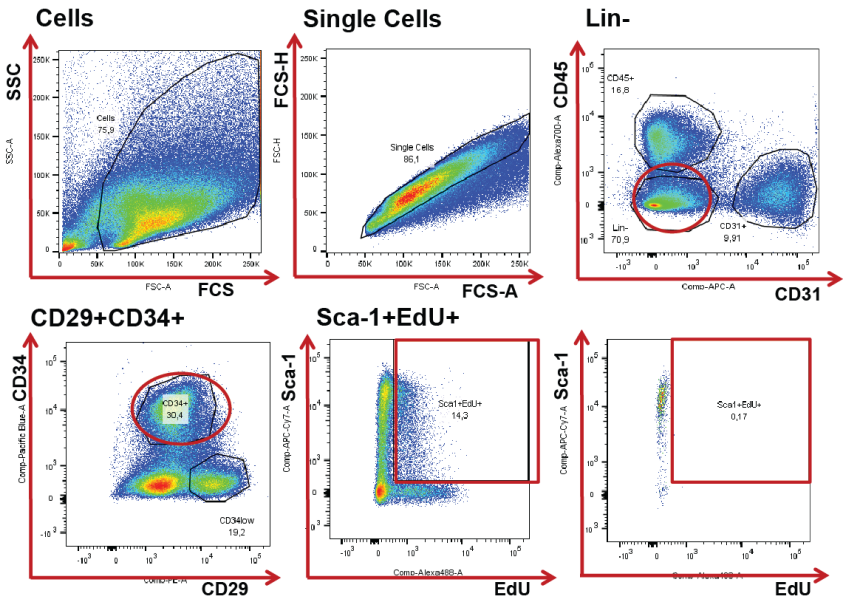

Figure 4.2: FACS gaiting for cell populations study. Using this analysis we were able to discriminate: endothelial cells - CD31+ CD45-; immune cells - CD45+ CD31-, Lin-cells - CD45- CD31-; pluripotent cells - Lin-CD29+CD34+ cells; fibrotic cells - Lin-CD29+CD34 CD34 ^{low} cells and adipose progenitors (APs) - Lin-CD29+CD34+Sca-1+ cells. Additionally in EdU-labeling experiments, we could distinguish EdU+ cells inside of subpopulation of interest, e.g. proliferating APs as Lin-CD29+CD34+Sca-1+EdU+. Gaiting for EdU was done based on fluorescence minus one (FMO) control, stained with all other antibodies and without EdU.

4.2.6 Immunofluorescence

LipidTox/DAPI staining

Cells were fixed with 4% paraformaldehyde (Fisher Scientific) for 10 min. and washed with 1xPBS. To discriminate lipid droplets samples were stained with HSC LipidTOXTM Red Neutral Lipid Stain (Life Technologies, Germany) 1:500 in PBS combined with 500ng/ml of 4,6-diamidino-2-phenylindole (DAPI) to label the cell nuclei for 30 min at RT in the dark.

EdU pulse and staining

For cell culture experiments Click-iT® Plus EdU Alexa Fluor® 594 Imaging Kit (C10639, Thermo Fisher Scientific) was used accordingly to manufacturer. Cell were pulsed with 10 µM EdU for 3 hours (normally 20 µM solution was prepared and only half of the culturing media was changed to prevent induction of cell proliferation from fresh media). After that cells were fixed with 4% paraformaldehyde (Fischer Scientific) for 15 min. and washed with 3%BSA in 1xPBS following by Click-iT protocol. To label nuclei 500ng/ml of 4,6-diamidino-2-phenylindole (DAPI) was used.

4.2.7 Microscopy

Fluorescence microscopy was performed using a motorized Cell Observer.Z1 microscope (Zeiss, Jena, Germany) equipped with the HXP 120 burner and with the AxioCam MRm CCD camera. The standard excitation/emission filters were used for visualizing DAPI (Zeiss filter 49), Alexa Fluor 488 (36HE), LipidTox (Zeiss 43 HE Cy3/DsRed filter).

For high-throughput data acquisition in co-culture experiments an automated wide field screening microscope (Olympus Biosystems IX81 inverted, Germany) were used in ViroQuant-CellNetworks RNAi Screening Facility, Bioquant, University of Heidelberg.

4.3 Molecular Biology

4.3.1 Pulverization of the tissues for RNA isolation

After dissection, tissues were frozen in liquid nitrogen and kept on -80°C. Tissue was transferred into pre-cooled in liquid nitrogen bucket with metal ball, placed in Mikro-Dismembrator S (Sartorius) and pulverized using 2500 rpm for 30 sec. Then powder was transferred back to tube in liquid nitrogen and 1 ml of Qiazol (Qiagen, Hilden, Germany) was added to bucket with residual tissue powder. Bucket was placed again to dismembrator and shacked for half a minute till Qiazol became a liquid back. Lysates were kept on -80°C till RNA isolation, but not longer than 1 month.

4.3.2 RNA isolation and quantification of nucleic acids

RNA was isolated from cell/tissue Qiazol lysates using RNeasy Micro or Mini Kit (Qiagen), respectively. Incubation of RNA on column with RNase-Free DNase Set (Qiagen) for 15 min was added to manufacture protocol. To determine concentration of RNA 1.5 µl were applied on blanked with H_2O NanoDrop ND-1000 Spectrophotometer (Thermo Fisher Scientific, Darmstadt, Germany) and absorbance was measured at 260 nm. To determine purity of RNA samples 2 ratios were assessed 260/280 and 260/230 = ~2.0.

4.3.3 cDNA synthesis and Quantitative Real-Time PCR

For cDNA synthesis QuantiTect Reverse Transcription Kit (Qiagen) was used according to manufacture protocol using 100-1000 ng of RNA as starting material. Briefly 100-1000 ng of RNA diluted with RNase-free water were incubated with 2 µl of gDNA wipeout buffer for 2 min. at 42°C in Thermomixer comfort MTP (Eppendorf), placed on ice and then mix solution (containing 1 µl of Quantiscript Reverse Transcriptase, 4 µl of Quantiscript RT Buffer and 1 µl of RT Primer Mix per sample) were added to sample. Samples were placed into Peqstar 2x gradient thermocycler (VWR Peqlab) for 30 min. at 42°C following by 3 min. at 95°C. To perform quantitative real time PCR (qPCR) samples

were diluted 1 to 10 and 5 µl of diluted cDNA was used. For qPCR the Taqman Gene Expression Master Mix (4369016, Applied Biosystems) and specific Gene Expression Assays (Applied Biosystems) were used in StepOnePlus Real-Time PCR System (Applied Biosystems). mRNA levels relative to TBP expression were calculated by the delta Ct method.

4.3.4 Gene Expression Profiling

RNA was isolated from gWAT or cell population and provided to Genomics and proteomics core facility (GPCF, DKFZ, Heidelberg) in concentration 50ng/µl not less than 500ng. Quality of RNA was assessed by Bioanalyzer in GPCF. Affymetrix GeneChip® Mouse Gene 2.0 ST Arrays, 4-5 chips per diet group per one time point were used.

4.4 Biochemistry

4.4.1 Enzyme-linked Immunosorbent Assay

Insulin

Insulin concentration in the blood serum was determined by Insulin (Mouse) ELISA Kit (80-INSMS-E01-AL, ALPCO) accordingly manufacture protocol. Briefly, serum samples were thawed on ice and 5µl of samples/standards/controls 2 replicates per sample were pipetted on microplate. Then 75µl Working Strength Conjugate was applied into each well. Plate were covered and shacked at 700 rpm on RT for 2h. Then plate was washed 6 times with Working Strength Washing Buffer following by applying of 100µl of TMB substrate into each well. Plate were covered and shacked at 700 rpm on RT for 15 min, 100 µl of stop solution were added. The absorbance was measured on microplate reader on 450 nm. Insulin concentration was determined using Elisa analysis web-resource (http://www.elisaanalysis.com/).

IGF-1

IGF-1 concentration in the blood serum was determined by Insulin-like Growth Factor 1 (Mouse) AssayMax ELISA Kit (EMI1001-1, AssayPro, USA) accordingly manufacture protocol. Briefly, serum samples were thawed on ice and diluted in 1:250 with 1x MiX Diluent in replicates. Standards were diluted accordingly to protocol starting from 10- 0.156 ng/ml through serial dilutions. Then 50µl of samples/standards per well were added to microplate, covered and incubated at RT for 2h. Then plate was washed 6 times with Washing buffer and 50µl of Mouse IGF-1 biotinylated antibody was added per well following by 30 min incubation at RT. After washing 50µl Streptavidin-Peroxidase Conjugate per well were added and plate was incubated at RT for 30min. After washing 50µl of Chromogen Substrate per

well were added and plate was incubated at RT for 12 min following by addition of 50µl of Stop solution. The absorbance was measured on microplate reader on 450 nm. IGF-1 concentration was determined using Elisa analysis web-resource (http://www.elisaanalysis.com/).

4.4.2 Serum Metabolite Assays

Triglycerides

To determine glycerol, total triglycerides and true (free) triglycerides 2 µl of serum in duplicates and commercial kit (T2449, Sigma) were used accordingly to manufacture protocol. Absorbance was measured on 550 nm using the Mithras Microplate Reader (Berthold).

Cholesterol

To determine cholesterol 2 µl of diluted 1:1 in 1xPBS serum in duplicates and commercial kit (CH200, Randox) were used. Briefly 100 µl of cholesterol reagent was added to the sample in 96-well plate and incubated on 37°C for 5 min following by absorbance detection on 505nm using the Mithras Microplate Reader (Berthold).

Non-esterified fatty acid (NEFA)

To determine NEFAs 2 µl of serum in duplicates and commercial kit (434-91795, 436-91995, Wako) were used accordingly to manufacture protocol. Absorbance was measured on 550 nm using the Mithras Microplate Reader (Berthold).

Ketone Bodies

To determine 2 µl of serum in duplicates and commercial kit (415-73301, Wako) were used accordingly to manufacture protocol. Absorbance was measured on 405 nm using the Mithras Microplate Reader (Berthold).

4.5 Computational Biology

4.5.1 Gene expression analysis:

Data RMA-normalization, visualization and quality controls were done via Affymetrix® Expression Console™ Software. Statistical analysis was performed via Chipster. Linear modelling (Smyth et al. 2005) was used for identifying interaction/main effect p values for 2 factors (type of diet and duration of diet) applying Benjamini and Hochberg's p value adjustment. To investigate enriched gene sets Gene set enrichment analysis (GSEA)

software from Broad Institute was used accordingly to available tutorial. Gene ontology (GO) gene set (Consortium 2000) was used for enrichment analysis. To prepare Venn diagrams Venny 2.1.0 – BioinfoGP was used http://bioinfogp.cnb.csic.es/tools/venny/index.html

4.5.2 Image processing

Adipocyte lipid droplet area

Adipocyte lipid droplet area was estimated automatically with constant settings using an ImageJ macro (http://rsbweb.nih.gov/ij). Briefly, Adipocytes were segmented as shown on Fig. 4.3 and area was measured. Adipocyte diameter and volume were estimated based on area using following formulas:

$$\text{Diameter} = 2\sqrt{\frac{\text{mean cell area}}{\pi}}\ \mu m \qquad \text{Volume} = \pi\frac{\text{diameter}^3}{6}\ \mu m^3$$

Number of adipocytes per gram of WAT was calculated as following: 1) convert the volume from μm^3 to a volume in picolitres (pl) (1 pl = 1000 μm^3). 2) calculate the mass of a cell, where mass = volume x density and the density of adipose tissue can be assumed to be 0.96 g ml^{-1}, mean cell mass = mean cell volume x 0.96. 3) calculate the number of cells per mg of tissue as number of cells per mg tissue = 1/mean cell mass, then to estimate absolute number of adipocytes per depot=number of adipocytes per gram x gram of tissue.

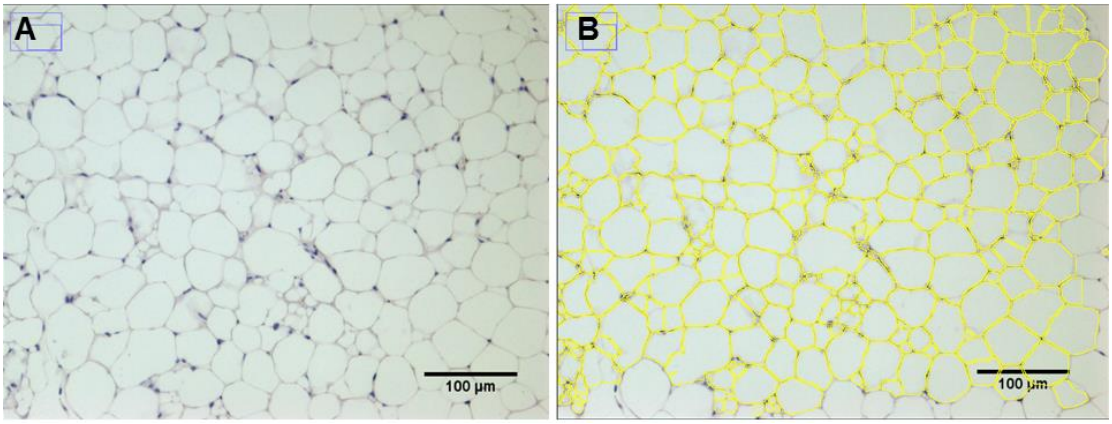

Figure 4.3: Illustration of adipocyte lipid droplet area measurement. A) Image of gWAT histology **B**) Lipid droplet areas recognized by automated algorithm.

EdU-labeled nuclei count

Count of EdU-labeled nuclei and all nuclei (labeled with DAPI) was performed automatically with constant settings using an ImageJ macro (http://rsbweb.nih.gov/ij). Briefly, nuclei were segmented, counted in both channels and then ratio of EdU-labeled nuclei to all nuclei in the field was calculated.

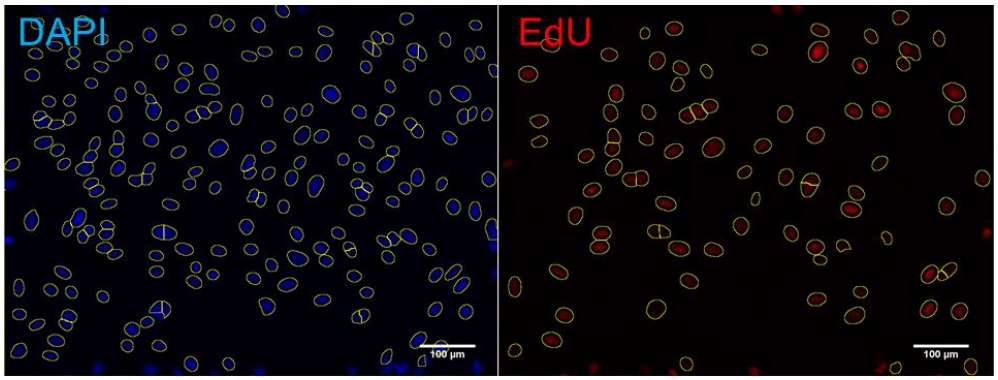

Figure 4.4: Illustration of EdU/DAPI-labeled nuclei recognition by automatic algorithm.

4.6 Statistical analysis

To asses significance of results statistics software GraphPad Prism (GraphPad Software, USA) version 5.04 was used. For one factor comparison in case of two groups the Mann–Whitney U test, in case three and more groups - one-way Anova with Tukey's post-hoc test was applied. For 2 factor analysis two-way ANOVA with post-hoc test by Bonferroni method was used. Statistical tests mentioned in the legend of figures.

5. APPENDIX

Appendix figures

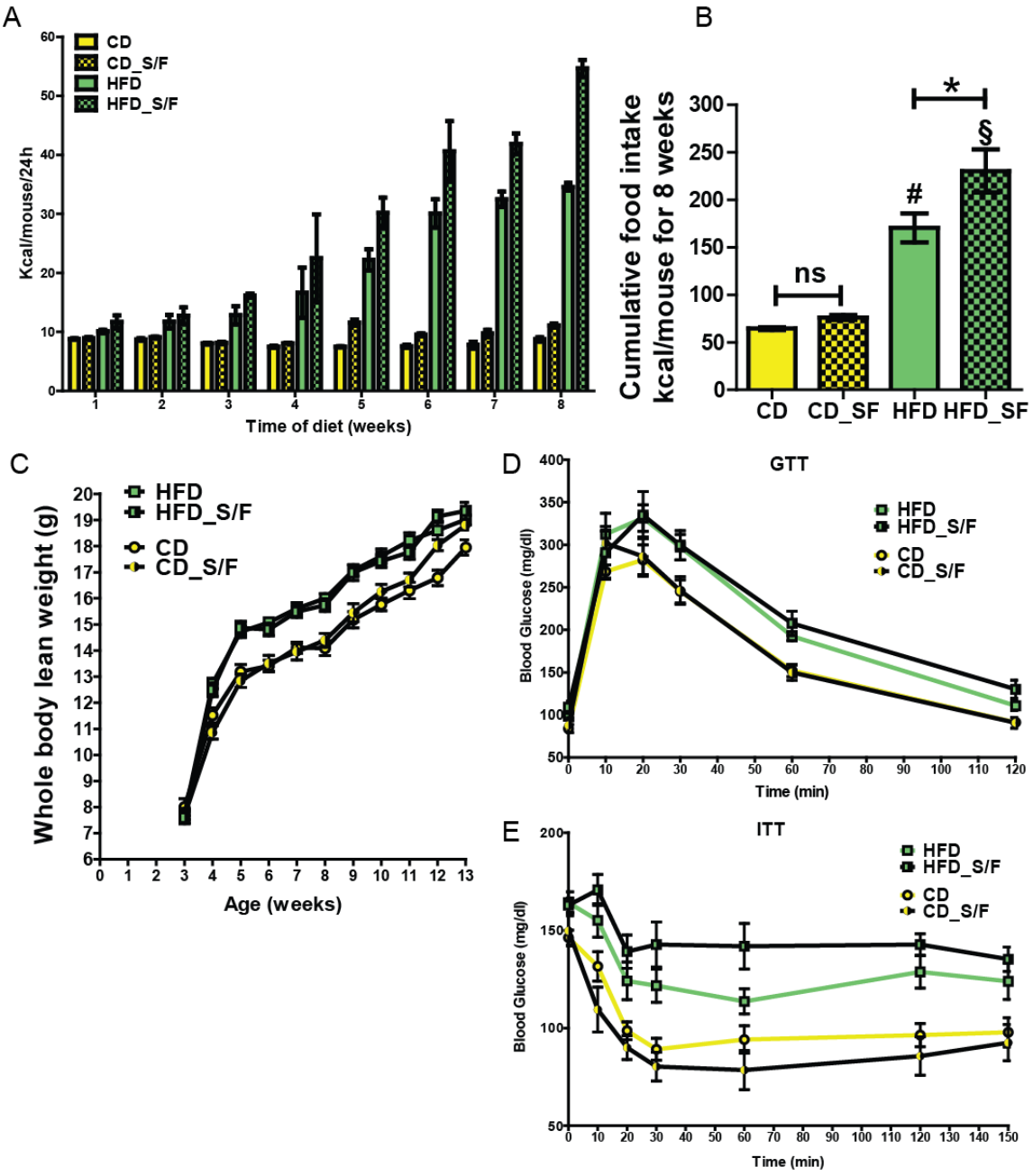

Appendix Figure 1: Long-term effects of high-fat diet and sucrose/fructose in early onset obesity. 40 two-week old female C57BL/6NCrl mice were acclimatized on control diet (CD) for one week and then fed with 4 different diets: CD with water, high-fat diet with water (HFD, 60% of fat), CD with (sucrose/fructose) S/F and HFD with S/F. Diets were applied for 15 weeks. For the first 5 weeks, low concentration of S/F (18.9/23.1 g/l) was applied to acclimatize mice to sweet drinks and for the remaining 10 weeks concentration was increased (94.5/115.5 g/l). **A)** Food intake in kcalories (kcal) calculated per mouse per 24 hours, data represented as mean ± SD from 2 cages per group. **B)** Cumulative food intake for 8 weeks, data represented as mean ± SD from 2 cages per group, two-way Anova with Bonferroni post-hoc test was used to assess significance, *, comparison between indicated groups, pV< 0.05, #, § comparison with CD, pV< 0.05. **C)** Weekly whole body lean mass (by EchoMRI) **D)** Glucose tolerance

test (GTT) was performed after overnight fasting for 16 hours. **E)** Insulin tolerance test (ITT) was performed after 5 hours fasting. C-E data represented as mean ± SEM.

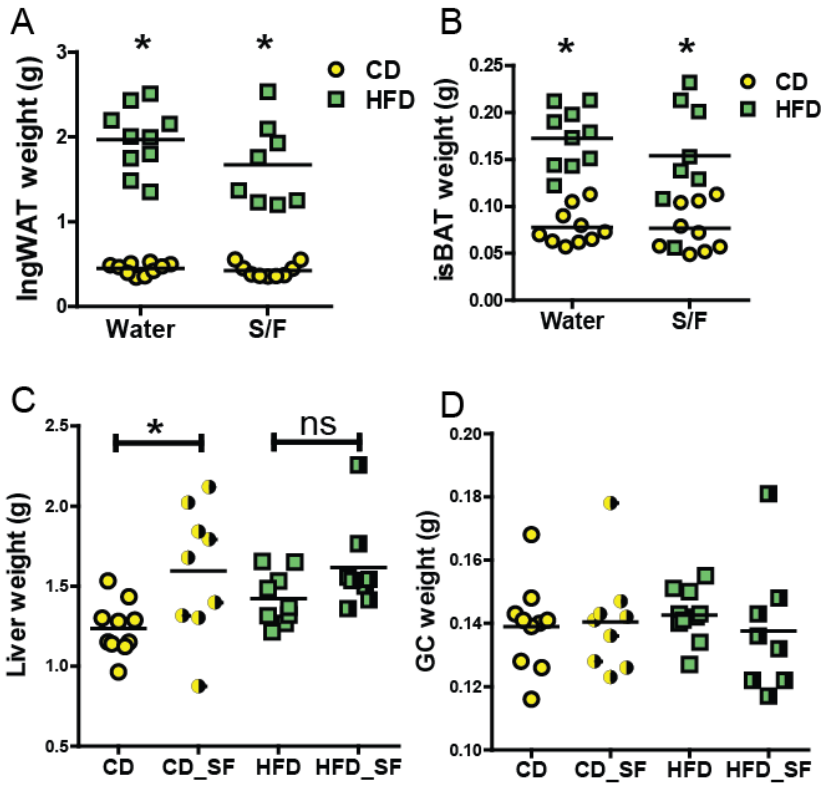

Appendix Figure 2: Long-term effects of high-fat diet and sucrose/fructose in early onset obesity. 40 two-week old female C57BL/6NCrl mice were acclimatized on control diet (CD) for one week and then fed with 4 different diets: CD with water, high-fat diet with water (HFD, 60% of fat), CD with (sucrose/fructose) S/F and HFD with S/F. Diets were applied for 15 weeks. For the first 5 weeks, low concentration of S/F (18.9/23.1 g/l) was applied to acclimatize mice to sweet drinks and for the remaining 10 weeks concentration was increased (94.5/115.5 g/l). **A**) Weight of ingunal WAT (IngWAT). **B)** Weight of interscapular brown adipose tissue (isBAT) **C)** Weight of liver **D)** Weight of gastrocnemius (Gc) muscles. A-D data represented as mean ± SEM, each dot represents individual mouse, line is mean of the group, two-way Anova with Bonferroni post-hoc test was used to assess significance, *, pV< 0.05, ns- no statistically significant difference.

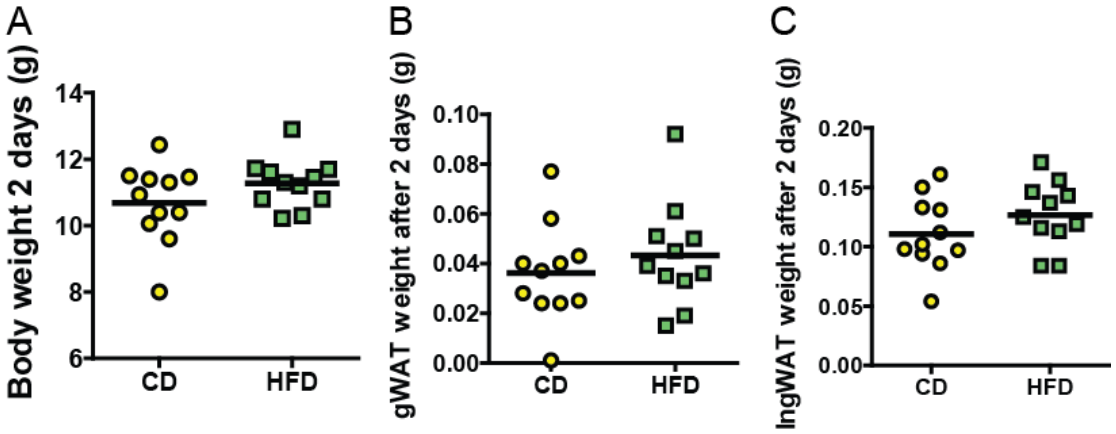

Appendix Figure 3: Body weight and WAT accumulation after two days of high-fat diet. 42 two-week old female C57BL/6NCrl mice were acclimatized on control diet (CD) for one week and then fed with high-fat (HFD) or CD for one week. **A)** Body mass weight. B) Perigonadal WAT (gWAT) weight in

day 2. F) inguinal WAT (IngWAT) weight in day 2. For A-C each dot represents individual mouse, line is mean of the group, Mann-Whitney t- test was used to assess significance.

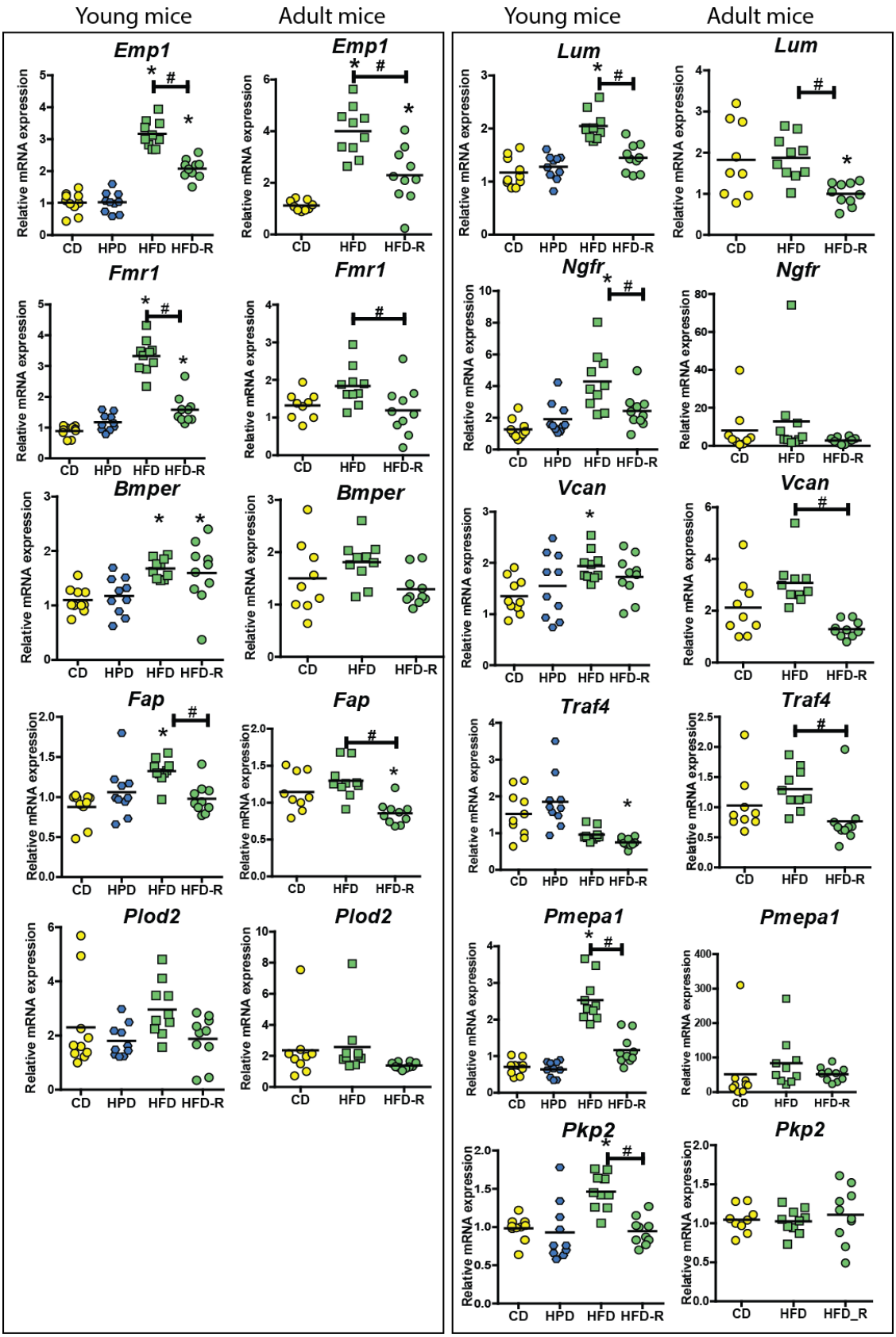

Appendix Figure 4: Validation of selected from expression profiles genes by qPCR. Each dot represents individual mouse, line is mean of the group, significance between groups were tested by one-

way Anova with Tukey's post-hoc test, *, comparison with CD, pV< 0.05, #, comparison with indicated group, pV< 0.05, ns, no statistically significant difference.

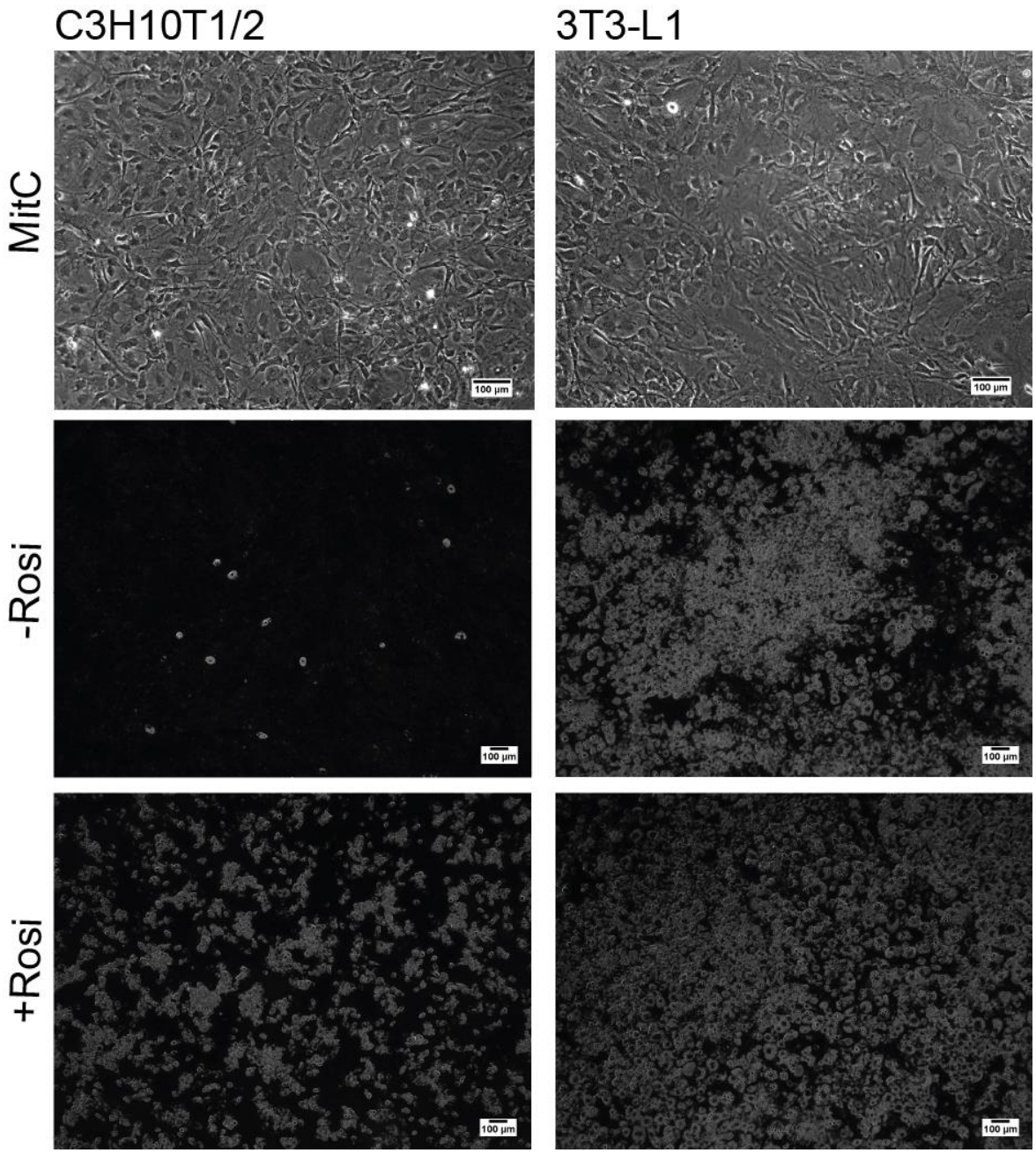

Appendix Figure 5: C3H10T1/2 and 3T3-L1 cell lines as different feeder systems. Upper panel - cells were treated with mitomycin C (MitC) to prevent overgrowth of culture, middle panel - cells were differentiated without rosiglitazone (Rosi) and bottom panel- cells were differentiated with Rosi, scale bar, 100 µm.

Appendix tables

Appendix table 1: The list of enriched gene sets after 2 and 7 days of HFD (vs. CD) (gWAT).

Name of gene set	**day 2**		**day 7**	
31 gene sets included exclusively in "HFD day2":	ES	FDR	ES	FDR
REGULATION OF T CELL ACTIVATION	**0.7**	**0.0000**	0.5	0.161
LIPID RAFT	**0.7**	**0.0030**	0.3	0.694
INTERLEUKIN RECEPTOR ACTIVITY	**0.7**	**0.0072**	0.5	0.127
LEUKOCYTE MIGRATION	**0.7**	**0.0088**	0.5	0.289
T CELL DIFFERENTIATION	**0.7**	**0.0106**	0.5	0.196
VASCULATURE DEVELOPMENT	**0.5**	**0.0131**	0.4	0.138
G PROTEIN COUPLED RECEPTOR BINDING	**0.5**	**0.0141**	0.4	0.138
ANGIOGENESIS	**0.5**	**0.0178**	0.4	0.167
REGULATION OF LYMPHOCYTE ACTIVATION	**0.6**	**0.0202**	0.5	0.128
LYMPHOCYTE DIFFERENTIATION	**0.6**	**0.0212**	0.4	0.243
POSITIVE REGULATION OF T CELL ACTIVATION	**0.6**	**0.0225**	0.5	0.151
ANATOMICAL STRUCTURE FORMATION	**0.5**	**0.0229**	0.4	0.245
POSITIVE REGULATION OF LYMPHOCYTE ACTIVATION	**0.6**	**0.0320**	0.5	0.128
INTERLEUKIN BINDING	**0.6**	**0.0342**	0.4	0.243
CHEMOKINE ACTIVITY	**0.5**	**0.0343**	0.5	0.143
T CELL PROLIFERATION	**0.6**	**0.0392**	0.5	0.128
GOLGI MEMBRANE	**0.5**	**0.0458**	#N/A	#N/A
CELL SURFACE	**0.4**	**0.0489**	#N/A	#N/A
PHAGOCYTOSIS	**0.6**	**0.0517**	0.5	0.386
REGULATION OF T CELL PROLIFERATION	**0.6**	**0.0682**	0.5	0.128
N ACYLTRANSFERASE ACTIVITY	**0.6**	**0.0768**	#N/A	#N/A
CATION HOMEOSTASIS	**0.4**	**0.0755**	0.3	0.292
N ACETYLTRANSFERASE ACTIVITY	**0.6**	**0.0743**	#N/A	#N/A
INFLAMMATORY RESPONSE	**0.4**	**0.0752**	0.3	0.294
CYTOKINE AND CHEMOKINE MEDIATED SIGNALING PATHWAY	**0.6**	**0.0771**	0.5	0.233
CELL MIGRATION	**0.4**	**0.0819**	0.3	0.246
CELLULAR CATION HOMEOSTASIS	**0.4**	**0.0795**	0.3	0.296
RECEPTOR SIGNALING PROTEIN ACTIVITY	**0.4**	**0.0850**	0.2	0.736
ION HOMEOSTASIS	**0.4**	**0.0881**	0.3	0.243
RESPONSE TO VIRUS	**0.5**	**0.0944**	0.4	0.401
TRANSMEMBRANE RECEPTOR PROTEIN KINASE ACTIVITY	**0.4**	**0.0961**	0.4	0.150
38 common gene sets in "HFD day 2" and "HFD day 7":				
HEMATOPOIETIN INTERFERON CLASSD200 DOMAIN CYTOKINE RECEPTOR ACTIVITY	**0.7**	**0.0000**	**0.5**	**0.027**
T CELL ACTIVATION	**0.6**	**0.0000**	**0.5**	**0.068**
CELLULAR DEFENSE RESPONSE	**0.6**	**0.0000**	**0.6**	**0.002**
IMMUNE RESPONSE	**0.5**	**0.0007**	**0.4**	**0.007**
DEFENSE RESPONSE	**0.5**	**0.0013**	**0.4**	**0.030**
IMMUNE SYSTEM PROCESS	**0.4**	**0.0016**	**0.4**	**0.007**
LYMPHOCYTE ACTIVATION	**0.6**	**0.0015**	**0.5**	**0.059**

LEUKOCYTE ACTIVATION	**0.5**	**0.0029**	**0.4**	**0.061**
EXTRACELLULAR MATRIX STRUCTURAL CONSTITUENT	**0.7**	**0.0027**	**0.6**	**0.007**
CYTOKINE METABOLIC PROCESS	**0.6**	**0.0031**	**0.6**	**0.003**
LOCOMOTORY BEHAVIOR	**0.5**	**0.0029**	**0.5**	**0.016**
POSITIVE REGULATION OF CYTOKINE BIOSYNTHETIC PROCESS	**0.7**	**0.0029**	**0.7**	**0.003**
POSITIVE REGULATION OF IMMUNE SYSTEM PROCESS	**0.6**	**0.0067**	**0.5**	**0.039**
CELL ACTIVATION	**0.5**	**0.0069**	**0.4**	**0.060**
REGULATION OF IMMUNE SYSTEM PROCESS	**0.5**	**0.0070**	**0.4**	**0.061**
CYTOKINE BIOSYNTHETIC PROCESS	**0.6**	**0.0069**	**0.6**	**0.003**
REGULATION OF CYTOKINE BIOSYNTHETIC PROCESS	**0.6**	**0.0086**	**0.5**	**0.017**
BEHAVIOR	**0.4**	**0.0112**	**0.5**	**0.006**
POSITIVE REGULATION OF TRANSLATION	**0.5**	**0.0222**	**0.6**	**0.003**
CYTOKINE BINDING	**0.5**	**0.0253**	**0.5**	**0.059**
CHEMOKINE RECEPTOR BINDING	**0.6**	**0.0248**	**0.5**	**0.096**
AUXILIARY TRANSPORT PROTEIN ACTIVITY	**0.6**	**0.0255**	**0.6**	**0.040**
REGULATION OF IMMUNE RESPONSE	**0.5**	**0.0350**	**0.6**	**0.009**
RESPONSE TO EXTERNAL STIMULUS	**0.4**	**0.0383**	**0.3**	**0.066**
RESPONSE TO OTHER ORGANISM	**0.5**	**0.0385**	**0.4**	**0.059**
IMMUNE EFFECTOR PROCESS	**0.5**	**0.0393**	**0.5**	**0.033**
CYTOKINE PRODUCTION	**0.4**	**0.0390**	**0.5**	**0.007**
POSITIVE REGULATION OF IMMUNE RESPONSE	**0.5**	**0.0460**	**0.6**	**0.018**
POSITIVE REGULATION OF CELLULAR PROTEIN METABOLIC PROCESS	**0.4**	**0.0684**	**0.4**	**0.063**
POSITIVE REGULATION OF PROTEIN METABOLIC PROCESS	**0.4**	**0.0674**	**0.4**	**0.061**
RESPONSE TO WOUNDING	**0.4**	**0.0828**	**0.4**	**0.083**
TRANSMEMBRANE RECEPTOR ACTIVITY	**0.3**	**0.0808**	**0.4**	**0.008**
LEUKOCYTE DIFFERENTIATION	**0.5**	**0.0865**	**0.5**	**0.061**
HEMOPOIETIC OR LYMPHOID ORGAN DEVELOPMENT	**0.4**	**0.0930**	**0.4**	**0.086**
POSITIVE REGULATION OF MULTICELLULAR ORGANISMAL PROCESS	**0.4**	**0.0940**	**0.5**	**0.049**
ADAPTIVE IMMUNE RESPONSE GO 0002460	**0.5**	**0.0973**	**0.7**	**0.008**
ADAPTIVE IMMUNE RESPONSE	**0.5**	**0.0976**	**0.6**	**0.005**
AXON GUIDANCE	**0.5**	**0.0974**	**0.6**	**0.021**
88 gene sets included exclusively in "HFD day 7":				
M PHASE OF MITOTIC CELL CYCLE	0.2	0.9904	**0.7**	**0.000**
SPINDLE	0.3	0.7050	**0.8**	**0.000**
MITOSIS	0.2	0.9787	**0.7**	**0.000**
CHROMOSOMEPERICENTRIC REGION	0.3	0.8029	**0.8**	**0.000**
M PHASE	#N/A	#N/A	**0.6**	**0.000**
MITOTIC CELL CYCLE	0.1	1.0000	**0.6**	**0.000**
KINETOCHORE	0.3	0.9530	**0.7**	**0.000**
CHROMOSOME SEGREGATION	0.3	0.7281	**0.7**	**0.000**
SPINDLE MICROTUBULE	#N/A	#N/A	**0.8**	**0.001**
CELL CYCLE PROCESS	#N/A	#N/A	**0.5**	**0.001**

REGULATION OF MITOSIS	0.3	0.8087	**0.6**	**0.001**
SISTER CHROMATID SEGREGATION	0.2	1.0000	**0.8**	**0.002**
MITOTIC SISTER CHROMATID SEGREGATION	0.1	0.9999	**0.8**	**0.002**
CELL CYCLE PHASE	#N/A	#N/A	**0.5**	**0.002**
SPINDLE POLE	0.3	0.9772	**0.7**	**0.002**
PROTEINACEOUS EXTRACELLULAR MATRIX	0.4	0.1008	**0.5**	**0.003**
MOTOR ACTIVITY	#N/A	#N/A	**0.6**	**0.003**
CHROMOSOMAL PART	#N/A	#N/A	**0.5**	**0.004**
MICROTUBULE CYTOSKELETON	0.2	0.9564	**0.5**	**0.004**
CELL DIVISION	0.3	0.6736	**0.7**	**0.004**
COLLAGEN	0.5	0.1234	**0.7**	**0.005**
CYTOKINESIS	0.3	0.8995	**0.7**	**0.006**
MICROTUBULE MOTOR ACTIVITY	0.3	0.9802	**0.7**	**0.008**
CHROMOSOME	#N/A	#N/A	**0.5**	**0.007**
RHODOPSIN LIKE RECEPTOR ACTIVITY	0.3	0.4875	**0.5**	**0.007**
CONDENSED CHROMOSOME	0.2	1.0000	**0.6**	**0.007**
EXTRACELLULAR MATRIX	0.4	0.1310	**0.5**	**0.008**
G PROTEIN COUPLED RECEPTOR ACTIVITY	0.3	0.2623	**0.4**	**0.015**
ESTABLISHMENT OF ORGANELLE LOCALIZATION	0.5	0.1534	**0.7**	**0.016**
MICROTUBULE	#N/A	#N/A	**0.6**	**0.017**
EXTRACELLULAR MATRIX PART	0.3	0.3107	**0.5**	**0.017**
CELL CYCLE GO 0007049	#N/A	#N/A	**0.4**	**0.018**
PEPTIDE RECEPTOR ACTIVITY	#N/A	#N/A	**0.5**	**0.017**
DNA PACKAGING	#N/A	#N/A	**0.5**	**0.020**
CENTROSOME	0.2	1.0000	**0.5**	**0.020**
MICROTUBULE BASED PROCESS	0.2	0.9877	**0.5**	**0.022**
PROTEOGLYCAN METABOLIC PROCESS	0.4	0.4838	**0.6**	**0.024**
NEUROPEPTIDE BINDING	0.4	0.5497	**0.6**	**0.025**
MICROTUBULE CYTOSKELETON ORGANIZATION AND BIOGENESIS	#N/A	#N/A	**0.5**	**0.025**
WOUND HEALING	0.4	0.2157	**0.5**	**0.026**
CARBOHYDRATE BINDING	0.4	0.2337	**0.5**	**0.027**
BRAIN DEVELOPMENT	0.4	0.2588	**0.5**	**0.027**
PATTERN BINDING	0.4	0.1751	**0.5**	**0.030**
HYDROLASE ACTIVITY HYDROLYZING O GLYCOSYL COMPOUNDS	0.4	0.1771	**0.6**	**0.032**
BLOOD COAGULATION	0.4	0.3587	**0.5**	**0.039**
INTEGRIN BINDING	0.4	0.4167	**0.5**	**0.040**
NEUROPEPTIDE RECEPTOR ACTIVITY	0.3	0.6850	**0.6**	**0.043**
G PROTEIN COUPLED RECEPTOR PROTEIN SIGNALING PATHWAY	0.3	0.1404	**0.4**	**0.043**
MITOTIC CELL CYCLE CHECKPOINT	#N/A	#N/A	**0.6**	**0.043**
PROTEIN HOMODIMERIZATION ACTIVITY	0.3	0.2580	**0.4**	**0.048**
CYTOSKELETAL PART	#N/A	#N/A	**0.4**	**0.048**
DEFENSE RESPONSE TO BACTERIUM	0.5	0.1272	**0.6**	**0.049**
PEPTIDE BINDING	0.2	0.7887	**0.4**	**0.052**
COAGULATION	0.3	0.3531	**0.5**	**0.052**

REGULATION OF BODY FLUID LEVELS	0.2	0.7892	**0.5**	**0.057**
G PROTEIN SIGNALING COUPLED TO CAMP NUCLEOTIDE SECOND MESSENGER	0.4	0.2547	**0.4**	**0.059**
PROTEASE INHIBITOR ACTIVITY	0.4	0.1342	**0.5**	**0.059**
POSITIVE REGULATION OF CELL PROLIFERATION	0.3	0.2736	**0.4**	**0.059**
REGULATION OF RESPONSE TO STIMULUS	0.4	0.2635	**0.4**	**0.059**
EXTRACELLULAR REGION	0.3	0.1503	**0.3**	**0.063**
MICROTUBULE ORGANIZING CENTER	#N/A	#N/A	**0.4**	**0.063**
REGULATION OF BLOOD PRESSURE	0.4	0.5309	**0.6**	**0.063**
HEMOSTASIS	0.3	0.5299	**0.5**	**0.062**
EXTRACELLULAR REGION PART	0.3	0.2619	**0.3**	**0.063**
AMINE RECEPTOR ACTIVITY	0.2	1.0000	**0.5**	**0.063**
REGULATION OF PROTEIN SECRETION	0.3	0.7478	**0.6**	**0.063**
CHROMOSOME ORGANIZATION AND BIOGENESIS	0.2	0.9246	**0.4**	**0.064**
CHROMATIN BINDING	#N/A	#N/A	**0.5**	**0.067**
CELL PROLIFERATION GO 0008283	0.2	0.3858	**0.3**	**0.068**
G PROTEIN SIGNALING ADENYLATE CYCLASE ACTIVATING PATHWAY	0.4	0.3232	**0.5**	**0.068**
IMMUNE SYSTEM DEVELOPMENT	0.4	0.1006	**0.4**	**0.070**
FATTY ACID OXIDATION	0.3	0.7183	**0.6**	**0.070**
ORGANELLE LOCALIZATION	0.4	0.2907	**0.5**	**0.070**
POLYSACCHARIDE BINDING	0.4	0.3227	**0.5**	**0.076**
HORMONE ACTIVITY	0.4	0.1579	**0.5**	**0.079**
REGULATION OF CELL PROLIFERATION	0.3	0.3982	**0.3**	**0.079**
RECEPTOR BINDING	0.3	0.1952	**0.3**	**0.079**
RESPONSE TO BACTERIUM	0.4	0.1948	**0.5**	**0.082**
POSITIVE REGULATION OF RESPONSE TO STIMULUS	0.4	0.1371	**0.5**	**0.092**
CAMP MEDIATED SIGNALING	0.3	0.3583	**0.4**	**0.095**
SENSORY PERCEPTION OF CHEMICAL STIMULUS	0.3	0.8191	**0.6**	**0.095**
NEGATIVE REGULATION OF CATALYTIC ACTIVITY	0.3	0.3691	**0.4**	**0.096**
PROTEIN DIMERIZATION ACTIVITY	0.3	0.3571	**0.3**	**0.099**
JAK STAT CASCADE	0.4	0.3564	**0.5**	**0.099**
CELL RECOGNITION	0.4	0.6019	**0.5**	**0.099**
GLYCOSAMINOGLYCAN BINDING	0.4	0.2218	**0.5**	**0.100**
ADENYLATE CYCLASE ACTIVATION	0.5	0.2858	**0.5**	**0.099**
SECOND MESSENGER MEDIATED SIGNALING	0.3	0.1999	**0.4**	**0.099**

Appendix table 2: The list of enriched gene sets after 2 and 7 days of CD (vs. HFD) (gWAT).

Name of gene set	Day 2		Day 7	
28 gene sets included exclusively in "day2":	ES	FDR	ES	FDR
CONTRACTILE FIBER PART	**-0.8**	**0.0000**	-0.3	0.9157
CONTRACTILE FIBER	**-0.8**	**0.0000**	-0.3	0.9414
STRUCTURAL CONSTITUENT OF MUSCLE	**-0.7**	**0.0000**	#N/A	#N/A
MYOFIBRIL	**-0.8**	**0.0002**	-0.2	0.9961
NUCLEOTIDE METABOLIC PROCESS	**-0.6**	**0.0018**	-0.5	0.1697
NUCLEOBASENUCLEOSIDE AND NUCLEOTIDE METABOLIC PROCESS	**-0.6**	**0.0100**	-0.4	0.3225
PROTEIN AMINO ACID O LINKED GLYCOSYLATION	**-0.7**	**0.0181**	-0.6	0.1217
CARBOHYDRATE METABOLIC PROCESS	**-0.4**	**0.0327**	-0.4	0.1125
AEROBIC RESPIRATION	**-0.7**	**0.0324**	-0.6	0.1043
CARBOHYDRATE CATABOLIC PROCESS	**-0.6**	**0.0340**	-0.3	0.6722
CELLULAR CARBOHYDRATE CATABOLIC PROCESS	**-0.6**	**0.0430**	-0.4	0.6659
VOLTAGE GATED CALCIUM CHANNEL ACTIVITY	**-0.6**	**0.0502**	-0.3	0.8825
VOLTAGE GATED CALCIUM CHANNEL COMPLEX	**-0.7**	**0.0528**	-0.4	0.6916
PHOSPHOTRANSFERASE ACTIVITY PHOSPHATE GROUP AS ACCEPTOR	**-0.6**	**0.0535**	-0.6	0.1193
RESPONSE TO ORGANIC SUBSTANCE	**-0.6**	**0.0559**	-0.5	0.1378
REGULATION OF HEART CONTRACTION	**-0.6**	**0.0560**	#N/A	#N/A
REGULATION OF CATABOLIC PROCESS	**-0.6**	**0.0652**	#N/A	#N/A
GENERATION OF PRECURSOR METABOLITES AND ENERGY	**-0.4**	**0.0704**	-0.4	0.1625
MYOSIN COMPLEX	**-0.6**	**0.0707**	-0.4	0.7789
OXIDOREDUCTASE ACTIVITY GO 0016616	**-0.5**	**0.0704**	-0.4	0.1204
CELLULAR CATABOLIC PROCESS	**-0.4**	**0.0703**	-0.4	0.1008
CELLULAR POLYSACCHARIDE METABOLIC PROCESS	**-0.6**	**0.0705**	-0.5	0.4540
CELLULAR CARBOHYDRATE METABOLIC PROCESS	**-0.4**	**0.0704**	-0.3	0.2442
RIBOSOME	**-0.5**	**0.0704**	-0.5	0.1529
CARBOHYDRATE KINASE ACTIVITY	**-0.6**	**0.0744**	-0.5	0.2686
THIOLESTER HYDROLASE ACTIVITY	**-0.6**	**0.0764**	-0.3	0.8844
RESPONSE TO TEMPERATURE STIMULUS	**-0.6**	**0.0758**	-0.6	0.1112
CATABOLIC PROCESS	**-0.4**	**0.0765**	-0.4	0.1316
40 common gene sets in "day2" and "day7":				
MITOCHONDRION	**-0.6**	**0.0000**	**-0.5**	**0.0000**
MITOCHONDRIAL PART	**-0.6**	**0.0000**	**-0.6**	**0.0000**
MITOCHONDRIAL INNER MEMBRANE	**-0.7**	**0.0000**	**-0.6**	**0.0000**
ORGANELLE INNER MEMBRANE	**-0.7**	**0.0000**	**-0.6**	**0.0003**
MITOCHONDRIAL ENVELOPE	**-0.6**	**0.0000**	**-0.6**	**0.0002**
COENZYME METABOLIC PROCESS	**-0.7**	**0.0000**	**-0.7**	**0.0009**
COFACTOR METABOLIC PROCESS	**-0.7**	**0.0000**	**-0.6**	**0.0003**
MITOCHONDRIAL MEMBRANE	**-0.6**	**0.0000**	**-0.6**	**0.0002**
MITOCHONDRIAL RESPIRATORY CHAIN COMPLEX I	**-0.9**	**0.0000**	**-0.7**	**0.0035**
RESPIRATORY CHAIN COMPLEX I	**-0.9**	**0.0000**	**-0.7**	**0.0061**
NADH DEHYDROGENASE COMPLEX	**-0.9**	**0.0000**	**-0.7**	**0.0038**

OXIDOREDUCTASE ACTIVITY ACTING ON NADH OR NADPH	**-0.8**	**0.0000**	**-0.6**	**0.0900**
MITOCHONDRIAL MATRIX	**-0.7**	**0.0000**	**-0.6**	**0.0004**
MITOCHONDRIAL LUMEN	**-0.7**	**0.0000**	**-0.6**	**0.0004**
COFACTOR BIOSYNTHETIC PROCESS	**-0.8**	**0.0000**	**-0.7**	**0.0024**
MITOCHONDRIAL RESPIRATORY CHAIN	**-0.8**	**0.0000**	**-0.7**	**0.0004**
ORGANELLAR RIBOSOME	**-0.8**	**0.0004**	**-0.7**	**0.0012**
MITOCHONDRIAL RIBOSOME	**-0.8**	**0.0005**	**-0.7**	**0.0008**
ORGANELLE ENVELOPE	**-0.5**	**0.0006**	**-0.5**	**0.0062**
MITOCHONDRIAL MEMBRANE PART	**-0.6**	**0.0005**	**-0.6**	**0.0021**
ENVELOPE	**-0.5**	**0.0006**	**-0.5**	**0.0088**
RIBOSOMAL SUBUNIT	**-0.8**	**0.0009**	**-0.8**	**0.0017**
OXIDOREDUCTASE ACTIVITY	**-0.5**	**0.0014**	**-0.4**	**0.0035**
ENERGY DERIVATION BY OXIDATION OF ORGANIC COMPOUNDS	**-0.6**	**0.0014**	**-0.5**	**0.0949**
PROTEASOME COMPLEX	**-0.7**	**0.0019**	**-0.8**	**0.0002**
CARBOHYDRATE TRANSMEMBRANE TRANSPORTER ACTIVITY	**-0.7**	**0.0024**	**-0.7**	**0.0116**
OXIDOREDUCTASE ACTIVITY ACTING ON CH OH GROUP OF DONORS	**-0.5**	**0.0058**	**-0.5**	**0.0621**
CARBOHYDRATE TRANSPORT	**-0.7**	**0.0067**	**-0.7**	**0.0103**
STRUCTURAL CONSTITUENT OF RIBOSOME	**-0.5**	**0.0069**	**-0.6**	**0.0020**
CELLULAR RESPIRATION	**-0.7**	**0.0071**	**-0.6**	**0.0367**
LIPID BIOSYNTHETIC PROCESS	**-0.5**	**0.0070**	**-0.5**	**0.0011**
HYDROGEN ION TRANSMEMBRANE TRANSPORTER ACTIVITY	**-0.6**	**0.0103**	**-0.6**	**0.0646**
STEROID BIOSYNTHETIC PROCESS	**-0.6**	**0.0226**	**-0.7**	**0.0119**
ALCOHOL METABOLIC PROCESS	**-0.5**	**0.0250**	**-0.5**	**0.0560**
GLUCOSE METABOLIC PROCESS	**-0.6**	**0.0392**	**-0.5**	**0.0821**
ELECTRON CARRIER ACTIVITY	**-0.5**	**0.0399**	**-0.5**	**0.0212**
RESPONSE TO OXIDATIVE STRESS	**-0.5**	**0.0501**	**-0.6**	**0.0034**
RNA POLYMERASE ACTIVITY	**-0.6**	**0.0651**	**-0.7**	**0.0235**
LIPID METABOLIC PROCESS	**-0.4**	**0.0692**	**-0.4**	**0.0293**
ORGANELLE MEMBRANE	**-0.4**	**0.0713**	**-0.4**	**0.0412**
29 gene sets included exclusively in "day7":				
PHOSPHATASE REGULATOR ACTIVITY	-0.5	0.2739	**-0.7**	**0.0074**
NUCLEOTIDYLTRANSFERASE ACTIVITY	-0.5	0.1495	**-0.5**	**0.0115**
PEROXISOME ORGANIZATION AND BIOGENESIS	-0.5	0.2233	**-0.7**	**0.0293**
TRANSLATION FACTOR ACTIVITY NUCLEIC ACID BINDING	-0.3	0.7380	**-0.5**	**0.0300**
TRANSLATION REGULATOR ACTIVITY	-0.3	0.8007	**-0.5**	**0.0359**
SECONDARY METABOLIC PROCESS	-0.4	0.4168	**-0.6**	**0.0478**
OXIDOREDUCTASE ACTIVITY ACTING ON THE ALDEHYDE OR OXO GROUP OF DONORS	-0.5	0.1635	**-0.6**	**0.0484**
TRANSLATIONAL INITIATION	-0.2	0.9972	**-0.5**	**0.0499**
TRANSFERASE ACTIVITY TRANSFERRING ALKYL OR ARYLOTHER THAN METHYLGROUPS	-0.5	0.2876	**-0.6**	**0.0549**
CELLULAR PROTEIN COMPLEX ASSEMBLY	-0.5	0.1386	**-0.6**	**0.0588**
OXIDOREDUCTASE ACTIVITY ACTING ON THE CH CH GROUP OF DONORS	-0.5	0.2733	**-0.6**	**0.0590**

PROTEIN N TERMINUS BINDING	-0.3	0.8801	**-0.5**	**0.0618**
LIGASE ACTIVITY	-0.4	0.2869	**-0.4**	**0.0686**
VITAMIN METABOLIC PROCESS	-0.5	0.2308	**-0.6**	**0.0750**
BIOSYNTHETIC PROCESS	-0.3	0.1962	**-0.4**	**0.0752**
NITROGEN COMPOUND CATABOLIC PROCESS	-0.5	0.1898	**-0.6**	**0.0762**
TRNA METABOLIC PROCESS	-0.4	0.6818	**-0.6**	**0.0763**
PHOSPHOLIPID BIOSYNTHETIC PROCESS	-0.4	0.4141	**-0.5**	**0.0766**
MONOVALENT INORGANIC CATION TRANSMEMBRANE TRANSPORTER ACTIVITY	-0.5	0.1335	**-0.5**	**0.0941**
RNA POLYMERASE COMPLEX	-0.3	0.9945	**-0.6**	**0.0941**
CELLULAR BIOSYNTHETIC PROCESS	-0.3	0.2632	**-0.4**	**0.0945**
PHOSPHOLIPID METABOLIC PROCESS	-0.4	0.3275	**-0.4**	**0.0954**
PEROXISOME	-0.4	0.4598	**-0.5**	**0.0955**
GOLGI VESICLE TRANSPORT	-0.2	1.0000	**-0.5**	**0.0957**
NUCLEAR DNA DIRECTED RNA POLYMERASE COMPLEX	-0.3	0.9894	**-0.6**	**0.0962**
MICROBODY	-0.4	0.4254	**-0.5**	**0.0965**
INTRACELLULAR TRANSPORT	-0.3	0.6275	**-0.4**	**0.0969**
TRANSLATION INITIATION FACTOR ACTIVITY	-0.3	0.9774	**-0.5**	**0.0978**
ER TO GOLGI VESICLE MEDIATED TRANSPORT	-0.4	0.8114	**-0.6**	**0.0994**

Appendix table 3: The list of enriched gene sets after 7 days of HFD vs. CD and HPD (gWAT).

Name of gene set	HFD vs. CD		HFD vs. HPD	
32 gene sets included exclusively in "HFD vs. CD":	**ES**	**FDR**	**ES**	**FDR**
KINESIN COMPLEX	**0.8**	**0.0013**	0.6	0.1756
BRAIN DEVELOPMENT	**0.5**	**0.0074**	0.3	0.5564
CYTOSKELETON ORGANIZATION AND BIOGENESIS	**0.4**	**0.0084**	0.4	0.2090
ACTIN CYTOSKELETON ORGANIZATION AND BIOGENESIS	**0.5**	**0.0085**	0.3	0.3341
CARBOHYDRATE BINDING	**0.5**	**0.0171**	0.5	0.1272
ACTIN POLYMERIZATION AND OR DEPOLYMERIZATION	**0.7**	**0.0186**	0.3	0.7999
CYTOSKELETON	**0.4**	**0.0277**	0.4	0.1527
POSITIVE REGULATION OF CELL CYCLE	**0.7**	**0.0319**	0.5	0.3561
POSITIVE REGULATION OF IMMUNE RESPONSE	**0.6**	**0.0325**	0.5	0.1621
PHOSPHOLIPASE C ACTIVATION	**0.7**	**0.0327**	0.7	0.1017
TISSUE DEVELOPMENT	**0.4**	**0.0327**	0.3	0.3786
LEADING EDGE	**0.5**	**0.0370**	0.5	0.1834
POSITIVE REGULATION OF IMMUNE SYSTEM PROCESS	**0.5**	**0.0371**	0.4	0.2539
ACTIN FILAMENT BASED PROCESS	**0.4**	**0.0416**	0.3	0.3608
MESODERM DEVELOPMENT	**0.6**	**0.0444**	0.5	0.3905
MICROTUBULE BASED PROCESS	**0.5**	**0.0544**	0.4	0.1782
CELL PROJECTION BIOGENESIS	**0.6**	**0.0546**	0.5	0.2203
CELL MIGRATION	**0.4**	**0.0561**	0.3	0.4381
CHROMOSOME ORGANIZATION AND BIOGENESIS	**0.4**	**0.0590**	0.4	0.2072
SUGAR BINDING	**0.6**	**0.0594**	0.5	0.1028
PROTEIN HETERODIMERIZATION ACTIVITY	**0.5**	**0.0646**	0.3	0.4966
PHOSPHOLIPASE C ACTIVITY	**0.6**	**0.0672**	0.3	0.8952
SULFURIC ESTER HYDROLASE ACTIVITY	**0.7**	**0.0768**	0.7	0.1435
COLLAGEN BINDING	**0.7**	**0.0796**	0.6	0.2169
PROTEIN DIMERIZATION ACTIVITY	**0.4**	**0.0888**	0.3	0.4386
ENDOPLASMIC RETICULUM LUMEN	**0.7**	**0.0893**	0.6	0.3592
REGULATION OF IMMUNE RESPONSE	**0.5**	**0.0914**	0.4	0.3253
RUFFLE	**0.5**	**0.0919**	0.4	0.3295
BASOLATERAL PLASMA MEMBRANE	**0.5**	**0.0922**	0.4	0.2983
POSITIVE REGULATION OF MULTICELLULAR ORGANISMAL PROCESS	**0.5**	**0.0931**	0.4	0.2362
ACTIN FILAMENT POLYMERIZATION	**0.7**	**0.0932**	0.5	0.6057
LAMELLIPODIUM	**0.6**	**0.0954**	0.5	0.2046
38 common gene sets in "HFD vs. CD" and "HFD vs. HPD":				
SPINDLE	**0.8**	**0**	**0.8**	**0.0000**
MITOSIS	**0.7**	**0**	**0.7**	**0.0000**
M PHASE OF MITOTIC CELL CYCLE	**0.7**	**0**	**0.7**	**0.0000**
M PHASE	**0.6**	**0**	**0.6**	**0.0000**
MITOTIC CELL CYCLE	**0.6**	**0**	**0.6**	**0.0000**
CELL CYCLE PROCESS	**0.5**	**0**	**0.5**	**0.0000**

MICROTUBULE CYTOSKELETON	**0.5**	**0**	**0.5**	**0.0008**
CHROMOSOMEPERICENTRIC REGION	**0.7**	**0**	**0.8**	**0.0000**
CELL CYCLE PHASE	**0.5**	**0**	**0.5**	**0.0001**
CHROMOSOME SEGREGATION	**0.7**	**0.00011**	**0.7**	**0.0001**
SPINDLE MICROTUBULE	**0.8**	**0.00032**	**0.8**	**0.0014**
DNA PACKAGING	**0.7**	**0.00062**	**0.6**	**0.0034**
REGULATION OF MITOSIS	**0.6**	**0.00068**	**0.7**	**0.0001**
CHROMOSOME	**0.5**	**0.00115**	**0.6**	**0.0001**
CELL CYCLE GO 0007049	**0.5**	**0.00122**	**0.5**	**0.0022**
SISTER CHROMATID SEGREGATION	**0.8**	**0.00135**	**0.8**	**0.0010**
SPINDLE ORGANIZATION AND BIOGENESIS	**0.8**	**0.00174**	**0.8**	**0.0302**
MICROTUBULE MOTOR ACTIVITY	**0.8**	**0.00176**	**0.7**	**0.0062**
CELLULAR DEFENSE RESPONSE	**0.6**	**0.00177**	**0.6**	**0.0248**
SPINDLE POLE	**0.7**	**0.00185**	**0.8**	**0.0017**
CHROMOSOMAL PART	**0.5**	**0.00188**	**0.6**	**0.0001**
MICROTUBULE CYTOSKELETON ORGANIZATION AND BIOGENESIS	**0.6**	**0.00208**	**0.6**	**0.0470**
MITOTIC SISTER CHROMATID SEGREGATION	**0.8**	**0.00209**	**0.8**	**0.0009**
CYTOSKELETAL PART	**0.5**	**0.00219**	**0.4**	**0.0219**
CONDENSED CHROMOSOME	**0.6**	**0.00259**	**0.7**	**0.0013**
KINETOCHORE	**0.7**	**0.0046**	**0.7**	**0.0009**
MICROTUBULE ORGANIZING CENTER	**0.5**	**0.00476**	**0.5**	**0.0387**
MOTOR ACTIVITY	**0.6**	**0.0048**	**0.6**	**0.0201**
CHROMOSOME CONDENSATION	**0.8**	**0.00481**	**0.9**	**0.0021**
CENTROSOME	**0.5**	**0.00507**	**0.5**	**0.0233**
CELL CYCLE CHECKPOINT GO 0000075	**0.6**	**0.01118**	**0.6**	**0.0017**
ESTABLISHMENT OF ORGANELLE LOCALIZATION	**0.7**	**0.01128**	**0.6**	**0.0598**
MICROTUBULE	**0.6**	**0.01331**	**0.6**	**0.0032**
MITOTIC CELL CYCLE CHECKPOINT	**0.6**	**0.03233**	**0.7**	**0.0180**
IMMUNE SYSTEM PROCESS	**0.4**	**0.03302**	**0.4**	**0.0347**
IMMUNE RESPONSE	**0.4**	**0.03639**	**0.4**	**0.0478**
CELL DIVISION	**0.6**	**0.03949**	**0.6**	**0.0466**
CYTOKINESIS	**0.6**	**0.05571**	**0.7**	**0.0213**
17 gene sets included exclusively in "HFD vs. HPD":				
HYDROLASE ACTIVITY HYDROLYZING O GLYCOSYL COMPOUNDS	0.5	0.12331	**0.6**	**0.0073**
EXTRACELLULAR MATRIX	0.4	0.15901	**0.5**	**0.0184**
PROTEINACEOUS EXTRACELLULAR MATRIX	0.4	0.10742	**0.5**	**0.0198**
HEMATOPOIETIN INTERFERON CLASSD200 DOMAIN CYTOKINE RECEPTOR ACTIVITY	0.5	0.17973	**0.6**	**0.0204**
EXTRACELLULAR MATRIX STRUCTURAL CONSTITUENT	0.5	0.15472	**0.6**	**0.0207**
HYDROLASE ACTIVITY ACTING ON GLYCOSYL BONDS	0.4	0.46074	**0.6**	**0.0270**
PROTEASE INHIBITOR ACTIVITY	0.5	0.23144	**0.6**	**0.0339**
DEFENSE RESPONSE	0.3	0.19153	**0.4**	**0.0522**
COLLAGEN	0.5	0.17333	**0.6**	**0.0675**
CELL SUBSTRATE ADHESION	0.5	0.1959	**0.5**	**0.0678**

DNA INTEGRITY CHECKPOINT	0.5	0.19197	**0.6**	**0.0699**
POSITIVE REGULATION OF CYTOKINE BIOSYNTHETIC PROCESS	0.5	0.26635	**0.6**	**0.0705**
INTEGRIN BINDING	0.5	0.15876	**0.6**	**0.0786**
INTERLEUKIN RECEPTOR ACTIVITY	0.5	0.23326	**0.6**	**0.0817**
REGULATION OF CELL CYCLE	0.4	0.12463	**0.4**	**0.0850**
INTERFERON GAMMA PRODUCTION	0.5	0.31058	**0.7**	**0.0976**
INTERFERON GAMMA BIOSYNTHETIC PROCESS	0.5	0.33754	**0.7**	**0.0985**

Appendix table 4: The list of enriched gene sets after 7 days of HFD-R vs. CD and HPD (gWAT).

Name of gene set	HFD-R vs. CD		HFD-R vs. HPD	
18 gene sets included exclusively in "HFD R vs. CD":	**ES**	**FDR**	**ES**	**FDR**
BRAIN DEVELOPMENT	**0.6**	**0.0012**	0.5	0.1687
AXON GUIDANCE	**0.7**	**0.0051**	0.5	0.2154
REGULATION OF MUSCLE CONTRACTION	**0.7**	**0.0068**	0.6	0.1875
CELL MATRIX JUNCTION	**0.7**	**0.0128**	0.6	0.1575
MORPHOGENESIS OF AN EPITHELIUM	**0.7**	**0.0188**	0.4	0.6587
BASOLATERAL PLASMA MEMBRANE	**0.6**	**0.0307**	0.5	0.2806
HEMATOPOIETIN INTERFERON CLASSD200 DOMAIN CYTOKINE RECEPTOR BINDING	**0.7**	**0.0313**	#N/A	#N/A
CYTOSKELETON ORGANIZATION AND BIOGENESIS	**0.4**	**0.0498**	0.3	0.2904
CELL SUBSTRATE ADHERENS JUNCTION	**0.6**	**0.0504**	0.6	0.2143
MICROTUBULE BASED PROCESS	**0.5**	**0.0588**	0.4	0.2806
SOLUTE SODIUM SYMPORTER ACTIVITY	**0.7**	**0.0596**	0.5	0.6263
NUCLEAR UBIQUITIN LIGASE COMPLEX	**0.7**	**0.0673**	0.5	0.4757
PROTEIN HOMODIMERIZATION ACTIVITY	**0.4**	**0.0711**	0.4	0.2049
MYELOID CELL DIFFERENTIATION	**0.5**	**0.0718**	0.5	0.2000
SMOOTH MUSCLE CONTRACTION GO 0006939	**0.7**	**0.0743**	0.5	0.4720
CYTOSKELETAL PROTEIN BINDING	**0.4**	**0.0833**	0.3	0.3277
ENDOTHELIAL CELL PROLIFERATION	**0.7**	**0.0837**	0.5	0.4882
MYOBLAST DIFFERENTIATION	**0.6**	**0.0849**	0.5	0.3099
44 common gene sets in "HFD R vs. CD" and "HFD R vs. HPD":				
SPINDLE	**0.8**	**0.0000**	**0.8**	**0.0000**
M PHASE	**0.6**	**0.0000**	**0.6**	**0.0000**
MITOSIS	**0.6**	**0.0000**	**0.7**	**0.0000**
M PHASE OF MITOTIC CELL CYCLE	**0.6**	**0.0000**	**0.7**	**0.0000**
MITOTIC CELL CYCLE	**0.6**	**0.0000**	**0.6**	**0.0000**
CHROMOSOMEPERICENTRIC REGION	**0.8**	**0.0000**	**0.8**	**0.0000**
CELL CYCLE PROCESS	**0.5**	**0.0000**	**0.6**	**0.0000**
CONTRACTILE FIBER	**0.8**	**0.0000**	**0.6**	**0.0139**
CHROMOSOME SEGREGATION	**0.7**	**0.0000**	**0.8**	**0.0000**
STRUCTURAL CONSTITUENT OF MUSCLE	**0.7**	**0.0000**	**0.7**	**0.0011**
CELL CYCLE PHASE	**0.5**	**0.0000**	**0.5**	**0.0001**
SPINDLE MICROTUBULE	**0.8**	**0.0001**	**0.9**	**0.0001**
KINETOCHORE	**0.7**	**0.0001**	**0.8**	**0.0001**

MYOFIBRIL	**0.8**	**0.0001**	**0.7**	**0.0315**
SARCOMERE	**0.9**	**0.0001**	**0.8**	**0.0012**
CONTRACTILE FIBER PART	**0.8**	**0.0002**	**0.7**	**0.0091**
CHROMOSOME	**0.5**	**0.0002**	**0.6**	**0.0000**
CHROMOSOMAL PART	**0.6**	**0.0002**	**0.6**	**0.0001**
MICROTUBULE	**0.7**	**0.0003**	**0.7**	**0.0003**
MICROTUBULE CYTOSKELETON	**0.5**	**0.0006**	**0.5**	**0.0001**
MICROTUBULE MOTOR ACTIVITY	**0.8**	**0.0007**	**0.7**	**0.0083**
ESTABLISHMENT OF ORGANELLE LOCALIZATION	**0.8**	**0.0007**	**0.7**	**0.0094**
CELL CYCLE GO 0007049	**0.5**	**0.0007**	**0.5**	**0.0003**
CHROMOSOME CONDENSATION	**0.9**	**0.0007**	**0.9**	**0.0010**
KINESIN COMPLEX	**0.8**	**0.0009**	**0.7**	**0.0660**
SISTER CHROMATID SEGREGATION	**0.8**	**0.0010**	**0.8**	**0.0002**
MITOTIC SISTER CHROMATID SEGREGATION	**0.8**	**0.0010**	**0.8**	**0.0002**
CONDENSED CHROMOSOME	**0.7**	**0.0010**	**0.7**	**0.0002**
ORGANELLE LOCALIZATION	**0.7**	**0.0013**	**0.6**	**0.0109**
CYTOSKELETAL PART	**0.5**	**0.0019**	**0.5**	**0.0006**
SPINDLE POLE	**0.7**	**0.0030**	**0.7**	**0.0038**
CHROMOSOME ORGANIZATION AND BIOGENESIS	**0.5**	**0.0051**	**0.5**	**0.0376**
DNA PACKAGING	**0.6**	**0.0051**	**0.6**	**0.0241**
SPINDLE ORGANIZATION AND BIOGENESIS	**0.8**	**0.0067**	**0.8**	**0.0063**
MOTOR ACTIVITY	**0.6**	**0.0074**	**0.6**	**0.0391**
CYTOKINESIS	**0.7**	**0.0121**	**0.8**	**0.0001**
CELL DIVISION	**0.7**	**0.0122**	**0.8**	**0.0002**
CENTROSOME	**0.5**	**0.0163**	**0.6**	**0.0012**
REGULATION OF MITOSIS	**0.6**	**0.0187**	**0.7**	**0.0002**
CYTOSKELETON	**0.4**	**0.0214**	**0.4**	**0.0532**
MICROTUBULE CYTOSKELETON ORGANIZATION AND BIOGENESIS	**0.6**	**0.0220**	**0.5**	**0.0680**
NEGATIVE REGULATION OF CELL DIFFERENTIATION	**0.6**	**0.0437**	**0.6**	**0.0757**
MICROTUBULE ORGANIZING CENTER	**0.5**	**0.0465**	**0.6**	**0.0013**
STRIATED MUSCLE CONTRACTION GO 0006941	**0.7**	**0.0651**	**0.8**	**0.0081**
19 gene sets included exclusively in "HFD R vs. HPD":				
HEMATOPOIETIN INTERFERON CLASSD200 DOMAIN CYTOKINE RECEPTOR ACTIVITY	0.5	0.2339	**0.6**	**0.0092**

CELL CYCLE CHECKPOINT GO 0000075	0.5	0.1901	**0.6**	**0.0132**
NEGATIVE REGULATION OF HYDROLASE ACTIVITY	0.6	0.2029	**0.8**	**0.0161**
REGULATION OF CELL CYCLE	0.4	0.1069	**0.4**	**0.0201**
DNA REPLICATION	0.4	0.2083	**0.5**	**0.0338**
DAMAGED DNA BINDING	0.3	0.8636	**0.7**	**0.0345**
HYDROLASE ACTIVITY ACTING ON GLYCOSYL BONDS	0.3	0.5780	**0.5**	**0.0489**
EXTRACELLULAR MATRIX	0.4	0.1330	**0.5**	**0.0501**
MITOTIC CELL CYCLE CHECKPOINT	0.6	0.1688	**0.6**	**0.0610**
REGULATION OF MITOTIC CELL CYCLE	0.5	0.3115	**0.6**	**0.0613**
HYDROLASE ACTIVITY HYDROLYZING O GLYCOSYL COMPOUNDS	0.4	0.3458	**0.6**	**0.0631**
MUSCLE DEVELOPMENT	0.4	0.2429	**0.5**	**0.0634**
ACTIN FILAMENT	0.6	0.1095	**0.6**	**0.0638**
PROTEINACEOUS EXTRACELLULAR MATRIX	0.4	0.1508	**0.5**	**0.0677**
NUCLEAR CHROMOSOME	0.4	0.3095	**0.5**	**0.0685**
REGULATION OF LIPID METABOLIC PROCESS	0.4	0.6910	**0.7**	**0.0744**
LIPID TRANSPORTER ACTIVITY	0.4	0.4514	**0.6**	**0.0769**
INTEGRIN BINDING	0.5	0.1878	**0.6**	**0.0805**
FATTY ACID OXIDATION	0.5	0.3119	**0.6**	**0.0959**

Appendix Figure 5: The list of genes differentially expressed upon 2 and 7 days of HFD vs. CD (gWAT).

Transcript ID	Gene Symbol	Accession	pV (Interaction)	pV (MainDiet)	FC (log) d2	pV d2	FC (log) d7	pV d7
17265268	**Cxcl16**	chemokine (C-X-C motif) ligand 16	**0.0596**	0.2738	0.22	0.33261	0.94	0.002585
17233993	**Egr2**	early growth response 2	**0.0596**	0.9609	0.02	0.96453	0.79	0.003397
17378741	**Nnat**	neuronatin	0.9930	**0.0000**	2.18	0.00018	2.49	4.00E-06
17346150	**Lrg1**	leucine-rich alpha-2-glycoprotein 1	0.3291	**0.0196**	0.71	0.03424	1.65	0.002585
17535208	**Fmr1**	fragile X mental retardation syndrome 1	0.2007	**0.0000**	0.89	0.00218	1.50	0.000172
17395091	**Pmepa1**	prostate transmembrane protein, androgen induced 1	0.9975	**0.0000**	1.37	0.00058	1.35	0.007351
17520364	**Plod2**	procollagen lysine, 2-oxoglutarate 5-dioxygenase 2	0.9930	**0.0471**	0.63	0.09751	1.14	0.011407
17463781	**Emp1**	epithelial membrane protein 1	0.9930	**0.0000**	0.93	0.00093	1.09	0.001549
17325206	**Adcy5**	adenylate cyclase 5	0.9930	**0.0100**	0.61	0.03894	0.92	0.01295
17462451	**Slc6a13**	solute carrier family 6 (neurotransmitter transporter, GABA), member 13	0.9930	**0.0064**	0.61	0.03868	0.91	0.009303
17486110	**Peg3**	paternally expressed 3	0.9930	**0.0046**	0.70	0.01291	0.86	0.03022
17232162	**Vnn1**	vanin 1	0.9948	**0.0098**	1.02	0.0457	0.84	0.10852
17346125	**Plin4**	perilipin 4	0.9975	**0.0008**	0.81	0.02517	0.78	0.010939
17283549	**Ifi27l2a**	interferon, alpha-inducible protein 27 like 2A	0.9930	**0.0003**	0.98	0.01865	0.78	0.010939
17325540	**Gpr156**	G protein-coupled receptor 156	0.9930	**0.0029**	0.63	0.03682	0.77	0.010939
17482943	**Il4ra**	interleukin 4 receptor, alpha	0.9930	**0.0029**	0.59	0.0506	0.76	0.005672
17305034	**Sncg**	synuclein, gamma	0.9956	**0.0282**	0.64	0.13742	0.75	0.025765
17497421	**Bnip3**	BCL2	0.9975	**0.0177**	0.74	0.07724	0.71	0.070535
17289196	**Lhfpl2**	lipoma HMGIC fusion partner-like 2	0.9956	**0.0049**	0.59	0.0457	0.67	0.02013
17425631	**Svep1**	sushi, von Willebrand factor type A, EGF and pentraxin domain containing 1	0.9930	**0.0001**	0.77	0.01377	0.65	0.007417
17227077	**Prelp**	proline arginine-rich end leucine-rich repeat	0.9966	**0.0031**	0.59	0.03651	0.63	0.025441
17438832	**Slc4a4**	solute carrier family 4 (anion exchanger), member 4	0.9975	**0.0228**	0.59	0.09187	0.62	0.068107

17509976	**Slc25a42**	solute carrier family 25, member 42	0.9956	**0.0039**	0.65	0.01301	0.58	0.105568
17341080	**Thbs2**	thrombospondin 2	0.9930	**0.0092**	0.72	0.0983	0.51	0.082842
17527917	**B930092H01Rik**	RIKEN cDNA B930092H01 gene	0.9930	**0.0395**	0.59	0.18892	0.45	0.141935
17430861	**Sesn2**	sestrin 2	0.9930	**0.0292**	0.64	0.09219	0.42	0.283575
17329361	**Kng2**	kininogen 2	0.2057	**0.0010**	-1.02	0.03496	0.08	0.840027
17516124	**Olfr878**	olfactory receptor 878	0.8036	**0.0172**	-0.64	0.09219	-0.02	0.973016
17387624	**Olfr1019**	olfactory receptor 1019	0.5417	**0.0471**	0.91	0.23859	-0.29	0.478422
17242376	**Pfkl**	phosphofructokinase, liver, B-type	0.9930	**0.0004**	-0.60	0.01169	-0.35	0.149665
17350671	**Gm5507**	predicted gene 5507	0.9930	**0.0007**	-0.60	0.02923	-0.43	0.059008
17427860	**Acot11**	acyl-CoA thioesterase 11	0.8957	**0.0009**	-1.19	0.0045	-0.44	0.432976
17251441	**Slc25a35**	solute carrier family 25, member 35	0.9930	**0.0039**	-0.58	0.04212	-0.46	0.095174
17409753	**Agl**	amylo-1,6-glucosidase, 4-alpha-glucanotransferase	0.9930	**0.0046**	-0.58	0.05969	-0.47	0.065319
17324835	**Tfrc**	transferrin receptor	0.9930	**0.0122**	-0.72	0.0983	-0.47	0.140277
17279277	**Aspg**	asparaginase homolog (S. cerevisiae)	0.9956	**0.0177**	-0.60	0.0716	-0.51	0.132116
17496408	**Aldoa**	aldolase A, fructose-bisphosphate	0.9930	**0.0014**	-0.66	0.01301	-0.55	0.071672
17328829	**Slc25a1**	solute carrier family 25 (mitochondrial carrier, citrate transporter), member 1	0.9930	**0.0004**	-0.69	0.01971	-0.58	0.017797
17273200	**Pcyt2**	phosphate cytidylyltransferase 2, ethanolamine	0.9960	**0.0135**	-0.53	0.13613	-0.59	0.012851
17447310	**Lrpap1**	low density lipoprotein receptor-related protein associated protein 1	0.9930	**0.0378**	-0.35	0.18584	-0.60	0.010695
17266335	**Traf4**	TNF receptor associated factor 4	0.9960	**0.0105**	-0.68	0.0457	-0.60	0.105568
17318983	**Tst**	thiosulfate sulfurtransferase, mitochondrial	0.9930	**0.0188**	-0.37	0.09009	-0.61	0.014042
17253461	**Tlcd1**	TLC domain containing 1	0.9940	**0.0438**	-0.50	0.23953	-0.61	0.014189
17505252	**Cyb5b**	cytochrome b5 type B	0.9930	**0.0193**	-0.47	0.15623	-0.61	0.009569
17371847	**Pdk1**	pyruvate dehydrogenase kinase, isoenzyme 1	0.9985	**0.0012**	-0.62	0.02603	-0.61	0.022871
17433040	**Pgd**	phosphogluconate dehydrogenase	0.9966	**0.0006**	-0.66	0.03022	-0.62	0.009569
17427746	**Prkaa2**	protein kinase, AMP-activated, alpha 2 catalytic subunit	0.9956	**0.0098**	-0.54	0.0429	-0.62	0.047859
17526861	**Dlat**	dihydrolipoamide S-acetyltransferase (E2 component of pyruvate dehydrogenase complex)	0.9960	**0.0006**	-0.57	0.01985	-0.62	0.010939

17319554	**Pmm1**	phosphomannomutase 1	0.9930	**0.0429**	-0.43	0.14248	-0.62	0.028678
17453124	**Psph**	phosphoserine phosphatase	0.9966	**0.0253**	-0.56	0.10793	-0.62	0.055638
17335540	**Pim1**	proviral integration site 1	0.9930	**0.0000**	-0.91	0.00103	-0.62	0.01793
17383832	**Gm13610**	predicted gene 13610	0.9977	**0.0055**	-0.61	0.07612	-0.63	0.017609
17220018	**Cnst**	consortin, connexin sorting protein	0.9930	**0.0025**	-0.54	0.02923	-0.64	0.018987
17467556	**Rpia**	ribose 5-phosphate isomerase A	0.9930	**0.0431**	-0.44	0.05522	-0.65	0.05515
17219156	**3110045C21Rik**	RIKEN cDNA 3110045C21 gene	0.9966	**0.0040**	-0.69	0.04242	-0.65	0.040242
17391861	**1700037H04Rik**	RIKEN cDNA 1700037H04 gene	0.9956	**0.0068**	-0.58	0.04242	-0.66	0.034099
17356216	**Pcx**	pyruvate carboxylase	0.9930	**0.0373**	-0.39	0.13207	-0.66	0.014016
17493432	**Thrsp**	thyroid hormone responsive	0.9930	**0.0000**	-0.86	0.00132	-0.66	0.020034
17388756	**Pdhx**	pyruvate dehydrogenase complex, component X	0.9930	**0.0083**	-0.53	0.09943	-0.68	0.007417
17268010	**Acsf2**	acyl-CoA synthetase family member 2	0.9930	**0.0228**	-0.46	0.15126	-0.68	0.008739
17505851	**Nudt7**	nudix (nucleoside diphosphate linked moiety X)-type motif 7	0.9960	**0.0204**	-0.62	0.11498	-0.68	0.031761
17485357	**Dhcr7**	7-dehydrocholesterol reductase	0.9930	**0.0485**	-0.56	0.17467	-0.71	0.034099
17535434	**Nsdhl**	NAD(P) dependent steroid dehydrogenase-like	0.9960	**0.0057**	-0.64	0.06055	-0.71	0.017609
17281843	**Dhrs7**	dehydrogenase	0.9959	**0.0015**	-0.65	0.03372	-0.71	0.010959
17303400	**Pdhb**	pyruvate dehydrogenase (lipoamide) beta	0.9974	**0.0000**	-0.71	0.00525	-0.74	0.003957
17359689	**Scd2**	stearoyl-Coenzyme A desaturase 2	0.9930	**0.0004**	-1.00	0.03022	-0.76	0.006219
17518007	**Pkm**	pyruvate kinase, muscle	0.9956	**0.0000**	-0.72	0.00487	-0.78	0.001713
17400048	**Rorc**	RAR-related orphan receptor gamma	0.9930	**0.0228**	-0.63	0.11639	-0.78	0.02151
17307588	**Fdft1**	farnesyl diphosphate farnesyl transferase 1	0.9930	**0.0047**	-0.56	0.03894	-0.78	0.009984
17418519	**Oscp1**	organic solute carrier partner 1	0.9956	**0.0007**	-0.87	0.00754	-0.79	0.035351
17231229	**Hsd11b1**	hydroxysteroid 11-beta dehydrogenase 1	0.9930	**0.0122**	-0.64	0.06513	-0.79	0.022871
17501041	**Casp3**	caspase 3	0.9930	**0.0101**	-0.57	0.10205	-0.80	0.005672
17428209	**9630013D21Rik**	RIKEN cDNA 9630013D21 gene	0.9930	**0.0376**	-0.55	0.20247	-0.82	0.007029
17254395	**Acaca**	acetyl-Coenzyme A carboxylase alpha	0.9975	**0.0000**	-0.85	0.00487	-0.83	0.002942
17351473	**Slmo1**	slowmo homolog 1 (Drosophila)	0.9930	**0.0008**	-0.62	0.01219	-0.83	0.007332

17468018	**Hk2**	hexokinase 2	0.9930	**0.0211**	-0.65	0.09009	-0.83	0.02468
17475498	**Cyp2f2**	cytochrome P450, family 2, subfamily f, polypeptide 2	0.9960	**0.0207**	-0.75	0.18584	-0.84	0.005517
17442187	**Tmem120b**	transmembrane protein 120B	0.9930	**0.0147**	-0.56	0.10802	-0.84	0.005949
17326567	**Gbe1**	glucan (1,4-alpha-), branching enzyme 1	0.9966	**0.0002**	-0.81	0.01007	-0.84	0.005672
17529398	**Me1**	malic enzyme 1, NADP(+)-dependent, cytosolic	0.9930	**0.0000**	-0.96	0.00215	-0.85	0.001713
17284037	**Mpc1**	mitochondrial pyruvate carrier 1	0.9930	**0.0029**	-0.62	0.04124	-0.86	0.005423
17370897	**Gpd2**	glycerol phosphate dehydrogenase 2, mitochondrial	0.9960	**0.0027**	-0.79	0.01469	-0.86	0.028633
17443185	**Mlxipl**	MLX interacting protein-like	0.9930	**0.0146**	-0.65	0.08166	-0.86	0.014409
17483007	**Sbk1**	SH3-binding kinase 1	0.9960	**0.0042**	-0.80	0.07724	-0.88	0.005124
17362595	**Fads2**	fatty acid desaturase 2	0.9930	**0.0011**	-0.59	0.03894	-0.89	0.001713
17298183	**Tkt**	transketolase	0.9971	**0.0000**	-0.93	0.00254	-0.90	0.005691
17525955	**Sc5d**	sterol-C5-desaturase (fungal ERG3, delta-5-desaturase) homolog (S. cerevisae)	0.9930	**0.0098**	-0.70	0.11155	-0.90	0.004499
17333079	**Mpc1**	mitochondrial pyruvate carrier 1	0.9930	**0.0114**	-0.69	0.04619	-0.91	0.020232
17285056	**Idi1**	isopentenyl-diphosphate delta isomerase	0.9930	**0.0039**	-0.70	0.04105	-0.91	0.008739
17281721	**Pygl**	liver glycogen phosphorylase	0.9930	**0.0000**	-1.08	0.01007	-0.93	0.001713
17501098	**Cldn22**	claudin 22	0.9966	**0.0137**	-1.02	0.08188	-0.94	0.05551
17361299	**2010003K11Rik**	RIKEN cDNA 2010003K11 gene	0.9930	**0.0034**	-0.72	0.0457	-0.94	0.005672
17396056	**Fabp5**	fatty acid binding protein 5, epidermal	0.9930	**0.0301**	-0.53	0.2211	-0.94	0.001549
17330463	**Gm19522**	predicted gene, 19522	0.9930	**0.0218**	-0.73	0.17153	-0.95	0.005014
17279317	**A530016L24Rik**	RIKEN cDNA A530016L24 gene	0.9930	**0.0445**	-0.56	0.20221	-0.96	0.005112
17531650	**Pth1r**	parathyroid hormone 1 receptor	0.9930	**0.0005**	-0.79	0.03894	-0.97	0.000667
17221360	**Lactb2**	lactamase, beta 2	0.9930	**0.0020**	-0.70	0.07612	-0.99	0.000612
17454382	**Adap1**	ArfGAP with dual PH domains 1	0.9938	**0.0211**	-0.84	0.12061	-1.01	0.015417
17340967	**Acat2**	acetyl-Coenzyme A acetyltransferase 2	0.9930	**0.0188**	-0.76	0.0716	-1.02	0.018987
17547610	**Fasn**	fatty acid synthase	0.9966	**0.0015**	-0.97	0.03496	-1.02	0.007539
17483133	**Fam57b**	family with sequence similarity 57, member B	0.9989	**0.0001**	-1.03	0.01157	-1.02	0.002168

17548238	**Gm3601**	predicted gene 3601	0.9930	**0.0366**	-0.57	0.15126	-1.06	0.004188
17435584	**Insig1**	insulin induced gene 1	0.9930	**0.0092**	-0.74	0.11915	-1.06	0.001713
17442719	**Aacs**	acetoacetyl-CoA synthetase	0.9930	**0.0038**	-0.85	0.0457	-1.07	0.005672
17472497	**Gys2**	glycogen synthase 2	0.9930	**0.0004**	-1.26	0.03022	-1.08	0.002168
17265096	**Slc2a4**	solute carrier family 2 (facilitated glucose transporter), member 4	0.9930	**0.0007**	-0.71	0.03022	-1.08	0.001549
17548717	**Gm3601**	predicted gene 3601	0.9930	**0.0235**	-0.60	0.12005	-1.08	0.003771
17442046	**Hvcn1**	hydrogen voltage-gated channel 1	0.9930	**0.0297**	-0.76	0.18644	-1.13	0.003425
17269521	**Acly**	ATP citrate lyase	0.9930	**0.0000**	-1.40	0.00093	-1.17	0.002585
17252912	**Tlcd2**	TLC domain containing 2	0.9930	**0.0206**	-0.89	0.13804	-1.19	0.005672
17399474	**Pmvk**	phosphomevalonate kinase	0.9930	**0.0001**	-1.07	0.00651	-1.21	0.001713
17406708	**Tmem79**	transmembrane protein 79	0.9930	**0.0071**	-0.95	0.04212	-1.25	0.010939
17406908	**Fdps**	farnesyl diphosphate synthetase	0.9930	**0.0025**	-1.08	0.03475	-1.29	0.007021
17355443	**Lipg**	lipase, endothelial	0.9930	**0.0092**	-0.90	0.0457	-1.30	0.008352
17439037	**Parm1**	prostate androgen-regulated mucin-like protein 1	0.9930	**0.0006**	-0.90	0.01985	-1.31	0.001549
17513681	**Mvd**	mevalonate (diphospho) decarboxylase	0.9930	**0.0107**	-0.87	0.07724	-1.31	0.005014
17525894	**Sorl1**	sortilin-related receptor, LDLR class A repeats-containing	0.9930	**0.0016**	-1.01	0.04212	-1.31	0.001762
17402558	**Elovl6**	ELOVL family member 6, elongation of long chain fatty acids (yeast)	0.9930	**0.0000**	-1.51	0.00093	-1.37	0.000535
17414747	**Orm2**	orosomucoid 2	0.9956	**0.0098**	-1.19	0.1048	-1.39	0.005112
17500543	**Ppp1r3b**	protein phosphatase 1, regulatory (inhibitor) subunit 3B	0.9960	**0.0050**	-1.57	0.00651	-1.40	0.109325
17445308	**Cyp51**	cytochrome P450, family 51	0.9930	**0.0016**	-0.92	0.03354	-1.44	0.00167
17515335	**Gm6484**	predicted gene 6484	0.9966	**0.0207**	-1.35	0.06708	-1.47	0.051943
17234552	**Lss**	lanosterol synthase	0.9930	**0.0010**	-1.16	0.03354	-1.49	0.001713
17440826	**Acacb**	acetyl-Coenzyme A carboxylase beta	0.9930	**0.0015**	-0.98	0.03424	-1.49	0.001549
17378359	**Acss2**	acyl-CoA synthetase short-chain family member 2	0.9985	**0.0000**	-1.51	0.0041	-1.50	0.001713
17357981	**Prune2**	prune homolog 2 (Drosophila)	0.9930	**0.0453**	-0.86	0.2487	-1.51	0.001549
17256388	**Ttc25**	tetratricopeptide repeat domain 25	0.9956	**0.0000**	-1.43	0.00093	-1.53	0.00167
17218965	**Adcy10**	adenylate cyclase 10	0.9930	**0.0010**	-1.33	0.01865	-1.63	0.004499

17421875	**Slc2a5**	solute carrier family 2 (facilitated glucose transporter), member 5	0.9930	**0.0000**	-2.51	7.90E-05	-2.09	0.000667
17524117	**Hephl1**	hephaestin-like 1	0.9930	**0.0068**	-1.54	0.09704	-2.28	0.001137
17359678	**Scd3**	stearoyl-coenzyme A desaturase 3	0.9956	0.0863	-0.61	**0.0429**	-0.75	0.157693
17480675	**P4ha3**	procollagen-proline, 2-oxoglutarate 4-dioxygenase (proline 4-hydroxylase), alpha polypeptide III	0.2007	0.6577	0.29	0.59665	1.69	**0.007627**
17302031	**Siah3**	seven in absentia homolog 3 (Drosophila)	0.2007	0.6530	0.21	0.53991	1.27	**0.009303**
17439535	**Bmp3**	bone morphogenetic protein 3	0.7553	0.0601	0.56	0.02923	1.25	**0.010939**
17491193	**Saa3**	serum amyloid A 3	0.8186	0.6614	0.29	0.72299	1.18	**0.010939**
17512809	**Hp**	haptoglobin	0.9930	0.0539	0.75	0.08166	1.15	**0.033421**
17263073	**Gm12248**	predicted gene 12248	0.7884	0.6185	0.27	0.63335	1.08	**0.020172**
17268210	**Ngfr**	nerve growth factor receptor (TNFR superfamily, member 16)	0.9930	0.0826	0.68	0.24235	0.95	**0.021848**
17538018	**Nrk**	Nik related kinase	0.9904	0.1088	0.38	0.13207	0.80	**0.02013**
17230918	**Cenpf**	centromere protein F	0.9930	0.7578	0.20	0.80339	0.80	**0.028162**
17491285	**Ptpn5**	protein tyrosine phosphatase, non-receptor type 5	0.7553	0.6718	0.18	0.65031	0.78	**0.034099**
17428017	**Zyg11a**	zyg-11 family member A, cell cycle regulator	0.9930	0.6413	0.24	0.71718	0.76	**0.026692**
17397932	**Sucnr1**	succinate receptor 1	0.9930	0.0559	0.58	0.26685	0.76	**0.009303**
17456934	**Mest**	mesoderm specific transcript	0.2007	0.8522	0.08	0.88287	0.76	**0.002942**
17284919	**Akr1c14**	aldo-keto reductase family 1, member C14	0.9930	0.4896	0.31	0.63111	0.75	**0.018719**
17228234	**Npl**	N-acetylneuraminate pyruvate lyase	0.9417	0.5187	0.24	0.54818	0.74	**0.040242**
17402797	**Cenpe**	centromere protein E	0.9930	0.7442	0.18	0.79443	0.72	**0.02635**
17482000	**Spon1**	spondin 1, (f-spondin) extracellular matrix protein	0.9930	0.3082	0.33	0.3886	0.72	**0.040242**
17381630	**Pfkfb3**	6-phosphofructo-2-kinase	0.9930	0.2137	0.44	0.38363	0.70	**0.04681**
17462351	**Il17ra**	interleukin 17 receptor A	0.4769	0.7400	0.12	0.75974	0.69	**0.016704**
17467232	**Gprin3**	GPRIN family member 3	0.9930	0.1467	0.42	0.36119	0.66	**0.020786**
17515478	**Bmper**	BMP-binding endothelial regulator	0.9930	0.0586	0.36	0.27317	0.64	**0.005672**
17404859	**Trpc3**	transient receptor potential cation channel, subfamily C, member 3	0.9930	0.1206	0.41	0.2367	0.64	**0.044802**
17430645	**Nkain1**	Na+/K+ transporting ATPase interacting 1	0.9930	0.1478	0.39	0.26848	0.64	**0.047859**
17358838	**Kif20b**	kinesin family member 20B	0.9930	0.9112	0.09	0.92723	0.62	**0.047859**

17449795	**4932430I15Rik**	RIKEN cDNA 4932430I15 gene	0.2555	0.9289	-0.05	0.92538	0.61	**0.034099**
17211305	**Pi15**	peptidase inhibitor 15	0.9930	0.2722	0.34	0.51511	0.60	**0.010979**
17294738	**Vcan**	versican	0.9553	0.2521	0.25	0.51101	0.60	**0.004492**
17323192	**Snai2**	snail homolog 2 (Drosophila)	0.7884	0.2284	0.23	0.46658	0.60	**0.005227**
17271751	**Gm11711**	predicted gene 11711	0.9930	0.1743	0.39	0.376	0.59	**0.036331**
17374488	**Thbs1**	thrombospondin 1	0.3884	0.7094	0.11	0.76346	0.58	**0.011683**
17481550	**Olfml1**	olfactomedin-like 1	0.9930	0.2278	-0.30	0.359	-0.59	**0.038812**
17280062	**Lpin1**	lipin 1	0.9930	0.8346	-0.12	0.86709	-0.59	**0.02961**
17255210	**Tob1**	transducer of ErbB-2.1	0.9930	0.0847	-0.36	0.25027	-0.59	**0.021501**
17435946	**Abhd1**	abhydrolase domain containing 1	0.9930	0.2994	-0.29	0.46674	-0.59	**0.02961**
17259383	**Slc25a10**	solute carrier family 25 (mitochondrial carrier, dicarboxylate transporter), member 10	0.9930	0.4581	-0.27	0.61392	-0.59	**0.028162**
17509629	**Sc4mol**	sterol-C4-methyl oxidase-like	0.9930	0.1297	-0.41	0.31711	-0.61	**0.035058**
17410251	**Enpep**	glutamyl aminopeptidase	0.9930	0.2472	-0.33	0.46397	-0.62	**0.015151**
17426981	**Plin2**	perilipin 2	0.9930	0.1081	-0.39	0.31003	-0.65	**0.014042**
17368349	**Fam69b**	family with sequence similarity 69, member B	0.9930	0.0557	-0.50	0.13751	-0.67	**0.048555**
17388371	**Mapk8ip1**	mitogen-activated protein kinase 8 interacting protein 1	0.9930	0.0591	-0.44	0.20247	-0.67	**0.018621**
17232763	**Ddo**	D-aspartate oxidase	0.9930	0.0906	-0.45	0.20826	-0.68	**0.036544**
17363429	**Aldh1a7**	aldehyde dehydrogenase family 1, subfamily A7	0.9930	0.1374	-0.53	0.35544	-0.69	**0.035196**
17294664	**Polr3g**	polymerase (RNA) III (DNA directed) polypeptide G	0.9930	0.1911	-0.38	0.35687	-0.70	**0.025441**
17386569	**Chn1**	chimerin (chimaerin) 1	0.8123	0.3910	-0.24	0.47587	-0.70	**0.018621**
17503650	**Nkd1**	naked cuticle 1 homolog (Drosophila)	0.9930	0.3901	-0.27	0.42445	-0.70	**0.042994**
17401480	**Dennd2d**	DENN	0.9553	0.4223	-0.26	0.55409	-0.71	**0.016801**
17355189	**Spire1**	spire homolog 1 (Drosophila)	0.9930	0.0698	-0.45	0.24329	-0.71	**0.012426**
17502233	**Slc27a1**	solute carrier family 27 (fatty acid transporter), member 1	0.9930	0.0826	-0.37	0.2648	-0.72	**0.007417**
17503094	**Podnl1**	podocan-like 1	0.2555	0.9395	-0.04	0.93351	-0.76	**0.015884**
17417146	**Pdzk1ip1**	PDZK1 interacting protein 1	0.9930	0.7658	-0.23	0.8364	-0.77	**0.011332**
17453714	**Sh2b2**	SH2B adaptor protein 2	0.9930	0.1194	-0.41	0.38363	-0.78	**0.002856**

17229466	**Hsd17b7**	hydroxysteroid (17-beta) dehydrogenase 7	0.9930	0.1264	-0.52	0.38448	-0.79	**0.007332**
17256537	**Mlx**	MAX-like protein X	0.9930	0.0512	-0.54	0.17153	-0.79	**0.02013**
17493461	**Aqp11**	aquaporin 11	0.9289	0.5904	-0.24	0.62291	-0.82	**0.03022**
17319050	**Mfng**	MFNG O-fucosylpeptide 3-beta-N-acetylglucosaminyltransferase	0.9930	0.3538	-0.33	0.46993	-0.83	**0.017579**
17311512	**Mal2**	mal, T cell differentiation protein 2	0.9930	0.4704	-0.51	0.63111	-0.88	**0.032011**
17378848	**Snhg11**	small nucleolar RNA host gene 11	0.9930	0.2525	-0.52	0.46658	-0.91	**0.012426**
17281084	**Egln3**	EGL nine homolog 3 (C. elegans)	0.9930	0.2007	-0.44	0.44467	-0.92	**0.003771**
17368171	**Bmyc**	brain expressed myelocytomatosis oncogene	0.9930	0.1288	-0.45	0.22718	-0.93	**0.012675**
17282158	**Rdh11**	retinol dehydrogenase 11	0.3884	0.0882	-0.37	0.2487	-0.97	**0.002168**
17300147	**Traj53**	T cell receptor alpha joining 53	0.8123	0.4776	-0.32	0.52068	-1.02	**0.02013**
17404073	**Fabp5**	fatty acid binding protein 5, epidermal	0.9930	0.1513	-0.58	0.27477	-1.03	**0.02182**
17522504	**Als2cl**	ALS2 C-terminal like	0.4769	0.1468	-0.38	0.14585	-1.04	**0.007961**
17509944	**Ncan**	neurocan	0.9930	0.1422	-0.76	0.28995	-1.07	**0.042777**
17245481	**Rassf3**	Ras association (RalGDS	0.2555	0.0534	-0.40	0.17146	-1.08	**0.001713**
17311807	**Sqle**	squalene epoxidase	0.9930	0.1850	-0.64	0.37558	-1.11	**0.01516**
17300247	**Trav9d-3**	T cell receptor alpha variable 9D-3	0.1821	0.9441	0.06	0.93994	-1.13	**0.008774**
17472271	**Slc15a5**	solute carrier family 15, member 5	0.8141	0.4223	-0.39	0.45695	-1.19	**0.018631**
17361996	**Ppp2r5b**	protein phosphatase 2, regulatory subunit B (B56), beta isoform	0.9930	0.0528	-0.75	0.22956	-1.37	**0.002168**
17300163	**Traj44**	T cell receptor alpha joining 44	0.8202	0.3532	-0.58	0.53879	-1.60	**0.002168**
17487805	**Atp1a3**	ATPase, Na+	0.4931	0.5716	-0.48	0.71437	-1.98	**0.000427**
17414738	**Orm3**	orosomucoid 3	0.9471	0.0801	-1.01	0.28436	-2.10	**0.001549**

Appendix table 6: List of genes differentially expressed upon 7 days of HFD vs. CD from second profiling (gWAT)

Transcript ID	Gene Symbol	Accession	FC (log)	pV
17378741	Nnat	neuronatin	1.91	0.03595
17421875	Slc2a5	solute carrier family 2 (facilitated glucose transporter), member 5	-1.81	0.01972
17487805	Atp1a3	ATPase, Na+	-1.43	0.02484
17414738	Orm3	orosomucoid 3	-1.38	0.04011
17359918	Elovl3	elongation of very long chain fatty acids (FEN1	-1.37	0.04011
17395091	Pmepa1	prostate transmembrane protein, androgen induced 1	1.29	0.01629
17535208	Fmr1	fragile X mental retardation syndrome 1	1.26	0.01629
17256388	Ttc25	tetratricopeptide repeat domain 25	-1.25	0.01629
17440826	Acacb	acetyl-Coenzyme A carboxylase beta	-1.23	0.00429
17218965	Adcy10	adenylate cyclase 10	-1.14	0.03595
17548559	Emp1	epithelial membrane protein 1	1.10	0.04011
17366746	Mir669k	microRNA 669k	-1.03	0.02605
17402558	Elovl6	ELOVL family member 6, elongation of long chain fatty acids (yeast)	-1.01	0.03595
17400048	Rorc	RAR-related orphan receptor gamma	-1.01	0.01938
17355443	Lipg	lipase, endothelial	-0.99	0.04342
17439037	Parm1	prostate androgen-regulated mucin-like protein 1	-0.97	0.04011
17463781	Emp1	epithelial membrane protein 1	0.95	0.01629
17231229	Hsd11b1	hydroxysteroid 11-beta dehydrogenase 1	-0.95	0.01685
17513681	Mvd	mevalonate (diphospho) decarboxylase	-0.95	0.03811
17483133	Fam57b	family with sequence similarity 57, member B	-0.94	0.01938
17340967	Acat2	acetyl-Coenzyme A acetyltransferase 2	-0.94	0.01972
17351473	Slmo1	slowmo homolog 1 (Drosophila)	-0.93	0.04375
17531650	Pth1r	parathyroid hormone 1 receptor	-0.90	0.01972
17282158	Rdh11	retinol dehydrogenase 11	-0.90	0.03775
17482943	Il4ra	interleukin 4 receptor, alpha	0.85	0.04011
17522504	Als2cl	ALS2 C-terminal like	-0.85	0.01629
17443185	Mlxipl	MLX interacting protein-like	-0.84	0.01629
17265096	Slc2a4	solute carrier family 2 (facilitated glucose transporter), member 4	-0.83	0.01938
17442046	Hvcn1	hydrogen voltage-gated channel 1	-0.83	0.04011
17527934	Kif23	kinesin family member 23	0.80	0.04923
17335540	Pim1	proviral integration site 1	-0.80	0.01629
17469627	Oxtr	oxytocin receptor	-0.79	0.03775
17502233	Slc27a1	solute carrier family 27 (fatty acid transporter), member 1	-0.78	0.04011
17470119	Ret	ret proto-oncogene	0.78	0.03595
17442719	Aacs	acetoacetyl-CoA synthetase	-0.77	0.01938
17245481	Rassf3	Ras association (RalGDS	-0.77	0.04078
17325206	Adcy5	adenylate cyclase 5	0.77	0.04787
17397907	Gm9696	arylacetamide deacetylase-like 2 pseudogene	-0.77	0.04923
17370897	Gpd2	glycerol phosphate dehydrogenase 2, mitochondrial	-0.75	0.01938
17333079	Mpc1	mitochondrial pyruvate carrier 1	-0.74	0.0173
17217914	Aspm	asp (abnormal spindle)-like, microcephaly associated (Drosophila)	0.73	0.04375

17479575	Prc1	protein regulator of cytokinesis 1	0.73	0.04923
17229433	Nuf2	NUF2, NDC80 kinetochore complex component, homolog (S. cerevisiae)	0.72	0.03811
17399474	Pmvk	phosphomevalonate kinase	-0.71	0.04078
17433145	Rbp7	retinol binding protein 7, cellular	0.71	0.04923
17268909	Top2a	topoisomerase (DNA) II alpha	0.71	0.04553
17234436	Chchd10	coiled-coil-helix-coiled-coil-helix domain containing 10	-0.70	0.01972
17397932	Sucnr1	succinate receptor 1	0.70	0.04078
17236811	Lum	lumican	0.68	0.0286
17523494	Kif15	kinesin family member 15	0.68	0.02605
17508025	Ckap2	cytoskeleton associated protein 2	0.68	0.04011
17498750	Cd209g	CD209g antigen	0.66	0.03979
17269521	Acly	ATP citrate lyase	-0.66	0.04011
17526881	Dixdc1	DIX domain containing 1	-0.65	0.02582
17371847	Pdk1	pyruvate dehydrogenase kinase, isoenzyme 1	-0.64	0.02484
17285867	Hist1h2ab	histone cluster 1, H2ab	0.64	0.04011
17531671	Tmie	transmembrane inner ear	-0.63	0.04553
17388756	Pdhx	pyruvate dehydrogenase complex, component X	-0.63	0.01938
17268010	Acsf2	acyl-CoA synthetase family member 2	-0.62	0.03811
17505851	Nudt7	nudix (nucleoside diphosphate linked moiety X)-type motif 7	-0.62	0.03348
17442187	Tmem120b	transmembrane protein 120B	-0.62	0.0337
17252609	P2rx5	purinergic receptor P2X, ligand-gated ion channel, 5	-0.61	0.03811
17456934	Mest	mesoderm specific transcript	0.60	0.04011
17217789	Kif14	kinesin family member 14	0.59	0.02697
17232763	Ddo	D-aspartate oxidase	-0.59	0.03811
17519910	Ttk	Ttk protein kinase	0.58	0.04078

Appendix table 7: List of genes differentially expressed upon 7 days of HFD vs. HFD-R from second profiling (gWAT)

Transcript ID	Gene Symbol	Accession	FC (log)	pV
17477979	Dbp	D site albumin promoter binding protein	1.99	0.0002
17515335	Gm6484	predicted gene 6484	-1.46	0.0076
17303625	Nr1d2	nuclear receptor subfamily 1, group D, member 2	1.41	0.0028
17524117	Hephl1	hephaestin-like 1	-1.39	0.0175
17500543	Ppp1r3b	protein phosphatase 1, regulatory (inhibitor) subunit 3B	-1.33	0.0118
17433328	Per3	period circadian clock 3	1.32	0.0007
17268884	Nr1d1	nuclear receptor subfamily 1, group D, member 1	1.30	0.0129
17310400	1700047G03Rik	RIKEN cDNA 1700047G03 gene	-1.27	0.0024
17481960	Arntl	aryl hydrocarbon receptor nuclear translocator-like	-1.23	0.0006
17375701	Slc27a2	solute carrier family 27 (fatty acid transporter), member 2	1.12	0.046
17309832	C6	complement component 6	-1.12	0.0129
17300183	Trav14d-3-dv8	T cell receptor alpha variable 14D-3-DV8	-1.11	0.0329

17285846	Hist1h4m	histone cluster 1, H4m	-1.09	0.0028
17491193	Saa3	serum amyloid A 3	-1.06	0.0136
17469627	Oxtr	oxytocin receptor	-1.05	0.0024
17467209	Fam13a	family with sequence similarity 13, member A	1.04	0.0027
17352710	Cables1	CDK5 and Abl enzyme substrate 1	-1.00	0.0425
17278261	Serpina3b	serine (or cysteine) peptidase inhibitor, clade A, member 3B	-0.99	0.0306
17400862	Hmgcs2	3-hydroxy-3-methylglutaryl-Coenzyme A synthase 2	0.99	0.0444
17313376	Tef	thyrotroph embryonic factor	0.99	0.0024
17212087	Npas2	neuronal PAS domain protein 2	-0.91	0.004
17300163	Traj44	T cell receptor alpha joining 44	-0.90	0.0432
17533282	Mid1ip1	Mid1 interacting protein 1 (gastrulation specific G12-like (zebrafish))	-0.90	0.0074
17520416	Paqr9	progestin and adipoQ receptor family member IX	-0.89	0.0007
17291019	Hist1h4m	histone cluster 1, H4m	-0.87	0.0307
17482230	Acsm5	acyl-CoA synthetase medium-chain family member 5	0.87	0.0106
17254065	Ccl8	chemokine (C-C motif) ligand 8	-0.86	0.0186
17502233	Slc27a1	solute carrier family 27 (fatty acid transporter), member 1	0.83	0.0024
17363086	Dtx4	deltex 4 homolog (Drosophila)	-0.83	0.0024
17472760	Bhlhe41	basic helix-loop-helix family, member e41	0.82	0.0136
17211405	Gsta3	glutathione S-transferase, alpha 3	-0.81	0.0214
17459074	BB365896	expressed sequence BB365896	0.81	0.0203
17408015	Hist2h3c2	histone cluster 2, H3c2	-0.81	0.0136
17300247	Trav9d-3	T cell receptor alpha variable 9D-3	-0.81	0.0399
17548559	Emp1	epithelial membrane protein 1	-0.80	0.0158
17241954	Gstt2	glutathione S-transferase, theta 2	0.78	0.0028
17543315	Asb12	ankyrin repeat and SOCS box-containing 12	-0.77	0.0425
17409816	D3Bwg0562e	DNA segment, Chr 3, Brigham & Women's Genetics 0562 expressed	-0.77	0.0419
17373521	Chst1	carbohydrate (keratan sulfate Gal-6) sulfotransferase 1	0.76	0.0006
17311807	Sqle	squalene epoxidase	-0.76	0.0182
17283742	Syne3	spectrin repeat containing, nuclear envelope family member 3	0.75	0.0029
17249853	Gm12236	predicted gene 12236	-0.75	0.0109
17441490	Fbxo21	F-box protein 21	0.74	0.0058
17361996	Ppp2r5b	protein phosphatase 2, regulatory subunit B (B56), beta isoform	-0.73	0.0214
17426097	Mup3	major urinary protein 3	-0.73	0.0136
17292634	Nfil3	nuclear factor, interleukin 3, regulated	-0.72	0.0071
17321474	Gm5620	tubulin, alpha 1B pseudogene	-0.71	0.0237
17500548	Gm20359	predicted gene, 20359	-0.71	0.0229
17449562	Rassf6	Ras association (RalGDS	0.70	0.0158
17222825	Nabp1	nucleic acid binding protein 1	-0.69	0.0251
17446793	Slc5a6	solute carrier family 5 (sodium-dependent vitamin transporter), member 6	0.69	0.0136
17535208	Fmr1	fragile X mental retardation syndrome 1	-0.68	0.0054
17409284	Celsr2	cadherin, EGF LAG seven-pass G-type receptor 2 (flamingo homolog,	0.68	0.0024

		Drosophila)		
17265365	Inca1	inhibitor of CDK, cyclin A1 interacting protein 1	0.68	0.0175
17310172	Ranbp3l	RAN binding protein 3-like	0.67	0.0129
17507374	Irs2	insulin receptor substrate 2	0.67	0.0205
17220475	Dusp10	dual specificity phosphatase 10	-0.67	0.0048
17364150	Pank1	pantothenate kinase 1	0.67	0.008
17218361	A930039A15Rik	RIKEN cDNA A930039A15 gene	0.67	0.0324
17471107	Plekhg6	pleckstrin homology domain containing, family G (with RhoGef domain) member 6	0.66	0.0199
17230725	Marc1	mitochondrial amidoxime reducing component 1	-0.66	0.0182
17464654	Pdk4	pyruvate dehydrogenase kinase, isoenzyme 4	0.66	0.0417
17230408	Adck3	aarF domain containing kinase 3	0.66	0.0158
17331720	Adamts5	a disintegrin-like and metallopeptidase (reprolysin type) with thrombospondin type 1 motif, 5 (aggrecanase-2)	-0.65	0.0027
17372621	Slc43a1	solute carrier family 43, member 1	0.65	0.0099
17340657	Gm9992	predicted gene 9992	0.64	0.0205
17290173	Hmgcs1	3-hydroxy-3-methylglutaryl-Coenzyme A synthase 1	-0.64	0.0016
17407934	Gm129	predicted gene 129	0.63	0.0158
17544878	Morc4	microrchidia 4	-0.62	0.0027
17333198	Gm16168	predicted gene 16168	0.61	0.0476
17515315	Ldlr	low density lipoprotein receptor	-0.61	0.0346
17484587	Cyp2e1	cytochrome P450, family 2, subfamily e, polypeptide 1	0.61	0.0151
17498502	Ccnd1	cyclin D1	-0.61	0.0137
17456545	Lep	leptin	-0.60	0.0251
17519364	Fam214a	family with sequence similarity 214, member A	0.60	0.0431
17507175	Cd209e	CD209e antigen	-0.59	0.0205
17495821	Cdr2	cerebellar degeneration-related 2	-0.59	0.0076
17290242	Net1	neuroepithelial cell transforming gene 1	0.59	0.0158
17326183	Gm6936	predicted gene 6936	-0.59	0.0352
17315860	Slc1a3	solute carrier family 1 (glial high affinity glutamate transporter), member 3	0.59	0.0175
17537861	Arxes2	adipocyte-related X-chromosome expressed sequence 2	0.58	0.0212
17401480	Dennd2d	DENN/MADD domain containing 2D	0.58	0.0307
17518378	Dennd4a	DENN/MADD domain containing 4A	-0.58	0.0136

6. SPECIAL ACKNOWLEDGEMENTS

In this part I would like to acknowledge who significantly contributed to my overall development as person and as scientist. I would like to acknowledge my first supervisor in Russia Dr. S.V. Anisimov, who shared with me all his US/Europe experiences, encourage me to learn English and thought me to write and speak. I also appreciate all support of Prof. A. Yu. Zaritskey, who sent me to international congresses. Great impact on my development was done by friend of mine Dr. Nikolay Samusik. Thank you for helping me with correction of applications, motivation letters and training with me for skype interviews.

I would like to thank my beloved mother who did not allow me to drop University in the moments of crises. Thank you for investing so much time, money and energy into my education. Since that frustrating moment, when during my childhood I was not able to discriminate numbers 7 and 8, you were never given up on me till the moment of success. I would not be here without all this years of permanent support. I would like specially acknowledge Luiz Gustavo Guedes Corrêa for daily support and for the nights correcting this thesis. Luiz, thank you for all your patience!

7. REFERENCES

Aeberli, I. et al., 2008. The increase of fatty acid-binding protein aP2 in overweight and obese children: interactions with dietary fat and impact on measures of subclinical inflammation. *International journal of obesity (2005)*, 32, pp.1513–20.

Andres, R., 1980. Effect of obesity on total mortality. *International journal of obesity*, 4(4), pp.381–386.

Arner, P. et al., 2013. Variations in the size of the major omentum are primarily determined by fat cell number. *Journal of Clinical Endocrinology and Metabolism*, 98(5), pp.897–901.

Baer, P.C., 2014. Adipose-derived mesenchymal stromal/stem cells: An update on their phenotype in vivo and in vitro. *World journal of stem cells*, 6(3), pp.256–65. Available at: http://www.ncbi.nlm.nih.gov/pubmed/25126376\nhttp://www.pubmedcentral.nih.gov/articlerender.fcgi?artid=PMC4131268.

Bangsow, T. et al., 2008. The epithelial membrane protein 1 is a novel tight junction protein of the blood-brain barrier. *Journal of cerebral blood flow and metabolism : official journal of the International Society of Cerebral Blood Flow and Metabolism*, 28(6), pp.1249–60. Available at: http://www.ncbi.nlm.nih.gov/pubmed/18382472 [Accessed February 12, 2015].

Berry, R. & Rodeheffer, M.S., 2013. Characterization of the adipocyte cellular lineage in vivo. *Nature cell biology*, 15(3), pp.302–8. Available at: http://www.pubmedcentral.nih.gov/articlerender.fcgi?artid=3721064&tool=pmcentrez&rendertype=abstract [Accessed May 23, 2014].

Berryman, D.E. et al., 2013. The GH/IGF-1 axis in obesity: pathophysiology and therapeutic considerations. *Nature reviews. Endocrinology*, 9(6), pp.346–56. Available at: http://www.ncbi.nlm.nih.gov/pubmed/23568441.

Bowers, R.R. et al., 2004. Sympathetic innervation of white adipose tissue and its regulation of fat cell number. *American journal of physiology. Regulatory, integrative and comparative physiology*, 286, pp.R1167–R1175.

Brestoff, J.R. et al., 2014. Group 2 innate lymphoid cells promote beiging of white adipose tissue and limit obesity. *Nature*, 519(7542), pp.242–246. Available at: http://www.nature.com/doifinder/10.1038/nature14115 [Accessed December 22, 2014].

Buettner, R. et al., 2006. Defining high-fat-diet rat models: Metabolic and molecular effects of different fat types. *Journal of Molecular Endocrinology*, 36(3), pp.485–501.

Butler, J.M. et al., 2012. Development of a vascular niche platform for expansion of repopulating human cord blood stem and progenitor cells Brief report Development of a vascular niche platform for expansion of repopulating human cord blood stem and progenitor cells. , 120(6), pp.1344–1347.

Choe, S.S. et al., 2016. Adipose tissue remodeling: Its role in energy metabolism and metabolic disorders. *Frontiers in Endocrinology*, 7(APR), pp.1–16.

Cinti, S. et al., 2005. Adipocyte death defines macrophage localization and function in adipose tissue of obese mice and humans. *Journal of lipid research*, 46(11), pp.2347–2355.

Cinti, S., 2012. The adipose organ at a glance. *Disease Models & Mechanisms*, 5(5), pp.588–594. Available at: http://dmm.biologists.org/cgi/doi/10.1242/dmm.009662.

Consequences, P. et al., 2013. Postnatal Overfeeding in Rodents by Litter Size Reduction Induces Major Short- and Long-Term. , pp.553–562.

Consortium, T.G.O., 2000. Gene ontologie: Tool for the unification of biology. *Nature Genetics*, 25(1), pp.25–29.

Coutinho, T. et al., 2011. Central obesity and survival in subjects with coronary artery disease: a systematic review of the literature and collaborative analysis with individual subject data. *Journal of the American College of Cardiology*, 57(19), pp.1877–1886.

Cunningham, S., Kramer, M.R. & Narayan, K.M.V., 2014. Incidence of childhood obesity in the United States. *The New England journal of medicine*, 370(5), pp.403–11.

Davison, Z. et al., 2011. Insulin-like growth factor-dependent proliferation and survival of triple-negative breast cancer cells: implications for therapy. *Neoplasia (New York, N.Y.)*, 13(6), pp.504–15.

Demirag, G.G. et al., 2016. Epithelial membrane protein 1 expression in ovarian serous tumors. *Oncology letters*, 11(3), pp.2140–2144. Available at: http://www.pubmedcentral.nih.gov/articlerender.fcgi?artid=4774438&tool=pmcentrez&rendertype=abstract [Accessed May 19, 2016].

Denis, G. V & Obin, M.S., 2013. “Metabolically healthy obesity”: Origins and implications. *Molecular Aspects of Medicine*, 34(1), pp.59–70. Available at: http://www.sciencedirect.com/science/article/pii/S0098299712001185.

Durgan, J. et al., 2015. SOS 1 and Ras regulate epithelial tight junction formation in the human airway through EMP 1. , 16(1).

Endocrinology, D., Israel, B. & Medical, D., 2012. Lipodystrophy : Pathophysiology and Advances in Treatment. , 7(3), pp.137–150.

Ferranti, R. et al., 2016. Sleep quality and duration is related with diet and obesity in young adolescent living in Sicily , Southern Italy. *Sleep Science*, 9(2), pp.117–122. Available at: http://dx.doi.org/10.1016/j.slsci.2016.04.003.

Fonseca, V., 2003. Effect of thiazolidinediones on body weight in patients with diabetes mellitus. *American Journal of Medicine*, 115(8 SUPPL. 1), pp.42–48.

Foster, M.T. & Bartness, T.J., 2006. Sympathetic but not sensory denervation stimulates white adipocyte proliferation. *American journal of physiology. Regulatory, integrative*

and comparative physiology, 291(6), pp.R1630-7. Available at: http://www.ncbi.nlm.nih.gov/pubmed/16887921.

Fox, K. et al., 1993. Abdominal fat deposition in 11-year-old children. *International journal of obesity and related metabolic disorders : journal of the International Association for the Study of Obesity*, 17(1), pp.11–16.

Frayn, K.N. & Humphreys, S.M., 2012. Metabolic characteristics of human subcutaneous abdominal adipose tissueafter overnight fast. *AJP: Endocrinology and Metabolism*, 302(4), pp.E468–E475.

Galescu, O.A. et al., 2016. A pilot study of the effects of niacin administration on free fatty acid and growth hormone concentrations in children with obesity. *Pediatric Obesity*.

Garten, A., Schuster, S. & Kiess, W., 2012. The insulin-like growth factors in adipogenesis and obesity. *Endocrinology and metabolism clinics of North America*, 41(2), pp.283–95, v–vi.

Garver, W.S. et al., 2013. The genetics of childhood obesity and interaction with dietary macronutrients. *Genes & nutrition*, 8(3), pp.271–87. Available at: http://www.pubmedcentral.nih.gov/articlerender.fcgi?artid=3639324&tool=pmcentrez&rendertype=abstract [Accessed June 13, 2014].

Gesta, S., Tseng, Y.H. & Kahn, C.R., 2007. Developmental Origin of Fat: Tracking Obesity to Its Source. *Cell*, 131(2), pp.242–256.

Giordano, A. et al., 2014. White, brown and pink adipocytes: The extraordinary plasticity of the adipose organ. *European Journal of Endocrinology*, 170(5).

Goran, M.I. et al., 2013. The obesogenic effect of high fructose exposure during early development. *Nature reviews. Endocrinology*, 9(8), pp.494–500. Available at: http://www.ncbi.nlm.nih.gov/pubmed/23732284 [Accessed October 24, 2014].

Habbout, A. et al., 2013. Postnatal overfeeding causes early shifts in gene expression in the heart and long-term alterations in cardiometabolic and oxidative parameters. *PloS one*, 8(2), p.e56981. Available at: http://www.pubmedcentral.nih.gov/articlerender.fcgi?artid=3582632&tool=pmcentrez&rendertype=abstract [Accessed October 24, 2014].

Hansen, J.B. & Kristiansen, K., 2006. Regulatory circuits controlling white versus brown adipocyte differentiation. *The Biochemical journal*, 398(2), pp.153–68. Available at: http://www.pubmedcentral.nih.gov/articlerender.fcgi?artid=1550312&tool=pmcentrez&rendertype=abstract.

Heo, J. et al., 2016. Gut microbiota Modulated by Probiotics and Garcinia cambogia Extract Correlate with Weight Gain and Adipocyte Sizes in High Fat-Fed Mice. *Scientific Reports*, 6(April), p.33566. Available at: http://www.nature.com/articles/srep33566.

Hill, J.O., Wyatt, H.R. & Peters, J.C., 2012. Energy balance and obesity. *Circulation*, 126(1),

pp.126–32. Available at: http://www.ncbi.nlm.nih.gov/pubmed/22753534.

Houpt, K. a., Houpt, T.R. & Pond, W.G., 1979. The Pig as a Model for the Study of Obesity and of Control of Food Intake: A Review. *The Yale journal of biology and medicine*, 52(3), pp.307–329.

Jeffery, E. et al., 2015. Rapid depot-specific activation of adipocyte precursor cells at the onset of obesity. *Nature cell biology*, 17(4), pp.376–85. Available at: http://dx.doi.org/10.1038/ncb3122.

Jeffery, E. et al., 2016. The Adipose Tissue Microenvironment Regulates Depot-Specific Adipogenesis in Obesity. *Cell Metabolism*, 24(1), pp.142–150.

Jeon, M., Rahman, N. & Kim, Y.-S., 2016. Wnt/β-catenin signaling plays a distinct role in methyl gallate–mediated inhibition of adipogenesis. *Biochemical and Biophysical Research Communications*, 479(1), pp.22–27. Available at: http://www.sciencedirect.com/science/article/pii/S0006291X16314425.

Jung, J.H. et al., 2016. Ultrasound measurement of pediatric visceral fat thickness: correlations with metabolic and liver profiles. *Annals of pediatric endocrinology & metabolism*, 21(2), pp.75–80. Available at: http://www.ncbi.nlm.nih.gov/pubmed/27462583\nhttp://www.pubmedcentral.nih.gov/articlerender.fcgi?artid=PMC4960018.

Kannel, W.B. et al., 1977. THE NHLBI TWIN STUDY OF CARDIOVASCULAR DISEASE RISK FACTORS : METHODOLOGY AND SUMMARY OF RESULTS Many prospective epidemiologic studies conducted during the past 20 years have firmly established the association between several physiologic characteristics . , 106(4), pp.284–295.

Kim, J.B. et al., 1998. ADD1/SREBP1 activates PPARgamma through the production of endogenous ligand. *Proceedings of the National Academy of Sciences of the United States of America*, 95(8), pp.4333–4337.

Kim, S.M. et al., 2014. Loss of white adipose hyperplastic potential is associated with enhanced susceptibility to insulin resistance. *Cell metabolism*, 20(6), pp.1049–58. Available at: http://www.pubmedcentral.nih.gov/articlerender.fcgi?artid=4715375&tool=pmcentrez&rendertype=abstract [Accessed August 19, 2016].

Klöting, N. et al., 2010. Insulin-sensitive obesity. *American Journal of …*, 299(3), pp.506–515. Available at: http://www.ncbi.nlm.nih.gov/pubmed/20570822\nhttp://ajpendo.physiology.org/content/299/3/E506.short.

Knittle, J.L. et al., 1979. The growth of adipose tissue in children and adolescents: Cross-sectional and longitudinal studies of adipose cell number and size. *The Journal of Clinical Investigation*, 63(February), pp.239–46. Available at:

http://www.pubmedcentral.nih.gov/articlerender.fcgi?artid=371945&tool=pmcentrez&rendertype=abstract.

Knittle, J.L. & Hirsch, J., 1968. Effect of early nutrition on the development of rat epididymal fat pads: cellularity and metabolism. *Journal of Clinical Investigation*, 47(9), pp.2091–2098.

Kreitschmann-Andermahr, I. et al., 2010. GH/IGF-I regulation in obesity - Mechanisms and practical consequences in children and adults. *Hormone Research in Paediatrics*, 73(3), pp.153–160.

Krotkiewski, M. et al., 1983. Impact of obesity on metabolism in men and women. Importance of regional adipose tissue distribution. *Journal of Clinical Investigation*, 72(3), pp.1150–1162.

Lackey, D.E. et al., 2014. Contributions of adipose tissue architectural and tensile properties toward defining healthy and unhealthy obesity. *American journal of physiology. Endocrinology and metabolism*, 306(3), pp.E233-46. Available at: http://ajpendo.physiology.org/content/306/3/E233.long.

Lasater, G., Piernas, C. & Popkin, B.M., 2011. Beverage patterns and trends among school-aged children in the US, 1989-2008. *Nutrition Journal*, 10(1), p.103. Available at: http://www.nutritionj.com/content/10/1/103.

Lee, J.J., Beretvas, S.N. & Freeland-Graves, J.H., 2014. Abdominal adiposity distribution in diabetic/prediabetic and nondiabetic populations: A meta-analysis. *Journal of Obesity*, 2014.

Lee, M.-W. et al., 2014. Activated Type 2 Innate Lymphoid Cells Regulate Beige Fat Biogenesis. *Cell*, pp.1–14. Available at: http://linkinghub.elsevier.com/retrieve/pii/S0092867414015815 [Accessed December 24, 2014].

Lee, Y.-H. et al., 2012. In vivo identification of bipotential adipocyte progenitors recruited by β3-adrenoceptor activation and high-fat feeding. *Cell metabolism*, 15(4), pp.480–91. Available at: http://www.pubmedcentral.nih.gov/articlerender.fcgi?artid=3322390&tool=pmcentrez&rendertype=abstract [Accessed May 25, 2014].

Lee, Y.-H., Mottillo, E.P. & Granneman, J.G., 2014. Adipose tissue plasticity from WAT to BAT and in between. *Biochimica et biophysica acta*, 1842(3), pp.358–69. Available at: http://www.ncbi.nlm.nih.gov/pubmed/23688783 [Accessed June 2, 2014].

Lee, Y.H., Petkova, A.P. & Granneman, J.G., 2013. Identification of an adipogenic niche for adipose tissue remodeling and restoration. *Cell Metabolism*, 18(3), pp.355–367. Available at: http://dx.doi.org/10.1016/j.cmet.2013.08.003.

Lin, G.G. & Scott, J.G., 2012. NIH Public Access. , 100(2), pp.130–134.

Lin, P.-H. et al., 2012. Dietary Saturated Fat Intake Is Negatively Associated With Weight Maintenance Among the PREMIER Participants. *Obesity*, 20(3), pp.571–575. Available at: http://dx.doi.org/10.1038/oby.2011.17/nature06264.

Luck, H. et al., 2015. Regulation of obesity-related insulin resistance with gut anti-inflammatory agents. *Cell Metabolism*, 21(4), pp.527–542. Available at: http://dx.doi.org/10.1016/j.cmet.2015.03.001.

Mersminn, H.J., Goodman, J.R. & Brown, L.J., 1975. Development of swine adipose tissue : morphology and chemical composition. , 16, pp.269–279.

Moitra, J. et al., 1998. Life without white fat : a transgenic mouse. , pp.3168–3181.

Nikitovic, D. et al., 2008. Lumican, a small leucine-rich proteoglycan. *IUBMB Life*, 60(12), pp.818–823.

Nishino, J. et al., 2008. Hmga2 Promotes Neural Stem Cell Self-Renewal in Young but Not Old Mice by Reducing p16Ink4a and p19Arf Expression. *Cell*, 135(2), pp.227–239. Available at: http://dx.doi.org/10.1016/j.cell.2008.09.017.

Nishtar, S., Gluckman, P. & Armstrong, T., 2016. Ending childhood obesity: A time for action. *The Lancet*, 387(10021), pp.825–827.

Pajvani, U.B. et al., 2005. Fat apoptosis through targeted activation of caspase 8: a new mouse model of inducible and reversible lipoatrophy. *Nature medicine*, 11(7), pp.797–803.

Paul, I.M. et al., 2011. Preventing obesity during infancy: a pilot study. *Obesity (Silver Spring, Md.)*, 19(2), pp.353–361. Available at: http://dx.doi.org/10.1038/oby.2010.182.

Peerani, R. et al., 2007. Niche-mediated control of human embryonic stem cell self-renewal and differentiation. *The EMBO Journal*, 26(22), pp.4744–4755. Available at: http://emboj.embopress.org/cgi/doi/10.1038/sj.emboj.7601896.

Peirce, V., Carobbio, S. & Vidal-Puig, A., 2014. The different shades of fat. *Nature*, 510(7503), pp.76–83. Available at: http://www.ncbi.nlm.nih.gov/pubmed/24899307 [Accessed July 21, 2014].

Perry, R.J. et al., 2016. Acetate mediates a microbiome-brain-beta-cell axis to promote metabolic syndrome. *Nature*, 534(7606), pp.213–217. Available at: http://www.ncbi.nlm.nih.gov/pubmed/27279214.

Petruzzelli, M. & Wagner, E.F., 2016. Mechanisms of metabolic dysfunction in cancer-associated cachexia. *Genes and Development*, 30(5), pp.489–501.

Poissonnet, C.M., Burdi, A.R. & Garn, S.M., 1984. The chronology of adipose tissue appearance and distribution in the human fetus. *Early human development*, 10(1–2), pp.1–11.

Primeau, V. et al., 2011. Characterizing the profile of obese patients who are metabolically healthy. *International journal of obesity (2005)*, 35(7), pp.971–981. Available at:

http://dx.doi.org/10.1038/ijo.2010.216.

Rabot, S. et al., 2016. High fat diet drives obesity regardless the composition of gut microbiota in mice. *Scientific Reports*, 6, p.32484. Available at: http://www.nature.com/articles/srep32484.

Raynaud, C.M. et al., 2013. Endothelial cells provide a niche for placental hematopoietic stem/progenitor cell expansion through broad transcriptomic modification. *Stem Cell Research*, 11(3), pp.1074–1090. Available at: http://dx.doi.org/10.1016/j.scr.2013.07.010.

Rodeheffer, M.S., Birsoy, K. & Friedman, J.M., 2008. Identification of White Adipocyte Progenitor Cells In Vivo. *Cell*, 135(2), pp.240–249.

Rosen, E.D. et al., 2000. Transcriptional regulation of adipogenesis Transcriptional regulation of adipogenesis. *Genes & Development*, 14, pp.1293–1307.

Rosen, E.D. & Spiegelman, B.M., 2014. What we talk about when we talk about fat. *Cell*, 156(1–2), pp.20–44. Available at: http://www.ncbi.nlm.nih.gov/pubmed/24439368 [Accessed July 11, 2014].

Rutkowski, J.M., Stern, J.H. & Scherer, P.E., 2015. The cell biology of fat expansion. *The Journal of cell biology*, 208(5), pp.501–512. Available at: http://www.ncbi.nlm.nih.gov/pubmed/25733711 [Accessed March 5, 2015].

Salans, L.B., Horton, E.S. & Sims, E.A.H., 1971. Experimental Obesity in Man : Cellular Character of the Adipose Tissue. , 50(4), pp.1005–1011.

Samuelsson, A.M. et al., 2013. Sucrose feeding in mouse pregnancy leads to hypertension, and sex-linked obesity and insulin resistance in female offspring. *Frontiers in Physiology*, 4 FEB(February), pp.1–11.

Scavo, L.M. et al., 2004. Insulin-like growth factor-I stimulates both cell growth and lipogenesis during differentiation of human mesenchymal stem cells into adipocytes. *J Clin Endocrinol Metab*, 89(7), pp.3543–3553.

Schulz, T.J. & Tseng, Y.-H., 2016. Emerging role of bone morphogenetic proteins in adipogenesis and energy metabolism. *Cytokine and Growth Factor Reviews*, 20(5), pp.523–531. Available at: http://dx.doi.org/10.1016/j.cytogfr.2009.10.019.

Senol-Cosar, O. et al., 2016. Tenomodulin promotes human adipocyte differentiation and beneficial visceral adipose tissue expansion. *Nature Communications*, 7, p.10686. Available at: http://www.nature.com/doifinder/10.1038/ncomms10686\nhttp://www.ncbi.nlm.nih.gov/pubmed/26880110.

Siegel, M.J. et al., 2007. Total and intraabdominal fat distribution in preadolescents and adolescents: Measurement with MR imaging. *Radiology*, 242(3), pp.846–856.

Sims, E.A.H., 2001. Are there persons who are obese, but metabolically healthy?

Metabolism: Clinical and Experimental, 50(12), pp.1499–1504.

Smith, P.J. et al., 1988. Insulin-like growth factor-I is an essential regulator of the differentiation of 3T3-L1 adipocytes. *The Journal of biological chemistry*, 263(19), pp.9402–9408.

Smyth, G.K., Michaud, J. & Scott, H.S., 2005. Use of within-array replicate spots for assessing differential expression in microarray experiments. *Bioinformatics*, 21(9), pp.2067–2075.

Spalding, K.L. et al., 2008. Dynamics of fat cell turnover in humans. *Nature*, 453(7196), pp.783–7. Available at: http://www.ncbi.nlm.nih.gov/pubmed/18454136 [Accessed January 12, 2015].

Spiegelman, B.M. et al., 1997. PPARγ and the control of adipogenesis. *Biochimie*, 79(2), pp.111–112. Available at: http://www.sciencedirect.com/science/article/pii/S0300908497815003.

Spiegelman, B.M. & Flier, J.S., 2001. Obesity and the regulation of energy balance. *Cell*, 104(4), pp.531–543.

Strissel, K.J. et al., 2007. Adipocyte death, adipose tissue remodeling, and obesity complications. *Diabetes*, 56(12), pp.2910–2918.

Stry, C.H.E. & Renold, A.E., 1965. by Incubated Rat Epididymal Adipose Tissue. *Transport*, 240(8).

Sun, G.G. et al., 2014. EMP1, a member of a new family of antiproliferative genes in breast carcinoma. *Tumour biology : the journal of the International Society for Oncodevelopmental Biology and Medicine*, 35(4), pp.3347–54. Available at: http://www.ncbi.nlm.nih.gov/pubmed/24402572 [Accessed February 11, 2015].

Sun, G.-G. et al., 2014. Epithelial membrane protein 1 negatively regulates cell growth and metastasis in colorectal carcinoma. *World journal of gastroenterology : WJG*, 20(14), pp.4001–10. Available at: http://www.pubmedcentral.nih.gov/articlerender.fcgi?artid=3983455&tool=pmcentrez&rendertype=abstract [Accessed February 11, 2015].

Tang, W. et al., 2011. Thiazolidinediones regulate adipose lineage dynamics. *Cell Metabolism*, 14(1), pp.116–122. Available at: http://dx.doi.org/10.1016/j.cmet.2011.05.012.

Tchoukalova, Y.D. et al., 2010. Regional differences in cellular mechanisms of adipose tissue gain with overfeeding. *Proceedings of the National Academy of Sciences of the United States of America*, 107(42), pp.18226–18231.

Vishvanath, L. et al., 2016. Pdgfrβ^{+} Mural Preadipocytes Contribute to Adipocyte Hyperplasia Induced by High-Fat-Diet Feeding and Prolonged Cold Exposure in Adult Mice. *Cell Metabolism*, 23(2), pp.350–359. Available at:

http://dx.doi.org/10.1016/j.cmet.2015.10.018.

Wang, B. et al., 2009. Dietary carbohydrate source alters gene expression profile of intestinal epithelium in mice. *Nutrition and cancer*, 61(1), pp.146–155.

Wernstedt Asterholm, I. et al., 2014. Adipocyte Inflammation Is Essential for Healthy Adipose Tissue Expansion and Remodeling. *Cell Metabolism*, 20(1), pp.103–118. Available at: http://linkinghub.elsevier.com/retrieve/pii/S1550413114002137 [Accessed June 13, 2014].

Whitaker, R.C. et al., 1997. Predicting Obesity in Young Adulthood from Childhood and Parental Obesity. *New England Journal of Medicine*, 337(13), pp.869–873. Available at: http://www.nejm.org/doi/abs/10.1056/NEJM199709253371301.

WHO, 2016. Report of the commission on ending childhood obesity. *Report of the commission on ending childhood obesity*.

Wilding, J., 2006. Thiazolidinediones, insulin resistance and obesity: Finding a balance. *International journal of clinical practice*, 60(10), pp.1272–80. Available at: http://www.ncbi.nlm.nih.gov/pubmed/16981971.

Wu, L.L. et al., 2015. Mitochondrial dysfunction in oocytes of obese mothers: transmission to offspring and reversal by pharmacological endoplasmic reticulum stress inhibitors. *Development*, 142(4), pp.681–691. Available at: http://dev.biologists.org/cgi/doi/10.1242/dev.114850 [Accessed February 10, 2015].

Yamauchi, T. et al., 2001. The Mechanisms by Which Both Heterozygous Peroxisome Proliferator-activated Receptor ?? (PPAR??) Deficiency and PPAR?? Agonist Improve Insulin Resistance. *Journal of Biological Chemistry*, 276(44), pp.41245–41254.

Yanovski, J. a, 2011. Intervening during infancy to prevent pediatric obesity. *Obesity (Silver Spring, Md.)*, 19(7), pp.1321–2. Available at: http://www.ncbi.nlm.nih.gov/pubmed/21706036 [Accessed June 25, 2014].